Investigation into pathophysiological mechanisms that alter ryanodine receptor function in cardiovascular disease



Abigail D. Wilson

Linacre College

University of Oxford

A thesis submitted for the degree of

Doctor of Philosophy

Trinity 2020

Acknowledgements

Firstly, thank you to Prof. Rebecca Sitsapesan for being such an incredible and supportive supervisor throughout the four years of my DPhil. I am very grateful for all the time and inspiration she has given to teach me how to be a great scientist. I would also like to thank all of the Sitsapesan group for their support and teamwork. In particular, thank you to Elisa Venturi for teaching me everything I know in the laboratory, as well as Babis Sigalas, Chris Lindsay, Tom Humberstone and Jianshu Hu. Thank you also to Dr. Ming Lei for supporting me to use his laboratory equipment.

Thank you to Prof. David Greaves for all his encouragement and for selecting me for the opportunity on the British Heart Foundation studentship programme. I am very grateful to the British Heart Foundation for funding my DPhil. It is also important to acknowledge all of the individuals and families affected by CPVT, such a devastating disease that has been the focus of my thesis.

Lisa Simpson and KC Park, thank you for all the friendship and support - it's been super fun to share this BHF journey with you. I am also so lucky to have met amazing friends in the Department of Pharmacology that have supported me along the way. Thank you so much to Kathryn Acheson, Ria Dinsdale, Lara Scofano and Razik Mu-u-Min, thank you for all the coffees and cakes. I hope we always stay in touch.

Thank you to all my friends at Hurst Street, Linacre College and beyond for all the good times in Oxford. And thank you to my Bristol pals and home gals for their support from afar.

I could not have done my DPhil without the most supportive and loving family - Mum, Dad, Tom and Ella.

And finally, thank you from the bottom of my heart to Andrew. We've had so much fun together and you've really kept me going through the hardest times. Thank you for your love, support and MATLAB expertise. *Is é Binn Ghulbain an chéad sliabh eile a dhreapfaimid le chéile!*

The year 2020 did not make it easy to complete my DPhil, but I am proud of myself for reaching the finish line.

Abstract

Catecholaminergic polymorphic ventricular tachycardia type 1 (CPVT1) is a highly malignant cardiac disease caused by mutations to the cardiac ryanodine receptor (RyR2). Mutations at RyR2, including the V2475F mutation, lead to inappropriate diastolic Ca^{2+} release thereby triggering arrhythmogenesis and sudden cardiac death (SCD).

In order to identify specific alterations to RyR2 caused by the V2475F mutation, this research utilised native RyR2 channels derived from heterozygous (+/-) V2475F-mutated mouse cardiac tissue in single-channel artificial bilayer experiments. Phospho-specific antibodies were used to quantify phosphorylation levels at S2808 of wild-type (WT) or CPVT1-mutated RyR2, and spontaneous Ca^{2+} release in intact cardiomyocytes was assessed using a Ca^{2+}-indicator.

These experiments revealed that the V2475F mutation caused highly aberrant RyR2 responses to cytosolic Ca^{2+} and Mg^{2+}, overall demonstrating a hyperactive RyR2 channel in nanomolar and low micromolar cytosolic [Ca^{2+}] alongside insensitivity to inhibition by cytosolic Mg^{2+}. Some V2475F(+/-) RyR2 channels even displayed an agonistic response to cytosolic Mg^{2+}. In agreement with these findings, intact cardiomyocytes derived from V2475F(+/-) hearts revealed a shorter latency to spontaneous Ca^{2+} release compared to WT. Furthermore, phosphorylation at S2808 was not altered but the Po at every quantified phosphorylation level was higher for RyR2 channels derived from V2475F(+/-) hearts compared to WT hearts.

Other novel findings were observed in this CPVT1-mutant RyR2, including modifications to single-channel Ca^{2+} conductance, and that atorvastatin was unable to inhibit these hyperactive channels. Moreover, modelling the V2475F single-channel behaviour against the proposed distribution of heterozygosity suggested that greater dysfunction may be caused by RyR2 channels with three or four mutated monomers per tetramer.

This work has revealed changes to RyR2 function that are specific to the V2475F mutation. Some of these dysfunctions have not been observed previously, highlighting the importance of comprehensive and patient-specific study of CPVT1-mutated RyR2 channels.

Statement of Covid-19 Disruption

Chapter not included: This thesis would have contained an additional chapter which characterised a "loss-of-function" CPVT1-mutation from a mouse model, A4860G. However, at the point of lockdown I did not have sufficient control experiments from the littermate controls. The results so far are very interesting and indicate that the mutation causes unusual changes in gating, Ca^{2+}-conductance and relative permeability of K^+/Ca^{2+}, but since the number of replicates was low, especially for controls, the data were not included in the thesis. This work will be continued October-January and written up for a manuscript.

Chapter 4: Mass spectrometry of WT and V2475F(+/-) SR preparations to determine phosphorylation levels at all serine sites of RyR2. The protocol had been optimised to have good coverage via a trypsin and elastase double-digestion protocol at known sites S2030, S2808 and S2814. This technique allows for greater resolution of level of phosphorylation than western blot and allows simultaneous measurements of all serine phosphorylation sites, as well as accurate comparisons of the intensity at each site. I had planned to run a phosphorylation treatment with CaMKII and PKA at 37∘C to induce a "catecholaminergic stress" protocol. These experiments would have given a more in-depth quantification of the alterations to phosphorylation sites at basal and under phosphorylated conditions, with comparison of WT and V2475F(+/-). The western blots in this chapter were only run to validate that at RT and under the specified conditions that we expected to see phosphorylation and dephosphorylation in the bilayer, and not for an accurate quantification of basal or treated phosphorylation levels.

Chapter 5: Further experiments would have been conducted on permeabilised cardiomyocytes with atorvastatin to investigate the effect of this statin at the whole cell level. The protocol had been optimised and some preliminary results were collected but this was unable to be completed following department closure and therefore were not included in this thesis. Further animal n numbers would also have been conducted for the intact cardiomyocyte experiments that were included in Chapter 4.

Contents

List of Figures **xi**

List of Tables **xvi**

List of Abbreviations **xvii**

1 Introduction **1**

1.1 Ca^{2+} signalling in the heart 2

1.1.1 Cardiac excitation-contraction coupling 2

1.1.2 Ultrastructure of cardiac diads 4

1.1.3 The β-adrenergic response in ECC 5

1.2 Ryanodine receptors 6

1.2.1 The discovery of ryanodine receptors 7

1.2.2 The structural basis of RyR2 8

1.2.3 Pore dynamics and conductance of RyR2 8

1.2.4 Ligand regulation of RyR2 11

1.2.5 RyR2 and associated proteins 13

1.2.6 Post-translational modification of RyR2 15

1.2.7 Spatial organisation of RyR2 clusters 17

1.3 Catecholaminergic polymorphic ventricular tachycardia 18

1.3.1 Clinical manifestations 18

1.3.2 Mutations that cause CPVT 19

1.3.3 Pathophysiological mechanisms of CPVT1 in the heart . . . 20

1.3.4 Helical domain 1 mutations 22

1.3.5 Current treatments for CPVT 23

1.3.6 Animal models of CPVT1 24
1.4 Statins and ryanodine receptors 25
1.5 Research aims 26

2 Methodology **29**
2.1 Mouse model of CPVT 30
2.1.1 Mouse model and ethical approval 30
2.1.2 Genotyping of the mouse model 31
2.2 Isolation of SR vesicles 32
2.2.1 Collection of cardiac tissue 32
2.2.2 Isolation of mixed membrane vesicles from mouse cardiac tissue 33
2.2.3 Isolation of heavy SR vesicles from sheep cardiac tissue . . . 34
2.2.4 Purification of heavy SR vesicles from sheep cardiac tissue . 35
2.3 Planar lipid bilayer technique 36
2.3.1 Planar lipid bilayer apparatus 36
2.3.2 Voltage-clamp configuration 38
2.3.3 Formation of planar lipid bilayers 39
2.3.4 Bilayer detection and estimate of the area 40
2.3.5 Incorporations of native RyR2 channels for recordings with Ca^{2+} as the permeant ion 41
2.3.6 Incorporations of native RyR2 channels for recordings with K^+ as the permeant ion 41
2.3.7 Incorporations of purified RyR2 channels for recordings with K^+ as the permeant ion 42
2.3.8 Recording conditions 43
2.4 Single-channel analysis 44
2.4.1 Data acquisition and filtering 44
2.4.2 Analysis of single-channel gating 45
2.4.3 Sub-conductance states 47
2.4.4 Single-channel lifetime distributions 47
2.4.5 Burst analysis 48

2.4.6 Population analysis 49
2.4.7 Single-channel conductance measurements 50
2.4.8 Liquid junction potentials 51
2.5 Phosphorylation studies 51
2.5.1 Bilayer treatments 51
2.5.2 Western blots for RyR2 53
2.6 Cardiomyocyte experiments 55
2.6.1 Isolation of cardiomyocytes 55
2.6.2 Ca^{2+} imaging set-up 57
2.6.3 Cardiomyocyte recording protocol 59
2.6.4 Analysis of spontaneous Ca^{2+} release from cardiomyocytes . 60
2.7 Chemicals and solutions 60
2.7.1 Measurement of free Ca^{2+} 60
2.7.2 Measurement of protein concentration 61
2.8 Statistics 61
2.8.1 Statistical tests 61
2.8.2 Models for linear and non-linear regression 63
2.8.3 Animal numbers 64
2.8.4 Randomisation and operator blinding 65

3 The V2475F mutation at RyR2 66
3.1 Introduction 67
3.2 Comparison of single-channel current fluctuations and conductance properties 68
3.3 Comparison of the RyR2 channel response to cytosolic Ca^{2+} 77
3.4 Effects of the V2475F mutation on channel response to 100 nM $[Ca^{2+}]$ 88
3.5 Populations of V2475F(+/-) channels 94
3.6 Alterations to other key regulators of RyR2 99

4 Phosphorylation and the V2475F mutation 111
4.1 Introduction 112

4.2 Phosphorylation at the single-channel level 112
4.3 Quantifying phosphorylation levels 116
4.4 β-adrenergic stimulation at the cardiomyocyte level 117

5 RyR2 and statins **120**

5.1 Introduction 121
5.2 Comparison of native and purified RyR2 channels 123
5.3 The effect of atorvastatin on purified RyR2 125
5.4 Atorvastatin modulation on a CPVT1- mutated RyR2 136

6 Discussion **142**

6.1 The pathophysiological effects of the V2475F mutation at single-channel RyR2 144
6.1.1 Alterations to modulation by cytosolic Ca^{2+} 144
6.1.2 Alterations to modulation by cytosolic Ca^{2+} at 100 nM . . . 147
6.1.3 Alterations to modulation by cytosolic Mg^{2+} 148
6.1.4 Differences in other key activators 150
6.1.5 Alterations to single-channel conductance 151
6.2 The contribution of phosphorylation to CPVT1 pathophysiology . . 153
6.2.1 Phosphorylation levels at S2808 were not altered 153
6.2.2 The relationship between S2808 phosphorylation levels and RyR2 single-channel function 154
6.2.3 β-adrenergic stimulation at the cardiomyocyte level 156
6.3 The interaction between RyR2 and atorvastatin 159
6.3.1 Comparison of purified and native RyR2 159
6.3.2 Atorvastatin modulates purified RyR2 gating 160
6.3.3 Statins as a therapeutic intervention for arrhythmic heart disease 162
6.4 Populations of single-channel behaviour 164
6.5 Structure-function relationship 170
6.6 Summary 172

6.6.1 Physiological implications 172
6.6.2 Other potential mechanisms 175
6.6.3 Generalised models of CPVT1 175
6.6.4 Concluding remarks 176

References **178**

List of Figures

1.1 Schematic of excitation-contraction coupling 3

1.2 β-adrenergic stimulation on a ventricular cardiomyocyte 5

1.3 Ryanodine locks RyR2 into a sub conductance state 8

1.4 Structure of RyR2 9

1.5 Adenosine derivatives refers to both adenosine and adenosine triphosphate 13

1.6 Schematic of generation of DADs in a cardiomyocyte with a CPVT1-mutation at RyR2 21

1.7 The chemical structure of atorvastatin 25

2.1 Example visualisation of resulting bands from genotyping of wildtype and transgenic V2475F(+/-) (Het) DNA samples 32

2.2 Schematic of the artificial planar bilayer set up 36

2.3 Equipment for data acquisition 38

2.4 Simplified electrical analogue of a bilayer 39

2.5 The osmotic gradient caused fusion of SR vesicles into the artificial lipid bilayer 42

2.6 Example schematic used throughout the thesis 43

2.7 Example of an idealisation of an RyR2 recording 46

2.8 Protocol for the phosphorylation and de-phosphorylation experiments 52

2.9 Schematic for isolation of cardiomyocytes 56

2.10 Equipment for image acquisition of spontaneous Ca^{2+} release 58

2.11 Schematic of the cardiomyocyte stress protocol 59

3.1 Comparison of single-channel Ca^{2+} current fluctuations 69

3.2 Comparison of single-channel Ca^{2+} conductance and current-voltage relationships 70

3.3 Comparison of single-channel K^+ current fluctuations 71

3.4 Comparison of single-channel K^+ conductance and current-voltage relationships 72

3.5 Comparison of single-channel recordings from relative Ca^{2+}/K^+ permeability 73

3.6 Comparison of single-channel relative Ca^{2+}:K^+ permeability 74

3.7 Comparison of the sub-conductance states 76

3.8 Effects of the V2475F mutation on the response to cytosolic Ca^{2+} (traces) 78

3.8 Effects of the V2475F mutation on the Ca^{2+}-response curve of RyR2 channels 79

3.9 The effects of cytosolic Ca^{2+} on RyR2 channel mean open and closed times 81

3.10 Representative open and closed lifetime distributions of single RyR2 channels in response to 1 μM cytosolic Ca^{2+} 83

3.11 Representative open and closed lifetime distributions of single RyR2 channels in response to 1 mM cytosolic Ca^{2+} 84

3.12 Comparison of the mean open lifetime parameters 86

3.12 Comparison of the mean closed lifetime parameters 87

3.13 The effect of the V2475F mutation on the response of RyR2 channels to 100 nM cytosolic Ca^{2+} 89

3.14 Open and closed lifetime distributions at 100 nM cytosolic Ca^{2+} . . 90

3.15 Burst analysis parameters at 100 nM cytosolic Ca^{2+} 92

3.16 Schematic of populations of V2475F(+/-) channels 94

3.17 Data displaying populations of V2475F(+/-) channels 96

3.18 The relationship between single-channel Ca^{2+} conductance and Po . 97

3.19 The quantification of protein concentration from WT and V2475F(+/-) SR vesicle isolations 98

3.20 Investigating differences in Po with single channels or multiple channels gating in the bilayer 99

3.21 Comparison of adenosine-based ligand activation of RyR2 from WT or V2475F(+/-) mouse hearts 100

3.22 Comparison of the effect of cytosolic Mg^{2+} on the gating of WT and V2475F(+/-) channels 102

3.23 The effects of cytosolic 500 μM Mg^{2+} on RyR2 channel mean open and closed times from WT or V2475F(+/-) mouse hearts 103

3.24 Populations of V2475F(+/-) channels that respond differently to Mg^{2+} inhibition 105

3.25 Effects of the V2475F mutation on open and closed lifetime distributions with the addition of 500 μM Mg^{2+} 107

3.26 Luminal Ca^{2+} regulation of WT and V2475F(+/-) channel gating . 109

3.26 Luminal Ca^{2+}-response curve 110

4.1 The contribution of phosphorylation to WT and V2475F(+/-) RyR2 gating 113

4.2 The contribution of phosphorylation to WT and V2475F(+/-) channel Po 114

4.3 The response of RyR2 gating with PKA-mediated phosphorylation . 115

4.4 The response of RyR2 Po to PKA-mediated phosphorylation . . . 116

4.5 S2808 phosphorylation levels of native RyR2 from SR vesicle preparations 117

4.6 Ca^{2+} release measured in intact cardiomyocytes isolated from mouse hearts 118

4.7 Survival of intact cardiomyocytes isolated from WT or V2475F(+/-) hearts following β-adrenergic stress protocol treatment 119

5.1 Comparison of single-channel K^+ current fluctuations of native mouse RyR2 channels and purified sheep RyR2 channels from sheep cardiac tissue 124

5.2 Comparison of current-voltage relationships in K^+ and Po in K^+ solutions of RyR2 channels derived from native mouse cardiac or purified from sheep cardiac tissue 125

5.3 Effects of atorvastatin on purified RyR2 channel gating 126

5.4 Effect of atorvastatin on purified RyR2 current-voltage relationships 127

5.5 Effects of atorvastatin on purified RyR2 channel gating 128

5.6 Relationships between dwell times and increasing atorvastatin concentration 129

5.7 Representative open and closed lifetime distributions of single purified RyR2 channels in response atorvastatin 130

5.8 Effects of atorvastatin on mean open and closed lifetime parameters for single purified RyR2 channels 132

5.9 Evidence of Ca^{2+}-independent openings with 50 μM atorvastatin . . 133

5.10 Lifetime analysis of Ca^{2+}-independent openings with 50 μM atorvastatin 134

5.11 Effects of atorvastatin on mouse native RyR2 channel gating 137

5.12 Percentage change in Po of mouse native RyR2 in response to atorvastatin 138

5.13 Open and closed lifetime distributions of a single RyR2 channel derived from V2475F(+/-) tissue that behaves similarly to a WT channel 139

5.14 Open and closed lifetime distributions of a single RyR2 channel derived from V2475F(+/-) tissue that behaves differently to a WT channel 140

6.1 Schematic depicting the alterations at RyR2 caused by the V2475F mutation 143

6.2 Schematic illustrating the complex biphasic relationship between RyR2 phosphorylation and Po 157

6.3 Schematic relating the distribution of V2475F(+/-) channel populations and the proportion of V2475F(+/-) channels with different behaviours to Mg^{2+} 165

6.4 Schematic relating the distribution of V2475F(+/-) channel populations and novel τ exponentials evidenced in lifetime analysis of open events at 1 μM and closed events at 1 mM cytosolic Ca^{2+} . 166

6.5 Schematic relating the distribution of V2475F(+/-) channel populations and the proportion of channels from V2475F(+/-) preparations that are insensitive to 1 nM inhibition by atorvastatin different to WT. 168

6.6 Structural domains of RyR2 170

6.7 Schematic depicting the predicted behaviour of RyR2 channels derived from WT or V2475F(+/-) cardiac tissue in diastolic conditions in a cardiomyocyte 173

6.8 The pathophysiological mechanism that lead to the induction of delayed-after-depolarisations (DADs) in CPVT1 caused by the mutation at V2475F 174

List of Tables

1.1 Identity alignment of RyR2 25

2.1 PCR genotyping protocol 31
2.2 Primers used for PCR genotyping 31
2.3 The compositions of buffers 33
2.4 The compositions of recording solutions 44
2.5 Phosphorylation experiment conditions 53
2.6 The compositions of buffers for western blots 54
2.7 The compositions of buffers for cardiomyocyte isolation 57

3.1 Burst analysis parameters at 100 nM cytosolic Ca^{2+} 93

List of Abbreviations

(+/-)	Heterozygous
(+/+)	Homozygous
A4860G	Alanine to guanine mutation at amino acid position 4860
ACN	Acetonitrile
AEBSF	4-(2-aminoethyl)benzenesulfonyl fluoride hydrochloride
AF	Atrial fibrillation
ANOVA	Analysis of variance
ATP	Adenosine triphosphate
BDM	2,3-Butanedione monoxime
BSA	Bovine serum albumin
CaM	Calmodulin
CaMKII	Calmodulin-dependent kinase II
cAMP	Cyclic adenosine monophosphate
CASQ	Calsequestrin
CHAPS	3-((3-cholamidopropyl)-dimethylammonio)-1-propane sulphonate
CICR	Ca^{2+} -induced-Ca^{2+}-release
Cis	*Cis* chamber / luminal side of the channel
CPVT	Catecholaminergic polymorphic ventricular tachycardia
CPVT1	Catecholaminergic polymorphic ventricular tachycardia type 1
Cryo-EM	Cryogenic electron microscopy
DAD	Delayed-after-depolarisation
DNA	Deoxyribonucleic acid
DTT	Dithiothreitol
EAD	Early-after-depolarisation

EC_{50} . . . . . Half maximal effective concentration

ECC . . . . . Excitation-contraction coupling

ECG . . . . . Electrocardiogram

EDTA . . . . . Ethylenediaminetetraacetic acid

EGTA . . . . . Ethylene glycol-bis(2-aminoethylether)-N,N,N',N'-tetraacetic acid

E_{REV} . . . . . Reversal potential

EtBr . . . . . Ethidium bromide

FKBP . . . . . FK506-binding protein

HD1 . . . . . Helical domain 1

HEPES . . . . 4-(2-hydroxyethyl)-1-piperazineethanesulfonic acid

HMG-CoA . . 3-hydroxy-3-methylglutaryl-CoA

IC_{50} . . . . . Half maximal inhibitory concentration

ICD . . . . . Implantable cardioverter defibrillator

ISO . . . . . Isoprenaline

KDE . . . . . Kernel density estimate

LJP . . . . . Liquid junction potential

LQT . . . . . Long QT interval

LTCC . . . . . L-type Ca^{2+} channels

mRNA . . . . Messenger ribonucleic acid

NaCl . . . . . Sodium chloride

NaF . . . . . Sodium fluoride

NCX . . . . . Na^+/Ca^{2+} exchanger

PC . . . . . L-α phosphatidylcholine

PCa^{2+}/PK^+ . Relative permeability of Ca^{2+} to K^+

PCR . . . . . Polymerase chain reaction

Pdf . . . . . Probability density function

PE . . . . . Phosphatidylethanolamine

PIPES . . . . . 1,4-Piperazinediethanesulfonic acid

PKA . . . . . Protein kinase A

PLB . . . . . Phospholamban

PMSF . . . . . Phenylmethylsulphonic fluoride

Po . . . . . Probability of opening

PP1 . . . . . Phosphatase protein 1

PS . . . . . Phosphatidylserine

RT . . . . . Room temperature

RyR1 . . . . . Skeletal ryanodine receptors / ryanodine receptor isoform 1

RyR2 . . . . . Cardiac ryanodine receptors / ryanodine receptor isoform 2

SAN . . . . . Sino-atrial node

SCD . . . . . Sudden cardiac death

SD . . . . . Standard deviation

SDS . . . . . Sodium dodecyl sulphate

SDS-PAGE . . Sodium dodecyl sulphate - polyacrylamide gel electrophoresis

SEM . . . . . Standard error of the mean

SERCA . . . . Sarcoplasmic reticulum Ca^{2+} ATPase

SR . . . . . Sarcoplasmic reticulum

TAE . . . . . Tris-acetate

TBS-T . . . . . Tris-buffered saline with 0.1% Tween 20 detergent

TCEP . . . . . Tris(2-carboxyethyl)phosphine

TEAB . . . . . Triethylammonium bicarbonate buffer

Trans . . . . . Trans chamber / cytosolic side of the channel

Tris . . . . . Tris(hydroxymethyl)aminomethane

V2475F . . . . Valine to phenylalanine mutation at amino acid position 2475

VT . . . . . Ventricular tachycardia

WT . . . . . Wild type

1 Introduction

Contents

1.1 Ca^{2+} signalling in the heart 2
1.1.1 Cardiac excitation-contraction coupling 2
1.1.2 Ultrastructure of cardiac diads 4
1.1.3 The β-adrenergic response in ECC 5
1.2 Ryanodine receptors 6
1.2.1 The discovery of ryanodine receptors 7
1.2.2 The structural basis of RyR2 8
1.2.3 Pore dynamics and conductance of RyR2 8
1.2.4 Ligand regulation of RyR2 11
1.2.5 RyR2 and associated proteins 13
1.2.6 Post-translational modification of RyR2 15
1.2.7 Spatial organisation of RyR2 clusters 17
1.3 Catecholaminergic polymorphic ventricular tachycardia 18
1.3.1 Clinical manifestations 18
1.3.2 Mutations that cause CPVT 19
1.3.3 Pathophysiological mechanisms of CPVT1 in the heart . 20
1.3.4 Helical domain 1 mutations 22
1.3.5 Current treatments for CPVT 23
1.3.6 Animal models of CPVT1 24
1.4 Statins and ryanodine receptors 25
1.5 Research aims 26

1.1 Ca^{2+} signalling in the heart

Calcium ions (Ca^{2+}) are a ubiquitous secondary messenger that regulate many processes in cells (Clapham, 2007). Extracellular solutions have high concentrations of Ca^{2+} in the millimolar range. Cells expend a lot of energy in order to maintain a high electrochemical gradient of Ca^{2+} thereby creating a large signalling gradient required for a range of physiological processes (Clapham, 2007). One of these Ca^{2+} critical physiological processes is contraction (Szent-Györgyi, 1975). The importance of Ca^{2+} in the contraction of the heart was discovered by Sydney Ringer as early as 1883 (Ringer, 1883).

1.1.1 Cardiac excitation-contraction coupling

Ca^{2+} is the critical signalling component of excitation-contraction coupling (ECC) in cardiac tissue, the process in which electrical excitation translates to contraction within cardiomyocytes (Bers, 2002). Ca^{2+} is both the intracellular secondary messenger in electrical excitation and the ligand that binds to myofilaments to initiate the physical contraction (Fabiato, 1983; Pan and Solaro, 1987). ECC is a coordinated process that orchestrates the cyclic contraction and relaxation in every cardiomyocyte (Bers, 2001). This translates to cardiac systole where the heart contracts followed by cardiac diastole in which the heart relaxes. This results in a rhythmic heartbeat with the necessary pump action with which to propel blood around the body followed by relaxation to allow the heart to fill with blood again (Bers, 2001).

At the molecular level, excitation-contraction coupling (ECC) is controlled by the functional coupling of ion channels in both the surface sarcolemmal membranes and the intracellular sarcoplasmic reticulum (SR) membranes. The process of ECC and the critical ion channels involved are displayed in Fig. 1.1. Firstly, cardiac systole is triggered by the propagation of a depolarising cardiac action potential that arises in the sinoatrial node (SAN) and transmits across the atria and down

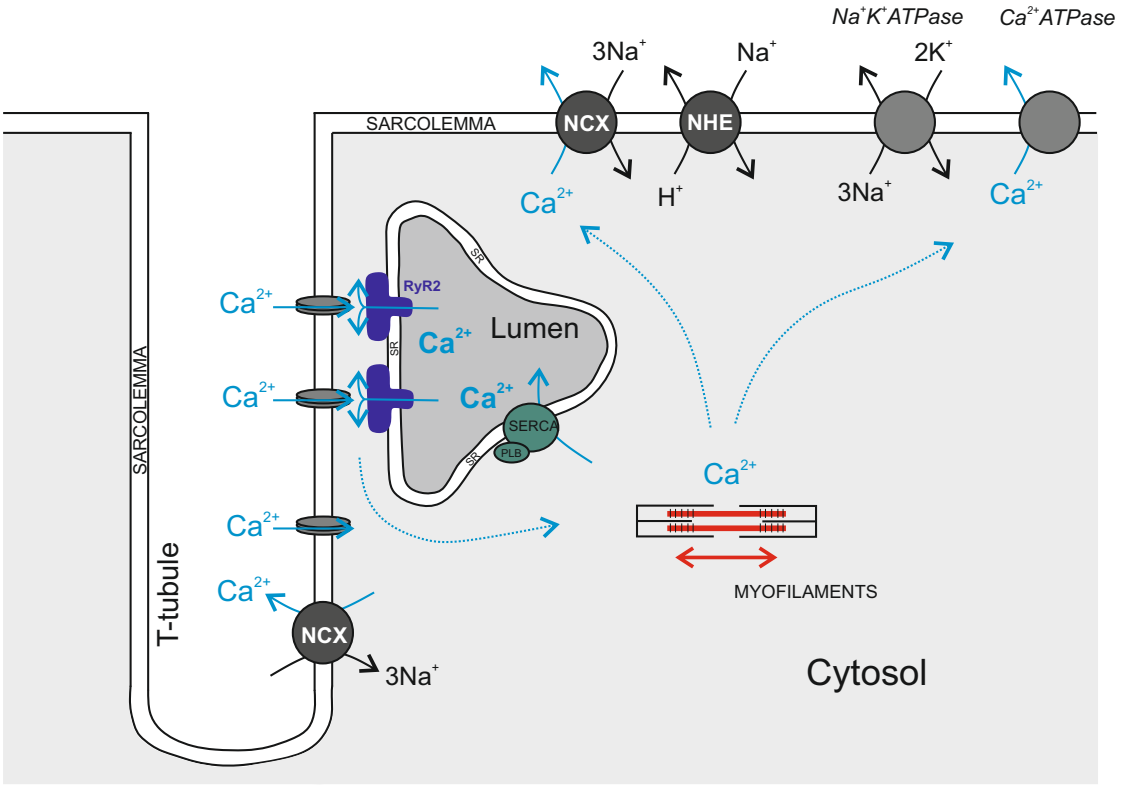


Figure 1.1: Schematic of excitation-contraction coupling, focusing on Ca^{2+} cycling in a ventricular cardiomyocyte Following the cardiac action potential, Ca^{2+} enters through L-type Ca^{2+} channels (LTCC) which in turn activate cardiac ryanodine receptors (RyR2) on the sarcoplasmic reticulum (SR) in a process called Ca^{2+}-induced-Ca^{2+}-release (CICR). The increased $[Ca^{2+}]$ binds to myofilaments causing contraction. Ca^{2+} is extruded via SR Ca^{2+} ATPase (SERCA) on the SR and via the Na^{+}/Ca^{2+} exchanger (NCX) and Ca^{2+} ATPase on the sarcolemma, thereby decreasing intracellular $[Ca^{2+}]$ for diastole. Na^{+}/H^{+} exchangers (NHE) are also expressed on the sarcolemma to modulate pH and intracellular $[Na^{+}]$. Adapted from (Bers, 2001).

to the ventricles (Rudy, 2008). This then depolarises the sarcolemmal membranes that initiates a small amount of Ca^{2+} entry via voltage-dependent L-type Ca^{2+} channels (LTCC) (Bean, 1985; Bers, 2001). The Ca^{2+} release through LTCC directly activates cardiac ryanodine receptors (RyR2) which are the main pathway of Ca^{2+} release from the SR (Fabiato, 1983; Smith et al., 1988). This mechanism is called Ca^{2+}-induced-Ca^{2+}-release (CICR) (Fabiato, 1983). The released Ca^{2+} causes an increase in the intracellular $[Ca^{2+}]$ which then binds to the myofilaments to induce contraction of the cardiomyocyte (Pan and Solaro, 1987).

Following CICR, Ca^{2+} is cycled out of the cytosol so that relaxation of the

cardiomyocytes can occur for cardiac diastole. The SR Ca^{2+} ATPase (SERCA) actively pumps Ca^{2+} back into the SR to replenish the luminal Ca^{2+} store (Bers and Bridge, 1989; Bassani et al., 1994). Ca^{2+} is also extruded across the sarcolemma, as the Na^{+}/Ca^{2+}-exchanger (NCX) passively exchanges 3 Na^{+} in for every extruded Ca^{2+} and the Ca^{2+}-ATPase actively pumps out Ca^{2+} (Bers and Bridge, 1989; Bassani et al., 1992; Bassani et al., 1994). The removal of Ca^{2+} therefore reduces the intracellular $[Ca^{2+}]$ and Ca^{2+} dissociates from the contractile proteins to allow relaxation and diastole (Pan and Solaro, 1987). During diastole in which the cytosolic $[Ca^{2+}]$ is approximately 100 nM, the activity of RyR2 and therefore the rate of spontaneous Ca^{2+} sparks is very low (Cheng and Lederer, 2008).

1.1.2 Ultrastructure of cardiac diads

The spatial organisation of sarcolemmal Ca^{2+} channels with RyR2 is critical for the mechanism of CICR (Stern, 1992). The sarcolemma is physically continuous with the transverse tubules (T-tubules) that penetrate the centre of cardiomyocytes (Fawcett and McNutt, 1969). In mammalian ventricles, it is largely the T-tubules that come into close proximity with the terminal cisternae of the SR (Page and Surdyk-Droske, 1979; Kawai et al., 1999). This forms a specialised structure called the cardiac diad (Franzini-Armstrong and Protasi, 1997). Within the diad is the functional couplon, in which RyR2 channels in the junctional SR are co-localised with cardiac LTCC in the adjacent sarcolemma (Sun et al., 1995; Carl et al., 1995).

Unlike for RyR1 in skeletal muscle, LTCCs are not physically associated with RyR2s, but instead are functionally coupled (Sham et al., 1995). There is approximately one LTCC for every 5-10 RyR2 channels (Sham et al., 1995; Protasi, 2002), and the co-localisation of these channels form Ca^{2+} release units or "couplons" (Franzini-Armstrong et al., 1999). In addition, a fraction of RyR2 channels exist that are not associated with LTCCs and these are suggested to have a secondary function to amplify Ca^{2+} release (Torres et al., 2014).

RyR2 channels are arranged in clusters of varying numbers of channels (Franzini-Armstrong et al., 1999). Ca^{2+} release from an RyR2 within a cluster will recruit neighbouring RyR2 channels within the same cluster to also open. This evokes a localised Ca^{2+} release event known as a Ca^{2+} spark (Cheng et al., 1993). The summation of discrete Ca^{2+} sparks across a cardiomyocyte equates to the global Ca^{2+} transient (Cheng and Lederer, 2008).

1.1.3 The β-adrenergic response in ECC

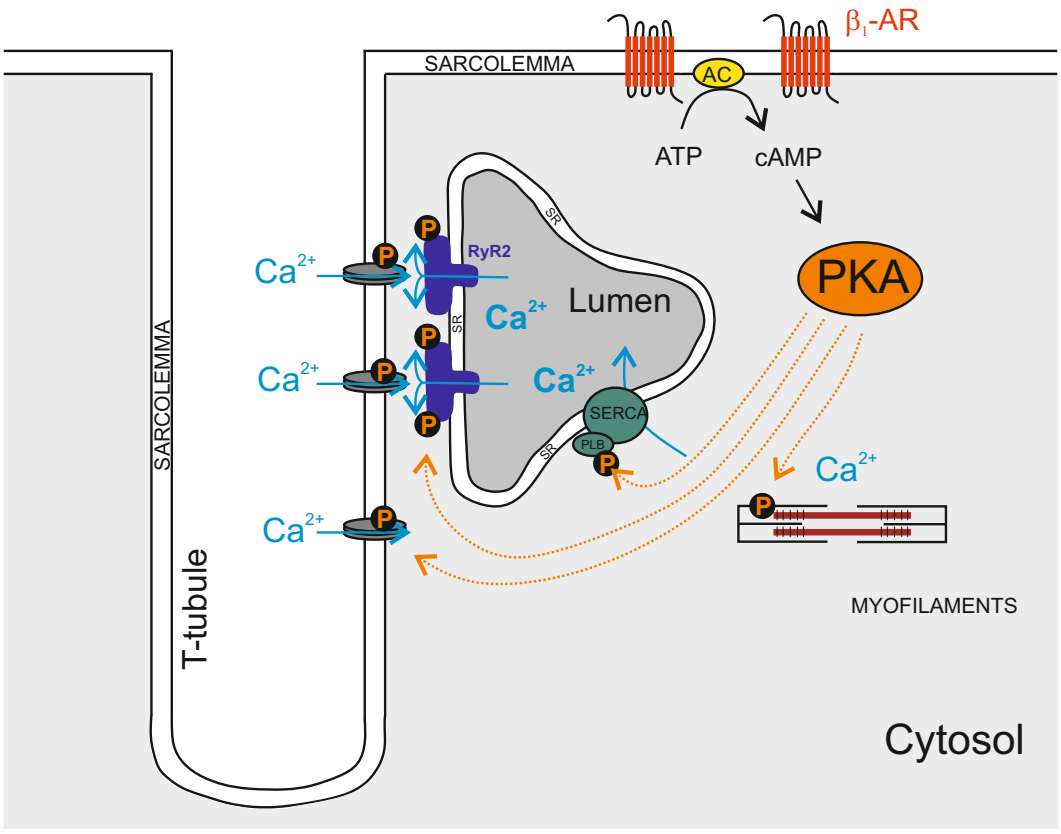


Figure 1.2: β-adrenergic stimulation on a ventricular cardiomyocyte and its implication on Ca^{2+} cycling via protein kinase A (PKA)-mediated phosphorylation β-adrenergic stimulation increases cyclic adenosine monophosphate (cAMP) levels and therefore activates PKA. PKA phosphorylates several key ECC proteins to upregulate Ca^{2+} cycling.

β-adrenergic stimulation upregulates Ca^{2+} cycling in the heart (Bers, 2002). This is an important physiological "fight or flight" mechanism to increase the capacity of the heart to circulate blood around the body. β_1-adrenergic receptors

reside on cardiomyocyte sarcolemmal membranes and are stimulated by circulating catecholamines and sympathetic innervation (Madamanchi, 2007). Binding of adrenaline or noradrenaline to the cardiac β_1-adrenergic receptor, which is a G-protein coupled receptor (GPCR), stimulates adenylate cyclase (AC) via the Gs alpha subunit to increase the intracellular concentration of cyclic adenosine monophosphate (cAMP) (Madamanchi, 2007). This in turn activates protein kinase A (PKA) which phosphorylates various targets: LTCCs are phosphorylated to increase inward Ca^{2+} current (Zhao et al., 1994); RyR2 channels are phosphorylated at multiple sites (Valdivia et al., 1995); phospholamban (PLB) phosphorylation increases Ca^{2+} loading back in the SR following contraction via SERCA (Sulakhe and Vo, 1995; Li et al., 2000); and phosphorylation of myofilament complexes increase the rate Ca^{2+} dissociation (Sulakhe and Vo, 1995; Kunst et al., 2000; Kentish et al., 2001). This is illustrated in Fig. 1.2. β_2-adrenergic receptors are also expressed in the heart, albeit at a lower level, and are thought to have a more localised effect as they solely phosphorylate LTCCs (Ye et al., 2000). The combination of the effect of the phosphorylation on these targets is increased capacity for Ca^{2+} cycling by increasing chronotropy (heart rate), inotropy (the force of contraction) and lusitropy (the rate of relaxation) (Bers, 2002).

1.2 Ryanodine receptors

Ryanodine receptors (RyR) are a family of homotetrameric Ca^{2+} release channels situated on intracellular sarcoplasmic reticulum and endoplasmic reticulum (SR/ER) (Takeshima et al., 1989; Franzini-Armstrong and Protasi, 1997). Their primary function is to regulate the release of Ca^{2+} from SR/ER stores to increase Ca^{2+} concentration in the cytosol. RyR are the largest ion channels in mammals with a tetrameric molecular mass of approximately 2 MDa (Takeshima et al., 1989). In mammals, ryanodine receptors exist in three isoforms. RyR type 1 (RyR1) is primarily the skeletal isoform (Takeshima et al., 1989). RyR type 2 (RyR2) is

the cardiac isoform but is also important in the brain (Otsu et al., 1990). RyR type 3 (RyR3) is expressed in relatively low levels in mature skeletal muscle (Perez et al., 2005), is expressed in the brain (Murayama and Ogawa, 1996) and has important roles in extraocular muscles (Sekulic-Jablanovic et al., 2015; Eckhardt et al., 2019). Since this thesis focuses on the pathophysiology of the cardiac isoform of the ryanodine receptor, (RyR2), this introduction will concentrate on mechanisms of RyR2-mediated Ca^{2+} release in cardiac tissue.

1.2.1 The discovery of ryanodine receptors

The mechanism of CICR was realised before the identification of the Ca^{2+}-release channel involved. Early studies by Fabiato (1985) revealed Ca^{2+}-dependent CICR from the SR of skinned cardiac Purkinje cells. Ryanodine, an alkaloid used as insecticide due to its paralytic action on skeletal muscle (Elison and Jenden, 1967), helped to pharmacologically identify the SR Ca^{2+} release channel. It was found that tritiated ([^{3}H]) ryanodine bound to the heavy fractions in an SR vesicle preparation. The heavy fractions correspond to the cardiac diad regions (Jones et al., 1979; Franzini-Armstrong and Protasi, 1997). This ryanodine binding complex was subsequently isolated and incorporated into a planar phospholipid bilayer (Pessah et al., 1985; Campbell et al., 1987; Smith et al., 1988; Lai et al., 1988a). This revealed that ryanodine bound to an SR Ca^{2+} permeable channel important in ECC. The ryanodine receptor was therefore named after ryanodine due to its unique action on the channel. Ryanodine locks RyR2 into a sub-conductance state as shown in Fig. 1.3 (Lai et al., 1988a). This distinct gating action on RyR2 explains the paralytic action observed in skeletal muscle and can be used for identity validation at the single-channel level. Following its discovery, a vast body of work has characterised the behaviour of RyR2. Since RyR2 is an intracellular ion channel, the only method to directly measure the electrophysiological behaviour of RyR2 and its gating kinetics is via artificial lipid bilayer electrophysiology.

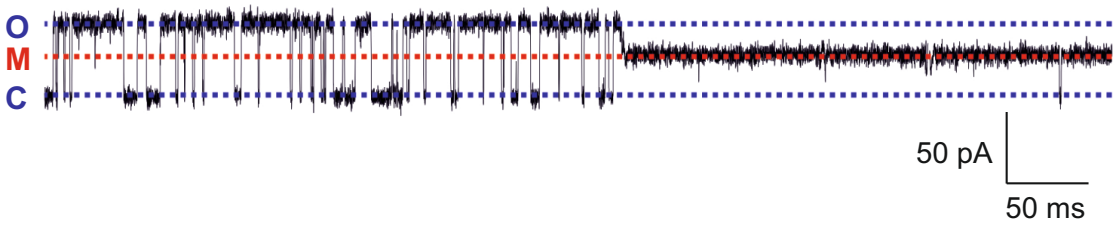


Figure 1.3: Ryanodine locks RyR2 into a sub conductance state Purified recombinant RyR2 recording following application of ryanodine. O, C and M indicate the open, closed and modified state, respectively.

1.2.2 The structural basis of RyR2

As shown in Fig. 1.4, RyR2 consists of a transmembrane pore domain and a large cytoplasmic region of over 4500 residues. The cytoplasmic domain serves as a surface for interactions with ligands and associated proteins. For example, between helical domains 1 and 2 exists a highly flexible P2 domain that is critical in the regulation of RyR2 via phosphorylation, encompassing the sites S2808 and S2814 (Peng et al., 2016).

RyR2 channels transition between open and closed states to regulate the passage of Ca^{2+} from the SR. Cryogenic electron microscopy (cryo-EM) studies indicate that the N-terminal domain, handle domain, and helical domain 1 move together to mediate the gating mechanism of RyR resulting in a coordinated "breathing" motion upon opening and closing (Bai et al., 2016; Wei et al., 2016; Peng et al., 2016; Samsó, 2017). The four repeating transmembrane segments below the cytoplasmic structure form the ion conducting pore. Upon channel opening, there is movement of the intracellular gate resulting in a dilation of the pore to allow the flux of cations (Peng et al., 2016).

1.2.3 Pore dynamics and conductance of RyR2

RyR2 contains a large water-filled pore which allows the passage of cations (Lindsay et al., 1991). RyR2 is poorly selective and permits both monovalent and divalent cation flux (Lindsay et al., 1991). The conductance through the pore of RyR2 for a particular permeant ion is based on the affinity of that ion with binding

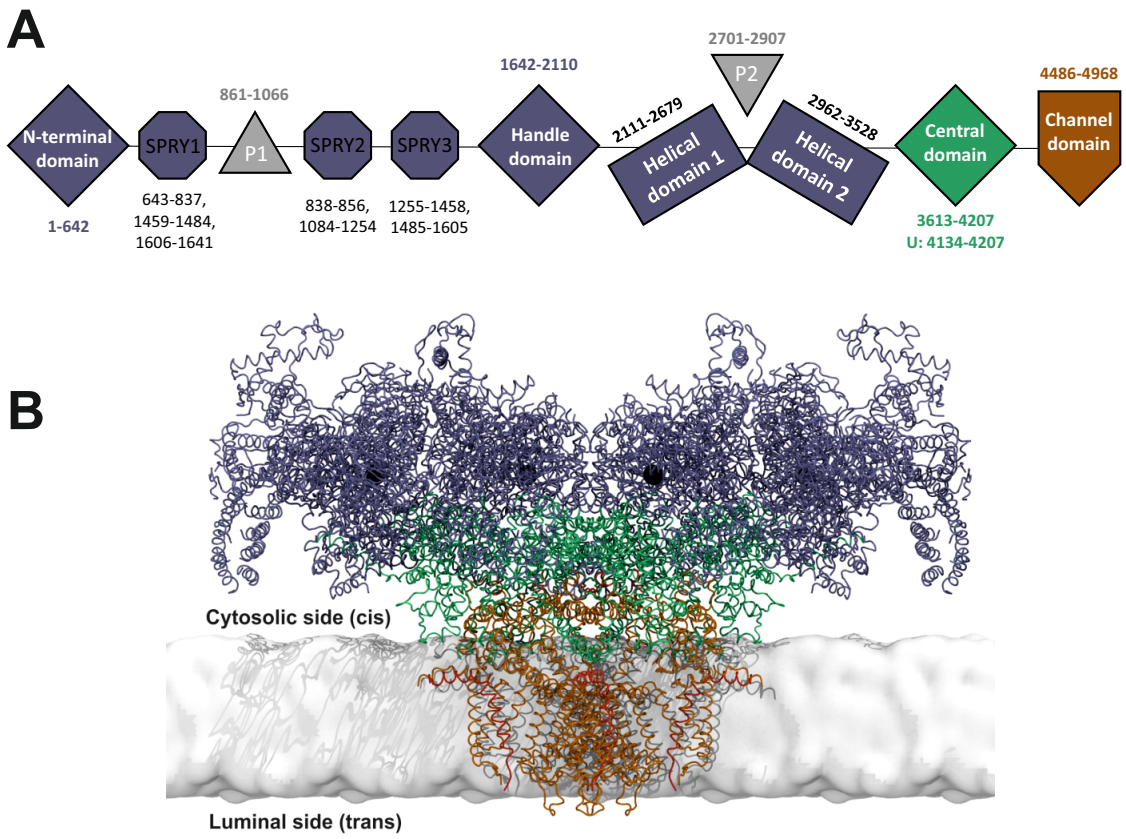


Figure 1.4: Structure of RyR2 (A) Domain organisation of an RyR2 protomer. The amino acid sequences are numbered below. P1 and P2 in grey indicate phosphorylation sites. Figure adapted from (Peng et al., 2016). **(B)** A single RyR2 channel incorporated into a lipid bilayer. The colours of each domain correspond to those of the domain organisation in (A). The four black beads indicates the site of the CPVT1-mutation, V2475F. Structural images were created in VMD. Figure adapted from (Lindsay et al., 2018).

sites within the conduction pathway. RyR2 favours the passage of divalent over monovalent ions since the central binding site during ion translocation has a higher affinity for divalent cations. RyR2 is approximately 6.5-fold more permeable to Ca^{2+} over K^{+} (Tinker and Williams, 1992). RyR2 has a saturable binding site, with single-ion occupancy, meaning ion translocations occur with one ion able to occupy the conduction pathway at a time (Lindsay et al., 1991). Native RyR2 channels derived from cardiac tissue are conventionally examined experimentally with high luminal $[Ca^{2+}]$ and with tris(hydroxymethyl)aminomethane ions ($Tris^{+}$) at the cytosolic face of the channel in order to examine Ca^{2+} flux and eliminate currents from native SR K^{+} or SR Cl^{-} channels in the single-channel recording (Ashley and

Williams, 1990). RyR2 is slightly permeable to $Tris^+$ (Lindsay et al., 1991).

Ca^{2+} selectivity is due to the electrostatic interactions of Ca^{2+} in the selectivity filter of RyR2. Ca^{2+} can coordinate with negative carboxyl groups of the aspartate (DDDD) locus within the selectivity filter which coordinates Ca^{2+} better than other permeant ions (Gillespie, 2008). The relatively small size of Ca^{2+} is preferential in the binding site as it occupies a relatively small space in the crowded selectivity filter of RyR2 (Gillespie et al., 2014). Taken together, the size/charge balance gives Ca^{2+} a significantly preferential permeability through the RyR2 pore compared to monovalent cations. Although RyR2 is poorly selective, the preference for divalent cations and high conductance means that physiologically, RyR2 is an effective Ca^{2+} release channel for conducting large Ca^{2+} flux over a relatively long time (>5 ms) (Tinker and Williams, 1992; Gillespie and Fill, 2008; Peng et al., 2016).

During ECC there is a large and rapid release of Ca^{2+} from the SR via RyR2. Despite the large and rapid efflux of positive ions from the SR, it has been observed that the membrane potential of the SR is maintained near 0 mV (Sanchez et al., 2018). Sanchez et al. (2018) quantified the SR membrane potential by using a voltage-sensing fluorescence resonance energy transfer (FRET) biosensor targeted to skeletal muscle SR and demonstrated no measurable change from 0 mV during muscle contraction (Sanchez et al., 2018). A counter-ion current is thereby required to compensate for this rapid loss of positive charge from the SR while maintaining the SR membrane potential at 0 mV. Without a counter-ion current, Ca^{2+} release would terminate in less than 1 ms as the reversal potential for Ca^{2+} would be rapidly reached (Gillespie and Fill, 2008; Zsolnay et al., 2018). During and between Ca^{2+} release events, other ions also move across the SR membrane (Berti et al., 2017) including K^+ and Cl^- via SR K^+ and Cl^- channels (Coronado et al., 1980; Rousseau et al., 1988) and via RyR2 itself which conducts Ca^{2+}, Mg^{2+} and K^+ (Tinker et al., 1993). The primary counter-ion current is believed to be meditated by the influx of K^+ into the SR, either via RyR2 providing its own counter-ion current (Gillespie and Fill, 2008) or by TRIC channels that are highly expressed

in the SR and permeable to monovalent cations (Fink and Veigel, 1996; Yazawa et al., 2007; Pitt et al., 2010; Venturi et al., 2013).

1.2.4 Ligand regulation of RyR2

The cytosolic face of RyR2 provides a vast surface area for the complex interactions involved in the regulation of RyR2. This includes several endogenous ligands and associated proteins. The luminal portion of RyR2 is much smaller but also critically involved in regulation of the channel. The critical ligands involved in regulation of RyR2 are described in this section.

1.2.4.1 Cytosolic divalent cations

Ca^{2+} is both a permeant ion and critical modulator of RyR2. As described previously, Ca^{2+} is the critical signalling component in CICR (Fabiato, 1983). RyR2s are activated by micromolar cytosolic [Ca^{2+}] and inhibited by millimolar cytosolic [Ca^{2+}] in a biphasic manner (Sitsapesan and Williams, 1994a; Laver et al., 1995). This implies that RyR2 has two cytosolic binding sites for Ca^{2+}, both a high affinity activation site and a low affinity inhibitory site (Chu et al., 1993; Meissner, 2017). RyR2 is activated by cytosolic Ca^{2+} with a steep Hill coefficient of between two to four due to the cooperative binding of Ca^{2+} in each of the four monomers (Sitsapesan and Williams, 1994a). RyR2 is inactivated by cytosolic Ca^{2+} with an IC_{50} of around 10 mM (Laver et al., 1995). Ca^{2+}-dependent increases in RyR2 probability of opening (Po), a measure of channel activity, are caused by an increase in frequency of opening (Ashley and Williams, 1990; Sitsapesan and Williams, 1994a) and increases in open lifetimes in high activity channels (Saftenku et al., 2001).

Mg^{2+} is an important inhibitory modulator of RyR2. Mg^{2+} inhibits RyR2 via competitive inhibition of Ca^{2+} at the activation site (Smith et al., 1986) but has a lower affinity than Ca^{2+} (Meissner et al., 1986). Mg^{2+} also binds to the Ca^{2+} inactivation site at millimolar levels, thereby both Ca^{2+} and Mg^{2+} can cause channel closure (Laver et al., 1997).

1.2.4.2 Luminal Ca^{2+}

It has been demonstrated that the amount of SR Ca^{2+} release is graded according to the level of Ca^{2+} in the SR (Fabiato and Fabiato, 1979). RyR2 are sensitive to luminal Ca^{2+} in order to regulate channel opening dependent on SR Ca^{2+} concentration (Sitsapesan and Williams, 1994b; Ching et al., 2000). The presence of luminal Ca^{2+} binding sites has been evidenced by tryptic digestion of the luminal side of RyR2 which results in abolishment of activation by luminal Ca^{2+} indicating that luminal activation is mediated by luminally situated sites and not governed by flow through to the cytosolic regions (Ching et al., 2000). Tryptic digestion also resulted in a decrease in RyR2 activity following an increase in luminal Ca^{2+}, revealing that a luminal inactivation site also exists, but with less effect on Po than the luminal activation site (Ching et al., 2000). It has been suggested that the E4872 residue located at the helix binding crossing region of RyR2 is part of the luminal Ca^{2+} activation binding site, since mutagenesis of this site to E4872A abolished the luminal Ca^{2+} sensitivity of recombinant purified mouse RyR2 channels (Chen et al., 2014). It has been established that optimum luminal Ca^{2+} activation requires the presence of cytosolic Ca^{2+} plus additional cytosolic activators; native RyR2 channels activated by only cytosolic Ca^{2+} presented no change in Po with increasing luminal [Ca^{2+}] (Sitsapesan and Williams, 1994b).

1.2.4.3 Adenosine derivatives

Adenosine triphosphate (ATP) is constitutively present at millimolar levels in cardiomyocytes (Chan et al., 2000). The importance of ATP bound to RyR2 is evidenced by the abolishment of CICR following reductions in intracellular ATP (Smith and O'Neill, 2001). ATP, adenosine and other ATP-metabolites can bind to the cytosolic face of RyR2 and act synergistically with Ca^{2+} to increase channel activity (Meissner, 1984; Kermode et al., 1998; Chan et al., 2000; Lindsay et al., 2018). For example, in the presence of an activating [Ca^{2+}], ATP can cause maximal activation of RyR2 via an increase in the frequency and duration

of openings (Kermode et al., 1998). However, at sub-activating [Ca^{2+}], ATP can also induce some long open durations although the overall RyR2 Po remains low (Kermode et al., 1998; Chan et al., 2000). Adenosine is also endogenously present and important in RyR2 regulation. Adenosine and ATP share the same binding site, but adenosine has a much lower efficacy since the triphosphate tail, or PPPi group, is essential for the full agonist properties of ATP, in particular for the induction of long openings (Lindsay et al., 2018). Unlike ATP, adenosine cannot phosphorylate RyR2 in the presence of endogenous kinases since the triphosphate moiety is not present (Fig. 1.5).

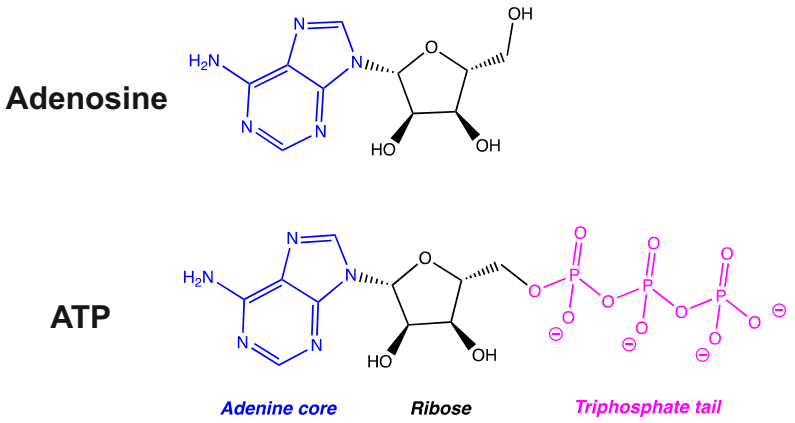


Figure 1.5: Adenosine derivatives refers to both adenosine and adenosine triphosphate (ATP) Adenosine has an adenine core attached to a ribose, and forms from the breakdown of ATP. ATP has an additional triphosphate tail (PPPi) attached to the ribose and is known as the "molecular currency of energy".

1.2.5 RyR2 and associated proteins

The large cytoplasmic domain of RyR2 provides a vast surface for complex regulation by a diverse range of ligands and associated proteins. The small luminal domain also interacts with ligands and intra-SR associated proteins. There are many closely associated proteins thought to be important in the function of RyR2 including calmodulin (CaM), cardiac calsequestrin (CASQ2), triadin, junctin and FK-506 binding proteins (FKBP12 and FKBP12.6) (Fill and Copello, 2002).

CaM functions as a sensor and mediator of signalling by Ca^{2+} for RyR2 (Potter et al., 1983; Ogawa and Tanokura, 1984). Both Ca^{2+}-free CaM (apoCaM) and Ca^{2+}-

bound CaM (CaCaM) can bind to RyR2, but with a higher affinity at nanomolar [Ca^{2+}] (Guo et al., 2011). The CaM binding domain on RyR2 resides between 3581-3610 and 4261-4286 (Balshaw et al., 2001; Huang et al., 2013). CaM is generally thought of as an inhibitor of RyR2 (Tripathy et al., 1995; Balshaw et al., 2001) however, physiological levels of CaCaM (50-100 nM) can increase RyR2 activity at the single-channel level but inhibits RyR2 at higher concentrations (Sigalas et al., 2009a; Sigalas et al., 2009b).

CASQ2 is closely associated with RyR2. CASQ2 is an intra-SR Ca^{2+} binding protein with the capacity to bind 20 to 80 Ca^{2+} ions with low affinity which functions therefore to buffer Ca^{2+} (Di Barletta et al., 2006). Triadin and junctin are membrane proteins that form complexes together with RyR2 and CASQ2 (Györke et al., 2004). The CASQ2/triadin/junctin complexes are thought to be important in the modulation of RyR2 from the luminal face as they have been determined experimentally to regulate the effects of luminal Ca^{2+} (Györke et al., 2004; Di Barletta et al., 2006; Chen et al., 2013).

Both FKBP12 and FKPB12.6 interact with RyR2 in the same binding site, but FKBP12 exists in cardiac cells at a higher concentration (Wagenknecht et al., 1996; Samsó et al., 2006; des Georges et al., 2016). At the single-channel level, it has been established that FKBP12 activates RyR2 with high affinity, and while FKBP12.6 also has high affinity, it has no measurable efficacy thereby antagonising the effects of FKBP12 by competitively binding in the same site (Galfré et al., 2012). The association between FKBPs and phosphorylation at RyR2 are controversial, with some authors reporting that hyperphosphorylation of RyR2 by PKA dissociates FKBP12.6 (Marx et al., 2000), with other authors reporting that this is not the case (Xiao et al., 2004). It was also reported that removal of FKBPs can cause sub-conductance state gating in RyR2 (Ahern et al., 1997; Marx et al., 2000), but again this has not been consistently reported (Xiao et al., 2007; Galfré et al., 2012).

RyR2 channels can form macromolecular complexes in which many regulatory proteins involved in altering the phosphorylation status of RyR2 are co-localised

(Marx et al., 2000; Carter et al., 2006; Huke and Bers, 2008; Camors and Valdivia, 2014; Dobrev and Wehrens, 2014). Regulation of the phosphorylation levels of various sites of RyR2 by these associated kinases can adapt the function of RyR2, as described in the following section.

1.2.6 Post-translational modification of RyR2

Post-translational modifications of RyR2 are important in the physiological regulation of RyR2 and provides adaptive regulation of the channel (Niggli et al., 2013; Denniss et al., 2018). RyR2 contains several serine, threonine and tyrosine residues that are predicted to be phosphorylation sites (Denniss et al., 2018), hence the regulation of RyR2 by phosphorylation is highly complex. Protein kinase A (PKA) and calmodulin-dependent protein kinase II (CaMKII) are protein kinases that are both closely associated with and implicated in modulating RyR2 activity (Marx et al., 2000; Carter et al., 2006; Huke and Bers, 2008; Camors and Valdivia, 2014). PKA is activated via the β-adrenergic cascade, and CaMKII is activated by auto-phosphorylation and a Ca^{2+}-dependent mechanism (Camors and Valdivia, 2014). RyR2 has many potential phosphorylation sites, but the sites that have been most extensively studied due to the availability of antibodies for these sites are S2030, S2808 and S2814. S2808 is a target for phosphorylation by both PKA and CaMKII (Rodriguez et al., 2003). S2030 has low basal phosphorylation, is targeted solely by PKA, and has been suggested to be important in the β-adrenergic response (Xiao et al., 2006; Huke and Bers, 2008; Potenza et al., 2019). S2814 is known as a CaMKII site (Wehrens et al., 2004). However, it is unlikely that each site is functionally independent. For example, S2808 and S2814 are situated close together on the P2 phosphorylation loop and examination of crystal structures have suggested that this highly flexible region can encircle PKA whereby phosphorylation at S2814 then increases the activity of PKA for phosphorylation at S2808 (Haji-Ghassemi et al., 2019).

Phosphorylation of RyR2 is also implicated in pathophysiological mechanisms of cardiac disease (Niggli et al., 2013; Denniss et al., 2018), but the critical phosphorylation sites that are involved is contested (Dobrev and Wehrens, 2014). For example, it has been suggested that the site S2808 is hyperphosphorylated in heart failure (Marx et al., 2000; Walweel et al., 2017), and a mouse model with genetic hyperphosphorylation of the S2808 site by S2808D mutagenesis exacerbated the progression of heart failure (Shan et al., 2010). In contradiction, work by a different group has shown genetic removal of the S2808 site by S2808A mutagenesis was not protective against the generation of heart failure (Benkusky et al., 2007). CaMKII phosphorylation at site S2814 is suggested to be important in heart failure since the genetic removal of the S2814 site by S2814A mutagenesis ameliorated the progression of non-ischemic heart failure (Respress et al., 2012). Furthermore, phosphorylation of RyR2 has been implicated in arrhythmic cardiac diseases, discussed further in Section 1.3.3.

The correlation between the phosphorylation status of various serine residues of RyR2 with the functional response of RyR2 is highly complex. For example, sheep RyR2 was found to have a biphasic activity in response to PKA phosphorylation at site S2808 (Carter et al., 2006). At this site, basal phosphorylation was found to be 75% of the maximum possible phosphorylation, with low channel activity. Hyperphosphorylation to maximal phosphorylation caused an increase in Po and single-channel conductance, however, dephosphorylation to near 0% phosphorylation levels also increased channel Po (Carter et al., 2006). Interestingly, the increase in channel activity due to hyperphosphorylation was not due to an increased sensitivity to Ca^{2+}, but instead due to an uncoupling from Ca^{2+} regulation, in which hyperphosphorylated channels gated with a high Po in the absence of activating levels of cytosolic [Ca^{2+}] (Carter et al., 2011).

In summary, further research into the association between post-translational modifications of RyR2 and RyR2 function in physiological and pathophysiological conditions are required to fully understand these complex mechanisms.

1.2.7 Spatial organisation of RyR2 clusters

The interaction of an RyR2 channel with its neighbouring RyR2 channels is important in their function. RyR2s assemble into clusters with variable numbers of channels within each cluster (Franzini-Armstrong et al., 1999). Most commonly, clusters exist with approximately 100 RyR2 channels (Franzini-Armstrong et al., 1999). but smaller clusters of 8 to 10 channels are also capable of producing Ca^{2+} release events (Galice et al., 2018). The way in which the clusters are configured and the number of channels in the cluster is highly dynamic and changes in response to different $[Ca^{2+}]$, $[Mg^{2+}]$ and phosphorylation levels in order to modulate Ca^{2+} release (Asghari et al., 2014, 2020). For example, in simulations, Galice et al. (2018) found a positive relationship between Ca^{2+} spark frequency and the number of RyRs within a cluster and this relationship became steeper upon increased sensitivity of the RyR2 channels with the cluster.

Clusters of RyR2 channels can exist in various different configurations which can be altered in response to their environment; this therefore suggests that the cluster configuration is important for function (Cabra et al., 2016). For example, in the configuration types of "centre-to-side" or "corner-to-corner", individual RyR2 channels are closely associated but without any physical overlap (Cabra et al., 2016). In "adjoining" or "oblique" configurations, RyR2s appear to be physically coupled with a fixed orientation in respect to each other (Cabra et al., 2016). In adjoining configurations there is an interaction between the two P1 domains of both RyR2s, while the helical domain 2 of each RyR2 contacts the neighbouring SPRY1 domain of the facing RyR2 (Fig. 1.4) (Cabra et al., 2016). In oblique configurations, RyR2s interact along their sides in which the P1 and SPRY1 domains are intertwined (Cabra et al., 2016). Both the helical domains and SPRY1 domains have known protein-protein interaction modules called armadillo-repeats that may explain this ability to physically couple (Tewari et al., 2010). The proportion of RyR2 clusters that are physically coupled and thereby in adjoining or oblique configurations increases in response to an increase in cytosolic $[Ca^{2+}]$, suggesting

that changes to the configurations of RyR2 clusters has important functional implications in ECC (Cabra et al., 2016).

1.3 Catecholaminergic polymorphic ventricular tachycardia

Catecholaminergic polymorphic ventricular tachycardia (CPVT) is a highly malignant genetic disease that causes life-threatening arrhythmias which can lead to sudden cardiac death (SCD) (Priori et al., 2002). CPVT is caused by mutations to proteins that are critical in the regulation of cardiac Ca^{2+} release in ECC (Priori et al., 2002). CPVT is most commonly caused by mutations to RyR2 which is defined as CPVT type 1 (CPVT1).

1.3.1 Clinical manifestations

CPVT is characterised in the clinic by episodes of syncope occurring during physiological stress of exercise or acute emotion (Priori et al., 2002). Patients with CPVT do not normally have any structural cardiac abnormalities, and the heart appears normal on the electrocardiogram (ECG) at rest. However, during an episode, patients present with fast ventricular tachycardia (VT) which is bidirectional or polymorphic on an ECG. These incidences of VT are the cause of syncope (Napolitano et al., 2016). The VT can recover spontaneously, but in serious cases may degenerate into ventricular fibrillation (VF) and SCD. CPVT tends to manifest in children, with the mean age of syncopal symptoms at 7 to 12 years old, although onset in patients of 40 years old has also been reported (Priori et al., 2002; Postma et al., 2005). Without treatment the prognosis is severe; around 30% of patients experience cardiac arrest and up to 80% of patients experience syncopal episodes (Napolitano et al., 2016).

The incidence of CPVT is low at 1:10,000 (Napolitano et al., 2016). However, this may be an underestimation of the real incidence due to missed cases or misdiagnosis.

For example, there are reports of CPVT being misdiagnosed as epilepsy in which patients present with convulsive syncope and are then found to be nonresponsive to anti-epileptic medications (Hazle et al., 2013). Further, a study of incidences of unexplained drownings found that around 20% of patients had CPVT1 which suggests a significant number of CPVT1 mutations may be overlooked (Choi et al., 2004). Furthermore, recent studies have revealed reduced penetrance in some CPVT1 mutations suggesting that the severity of the disease may be variable between patients, and that this variability may be associated with the location of the mutation in RyR2 (Liu et al., 2017).

1.3.2 Mutations that cause CPVT

Around 50% of CPVT patients are found to have mutations to RyR2. Mutations at RyR2 that cause CPVT1 have been associated with at least 160 different residues (Priori and Chen, 2011). Approximately 50% of patients obtain the mutation via familial inheritance in which these mutations are inherited in an autosomal dominant manner. This means that the patients are heterozygous for the mutation at RyR2. Other patients have a *de novo* pathogenic variant meaning the mutation has arisen from the germ cell or the fertilised egg thereby occuring for the first time in a family. The proportion of *de novo* mutations is presumably so high since RyR2-related CPVT1 patients historically did not reach reproductive age (Napolitano et al., 2016). Although the cause of CPVT in most patients is due to mutations to RyR2, mutations in genes encoding for other proteins are also possible. These include calmodulin (CALM1), calsequestrin (CASQ2) and triadin (TRDN) which each account for around 2% of CPVT patients (Napolitano et al., 2016). The remaining 40% of CPVT patients have unknown causes (Napolitano et al., 2016). This thesis investigates a mutation to RyR2 that causes CPVT1.

1.3.3 Pathophysiological mechanisms of CPVT1 in the heart

As described so far, RyR2 is the primary Ca^{2+} release channel in the SR. Since RyR2 has such a critical role in the mechanism of CICR and the generation of Ca^{2+} sparks, mutations that alter the function of RyR2 impact on Ca^{2+} handling in the heart. RyR2 mutations tend to cause diastolic Ca^{2+} release which is most commonly caused by a dysfunction to RyR2 behaviour that causes channel 'hyperactivity' (Liu et al., 2006; Uehara et al., 2017). Mutations that cause hyperactive RyR2 increase the propensity for RyR2 opening and thereby increase the likelihood of Ca^{2+} release during diastole, independent of the normal depolarising trigger (George et al., 2003; Jiang et al., 2004). This spontaneous Ca^{2+} release can lead to a type of arrhythmogenesis called delayed-after-depolarisations (DADs) (Marban et al., 1986; Cheng et al., 1996; Liu et al., 2006; Loaiza et al., 2013). The canonical pathway for DADs is illustrated in Fig. 1.6. Inappropriate RyR2 openings during diastole leads to an increase in cytosolic Ca^{2+} (Györke, 2009). This increase in intracellular $[Ca^{2+}]$ triggers extrusion of Ca^{2+} via the electrogenic NCX, as it extrudes one Ca^{2+} in return for three Na^{+}. This leads to depolarisation caused by transient inward current (I_{ti}) which, if significant enough, can reach the voltage threshold for Na^{+} channel activation and cause a triggered action potential (Mohamed et al., 2007). Propagation of an action potential across the entire heart causes extra-systolic beats and life-threatening arrhythmias (Scoote and Williams, 2002; Liu et al., 2006; Venetucci et al., 2012). In CPVT1, this can lead to VT and/or VF (Mohamed et al., 2007). This may ultimately lead to SCD without intervention (Napolitano et al., 2016).

It is widely accepted that CPVT1 mutations effect RyR2 in such a way that the propensity of spontaneous Ca^{2+} release events is increased. However, the mechanism for how this occurs is under debate. Some RyR2 mutations appear to modify RyR2 channels whereby their sensitivity to luminal Ca^{2+} is increased (Jiang et al., 2004). Some groups have suggested that this may result in a lowering of

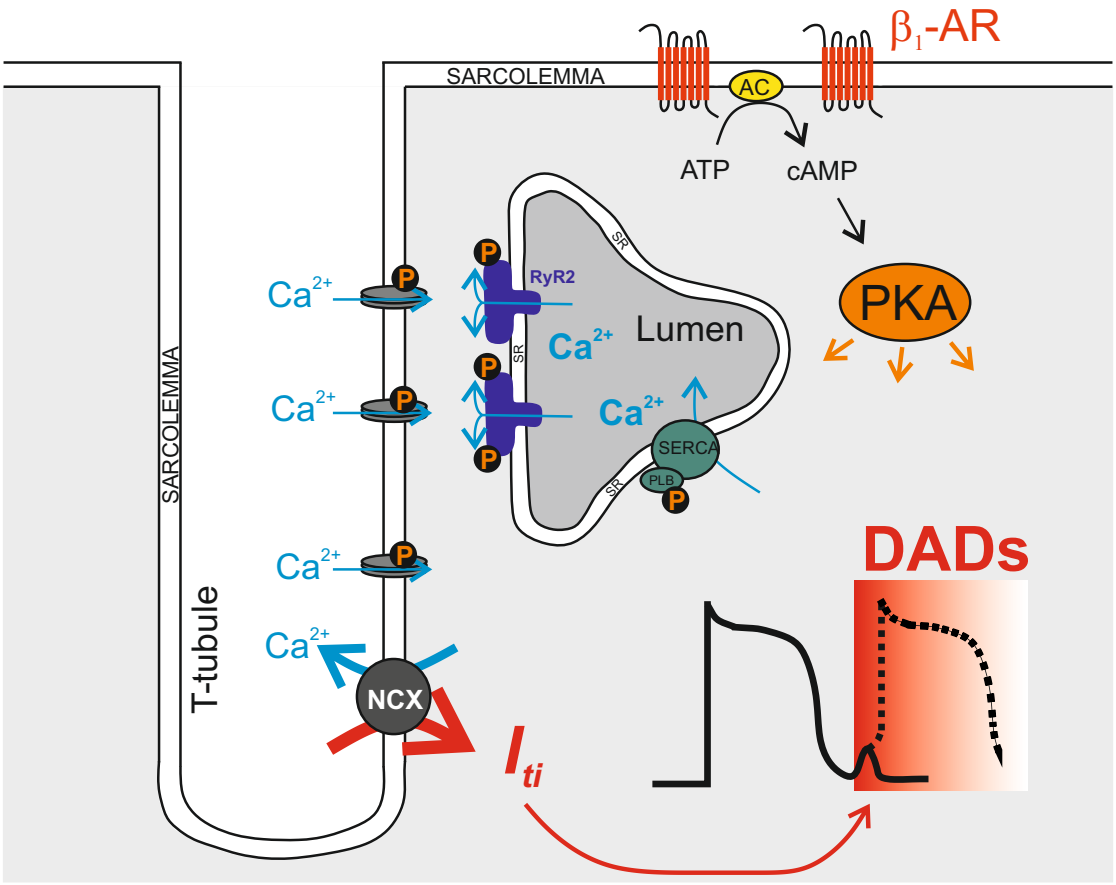


Figure 1.6: Schematic of generation of DADs in a cardiomyocyte with a CPVT1-mutation at RyR2 β-adrenergic stimulation induces phosphorylation of key proteins in ECC, including RyR2. Spontaneous Ca^{2+} release from RyR2 during diastole triggers an inward transient current (I_{ti}) which leads to DADs and triggered cardiac arrhythmias.

the SR Ca^{2+} threshold required for RyR2 opening, thereby causing inappropriate Ca^{2+} release events (Jiang et al., 2004, 2005). However, this cannot account for all CPVT1 RyR2 mutations, as not all of them exhibit increased luminal Ca^{2+} sensitivity (Meli et al., 2011). It has also been proposed that RyR2 mutations that cause CPVT1 disrupt the structural conformation of RyR2 in which there is a decreased stability for the closed state. This is known as "domain unzipping", in which it is proposed that the intradomain interactions that hold the channel closed are disrupted by the mutation, thereby leading to an RyR2 channel that is opened more readily in response to cytosolic Ca^{2+}, thus allowing spontaneous Ca^{2+} release (Yamamoto et al., 2008; Uchinoumi et al., 2010). Overall, there is general disagreement concerning the molecular mechanisms that cause RyR2 dysfunction

in CPVT1 highlighting that further investigation is essential.

It is important to note that in CPVT1, adverse cardiac events seem to occur under physiological stress with increased levels of circulating catecholamines thereby following activation of the β-adrenergic cascade (Priori et al., 2002). As described previously, β-adrenergic stimulation will phosphorylate key ECC proteins which will alter the Ca^{2+} handling in a cardiomyocyte (Fig. 1.2). Even under extreme β-adrenergic stimulation in healthy cardiomyocytes it is possible to observe DADs (Priori and Corr, 1990). It is generally believed that β-adrenergic stimulation may result in the CPVT1-mutated RyR2 behaving differently to normal RyR2. For example, it has been proposed that the response to β-adrenergic stimulation may exacerbate the effect of a mutation at RyR2 due to the increased SR Ca^{2+} load resulting from SERCA upregulation (Jiang et al., 2004; Ginsburg and Bers, 2004; Kashimura et al., 2010), or alternatively, may be related to the degree of RyR2 channel phosphorylation by PKA and CaMKII thereby causing an increased RyR2 sensitivity (Fernández-Velasco et al., 2009; Venetucci et al., 2012). Although there is conflicting evidence for the specific mechanisms involved, most proposed mechanisms suggest there is a resultant aberrant increase in spontaneous Ca^{2+} release events during diastole thereby producing DADs (Mohamed et al., 2007).

1.3.4 Helical domain 1 mutations

As described in section 1.2.2, the helical domain 1 (HD1) is a highly flexible cytoplasmic domain of RyR2 that interacts with associated proteins and is important for intradomain interactions (Peng et al., 2016). The HD1 is associated with mutations that cause CPVT1, including V2475F, R2474S and P2328S, amongst others (Lehnart et al., 2008; Loaiza et al., 2013; Salvage et al., 2019). The V2475F mutation causing CPVT1 was first identified by genetic screening of a young boy following a case of unexplained drowning (Tester et al., 2005). The V2475F mutation causes an amino acid mutation of valine to phenylalanine in which the isopropyl moiety is substituted with a benzyl group while preserving the hydrophobicity of

the side chain. The site of this mutation on the RyR2 structure is marked by black beads in Fig. 1.4. This region appears to be susceptible to dysfunction caused by single point mutations since a mutation at the neighbouring residue, R2474S, was also found to cause CPVT1 (Lehnart et al., 2008).

1.3.5 Current treatments for CPVT

Currently, the therapeutic interventions for patients with CPVT1 are limited. Beta-blockers are commonly prescribed to inhibit the β-adrenergic response associated with triggering episodes of VT (Priori et al., 2002). Flecainide, a sodium channel blocker, has been shown to improve arrhythmia control in CPVT patients (Watanabe et al., 2009). Some groups have implied that flecainide has a direct action on RyR2 (Watanabe et al., 2009), however this is contested since in single-channel experiments flecainide does not block RyR2 when current is in a physiological luminal-to-cytosolic direction (Bannister et al., 2015). A third of patients have an implantable cardioverter defibrillator (ICD) fitted, yet ICD implantation holds significant morbidity risk and is used in conjunction with pharmacological interventions to avoid the necessity of firing (Miyake et al., 2013).

A study by Bongianino et al. (2017) used RNA interference to induce allele specific silencing of the mutated monomers in the heterozygous R4496C CPVT1 mutant mouse model. It was reported that a 1:1 to 2:1 ratio increase of WT to mutant RyR2 mRNA reduced the incidence of DADs in cardiomyocytes isolated from this mutant mouse and decreased the occurrence of VT in the mice, indicating that even a shift in the number of mutated monomers can normalise the CPVT1-phenotype (Bongianino et al., 2017). However, gene therapy in general has safety advances to make before its potential can be used in the clinic.

The inhibition of RyR2 single-channel activity is a potential therapeutic target for CPVT1 (Hwang et al., 2011). Currently, there are no clinically-used drugs proven to bind directly with RyR2, but several groups are undertaking high throughput screening of RyR2 inhibitors to identify possible drug candidates (Rebbeck et

al., 2017; Murayama et al., 2018). Studies in an induced pluripotent stem cell (iPSC) model of CPVT1 have identified that dantrolene, used to treat malignant hyperthermia by inhibiting RyR1, was found to rescue DADs, possibly via RyR2 inhibition (Jung et al., 2012). However, the inhibitory mechanism of dantrolene on RyR2 remains controversial as it is not observed at the single-channel level and therefore its effect may be mediated through an RyR2-associated protein or even via a different ion channel (Oo et al., 2015; Diszházi et al., 2019). On this account, the use of an RyR2 inhibitor as a means for a therapeutic intervention for CPVT1 requires further investigation.

1.3.6 Animal models of CPVT1

Mouse models have provided valuable tools to study the human disease of CPVT1 (Liu et al., 2006; Loaiza et al., 2013). The mouse species is genetically tractable and therefore provides a useful experimental tool to study single point mutations. RyR2 mutations that cause CPVT1 are heterozygous for the disease in humans (Priori et al., 2001), and since RyR2 channels are homo-tetrameric, this means that the RyR2 channels in a patient with CPVT1 will contain a mixture of RyR2 channels with different numbers of mutated monomers per tetramer (Loaiza et al., 2013). It can therefore be argued that it is more physiological to study heterozygous RyR2 channels and some mouse models, including the V2475F mutation, exhibit homozygous lethality thereby demonstrating that homozygous expression of some RyR2 mutations is fatal (Lehnart et al., 2008; Loaiza et al., 2013; Zhao et al., 2015).

RyR2 is a highly conserved protein with >90% sequence alignment across different mammalian species. Table 1.1 shows the identity alignment of RyR2 calculated across important experimental mammalian species compared to human (The UniProt Consortium, 2017). For example, the mouse and human have a 97% sequence identity alignment, suggesting the mouse model will produce RyR2 single channel proteins that are highly similar to human and other mammalian species.

Table 1.1: Identity alignment of RyR2 Percentage of aligned amino acids calculated on BLAST sequence alignment (The UniProt Consortium, 2017): mouse (E9Q401); rat (B0LPN4); sheep (W5P0Y1); human (Q92736); and pig (A0A5G2R1W3_PIG)

	Mouse	**Rat**	**Sheep**	**Human**	**Pig**
Mouse	≡	98.6	91.7	97.4	96.6
Rat		≡	91.9	97.0	96.2
Sheep			≡	93.1	93.3
Human				≡	98.1
Pig					≡

1.4 Statins and ryanodine receptors

Statins are a class of competitive inhibitors of 3-hydroxy-3-methylglutaryl-CoA (HMG-CoA) reductase, a critical enzyme in the synthesis of cholesterol (Dansette et al., 2000). They are commonly prescribed due to their plasma lipid lowering effect and are highly effective in treating hypercholesteremia (Shepherd et al., 1995). Clinical trials suggest that statin treatment reduces the incidence of coronary heart disease and strokes (Sirtori, 2014). Last year alone, the synthetic statin analogue, atorvastatin, was reported to be the most-prescribed drug in England with 45.8 million items dispensed (Connor, 2019). The chemical structure of atorvastatin is illustrated in Fig. 1.7.

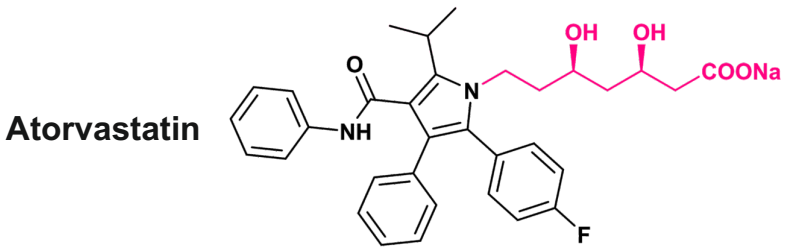


Figure 1.7: The chemical structure of atorvastatin, a synthetic statin analogue

Many large clinical trials have provided evidence that patients with cardiovascular disease will benefit from statin treatment (Collins et al., 2016), however statins do have pleiotropic effects, both positive and negative (Armitage, 2007; Schirris et al., 2015). Negative pleiotropic effects of statins include muscle pain, weakness and in

extreme cases can cause rhabdomyolysis which is not correlated to the potency at HMG-CoA reductase (Armitage, 2007). In particular, cerivastatin was withdrawn from the market due to incidences of fatal rhabdomyolysis (Charatan, 2001).

Statins also exhibit positive pleiotropic cardiovascular effects. In patients with severe cardiovascular disease, it was found that patients on statin treatment experienced lower incidences of ventricular arrhythmia compared to those without (De Sutter et al., 2000). Statins are also associated with a decrease in instances of atrial fibrillation (AF) in patients (Siu et al., 2003; Amar et al., 2005; Fauchier et al., 2008), and in animal models statin treatment has shown a reduction in VF (Liu et al., 2009) and faster termination of re-entrant tachycardia (Khori et al., 2015). These reported reductions in arrhythmias were not entirely dependent on the effect of lowering cholesterol levels suggesting an off-target effect that was not mediated by the interaction with HMG-CoA reductase (De Sutter et al., 2000; Khori et al., 2015). This clinical and experimental evidence of the electrophysiological stabilisation of the heart by statin therapy requires further investigation.

Our laboratory has studied the effect of statins on RyR1 and RyR2 function to investigate if an RyR-mediated action of statins could contribute to the poly-pharmacological effects associated with statin treatment. It was demonstrated that, at the bimolecular level, simvastatin concentrations greater than 1 μM can activate RyR1, in both the hydroxy acid and lactone forms (Venturi et al., 2018). We also demonstrated that 1 μM simvastatin inhibits RyR2 at the single-channel level, as well as decreasing the frequency of Ca^{2+} sparks in permeabilised cardiomyocytes (Venturi et al., 2018; Wilson et al., 2018).

1.5 Research aims

CPVT1 is a devastating disease caused by mutations to RyR2 yet the fundamental changes to RyR2 channel gating in response to a range of critical ligands and/or conductance caused by each specific mutation are not routinely examined. The work

in Chapter 3 therefore aims to give a detailed and comprehensive characterisation of the effects that the V2475F mutation has on RyR2 single-channel function, in order to better understand the pathophysiological effects at the molecular level that ultimately led to sudden cardiac death in a patient with the V2475F mutation. As part of this aim, investigation into the contribution of RyR2 function that occurs in a heterozygous population of V2475F mutated RyR2 channels was investigated, as would be the case in CPVT1 patients with an RyR2 mutation.

As described in the introduction, the contribution of β-adrenergic stimulation is important in the manifestation of cardiac events in CPVT1. Chapter 4 therefore aims to investigate the complex contribution of RyR2 phosphorylation levels on WT and CPVT1-mutated RyR2 channel function. This will be conducted by quantifying phosphorylation levels at S2808 in WT and V2475F(+/-)-mutated channels, as well as examining the effects of PKA and PP1 treatment on the behaviour of WT and V2475F(+/-)-mutated RyR2 channels at the single-channel level.

CPVT1 patients currently have a poor prognosis and few prospects for treatment. Current therapeutic interventions involve treating the morbidity risks associated with the disease, rather than acting at the level of the dysfunctional RyR2. Could modulation at RyR2 provide a therapeutic target for CPVT1? This question is explored in chapter 5 by utilising atorvastatin that has been shown to reduce RyR2 activity (Venturi et al., 2018; Wilson et al., 2018).

The specific aims of this thesis are summarised here:

Chapter 3

- To study the effect of the V2475F mutation on native RyR2 single-channel conductance
- To characterise the effect of the V2475F mutation on native RyR2 single-channel activity in response to key regulatory ligands
- To understand the influence of the heterozygosity of the V2475F-mutated RyR2 channels derived from cardiac tissue

Chapter 4

- To examine the contribution of phosphorylation on CPVT1-mutated RyR2 activity
- To evaluate the effect of the V2475F mutation on RyR2 activity at the cardiomyocyte level under β-adrenergic conditions

Chapter 5

- To investigate the mechanism of action of atorvastatin modulation of RyR2
- To assess whether low dose statins could be repurposed as inhibitors of RyR2 in CPVT1

2

Methodology

Contents

2.1 Mouse model of CPVT 30
2.1.1 Mouse model and ethical approval 30
2.1.2 Genotyping of the mouse model 31
2.2 Isolation of SR vesicles 32
2.2.1 Collection of cardiac tissue 32
2.2.2 Isolation of mixed membrane vesicles from mouse cardiac tissue 33
2.2.3 Isolation of heavy SR vesicles from sheep cardiac tissue 34
2.2.4 Purification of heavy SR vesicles from sheep cardiac tissue 35
2.3 Planar lipid bilayer technique 36
2.3.1 Planar lipid bilayer apparatus 36
2.3.2 Voltage-clamp configuration 38
2.3.3 Formation of planar lipid bilayers 39
2.3.4 Bilayer detection and estimate of the area 40
2.3.5 Incorporations of native RyR2 channels for recordings with Ca^{2+} as the permeant ion 41
2.3.6 Incorporations of native RyR2 channels for recordings with K^+ as the permeant ion 41
2.3.7 Incorporations of purified RyR2 channels for recordings with K^+ as the permeant ion 42
2.3.8 Recording conditions 43
2.4 Single-channel analysis 44
2.4.1 Data acquisition and filtering 44
2.4.2 Analysis of single-channel gating 45
2.4.3 Sub-conductance states 47
2.4.4 Single-channel lifetime distributions 47
2.4.5 Burst analysis 48

2.4.6 Population analysis 49
2.4.7 Single-channel conductance measurements 50
2.4.8 Liquid junction potentials 51
2.5 Phosphorylation studies 51
2.5.1 Bilayer treatments 51
2.5.2 Western blots for RyR2 53
2.6 Cardiomyocyte experiments 55
2.6.1 Isolation of cardiomyocytes 55
2.6.2 Ca^{2+} imaging set-up 57
2.6.3 Cardiomyocyte recording protocol 59
2.6.4 Analysis of spontaneous Ca^{2+} release from cardiomyocytes 60
2.7 Chemicals and solutions 60
2.7.1 Measurement of free Ca^{2+} 60
2.7.2 Measurement of protein concentration 61
2.8 Statistics 61
2.8.1 Statistical tests 61
2.8.2 Models for linear and non-linear regression 63
2.8.3 Animal numbers 64
2.8.4 Randomisation and operator blinding 65

2.1 Mouse model of CPVT

2.1.1 Mouse model and ethical approval

The V2475F heterozygous (+/-) mouse model was kindly given to us by Professor Héctor Valdivia, University of Wisconsin (Loaiza et al., 2013). All procedures with mice were approved by the University of Oxford Ethics Committee and followed the UK Scientific Procedures (Animals) Act, 1968. All animal work was conducted in accordance with the United Kingdom Home Office guidelines. All mice used in this study were maintained in a pathogen-free facility at the University of Oxford. Mice were given *ad libitum* access to food and water. The V2475F mutation is autosomal dominant and was found to produce a non-Mendelian propagation due to homozygous lethality (Loaiza et al., 2013). Mice were bred with one heterozygous and one wild-type (WT) pairing to produce a 1:1 WT to heterozygous mutant ratio of offspring, therefore WT mice were littermate controls. The use of mice was shared between members of the laboratory, in which cardiac, skeletal and brain

tissue were taken from the same mouse wherever possible in order to comply with the "three Rs" principles (Fenwick et al., 2009).

2.1.2 Genotyping of the mouse model

All V2475F(+/-) mice were genotyped to identify each mouse as WT or heterozygous for the V2475F mutation. Tissue samples of ear clips or tails were lysed overnight at 56°C in a lysis buffer of 100 mM Tris, 250 mM NaCl, 5 mM EDTA and 0.2% SDS made up in sterile H_2O, with 1:100 of proteinase K (Am2548, Life Technologies Ltd, UK) added fresh. Samples were then centrifuged at 13,000 rpm at 20°C for 3 min (Sorvall, UK). The supernatant was collected and diluted 1:5 in PCR-grade sterile H_2O. A polymerase chain reaction (PCR) was used to amplify and thereby detect the presence of the mutated portion of the RyR2 gene (Loaiza et al., 2013). 2 μl of each DNA sample was added to PCR reaction solution of Master Mix (Promega, UK), 1 μM forward primer, 1 μM reverse primer, made up in PCR-grade H_2O to a total volume of 25 μl. The PCR reaction consisted of an initial 94°C denaturing step before 30 cycles involving brief steps for denaturing, annealing, and amplification. This was followed by a final elongation period of 10 min at 72°C. The exact PCR primers and cycle protocol are reported in tables 2.1 and 2.2 below.

Table 2.1: PCR genotyping protocol

Temperature (°C)	Time (s or min)	Cycles
94	3 min	1
94	30 s	30
55	45 s	
72	1 min	
72	10 min	1
4	Hold	

Table 2.2: Primers used for PCR genotyping

Primer Name	Primer Sequence
V2475F(+/-) forward 5'	GTAGATGGGAAGGTGGTG
V2475F(+/-) reverse 3'	GATATCCCTATGACCCCCC

PCR products were then mixed with 5x loading dye (Qiagen, Germany) and run on a 1.5% agarose gel containing 0.8 μg/ml ethidium bromide (EtBr) in tris-acetate (TAE) buffer (EMD Millipore, UK) for 45 min at 90 mV. EtBr is a fluorescent DNA intercalator which increases its fluorescence approximately 25-fold upon binding DNA (Severini and Morgan, 1991). EtBr is excited at 526 nm and emits at a wavelength of 590 nm and therefore allows visualisation of DNA bands on the agarose gel by exposure to ultraviolet light (Severini and Morgan, 1991). The diagram below shows how representative bands identified the genotype of each mouse.

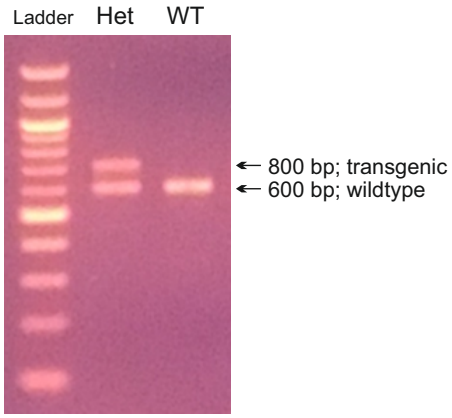


Figure 2.1: Example of resulting bands from genotyping of WT and V2475F(+/-) DNA samples from littermates of the V2475F colony

2.2 Isolation of SR vesicles

2.2.1 Collection of cardiac tissue

C57Bl6/j mice were culled by cervical dislocation, and hearts were dissected and immediately snap frozen and stored in liquid nitrogen. For mouse cardiac SR vesicle preparations, 10 hearts were used, at a 1:1 male: female ratio. WT littermates were used as the appropriate control to the transgenic V2475F(+/-) mouse model. For sheep cardiac SR vesicle preparations, half of the left ventricle was used. Sheep hearts were obtained from a local abattoir and transported to the laboratory in cardioplegic solution containing 102 mM NaCl, 21.4 mM KCl, 16 mM $MgCl_2$, 28.7 mM Na-lactate, 2.4 mM $CaCl_2$, 1 mM procaine at 4°C . The left ventricle was

isolated and fat and connective tissue was removed. The cardiac muscle was then snap frozen and stored in liquid nitrogen (Venturi et al., 2018).

2.2.2 Isolation of mixed membrane vesicles from mouse cardiac tissue

Table 2.3: Details of the composition of the buffers used for SR vesicle isolation

Buffer	Composition
Protease inhibitor cocktail (P8340, Sigma, UK)	104 μM 4-(2-aminoethyl)benzenesulfonyl fluoride hydrochloride (AEBSF), 80 nM aprotinin, 4 μM bestatin, 1.4 μM E-64, 2 μM leupeptin, 1.5 μM pepstatin A
Solution A	300 mM sucrose, 20 mM PIPES ‡ 5 mM sodium fluoride (NaF), 2.5 mM dithiothreitol (DTT), 1 mM phenylmethylsulphonic fluoride (PMSF), pH 7.2 by KOH
Solution B	400 mM KCl, 0.1 mM $CaCl_2$, 0.1 mM $MgCl_2$, 0.1 mM EGTA‡, 5 mM PIPES‡, pH 7.2
Solution C	0.4 M sucrose, 5 mM HEPES‡, pH 7.2 with Tris‡
Solution D	0.4 M KCl
Solubilisation buffer	1 M NaCl, 0.1 mM EGTA‡, 0.15 mM $CaCl_2$, and 25 mM PIPES‡, 25 mM NaOH with 0.5% (w/v) 3-((3-cholamidopropyl)-dimethylammonio)-1-propane sulphonate (CHAPS) and 2.5 mg/ml L-α phosphatidylcholine (PC), pH 7.4
Dialysis buffer†	0.1 M NaCl, 10 μM EGTA‡, 15 μM $CaCl_2$, and 0.25 mM PIPES‡, 0.25 mM NaOH, pH 7.4

‡ *Abbreviations are used for common chemicals:*
EGTA is ethylene glycol-bis(2-aminoethylether)-N,N,N',N'-tetraacetic acid
HEPES is 4-(2-hydroxyethyl)-1-piperazineethanesulphonic acid
PIPES is Piperazine-N,N'-bis(2-ethanesulphonic acid)
Tris is tris(hydroxymethyl)aminomethane
† *Dialysis buffer is a 10-fold dilution of the solubilisation buffer*

The compositions of the solutions used for the isolation of SR vesicles described below are outlined in Table 2.3. All solutions and equipment were maintained at 4°C during the isolation procedure. 10 snap frozen mouse hearts were homogenised by an Ultra-Turrax (IKA Werke GmbH & Co. KG, Germany) in solution A containing a protease inhibitor cocktail (Table 2.3). The homogenised tissue in solution was centrifuged for 20 min at 6,000 g in an Optima XPN-80 Ultracentrifuge with a type-45 Ti rotor (Beckman Coulter, UK) to pellet insoluble material. The remaining

supernatant was centrifuged at 120,000 g for 1 h. The resulting pellet containing mixed membrane vesicles were re-suspended in a glass homogeniser in a minimum volume of solution C with 5 mM sodium fluoride (NaF). This final suspension of vesicles was aliquoted, snap frozen and stored at -80°C and used within 3 weeks for bilayer experiments. RyR2 channels obtained in this way are referred to as native RyR2 channels, as they remain in their native membranes before incorporation into planar phospholipid bilayers under voltage-clamp.

2.2.3 Isolation of heavy SR vesicles from sheep cardiac tissue

All solutions and equipment were maintained at 4°C. Sheep cardiac tissue was first pulverised using a pestle and mortar before being homogenised by a coarse blender and then finely homogenised by an Ultra-Turrax in solution A with a protease inhibitor cocktail (Table 2.3) (Sitsapesan et al., 1991; Venturi et al., 2018). The homogenised tissue in solution was centrifuged at 4°C for 20 min at 6,000 g in an RC6+ centrifuge (Sorvall Thermo Fisher, UK) using a F14S-6x250y rotor (Beckman Coulter, UK) to pellet insoluble material. The remaining supernatant was centrifuged at 100,000 g for 1 h in an Optima XPN-80 Ultracentrifuge using the type-45 Ti rotor. The resulting pellet containing mixed membrane vesicles was resuspended in a glass homogeniser in solution B with 10% w/v sucrose (Table 2.3). Sucrose solutions at 20%, 30% and 40% w/v of sucrose were prepared in solution B. The mixed membrane suspension was loaded on a discontinuous sucrose gradient of 20%, 30% and 40% w/v and centrifuged for 2 h using a SW 32 Ti swinging bucket-type rotor (Beckman Coulter, UK). According to their weight, different membrane fractions were separated at the sucrose interfaces. Heavy SR was collected at the 30-40% sucrose interface which contained the highest contribution of RyR2 channels (Jones et al., 1979; Sitsapesan et al., 1991). This membrane fraction was suspended in solution D and ultra-centrifuged in the type-45 Ti rotor for 1 h at 100,000 g. The final pellets were re-suspended in a minimum volume

of solution C. This final suspension of vesicles was aliquoted, snap frozen and stored at -80°C (Sitsapesan et al., 1991).

2.2.4 Purification of heavy SR vesicles from sheep cardiac tissue

Heavy SR vesicles (2 mg/ml) were solubilised in solubilisation buffer (Table 2.3) for 1 h on ice. Unsolubilised material was separated by centrifugation for 45 min at 100,000 g in an Optima TLX Ultracentrifuge with a TLA-110 rotor (Beckman Coulter, UK) at 4°C. The supernatant containing solubilised RyR2 was loaded on top of a continuous linear sucrose gradient of 5-25% (w/v) and centrifuged overnight at 100,000g in SW 32 Ti rotor at 4 °C (Sitsapesan et al., 1991; Sitsapesan and Williams, 1994a). Gradient fractions were needle extracted sequentially from the base of the tube, and high RyR2 containing fractions were identified by a radioligand binding assay. Aliquots of each fraction were made up in 1 M KCl, 5 nM [^{3}H]-ryanodine and 1:1000 protease inhibitors (AEBSF) and incubated for 90 min in a 37°C shaking water bath. The bound and free ligand in incubated solutions were then separated by rapid filtration through Whatman GF/B glass microfibre filters (Sigma, UK) prepared in polyethylenimine solution. Filters were dissolved in emulsifier for 2 min with shaking, and the presence of bound [^{3}H]-ryanodine was quantified by liquid scintillation spectrometry with a scintillation counter (Hidex 300SL, Finland). This indicated fractions with a high concentration of RyR2 channels (Jones et al., 1979). Typically, RyR2 resides in membrane fractions of 17-28% (w/v) sucrose (Sitsapesan and Williams, 1994a). Fractions containing high [RyR2] were then dialysed to remove detergent in dialysis cassettes with a 10k molecular weight cut-off (Slide-a-Lyzer, Thermo Fisher, UK) using a dialysis buffer (table 2.3) changed every hour for 4 h then left overnight at 4 °C. The sucrose concentration of the RyR2 preparation was adjusted to 0.5 M and incubated for 1 h before snap freezing. RyR2 channels isolated and functionally purified by this methodology are referred to as purified RyR2 channels (Sitsapesan and Williams, 1994b; Sigalas et al., 2009a).

2.3 Planar lipid bilayer technique

2.3.1 Planar lipid bilayer apparatus

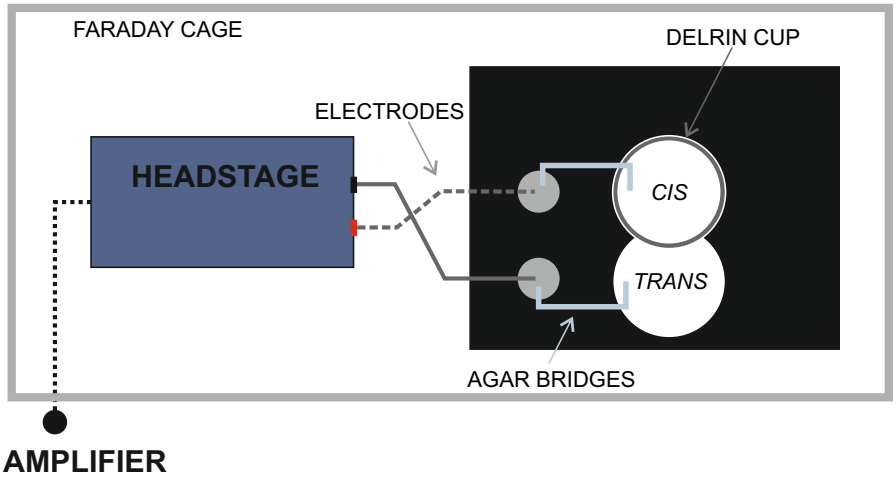


Figure 2.2: Schematic of artificial planar bilayer set up The large chambers encompass the *cis* and *trans* side of the bilayer formed by the cup and the block chamber, respectively. They are connected via agar bridges to smaller chambers, housing the electrodes and filled with 3 M LiCl. These electrodes connect to the headstage which is integrated with the amplifier. The Faraday cage sheilds the set-up to reduce noise.

The bilayer set up was a 2-part system comprising a Delrin cup and a block chamber (Warner Instruments, Harvard Bioscience, USA). The cup had a precision machined aperture of 150 μm in which the bilayer was formed (Miller, 1978). With the cup inserted into the chamber, the setup was designed so that a 1 ml volume each side of the aperture resulted in a balanced solution height to eliminate mechanical gradients across the bilayer membrane. The chamber and cup included a 0.5 mm well in the base to confine motion of the magnetic stir bars to minimise mechanical noise artefacts. The two larger chambers were connected by the aperture in the cup; the cup forms the *cis* side of the bilayer, and the chamber creates the *trans* side. Two smaller chambers contained 3 M LiCl solution and housed the Ag/AgCl electrodes connected to the headstage. These smaller chambers were connected to the large chambers via agar bridges. The agar bridges were made from capillary glass filled with 3 M LiCl and 2% agar, creating an electrical connection between the LiCl solution and recording solution in the *cis* and *trans*

chambers (Alvarez, 1986; Miller, 1978). All experiments were conducted at room temperature (RT) defined as 21 ± 1°C.

The equipment used to acquire single channel recordings was comprised of:

- BC-525D bilayer clamp amplifier (Warner Instruments, Harvard Bioscience, USA) to voltage-clamp the bilayer and record current flowing across the membrane through open ion channels. It was integrated with a resistive feedback head-stage (Fig. 2.2)
- Digidata 1440A (Axon CNS, Molecular Devices, USA) high-resolution low-noise data acquisition system, to send and receive signals from the amplifier or stimulators to communicate with the computer to acquire channel recordings
- Computer and hard drive (Microsoft Windows, UK)
- Low-pass 8 pole Bessel filter (Frequency Devices, USA) to filter signal for real-time display on to the oscilloscope
- Oscilloscope (TDS 1012C-EDU, Tektronix, USA) for real time display of recording channels
- Magnetic stirrer system (Spin-2 stir-plate, Warner Instruments, Harvard Bioscience, USA), two-part switch and stirrer plate
- Custom-made Faraday cage, housing the head-stage, block and cups and stirrer plate, to shield the experiment from background electrical noise

A good signal-to-noise ratio is critical; current recordings as small as 3 pA need to be resolved. To achieve a high signal to noise ratio, the set-up was grounded to the central ground on the amplifier. The stir-plate was connected to the Faraday cage, then directly grounded to the central ground.

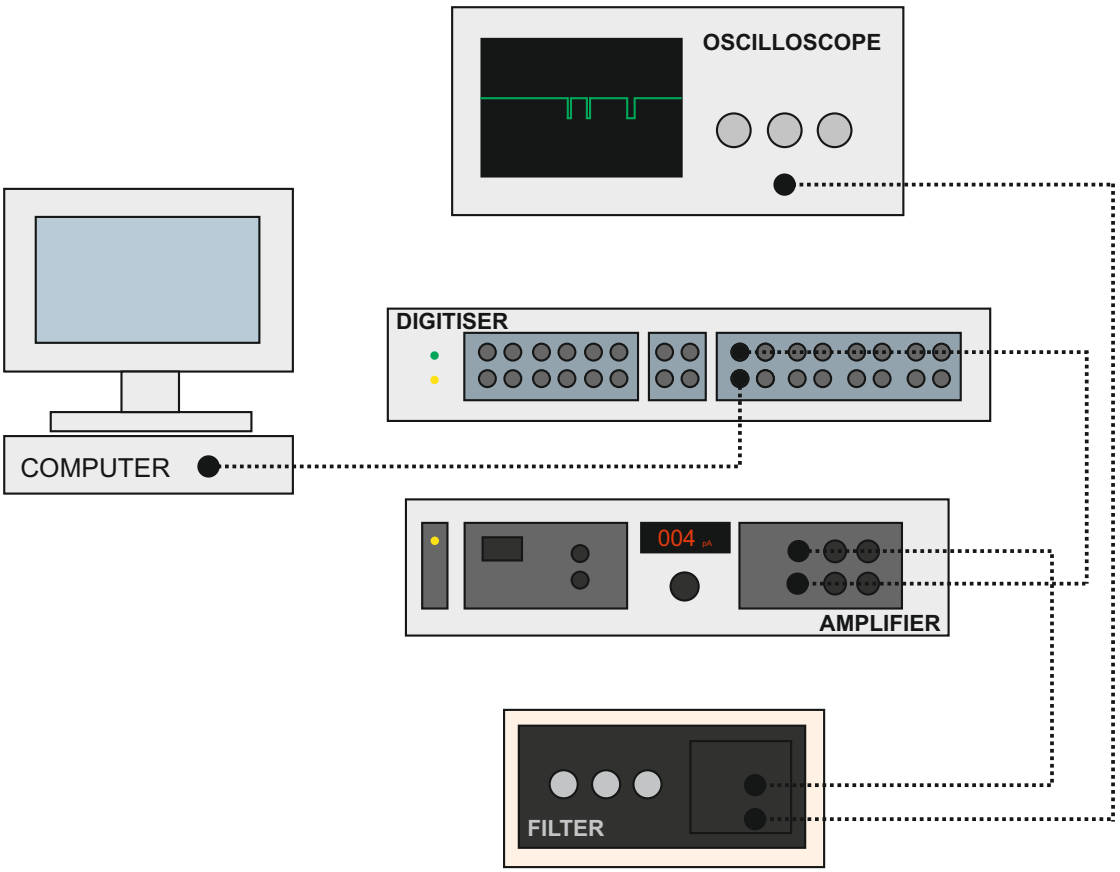


Figure 2.3: Equipment for data acquisition The signal from single-channel current fluctuations is received from the headstage to the amplifier. The signal is then converted to a digital format by the digitiser and saved on the computer hard drive. The signal is simultaneously filtered and displayed in real time on the oscilloscope.

2.3.2 Voltage-clamp configuration

An artificial membrane, in which a single ion channel is reconstituted, can be represented by a simplified circuit. A bilayer, with its double layer of lipids, behaves as a capacitor (C_b), storing energy as electrical charge on both sides of the membrane. An ion channel, in this case RyR2, acts as a resistor (R); in symmetrical ionic conditions with a voltage difference across the membrane, the ion channel allows the selective passage of ions when in an open state.

The total current through the bilayer, I_b, is then the sum of two components; a current through the bilayer capacitor, C_b, due to charge and a subsequent discharge of the membrane and a second component due to the ionic current, I_i, flowing

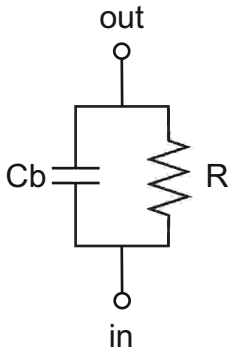


Figure 2.4: Simplified electrical analogue of a bilayer in which ion channels are reconstituted C_b is the bilayer capacitor and R the resistor representing the ion channel. "In" and "out" indicate the potentials at the two sides of the membrane.

through the ion channel. The total current I_b is shown in the following equation:

$$I_b = I_i + C_b \frac{dV}{dt} \tag{2.1}$$

During single-channel experiments the ionic current is measured using the voltage-clamp technique, first developed by Hodgkin and Huxley (1952). Voltage-clamping the artificial membrane holds the voltage at a constant, thus eliminating the contribution of the capacitance, C_b, since dV/dt will equal 0. The resultant current that is obtained by the amplifier is then the ionic current through the RyR2 incorporated into the bilayer, with a conductance limit.

2.3.3 Formation of planar lipid bilayers

Planar phospholipid bilayers were formed with modification to the method first described by Miller (1978). Bilayers were formed with a 1:1 phosphatidylethanolamine (PE): phosphatidylserine (PS) mixture (Avanti Polar Lipids, USA) for native RyR2 channel experiments. Lipids were stored in chloroform at -80°C. The chloroform was evaporated and the lipids were resuspended in decane at 20 mg/ml for experimental use. For purified channels, PE lipids only were used to form bilayers, resuspended at 35 mg/ml. The cup was primed by applying a small amount of PE lipid mixture onto the interior of the aperture and pressure was applied to force the lipid through the aperture. A

second layer of lipids was applied after 5 min. The priming of the cup allows a lipid surface interaction for a bilayer to form (White, 1986). A bilayer was formed in symmetrical solutions by "painting" lipid over the aperture. The lipids form a thick torus at the cup aperture, with a small area at the centre of the aperture in which lipids will self-organise to form a bilayer (White, 1986). The bilayer consists of two layers of phospholipids with fatty acid chains that form a hydrophobic interior and polar head groups that make the hydrophilic exterior. When the amplifier reports zero-current upon application of a voltage potential, a stable bilayer has been formed, creating an artificial bilayer between the *cis* and *trans* chambers (Miller, 1978). In this model, the bilayer mimics the intracellular membrane of the SR.

2.3.4 Bilayer detection and estimate of the area

The BC-525D bilayer clamp amplifier measures the capacitance of the bilayer in the "CAPTEST" configuration to monitor the formation and the stability of the bilayer membrane. A triangle waveform was applied to the command input and the amplitude of the resulting square wave was proportional to the membrane capacitance. In absence of a bilayer membrane the amplifier returned the same triangular wave applied which was 10 V peak to peak. When the bilayer was formed, a capacitor was then included in the circuit and the resulting waveform in output became square, with the amplitude proportional to the membrane capacitance. In these conditions it is possible to have an estimate of the area forming the bilayer. The output is scaled at 1 mV/pF when in 'CAPTEST' configuration. The capacitance of the membrane was the result of the amplitude of the square wave divided by the amplifier gain which was set at 10 mV/pA. For example, a resulting square wave of peak to peak 1000 mV was obtained when the bilayer had a capacitance of 100 pF. This read out was displayed on the amplifier, and also represented by a tone from the amplifier; the higher the pitch the larger the capacitance. A bilayer capacitance of 70 to 120 pF formed stable and fusigenic bilayers for incorporation of SR vesicles or liposomes.

2.3.5 Incorporations of native RyR2 channels for recordings with Ca^{2+} as the permeant ion

Native RyR2 channels were incorporated as follows. Both chambers were filled with symmetrical 50 mM ChCl. A stable bilayer was formed in the aperture of the cup. Next, an osmotic gradient was created across the membrane by addition of 200 μl of 3 M KCl in the *cis* chamber. 1 μl of SR vesicles were added to the *cis* chamber whilst stirring. Stirring the *cis* chamber helps to align the vesicles on the bilayer. The osmotic gradient causes swelling of the vesicles in contact with the bilayer, which eventually burst and fuse with the bilayer (Cohen, 1986), as depicted in Fig. 2.5. Fusion of vesicles containing gating ion channels created a large increase in current which was detected by the amplifier and visualised on the oscilloscope. Incorporations of RyR2 channels were easily detected because of their high K^+ permeability. After incorporation, the *cis* and *trans* chamber were perfused with the appropriate recording solutions (see table 2.4). The *cis* chamber was perfused with 125 mM Tris, 250 mM HEPES, 1 mM EGTA and 100 nM free [Ca^{2+}]. The *trans* chamber was perfused with 250 mM glutamic acid, 10 mM HEPES, 50 mM free [Ca^{2+}] with $Ca(OH)_2$ (Venturi et al., 2018). The perfusion was performed with a peristaltic pump system by perfusing the chambers with 10 ml of solution whilst stirring. This prevented further fusion of vesicles.

2.3.6 Incorporations of native RyR2 channels for recordings with K^+ as the permeant ion

Native RyR2 channels for experiments with K^+ as the permeant ion were incorporated in a similar way as for experiments with Ca^{2+} as the permeant ion, but with the following modifications. Both chambers were filled with symmetrical 210 mM KPIPES. A stable bilayer was formed in the aperture of the cup. Next, an osmotic gradient was created across the membrane by addition of 200 μl of 3 M KCl in the *cis* chamber. 1 μl of SR vesicles were added to the *cis* chamber whilst

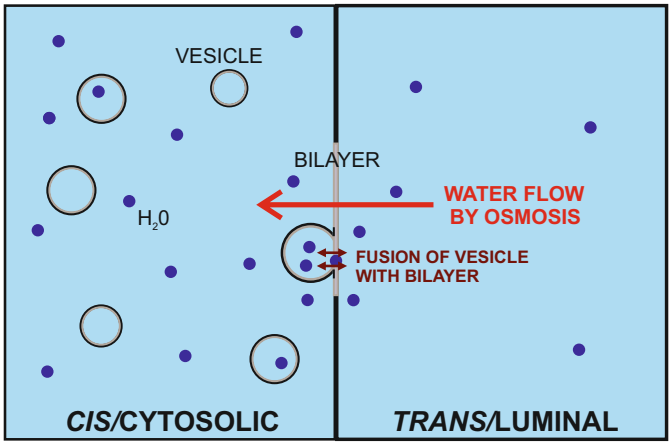


Figure 2.5: Osmotic gradient causes fusion of SR vesicles into the artificial lipid bilayer Addition of high [salt] to the cytosolic (*cis*) chamber caused water flow from the *trans* to *cis* chamber via osmosis. This caused swelling of the vesicles and allowed for fusion with the bilayer. Ion channels in the vesicles were then incorporated into the planar lipid bilayer

stirring. After incorporation, the *cis* chamber was perfused with 210 mM KPIPES to remove the gradient and vesicles.

2.3.7 Incorporations of purified RyR2 channels for recordings with K^+ as the permeant ion

Purified RyR2 channels for experiments with K^+ as the permeant ion were incorporated in a similar way as for experiments with native RyR2 channels, but with the following modifications. Both chambers were filled with symmetrical 210 mM KCl. A stable bilayer was formed in the aperture of the cup. Next, an osmotic gradient was created across the membrane by addition of 200 μl of 3 M KCl in the *cis* chamber. 1 μl of SR vesicles were added to the *cis* chamber whilst stirring (Sitsapesan and Williams, 1994a). After incorporation, the *cis* chamber was perfused with 210 mM KCl to remove the gradient and vesicles.

Channels within SR native vesicles are highly oriented once incorporated into the artificial bilayer by this technique. This is due to the way that the highly asymmetric native SR membrane vesicles fuses with the artificial bilayer (Miller and Rosenberg, 1979; Ashley and Williams, 1990). It has been determined experimentally that,

given the above protocol for fusion of membrane vesicles or liposomes, both native and purified RyR channels incorporate into bilayers in a fixed orientation, with the cytosolic side of the channel facing the *cis* chamber, and the luminal portion facing the *trans* chamber (Ashley and Williams, 1990; Sitsapesan and Williams, 1994a). Subsequently, in this thesis the *cis* chamber will be referred to as the cytosolic chamber and the *trans* chamber will be referred to as the luminal chamber.

2.3.8 Recording conditions

A schematic of the solutions used in an experiment to investigate the effects of luminal Ca^{2+} using native RyR2 channels is depicted in Fig. 2.6. This format of schematic will be used throughout the thesis to indicate the ionic composition of the cytosolic and luminal chambers, the holding potential and the direction of current flow for each type of experiment.

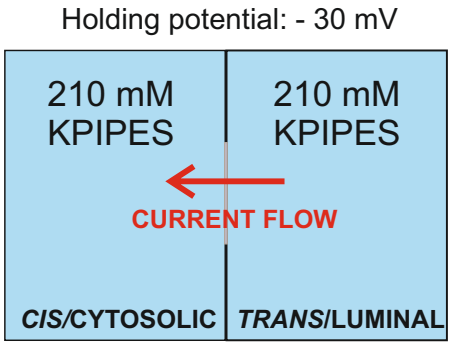


Figure 2.6: Example schematic used throughout the thesis to indicate the key experimental conditions For each set of experiments, the solutions and holding potential are displayed like this schematic. The red arrow indicates the direction of current flow through RyR2. In this case, current flow is in a physiological luminal to cytosolic direction

The solutions used for each experimental condition in this thesis are described in Table 2.4. All solutions for bilayer experiments were made in deionised water (MilliQ, Merck, UK), maintained at pH 7.2 and RT.

Table 2.4: Details of the composition of the recording solutions used for RyR2 single-channel experiments

Experiment	Holding potential (mV)	Cytosolic chamber (*cis*)	Luminal chamber (*trans*)
Native RyR2 with Ca^{2+} as the permeant ion	0	125 mM Tris, 250 mM HEPES, 1 mM EGTA, 100 nM free [Ca^{2+}] by $CaCl_2$ addition (plus [ligand])	250 mM glutamic acid, 10 mM HEPES, 50 mM free [Ca^{2+}] with $Ca(OH)_2$
Native RyR2 with K^+ as the permeant ion	-30	210 mM KPIPES, 1 mM ATP, 1 μM free [Ca^{2+}]	210 mM KPIPES (plus appropriate [Ca^{2+}])
Relative Ca^{2+}/K^+ permeability	-60 to +60	210 mM KPIPES, 20 mM HEPES, 1 mM ATP	210 mM $CaCl_2$, 40 mM HEPES
Purified RyR2	-40	210 mM KCl, 20 mM HEPES (plus [ligand])	210 mM KCl, 20 mM HEPES

2.4 Single-channel analysis

2.4.1 Data acquisition and filtering

During an experiment, single-channel current fluctuations were filtered at 800 Hz and displayed on an oscilloscope in real time. Measurements of the current flow were acquired by the amplifier and the signal was then digitised by the Digidata and stored on a computer hard drive recording via the Clampex software. The Nyquist-Shannon Sampling Theorem (Nyquist, 1928) states that the sampling frequency must be at least twice the frequency of the filtering rate to prevent aliasing and distortion of the acquired signal. Since the amplifier's internal low-pass 8-pole Bessel filter used was 5 kHz, sampling at 20 kHz was used to ensure no aliasing of the signal.

For single-channel analysis, digitised recordings were subsequently low-pass filtered which was set at specific frequencies depending on the experimental conditions. Low pass filtering is critical to remove background noise, particularly from external power sources. The level of filtering was selected to optimise the signal-to-noise ratio whilst minimising omission of real channel gating events.

For experiments with native RyR2 in Tris-HEPES/Ca^{2+} glutamate solutions where Ca^{2+} was the permeant ion, the data was filtered at 800 Hz using Clampfit (v 10.7, pCLAMP, Molecular Devices, USA) to remove high frequency noise. 800 Hz was chosen by testing the application of 50% threshold analysis to a sample of recordings with the greatest noise. 800 Hz was the optimum level of filtering that provided an idealised trace which included true channel openings without events caused by the noise in the bilayer. A square wave pulse at 800 Hz was generated to determine the frequency at which 50% attenuation of the signal was obtained. This occurred at < 1 ms therefore 1 ms was termed the *tmin*.

For experiments with native RyR2 channels in KPIPES with K^+ as the permeant ion, the high current amplitudes of the channel openings allowed the filter to be set at 2 kHz. The filtering rate was determined in recordings with the highest luminal [Ca^{2+}] and with contamination from SR K^+ channels.

In experiments in KCl using purified RyR2, the data was filtered at 4 kHz filtering rate. The filtering rate and subsequent *tmin* were determined as described above and set at 4 kHz with a *tmin* of 0.2 ms.

2.4.2 Analysis of single-channel gating

The analysis of single-channel recordings requires estimation of the time point and amplitude of each transition between an open and closed state. A list of these values can be made from an idealised record. Idealisations were performed in Clampfit using the 50% threshold method (Colquhoun and Sigworth, 1995). First, cursors were placed manually to define the open and closed states as in Fig. 2.7. The closed state was defined as the state in which the channel does not conduct ions, and is therefore the zero-current level. Transitions between open and closed states were classified as events only when the current amplitude crossed the 50% threshold level, the level halfway between the closed and fully open state. This method is appropriate for the analysis of RyR2 since it normally gates between the closed state and the full open channel state and only rarely visits sub-conductance levels.

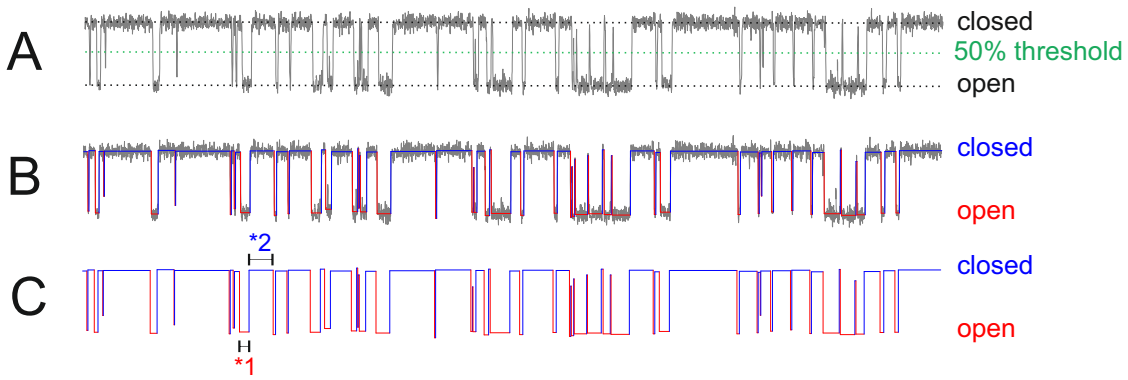


Figure 2.7: Example of idealisation of RyR2 recording (A) 2 kHz filtered recording of a native WT RyR2 channel in symmetrical 210 mM KPIPES held at –30 mV. **(B)** Idealisation of the open and closed events detected with the 50% threshold method superimposed on the single-channel recording. **(C)** Idealisation of the single channel recording. *1 and *2 illustrate an open and a closed event, respectively. The durations of these events are each marked by a segment and denoted as t_{open} or t_{closed}, respectively.

Fig. 2.7 shows how a recording was quantified by an idealisation. For each open and closed event that was detected, their durations were recorded. The sums of the times spent in the open or closed states were then used to calculate the probability of opening (Po) from at least 3 min steady state recording (Ashley and Williams, 1990). The open time and closed time, t_{open} or t_{closed}, are the times spent in each state, respectively. Po was calculated by Clampfit with the following equation:

$$Po = \frac{t_{open}}{t_{open} + t_{closed}} \tag{2.2}$$

Where multiple RyR2 channels were incorporated into the bilayer, further open levels were defined with the cursors, and equation 2.3 was used to determine NPo:

$$NPo = \frac{T_{open1} + 2\,(T_{open2}) + 3\,(T_{open3}) + \ldots\ n(T_{openN})}{T_{total}} \tag{2.3}$$

where NPo is the sum of the Po of multiple channels, N is the number of channels gating in the bilayer, T_{open1}, T_{open2} and T_{open3} are the durations in which the channels open in the first, second and third level, respectively, and T_{total} is the total time of the recording (3 min). A mean Po ($avgPo$) was then derived by dividing the NPo value by the number of channels (N), as indicated in the equation:

$$avgPo = \frac{NPo}{N} = \frac{Po_1 + 2Po_2 + 3Po_3 + \ldots nPo_n}{N} \quad (2.4)$$

where Po_1, Po_2 and Po_3 are the probability of dwelling in the first, second or third channel level, respectively.

2.4.3 Sub-conductance states

A sub-conductance state is described as a channel opening to a conductance state lower than that of the conductance of a full opening (Rousseau et al., 1987). At 800 Hz filtering level, a sub-conductance state was defined as an event > 2 ms, to distinguish a sub-conductance state from a truncated brief full open event. Where possible, the current amplitude was measured (see section 2.4.7).

2.4.4 Single-channel lifetime distributions

A channel is predicted to exist in an infinite number of conformational states, with a limited number of conformations that are stable (Colquhoun and Sigworth, 1995). A number of stable conformations can be revealed by analysis of the open or closed duration frequency distributions. This is called lifetime analysis and can be applied to either the open or the closed state (Colquhoun and Sigworth, 1995). Lifetime analysis can only be performed when a single channel is gating in the bilayer and provides information about the duration of individual states that are long enough to resolve. The durations of the open or closed states are random and continuous variables, and this form of variability can be described by a probability distribution (Colquhoun and Sigworth, 1995). A probability density function (pdf) as a function of time can be used to calculate the area under the curve up to a particular time (τ) that represents the probability that the lifetime is $\leq \tau$ at any given moment. A pdf is the sum of several exponential components each characterised by a time constant as described by equation 2.5:

$$f(t) = \sum_{i=1}^{n} \frac{P_i}{\tau_i} e\left(\frac{-t}{\tau_i}\right) + C \quad (2.5)$$

where P_i is the proportional area under the curve corresponding to the time constant τ_i, i is the number of exponential components of the distribution, and C is the constant y-offset for each component i. Logarithmic binning is preferential to conventional linear binning due to better visualisation of time constants (Sigworth and Sine, 1987), therefore the log-transformed pdf was used as described below:

$$f(t) = \sum_{i=1}^{n} P_i \; e^{[ln(t)-ln(\tau_i)]e^{ln(t)-ln(\tau_i)}} \tag{2.6}$$

where t is the log dwell-time data, P_i is the proportional area (%) under the curve corresponding to the time constant τ_i, and i is the number of exponential components of the distribution.

For the generation of lifetime distributions, to avoid including events distorted by the filtering process, events were stripped below their measured *tmin* (as described in Section 2.4.1). The stripped events were then binned into a logarithmic frequency histogram in Clampfit. Clampfit was used to fit a log-pdf for the lifetime histogram chosen by the maximum likelihood method. The maximum likelihood method is an iterative algorithm to calculate the optimum value of the log of likelihood (L) (Colquhoun and Sigworth, 1995). The number of exponentials that best fit the distribution were then determined using the likelihood ratio test (Colquhoun and Sigworth, 1995). The pdf calculates lifetime parameters including a τ value for each exponential, and a proportional area under the curve for each exponential. This mathematical approach can elucidate the mechanisms underlying the gating of a channel under specific conditions and estimate the number of resolvable stable open and closed state conformations.

2.4.5 Burst analysis

Many types of ion channels open and shut non-randomly under steady-state conditions so that the openings are grouped into "bursts" of activity that are separated by longer periods of inactivity (Magleby and Pallotta, 1983). RyR2s can gate in bursts and analyses of the burst kinetics can give further information

underlying the molecular mechanisms of the channel (Magleby and Pallotta, 1983; Sitsapesan and Williams, 1994a; Mukherjee et al., 2012). Burst analysis was therefore conducted to investigate changes to the mechanisms of gating caused by the V2475F mutation. The interval between bursts (T) was defined and calculated according to the method of Magleby and Pallotta (1983) by the equation below:

$$A_s \, .e^{-T/\tau_s} \; + \; A_m \, .e^{-T/\tau_m} \; = \; A_L \, .(1 \; - \; e^{-T/\tau_L}) \tag{2.7}$$

Where A was the area and τ was the tau value of a lifetime distribution of short (S), intermediate (I) and long (L) shut intervals. The interval between bursts was thereby set at 50 ms. Single events were considered as a burst initially, but were also subsequently separated in analysis in order to compare bursts with one or more than one event.

2.4.6 Population analysis

Due to the high number of single-channel recordings obtained at 1 μM free cytosolic Ca^{2+}, it was possible to construct Po frequency histograms for WT and V2475F(+/-) channels with this data. A pdf could be fit to the distribution of WT Po values, similarly to the fitting of pdfs to channel open and closed lifetimes described above. This was not possible for the V2475F(+/-) channel data, although several distinct peaks were observed by eye. A kernel density estimate (KDE) is a non-parametric estimate of the probability density function, in which data smoothing is used to make estimations of populations within the data and can be described by:

$$KDE_h(x) \; = \; \frac{1}{nh} \sum_{i \, = \, 1}^{n} K \left(\frac{x \; - \; x_i}{h} \right) \tag{2.8}$$

where x are random samples from an unknown distribution, n is the sample size, K is the kernel smoothing function, and h is the bandwidth set at 0.05. A KDE was therefore used to estimate the Po values at the population peaks within the overall distribution of Po values for the V2475F(+/-) channels (Hill, 1985). These were calculated in a custom-made MATLAB (2018) script. Every peak of

the distribution was then quantified to determine an estimate of a Po activity level for each population group.

2.4.7 Single-channel conductance measurements

Ion channels provide a conductive pathway across the barrier of the lipid membrane. The amplitude of the ionic current through an RyR2 was assessed by manually controlled cursors in Clampfit. Amplitude was measured only using full open events that were clearly resolved, for example, using openings longer than 1 ms after filtering at 800 Hz. The current amplitude was measured at 10 mV incremental step voltages from – 40 mV to + 40 mV in Tris/HEPES and Ca^{2+} glutamate solutions, and from -60 to +60 mV in KPIPES or KCl recording solutions. The slope of this relationship is the conductance of the channel in the recording conditions used, as per Ohm's Law:

$$I = g\,V \tag{2.9}$$

in which I is the current flowing through the RyR2, g is the conductance, and V the potential difference applied across the bilayer. The gradient of the slope was obtained from current measurements between -60 to +60 mV in KPIPES or KCl solutions. The gradient of the slope was considered between – 40 mV and +20 mV in Tris/HEPES and Ca^{2+} glutamate solutions. RyR2 channels are slightly permeable to $Tris^{+}$ (Lindsay et al., 1991) and therefore the current-voltage relationship in $Tris^{+}$-containing solutions becomes non-linear at positive voltage potentials.

To compare the relative Ca^{2+} to K^{+} permeability ratios (PCa^{2+}/PK^{+}) for RyR2 channels, the zero-current reversal potential (E_{REV}) was measured under bi-ionic conditions as described in Table 2.4, correcting for the measured liquid junction potential (LJP) as described in Section 2.4.8. The Goldman-Hodgkin-Katz (GHK) equation which describes ion permeability and selectivity across biological membranes for monovalent anions and cations (Hodgkin and Huxley, 1952) is shown below:

$$V_m = \frac{RT}{F} \ln \left(\frac{\sum_{X^+} \langle P_{X^+} [X^+]_{out} \rangle + \sum_{Y^-} \langle P_{Y^-} [Y^-]_{in} \rangle}{\sum_{X^+} \langle P_{X^+} [X^+]_{in} \rangle + \sum_{Y^-} \langle P_{Y^-} [Y^-]_{out} \rangle} \right) \tag{2.10}$$

where V_m is the membrane potential, P is the permeability of the membrane to a particular ion, X^+ is a monovalent cation and Y^- is a monovalent anion, and $[X^+]$ and $[Y^-]$ are the concentrations thereof. The Fatt-Ginsborg equation (Fatt and Ginsborg, 1958) is a modification of the GHK equation which is used to calculate the relative permeability of two ions. The modification of the GHK equation is required since Ca^{2+} and K^+ have different valences. To calculate PCa^{2+}/PK^+ the Fatt and Ginsborg (1958) equation was used and the E_{REV} was measured experimentally. The equation is described below (Tinker and Williams, 1992):

$$\frac{PCa^{2+}}{PK^+} = \frac{e^{(E_{REV} \cdot F/RT)} \cdot \left(e^{E_{REV} \cdot F/RT} + 1 \right)}{4} \tag{2.11}$$

2.4.8 Liquid junction potentials

The liquid junction potential (LJP) arises from the interface of two different salt solutions. For calculations of relative permeability, it was essential to make accurate measurements of the E_{REV}. Since the solutions in the cytosolic and luminal chamber were different and would create an LJP (see table 2.4), this needed to be accounted for in the actual E_{REV} (Tinker and Williams, 1992). The LJP was measured by ensuring the amplifier offset was at 0 mV, painting a bilayer, perfusing to solution conditions, then breaking the bilayer and measuring the offset potential readout.

2.5 Phosphorylation studies

2.5.1 Bilayer treatments

Native RyR2 channels have a basal level of phosphorylation (Carter et al., 2006; Alvarado et al., 2017). To investigate the functional changes of RyR2 single-channel gating dependent on their phosphorylation levels, native RyR2 channels were treated with phosphatases or serine/threonine kinases to alter their phosphorylation level

from the basal level after channels were incorporated into the bilayer. The catalytic subunit of protein kinase A (PKA P2645, Sigma, UK) was used to phosphorylate RyR2 channels and the catalytic subunit of protein phosphatase 1 (PP1 P7937, Sigma, UK) was used to de-phosphorylate the RyR2 channels via addition to the cytosolic side of RyR2 (Carter et al., 2006).

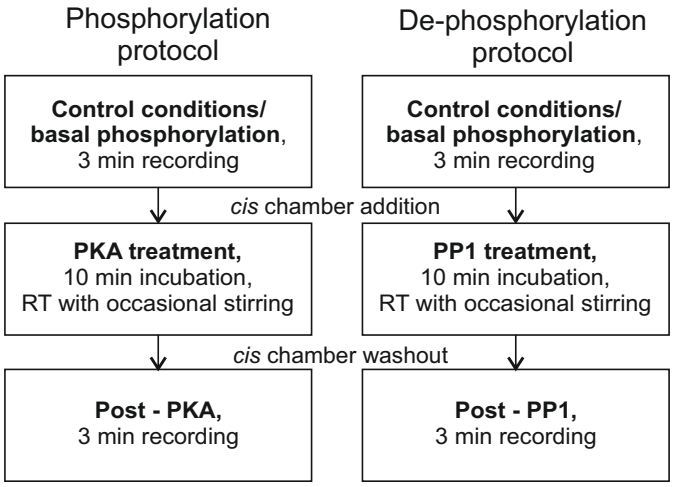


Figure 2.8: Protocol followed for the phosphorylation and de-phosphorylation experiments.

The conditions and protocols used for the phosphorylation and de-phosphorylation experiments are outlined in Table 2.5 and Fig. 2.8. "Control conditions" refers to the basal level of phosphorylation of native RyR2 channels isolated from mouse cardiac tissue. The single-channel recording conditions used before and after treatments were the same, in order to directly compare the Po at basal levels of phosphorylation (control) to the Po occurring with the phosphorylation level after treatment (post-PKA or post-PP1). Native preparations can contain endogenous kinases that are incorporated into the bilayer with the RyR2 channel (Carter et al., 2011). Thus, for the PP1 experiment, adenosine was used rather than ATP as a channel activator to ensure that no influence of phosphorylation from endogenous kinases would affect Po.

Table 2.5: Composition of the cytosolic chamber for each stage in the phosphorylation and de-phosphorylation experiments

Experiment	Condition	Cytosolic chamber composition
Phosphorylation	Control	Tris/HEPES with 1 μM free Ca^{2+}
	PKA treatment	20 units of PKA[§], 100 μM Ca^{2+}, 10 mM ATP, 15 mM Mg^{2+}
	Post-PKA	Tris/HEPES with 1 μM free Ca^{2+}
De-phosphorylation	Control	Tris/HEPES with 1 μM Ca^{2+} and 1 mM adenosine
	PP1 treatment	5 units of PP1[†]+ 100 μM $MnCl_2$
	Post-PP1	Tris/HEPES with 1 μM Ca^{2+} and 1 mM adenosine

[§] *PKA, catalytic subunit from bovine heart (Sigma, UK)*
[†] *PP1, recombinant catalytic subunit, α-isoform from rabbit (Sigma, UK)*

2.5.2 Western blots for RyR2

Western blots were used to quantify the level of phosphorylation at S2808 of RyR2 in the isolated SR preparations using antibodies specific for both the phosphorylated state of S2808 and the dephosphorylated state of S2808 (Badrilla, UK) (Rodriguez et al., 2003). The composition of buffers used are described fully in Table 2.6. To estimate the levels of phosphorylation and de-phosphorylation of RyR2 channels in the bilayer experiments outlined in section 2.5.1, SR vesicles were subjected to treatments designed to mimic those used in the bilayer experiments before western blot analysis. For an estimate of the basal control level of phosphorylation at S2808, 0.6 μg/μl of vesicles were incubated in basal buffer (Table. 2.6). For the phosphorylation treatment by PKA, 0.6 μg/μl of vesicles were incubated in phosphorylation buffer. For the dephosphorylation treatment by PP1, 0.6 μg/μl of vesicles were incubated in dephosphorylation buffer. The compositions of these buffers is described in Table 2.6. All incubations were conducted at RT for 10 min in a volume of 100 μl.

Following the phosphorylation or dephosphorylation treatment of the SR vesicles described above, 100 μl of ice-cold Tris-HEPES solution with 15 mM NaF was added before centrifugation at 13,000 rpm for 30 min at 4°C (Sorvall, Thermo Fisher, UK).

Table 2.6: Details of the composition of the buffers used for western blots

Buffer	Composition
Basal buffer	125 mM Tris, 250 mM HEPES, pH 7.2
Phosphorylation buffer	125 mM Tris, 250 mM HEPES, PKA at 0.2 U/μg of protein, 100 μM Ca^{2+}, 10 mM ATP, 15 mM Mg^{2+}, pH 7.2
Dephosphorylation buffer	125 mM Tris, 250 mM HEPES, PP1 at 0.1 U/μg of protein, 100 μM $MnCl_2$, 1 mM adenosine, 1 μM Ca^{2+}, pH 7.2
Separating gel buffer	6% acrylamide, 0.375 M Tris, 0.1% SDS, 0.1% APS, 1:1000 TEMED, pH 8.8
Stacking gel buffer	5% acrylamide, 0.13 M Tris, 0.1% SDS, 0.1% APS, 1:1000 TEMED, pH 6.8
Sample buffer	0.4 M sucrose, 5 mM HEPES, pH 7.2 with TRIS, 4x laemmli buffer (BioRad) + β -mercaptoethanol (BME)
Running buffer	25 mM Tris, 190 mM glycine, 0.1% SDS
Transfer buffer	25 mM Tris, 190 mM glycine, 10 % methanol, 0.02% SDS
TBS-T	50 mM Tris, 150 mM NaCl, 1:1000 Tween20
Coomassie blue buffer	0.25% Coomassie Blue R-250, 50% methanol, 10% acetic acid
De-stain buffer	5% acetic acid, 25% methanol

The resulting pellet was resuspended in sample buffer and incubated at 55°C for 15 min. Each sample was loaded into 3 wells of the gel alongside a ladder (Precision Plus Proteins, BioRad, UK). 60 μg of protein was loaded per well. Gels were cast in glass slides and consisted of a 6% separating gel and a 5% stacking gel. The gels were run in a mini-PROTEAN system (BioRad, UK) with running buffer (Table 2.6). Proteins were separated electrophoretically at 70 V for 30 min, then 110 V for a further 3.5 h. Proteins were then transferred to a nitrocellulose membrane for 2 h at 100 mV in transfer buffer (Towbin et al., 1979). High [methanol] and addition of sodium dodecyl sulphate (SDS) was required to ensure efficient transfer due to the large size of RyR2 (560 kDa per monomer (Takeshima et al., 1989)). Membranes were then blocked overnight in 5% non-fat milk in TBS-T solution (Table 2.6).

Membranes were probed for 1 h at RT with a primary antibody for RyR2 (34C, Abcam, 1:1000 dilution), phospho-S2808 or dephospho-S2808, (1:5000 or 1:1000 dilution, respectively; Badrilla, UK) (Rodriguez et al., 2003), and subsequently

incubated with 1:5000 dilution of horseradish peroxidase-linked anti-rabbit IgG for phospho-antibodies or anti-mouse IgG for the RyR2 (34C) antibody (Thermo Fisher, UK). Immunoreactive proteins were probed with an enhanced chemiluminescent detection substrate (Thermo Fisher, UK), and images were taken in a ChemiDoc XRS imager (BioRad, UK). Blot intensity was quantified by densitometry using ImageJ software (NIH).

2.6 Cardiomyocyte experiments

2.6.1 Isolation of cardiomyocytes

Mouse cardiomyocytes were isolated using a non-Langendorff perfusion method (Ackers-Johnson et al., 2016). This had advantages over the traditional Langendorff method including: antegrade rather than retrograde perfusion; no requirement to cannulate the mouse aorta with is technically difficult; and a smaller volume of expensive collagenase enzyme required (Ackers-Johnson et al., 2016). This method achieved a consistent yield of viable cardiomyocytes. The mouse was intraperitoneally injected with 0.2 ml of 2.5% avertin and 200 U heparin. After 10 min, the mouse was sacrificed by cervical dislocation and the heart was exposed by dissection. Under the left lung, the descending aorta and inferior vena cava were cut. The protocol follows the schematic depicted in Fig. 2.9.

The heart was then injected via the right ventricle (RV) with 7 ml of ethylenediaminetetraacetic acid (EDTA) solution (Table 2.7) within 1 min to clear blood from the heart. This caused contractions to quickly cease and the heart lightened in colour. The ascending aorta was then clamped, and the heart dissected out of the thoracic cavity and submerged in a Petri dish of EDTA solution with the left ventricle (LV) facing upwards. Next, 10 ml of EDTA solution was injected into the LV at a rate of 0.5 ml/min giving just enough pressure for the heart to inflate to ensure adequate perfusion. The coronary circulation then cleared as the surface of the heart became pale. Next, the heart was transferred into a dish

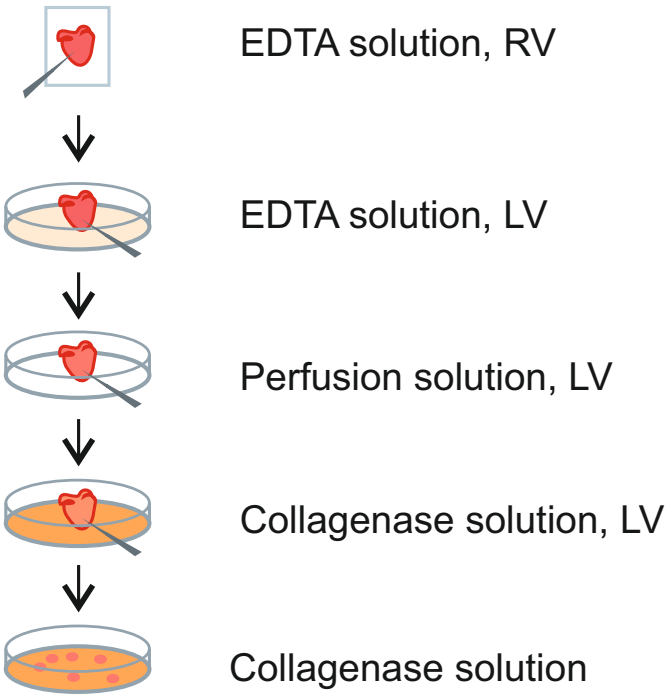


Figure 2.9: Schematic of the protocol for isolation of cardiomyocytes from murine heart RV indicates the injection was made into the right ventricle, and LV indicates injection into the left ventricle. All buffers are described fully in Table 2.7.

of perfusion solution, and 3 ml of perfusion solution was injected into the same injection site to clear the EDTA, as this could have hindered the activity of the collagenase. The heart was further transferred into a dish of collagenase solution and injected with collagenase solution at 37 °C, again into the same site. For the digestion procedure, the heart was maintained at 37 °C for optimal collagenase activity. The rate of injection was around 2 ml/min but this increased as the procedure progressed and the structural integrity of the heart was weakened. The time taken to perfuse with collagenase solution could vary, for example, it could take more time to perfuse a larger heart. Complete digestion of the heart was confirmed by: a noticeable reduction in injection pressure; holes and loss of external structure to the heart; and the ejection of cardiomyocytes into the effluent buffer just about visible by eye (Ackers-Johnson et al., 2016).

After sufficient digestion, the ventricles were dissected and placed into 3 ml of fresh collagenase solution. The tissue was gently teased apart with tweezers, then triturated for 2 min with a custom-made glass pipette with a wide bore tip to

reduce shear stress. 5 ml stop solution was added to the cells to halt enzymatic digestion, followed by further trituration. Cardiomyocytes were inspected under a light microscope to check for yield and health. Cell suspensions were passed through a 100 μm cell strainer and washed through with 5 ml stop solution. Cells were gravity settled for 10 min, during which time viable cardiomyocytes settled and other cell types and cellular debris remained in suspension. Sequential gravity settling was repeated 3 times to purify the cells, and [Ca^{2+}] was gradually increased to the working solution of 1 mM Ca^{2+} for intact cellular experiments; this minimised spontaneous contractions and obtained Ca^{2+} tolerant cells (Ackers-Johnson et al., 2016).

Table 2.7: Composition of solutions required for cardiomyocyte isolation and experiments

Buffer	Composition
EDTA solution	130 mM NaCl, 5 mM KCl, 0.5 mM NaH_2PO_4, 10 mM HEPES, 10 mM glucose, 10 mM BDM, 10 mM taurine, 5 mM EDTA
Perfusion solution	130 mM NaCl, 5 mM KCl, 0.5 mM NaH_2PO_4, 10 mM HEPES, 10 mM glucose, 10 mM BDM, 10 mM taurine, 1 mM $MgCl_2$
Collagenase solution	0.5 mg/ml collagenase 2 (Worthington, LS004176), 0.5 mg/ml collagenase 4 (LS004188), 0.05 mg/ml protease XIV (P5147, Sigma, UK)
Stop solution	5% FBS in perfusion solution
Kreb's solution	128 mM NaCl, 4.8 mM KCl, 22 mM $NaHCO_3$, 11 mM glucose, 1 mM $MgCl_2$, 1 mM $CaCl_2$

2.6.2 Ca^{2+} imaging set-up

Isoprenaline (ISO) perfusion of isolated intact (or unpermeabilised) cardiomyocytes was used to mimic β-adrenergic stress of cardiomyocytes from WT or V2475F(+/-) mice (Capel et al., 2015). ISO is a non-selective β-adrenoreceptor agonist and therefore mimics an increase in circulating catecholamines by activating the β-adrenergic pathway (Shen, 2006). Ca^{2+} release from cardiomyocytes was visualised by Fluo-4 AM (Thermo Fisher, UK), a cell permeant Ca^{2+} indicator that increases >100-fold in fluorescence excitation at 488 nm upon binding Ca^{2+} (Ohata et al., 1999). The imaging set up consisted of a custom-made optical imager, as depicted

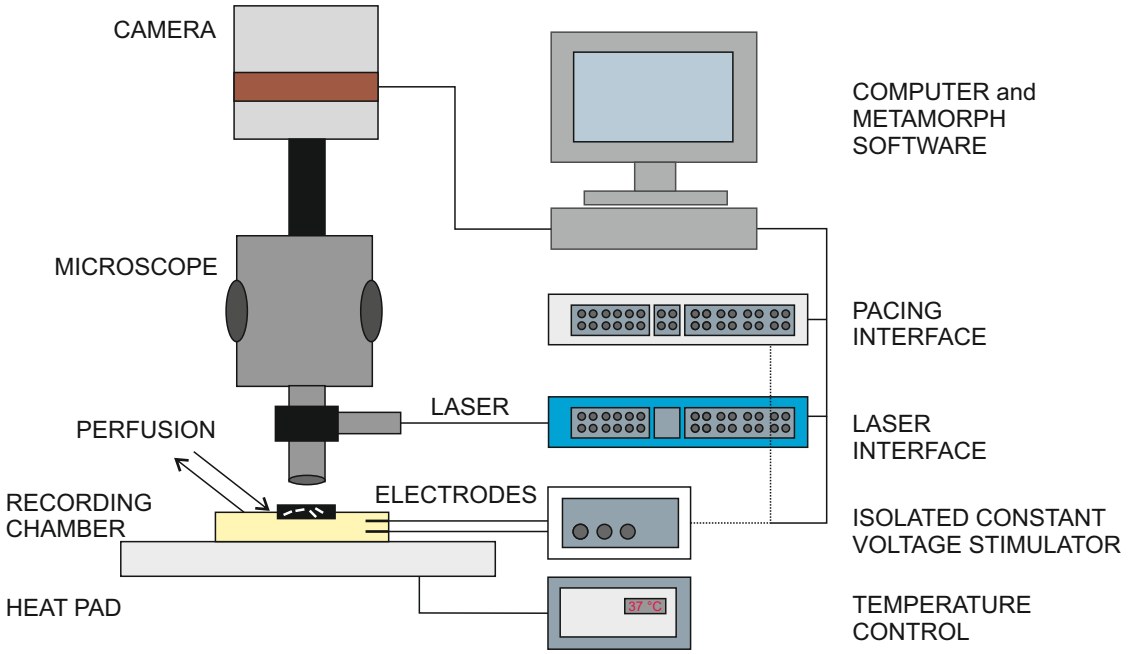


Figure 2.10: Equipment for image acquisition The fluorescence of the dye-containing cardiomyocytes was recorded on the computer via the camera, imaged through the microscope. The chamber contains electrodes that conduct the pacing stimulus to the cardiomyocytes, which is integrated with the isolated constant voltage stimulator, the interface and the computer. The cardiomyocytes were constantly perfused and temperature maintained by the heat pad and temperature control.

in Fig. 2.10. The camera (Photometrics Technology, Evolve) was integrated with the Metamorph software (Molecular Devices, USA) on a computer. This system recorded the fluorescence of dye-loaded cardiomyocytes which were visualised with blue light (470 nm) under a microscope (Olympus MVX10). The recording chamber was set up as follows: the glass slide where cardiomyocytes were placed was fixed in a chamber with silicone gel; the chamber sat on a heat pad to maintain the experimental temperature at 37°C; the Kreb's solution was maintained at 37°C in a heated bath immediately prior to perfusion; the chamber housed electrodes which produced a field stimulation in the recording chamber; the electrodes were attached to an isolated constant voltage stimulator (DS2A, Digitimer, USA) which paced the cardiomyocytes at 0.5 Hz at 20 V with a plateau of 4 ms; the pacing protocol was set by a pacing programme (Spike 2 software, Cambridge Electronic Design, UK) integrated with an interface (CED 1401, Cambridge Electronic Design, UK) connected to the isolated constant voltage stimulator (Wang et al., 2016).

Recordings were saved onto a computer hard drive via the Metamorph software.

2.6.3 Cardiomyocyte recording protocol

Prior to a recording, cardiomyocytes were incubated in 10 μM Fluo-4 AM supplemented with pluronic acid (Thermo Fisher,UK) for 20 min at 37°C. Isolated cardiomyocytes were suspended in Kreb's solution containing 1 mM Ca^{2+} After incubation, cardiomyocytes were added to a fresh glass slide, and a suspended cover slip was placed on top. Cells were left to settle for 5 mins to adhere. Next, the perfusion system was switched on, and cardiomyocytes were perfused with Kreb's solution containing 1 mM Ca^{2+} (Table 2.7). The recording protocol is depicted below (Fig. 2.11). Cardiomyocytes were recorded every 30 s. Cardiomyocytes were only visualised for 10 s every 30 s to minimise dye bleaching and damage to the cardiomyocytes from the laser. The fluorescence of the cardiomyocytes was recorded for control without 50 nM ISO, with and without the pacing protocol. The chamber was then perfused with 50 nM ISO in Kreb's solution for 1.5 min to ensure adequate perfusion of the cells. The ISO solution was made up fresh, immediately before perfusion for every experiment. Cardiomyocyte fluorescence was then recorded every 30 s for 3.5 min. After this, pacing was turned off for 1 min before a further recording was taken.

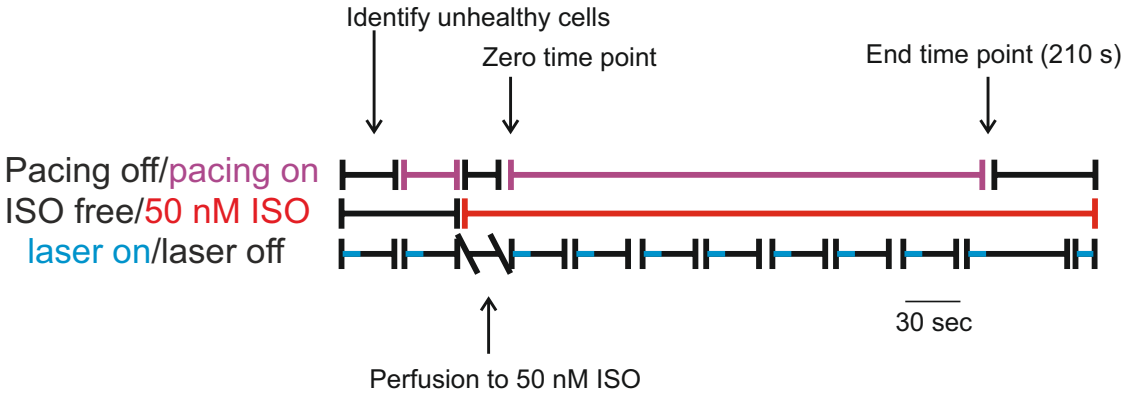


Figure 2.11: Schematic of the cardiomyocyte β-adrenergic stress protocol Blue "laser on" periods indicate when cardiomyocyte Ca^{2+} release was recorded. The blue section of the bar indicates a 10 s recording period in every 30 s period. The first recording period allows for identification of unhealthy cells. The angled bar represents a 1.5 min perfusion duration of ISO.

2.6.4 Analysis of spontaneous Ca^{2+} release from cardiomyocytes

Unhealthy cardiomyocytes were defined as cardiomyocytes that spontaneously released Ca^{2+} independently of the pacing stimulus. These cells were identified in the initial recording without pacing stimulus and eliminated from the analysis. Each individual cardiomyocyte was highlighted as a region of interest in the Metamorph programme, and data was quantified as a measure of fluorescence (A.U.). Recording values were exported into Excel prior to further analysis by a bespoke MATLAB (2018b, Mathworks, USA) protocol. This script made graphical visualisations of the fluorescence recordings from each cell in a time series graph, and time to first spontaneous wave or non-recoverable wave was recorded from this identified time point. A first spontaneous wave was defined by a Ca^{2+} release event independent of a pacing stimulus with subsequent Ca^{2+} release events returning to synchrony with the pacing. A non-recoverable wave was defined as a Ca^{2+} release event(s) independent of the pacing stimulus that did not return to normal Ca^{2+} release events within 5 s. The time to first spontaneous wave or non-recoverable wave was plotted as a survival curve using a log-rank method (Bland and Altman, 2004) in Prism 8 (GraphPad, USA) to compare WT and V2475F(+/-) cardiomyocytes.

2.7 Chemicals and solutions

2.7.1 Measurement of free Ca^{2+}

The free [Ca^{2+}] of solutions was measured using a Ca^{2+} electrode and a Ross-type pH electrode (Orion 93-20/Orion 81-55, Thermo Fisher, UK). The Ca^{2+} electrode was calibrated to solutions with a known [Ca^{2+}] to produce a standard curve for [Ca^{2+}] (Sitsapesan et al., 1991). Tris-HEPES solution was buffered with 1 mM EGTA, and $CaCl_2$ was added to titrate the free Ca^{2+} concentration to 100 nM according to the [Ca^{2+}] standard curve. Further measurements were made to calculate the amount of $CaCl_2$ required to increase free [Ca^{2+}] from 100 nM to 10 mM in 10-fold increments.

Since the Ca^{2+} electrode loses accuracy at < 100 nM $[Ca^{2+}]$, the MaxChelator software (maxchelator.stanford.edu) was used to predict the $[Ca^{2+}]$ in solutions with concentrations less than 100 nM. The approximate free $[Ca^{2+}]$ of solutions where 1 mM EGTA was added without additions of $CaCl_2$ was predicted to be < 1 nM.

2.7.2 Measurement of protein concentration

The protein concentration of the SR vesicle preparations was measured using the Bradford protein assay; the Bradford protein assay is a spectroscopic analytical procedure used to measure [protein] in a solution (Bradford, 1976). Standards of 1, 0.75, 0.5, 0.25, 0.125, 0 mg of protein/ml were made with bovine serum albumin (BSA, Sigma, UK) in H_2O. 20 μl of standards were added to 1 ml of 1:4 diluted Bradford reagent dye, and a standard curve was produced by measuring the absorbance at wavelength 595 nm with a NanoPhotometer (Implen, Germany). Each SR vesicle preparation was diluted 1:10, 1:20 and 1:30, and absorbance was measured and averaged to obtain the final protein concentration by extrapolation from the standard curve.

2.8 Statistics

2.8.1 Statistical tests

Statistical significance for grouped numerical data was determined with unpaired t-tests where two groups were compared. For more than two numerical groups with one independent variable, a one-way analysis of variance (ANOVA) was conducted (Welch, 1951). Post-hoc multiple comparisons were conducted after the ANOVA, to inform which specific groups in the one-way ANOVA differed significantly. For post-hoc multiple comparisons, Sidak's correction was used, to avoid overestimation of the p value (Šidák, 1967).

A two-way ANOVA was used to compute statistical significance in an experiment with two independent variables (Fisher, 1992). The two-way ANOVA is more

accurate than a one-way ANOVA in this case since the two-way ANOVA partitions the variance between the two independent factors. The primary purpose of the two-way ANOVA is to understand whether there is an interaction between two independent variables on the dependent variable. In this thesis, the two independent variables were usually experimental condition and genotype, so the two-way ANOVA informed whether there was an interaction between, for example, the effect of $[Ca^{2+}]$ and genotype. The interaction term informs whether the effect of one of the independent variables on the dependent variable is the same for all values of the other independent variable (Krzywinski and Altman, 2014). Hence, in the above example, is the effect of $[Ca^{2+}]$ on RyR2 channel Po influenced by genotype and vice versa? The two-way ANOVA also calculates two main effects for each independent variable. Thus, in the above example, a separate p value for the main effect of $[Ca^{2+}]$ and a p value for the main effect of genotype would also be computed. Throughout this thesis, to report the two-way ANOVA, the p value for the interaction and the main effects are not indicated on the graph but are described in the figure legend. The p value for the interaction will be stated in the relevant figure legend as "independent variable 1-by-independent variable 2 interaction", followed by the p values for the main effects. For example: Two-way ANOVA: Ca^{2+}-by-genotype interaction, p = X; main effect of $[Ca^{2+}]$, p = X; main effect of genotype, p = X.

When an interaction is significant, it is informative to look at the p values for the post-hoc multiple comparisons to understand where the significant differences lie when comparing each group. Sidak's correction for multiple comparisons was used (Šidák, 1967). The p value obtained for the significant difference between two groups is stated in the figure legends and further indicated on the figure by asterisks (*).

Chi-squared (χ^2) analysis was conducted to compare whether there was a significant difference between expected and observed frequencies in categorical data (Pearson, 1900).

All statistical analysis was performed in Prism 8 unless otherwise stated. Data was expressed as mean ± SEM with $n \geq 5$, unless otherwise stated. Statistical

analysis was not conducted in cases where n < 5 because it was not possible to assess the normality of the distribution of the data with small sample sizes. For all statistical tests, p < 0.05 was considered significant. Significance was denoted on figures as follows: * p < 0.05, ** p < 0.01, *** p < 0.001, **** p < 0.0001. Statistical tests are described in the legend for each figure.

2.8.2 Models for linear and non-linear regression

All linear or non-linear plotted lines described here were fitted in Prism 8 by a least squares fit. To calculate the slope of a linear relationship, a linear regression was fit to the equation:

$$Y = aX + b \tag{2.12}$$

where a is the gradient of the line, and b is the Y-intercept.

For log[ligand]-response curves, the following models for a non-linear variable slope were used depending on whether the ligand was an agonist or an antagonist, respectively:

$$Y = \frac{B\ (T - B)}{1 + 10^{(LogEC50\ -\ X)\ .\ nH}} \tag{2.13a}$$

$$Y = \frac{B\ (T - B)}{1 + 10^{(LogIC50\ -\ X)\ .\ nH}} \tag{2.13b}$$

where T and B are the top and bottom which refers to the plateaus of the curve in the units of Y, where nH is the Hill slope which describes the steepness of the curve, and where Log_{EC50} and Log_{IC50} are the concentrations that give half-maximal stimulatory and inhibitory effects in the same units as X.

To fit a biphasic log[ligand]-response curve, a non-linear bell-shaped model was used as described below. To calculate the span (the Y-height) of the curve:

$$Span1 = Plateau1 - Peak \tag{2.14a}$$

$$Span2 = Plateau2 - Peak \tag{2.14b}$$

Where $plateau1$ and $plateau2$ are the plateaus at the extremities of the curve, in the same units as Y. $Peak$ is the plateau in the middle of the curve, in the units of Y. These values are then used to calculate the two sections of the curve:

$$Section\ 1 = \frac{Span1}{1 + 10^{(LogEC50 - X)\ .\ nH1}} \tag{2.15a}$$

$$Section\ 2 = \frac{Span2}{1 + 10^{(X - LogIC50)\ .\ nH2}} \tag{2.15b}$$

Where $nH1$ and $nH2$ are the unitless slope factors or Hill slopes for the stimulation and inhibition portion of the curves, respectively. Using equation 2.15, a non-linear bell-shaped curve was fitted by:

$$Y = Peak + Section1 + Section2 \tag{2.16}$$

2.8.3 Animal numbers

Since 10 hearts were required per SR preparation and it was planned that experiments would be obtained from at least 3 preparations to ensure no differences between preparations of the same genotype, it was calculated that 60 mice would be required per colony for single-channel experiments (30 WT + 30 V2475F(+/-)). Samples used for western blot experiments were taken from SR preparations that were made for single-channel experiments, so no additional animal numbers were required for these experiments. To reduce the number of experimental animals used and to comply with the "three Rs" from the same animal and used for other experiments carried out in the laboratory (Fenwick et al., 2009). This was not possible for cardiomyocyte isolations since the heparin injection meant other tissues were compromised. For cardiomyocyte experiments, G*power (HHU, Germany) was used to determine the number of cardiomyocytes, and therefore the number of

animals, required in this study (Faul et al., 2007). Experimental data from Professor Derek Terrar's laboratory (Department of Pharmacology, University of Oxford) was used to estimate the effect size, a significant level of 0.05 was used with a power value of 0.8 (Festing and Altman, 2002).

2.8.4 Randomisation and operator blinding

Randomisation was carried out as effectively as possible throughout these experiments. Hearts used for generation of SR vesicle preparations were selected randomly within each genotype group. Cardiomyocytes were randomly selected for experiments. The operator was blind to the genotype during the analysis of the cardiomyocyte experiments. Unhealthy cardiomyocytes were determined by whether they had spontaneous waves at rest before the experiments, and otherwise all included. Every RyR2 channel successfully incorporated into the bilayer was experimented on. Wherever possible, randomisation was achieved by altering the order in which ligands were applied to the channel. For example, some high dose ligands were added immediately after the control period, and not always sequentially. Although it was not possible to conduct single-channel experiments blinded, single-channel analysis was conducted blinded to the genotype.

3

The V2475F mutation at RyR2

Contents

3.1 Introduction 67
3.2 Comparison of single-channel current fluctuations and conductance properties 68
3.3 Comparison of the RyR2 channel response to cytosolic Ca^{2+} 77
3.4 Effects of the V2475F mutation on channel response to 100 nM [Ca^{2+}] 88
3.5 Populations of V2475F(+/-) channels 94
3.6 Alterations to other key regulators of RyR2 99

3.1 Introduction

Single-point mutations to RyR2 cause the arrhythmic cardiac disease, CPVT1 (Priori et al., 2001). The mutation, V2475F, was found to be the cause of death in a young boy (Tester et al., 2005). Experiments in this chapter aim to elucidate the molecular pathophysiological mechanisms that give rise to dysfunction at RyR2 caused by the V2475F mutation. The experiments in this Chapter utilise native RyR2 channels derived from the cardiac tissue of V2475F heterozygous (+/-) mice and the littermate WT RyR2 controls (Loaiza et al., 2013). In order to understand the ways in which the V2475F-mutated RyR2 channels are dysfunctional, the single-channel responses to known important physiological RyR2 regulators were individually examined. As a rise in cytosolic Ca^{2+} is the trigger for SR Ca^{2+} release in the heart and as the effects of cytosolic Ca^{2+} are heavily dependent on the modulating actions of Mg^{2+}, adenine nucleotides and luminal Ca^{2+}, the effects of these agents were investigated primarily.

CPVT1 is an autosomal dominant expressed disease (Priori et al., 2001). This means that CPVT1-mutated RyR2 channels will exist as a population of channels with a different number of mutated monomers per RyR2 tetramer 3.16. Native RyR2 channels were therefore derived from the cardiac tissue of mice that were heterozygous (+/−) for the V2475F mutation (Loaiza et al., 2013) and the contribution of the heterozygosity to the single-channel function of RyR2 channels was examined.

Disruption to conductance properties of RyR2 caused by a CPVT1 mutation are not routinely examined. Therefore, in addition to exploring possible changes in ligand regulation of RyR2, the potential dysfunction to ion permeation caused by the V2475F mutation was explored. The single-channel conductance in Ca^{2+} and K^+ solutions was therefore subsequently investigated, as well as the permeability of Ca^{2+} relative to K^+.

3.2 Comparison of single-channel current fluctuations and conductance properties of RyR2 channels from WT and V2475F(+/-) mouse hearts

Typical single-channel recordings of native RyR2 channels derived from the hearts of WT or V2475F(+/-) mice in recording solutions of Tris/HEPES (cytosolic) and Ca^{2+} glutamate (luminal) with Ca^{2+} as the permeant ion are shown in Fig. 3.1. At this free cytosolic [Ca^{2+}] (1 μM), both sets of channels were characterised by very short open and closed events. It can also be seen that the current amplitudes of the V2475F(+/-) channel openings appeared to be slightly lower than those of WT channels. Fig. 3.2A displays the mean voltage-current relationships from -40 mV to + 40 mV in these same solutions. The V2475F mutation significantly reduced single-channel Ca^{2+} conductance from 114.1 ± 2.5 pS for WT to 104.3 ± 2.4 pS for V2475F(+/-) channels (mean ± SEM) as shown in Fig. 3.2B.

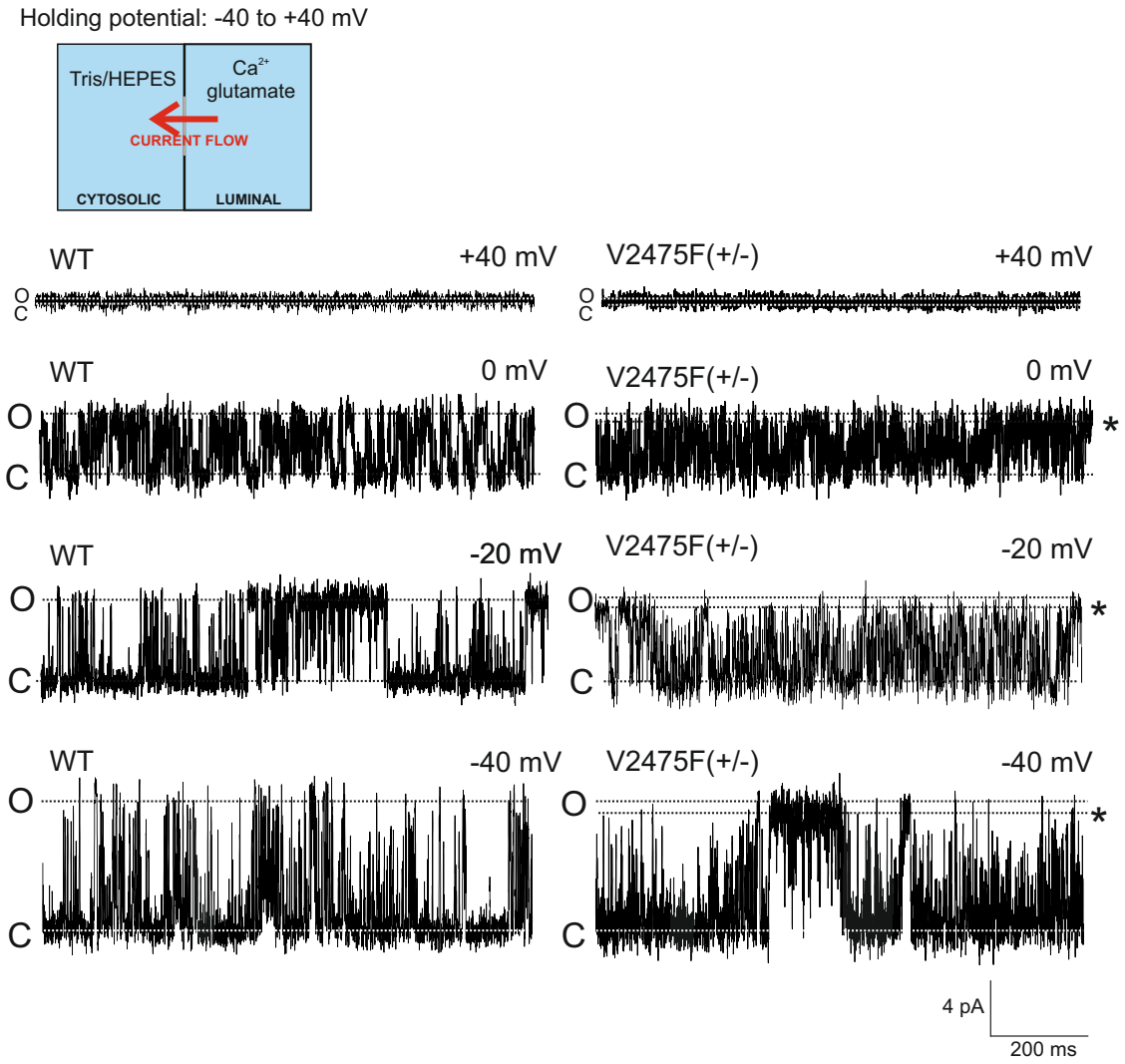


Figure 3.1: Comparison of single-channel Ca^{2+} current fluctuations and Ca^{2+} conducting properties of RyR2 channels from WT and V2475F(+/-) mice Representative single-channel recordings in Tris/HEPES and Ca^{2+} glutamate solutions illustrating the effects of varying holding potential on single-channel current amplitude for WT (left) and V2475F(+/-) (right) RyR2 channels. A simplified model of the experimental conditions is shown above the traces. Cytosolic free [Ca^{2+}] was 1 μM and luminal Ca^{2+} was approximately 50 mM. Ca^{2+} was the permeant ion flowing in the luminal to cytosolic direction. Traces were filtered at 800 Hz. O and C represent the fully open and closed levels for WT channels, respectively. * indicates the level of the fully open V2475F(+/-) channels.

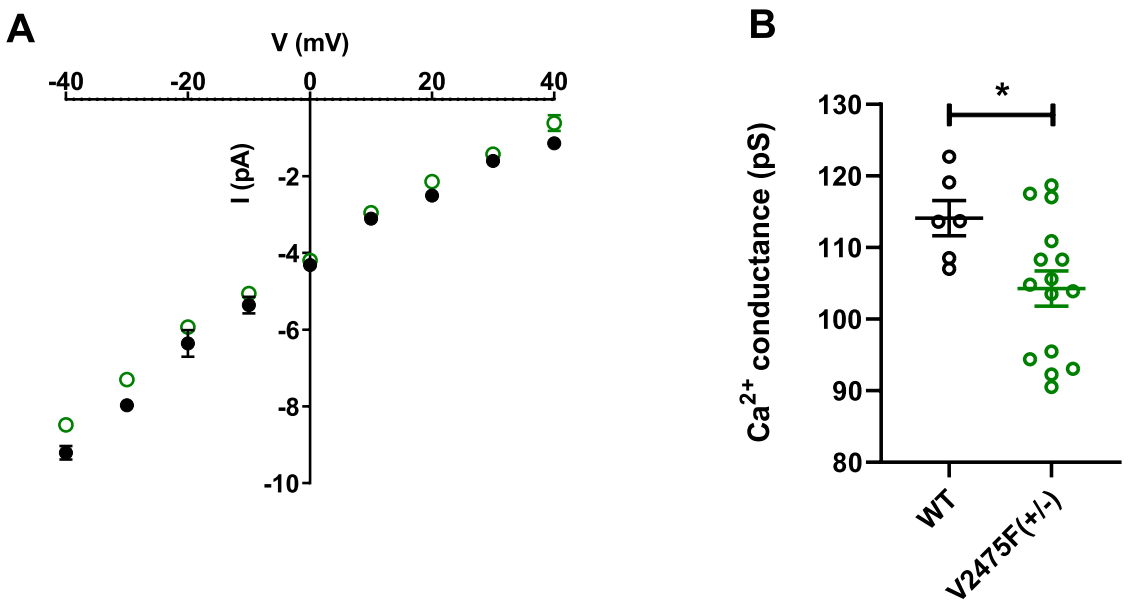


Figure 3.2: Comparison of single-channel Ca^{2+} conductance and current-voltage relationships of RyR2 channels from WT and V2475F(+/-) mice (A) Single-channel current-voltage relationships with the same solutions as (Fig. 3.1). Mean values ± SEM (n ≥ 5) are shown for WT (black filled circles) and V2475F(+/-) (green open circles) channels. Where not shown, error bars are within the symbol. **(B)** The data from (A) was used to calculate the individual linear single-channel Ca^{2+} conductance values of WT (black) and V2475F(+/-) (green) channels (Mean ± SEM; *p = 0.03). RyR2 is slightly permeable to $Tris^{+}$ (Lindsay et al., 1991) and therefore the current-voltage relationship in (A) is not linear. Linear single-channel conductance values were therefore obtained by plotting a straight line of best fit between holding potentials of -40 to +20 mV.

Representative single-channel recordings of native RyR2 channels derived from the hearts of WT or V2475F(+/-) mice hearts in recording solutions of symmetrical 210 mM KPIPES with K^{+} as the permeant ion are shown in Fig. 3.3. The reversal potential was 0 mV. Fig. 3.4A displays the voltage-current relationships (plotted from -60 mV to + 60 mV) in these same solutions. The single-channel K^{+} conductance was 698.4 ± 18.6 pS for WT channels and 703.0 ± 20.7 pS (mean ± SEM) for V2475F(+/-) channels as shown in Fig. 3.4B. This indicated that the V2475F mutation does not alter single-channel K^{+} conductance.

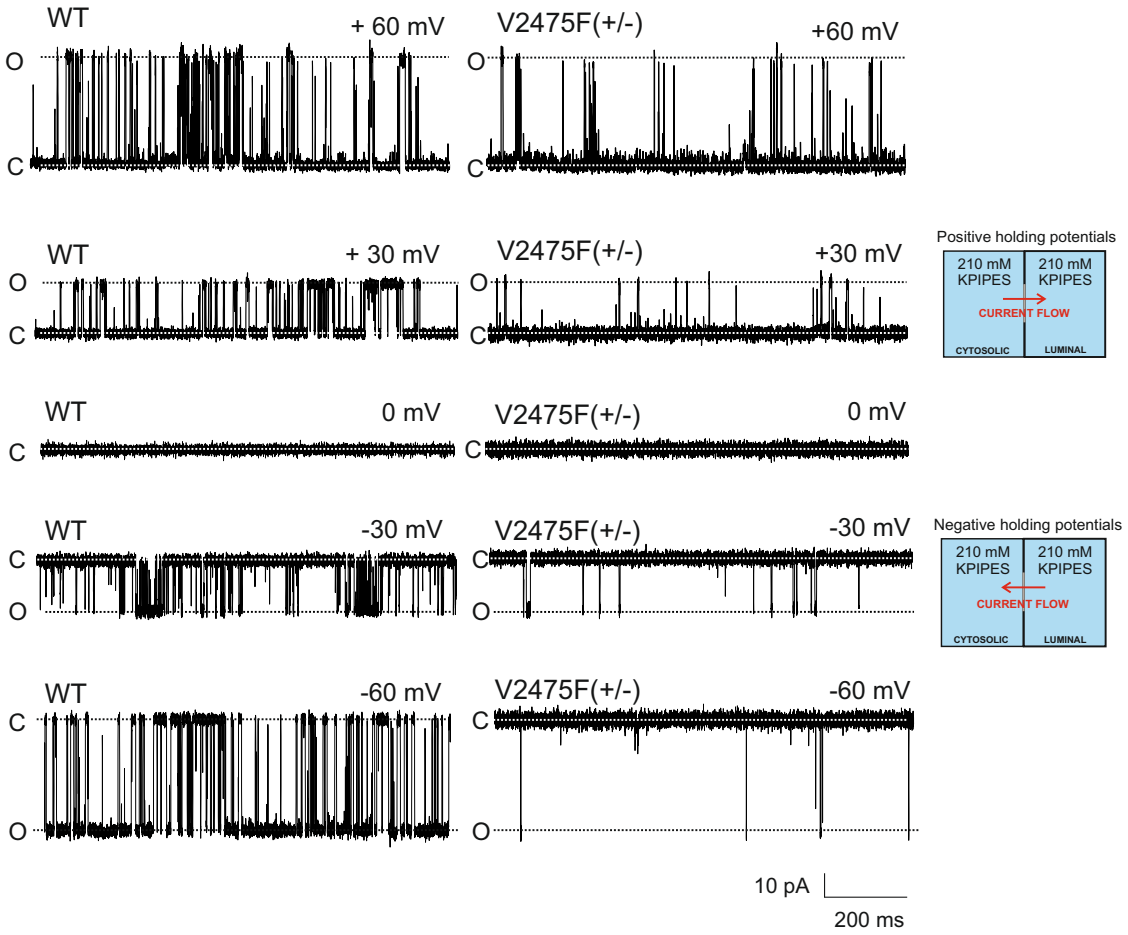


Figure 3.3: Comparison of single-channel K^+ current fluctuations of RyR2 channels from WT and V2475F(+/-) mice Representative single-channel recordings in symmetrical 210 mM KPIPES solutions illustrating the effects of varying holding potential on gating and current amplitude for WT (left) and V2475F(+/-) (right) RyR2 channels with K^+ as the permeant ion. A simplified model of the experimental conditions is shown to the right of the traces. Channels were activated by 0.5 μM cytosolic Ca^{2+} and 1 mM cytosolic ATP. The luminal [Ca^{2+}] was 2 μM. Traces were filtered at 2 kHz. O and C represent the fully open and closed levels, respectively.

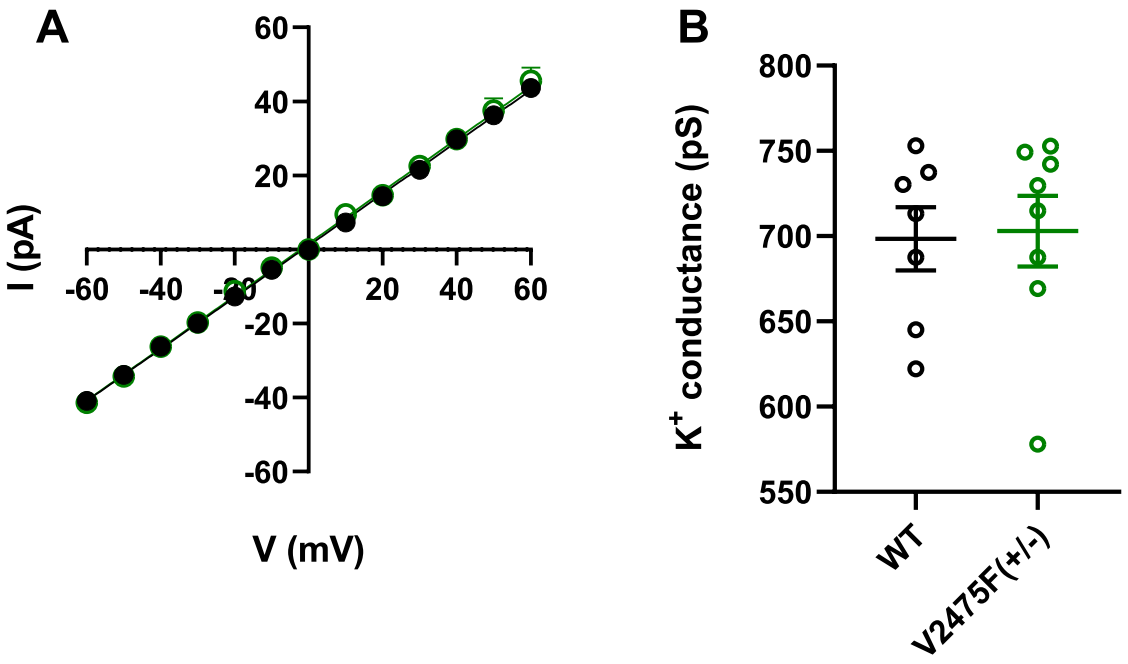


Figure 3.4: Comparison of single-channel K^+ conductance and current-voltage relationships of RyR2 channels from WT and V2475F(+/-) mice (A) Single-channel current-voltage relationships with the same solutions as in Fig. 3.3. Mean values ± SEM (n ≥ 7) for WT (black filled circles) and V2475F(+/-) (green open circles) channels. Where not shown, error bars are within the symbol. **(B)** The data from (A) was used to calculate the individual single-channel conductance values of WT (black) and V2475F(+/-) (green) channels (Mean ± SEM; p = 0.88). Single-channel conductance values were obtained from the slope of the linear regression line determined between holding potentials of -60 to +60 mV.

Typical single-channel recordings of native RyR2 channels derived from the hearts of WT or V2475F(+/-) mice in recording solutions of 210 mM KPIPES (cytosolic) and 210 mM $CaCl_2$ (luminal) with K^+ and Ca^{2+} as the only permeant ions are shown in Fig. 3.5. Fig. 3.6 displays the voltage-current relationships in these solutions. Under these bi-ionic conditions there was no difference in reversal potential (E_{REV}) measured as 34.8 ± 0.4 mV and 34.9 ± 0.3 mV (mean ± SEM, n = 5) for WT and V2475F(+/-) RyR2 channels, respectively. The relative permeability of Ca^{2+} and K^+ (PCa^{2+}/PK^+) was calculated from the E_{REV} by the Fatt and Ginsborg (1958) equation to be 7.13 ± 0.30 and 7.15 ± 0.62 (mean ± SEM; n = 5) for WT and V2475F(+/-) channels, respectively. This indicates that both the WT and V2475F(+/-) mouse RyR2 channels were approximately 7-fold

more permeant to Ca^{2+} than K^+, similar to values calculated previously for sheep RyR2 (Tinker and Williams, 1992). This suggests that the V2475F mutation does not alter the permeability of Ca^{2+} relative to K^+.

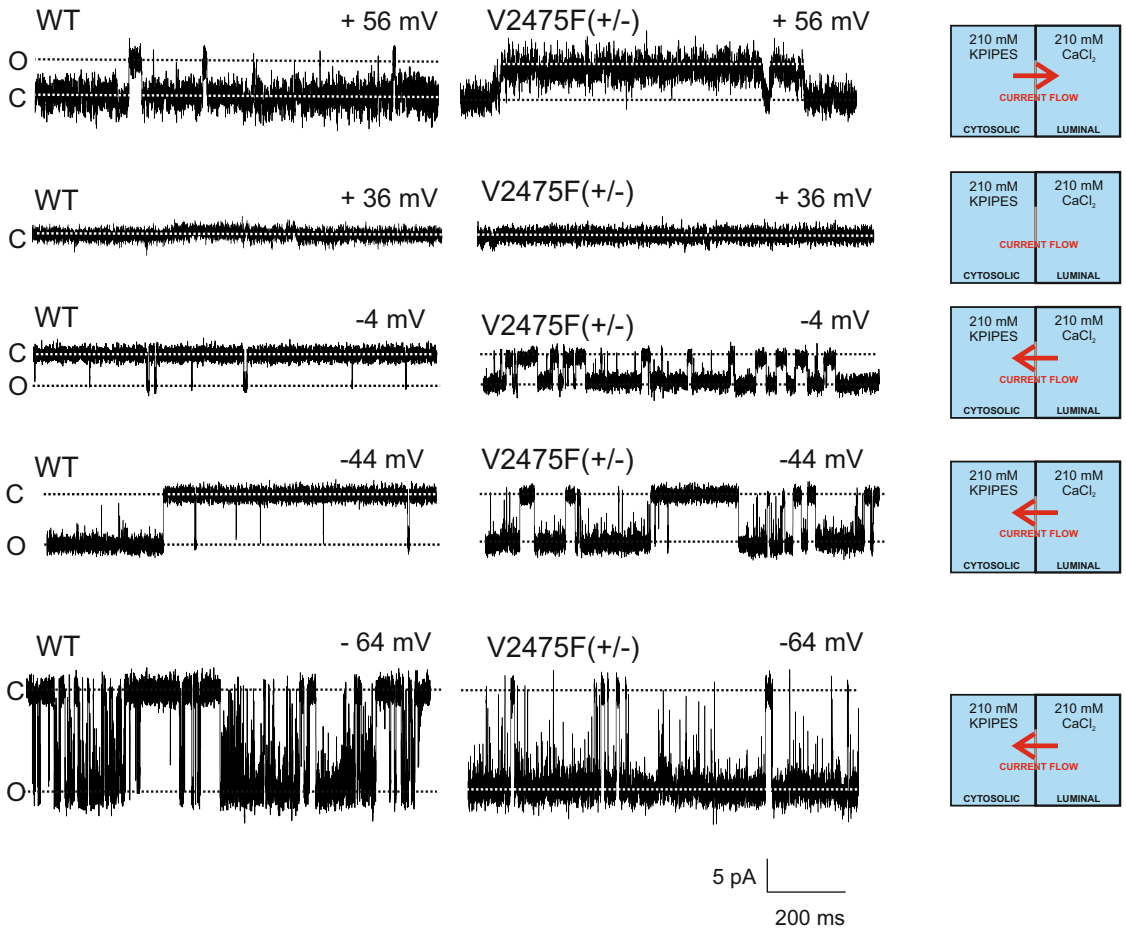


Figure 3.5: Comparison of single-channel relative Ca^{2+}/K^+ permeability of RyR2 channels from WT and V2475F(+/-) mice Representative single-channel recordings in 210 mM KPIPES, pH 7.2 (cytosolic) and 210 mM CaCl2 (luminal) at various holding potentials for WT (left) and V2475F(+/-) (right). A simplified model of the experimental conditions is shown to the right of the traces. In these conditions, 210 mM K^+ and 210 mM Ca^{2+} were the only permeant ions. Traces were filtered at 2 kHz. O and C represent the fully open and closed levels, respectively.

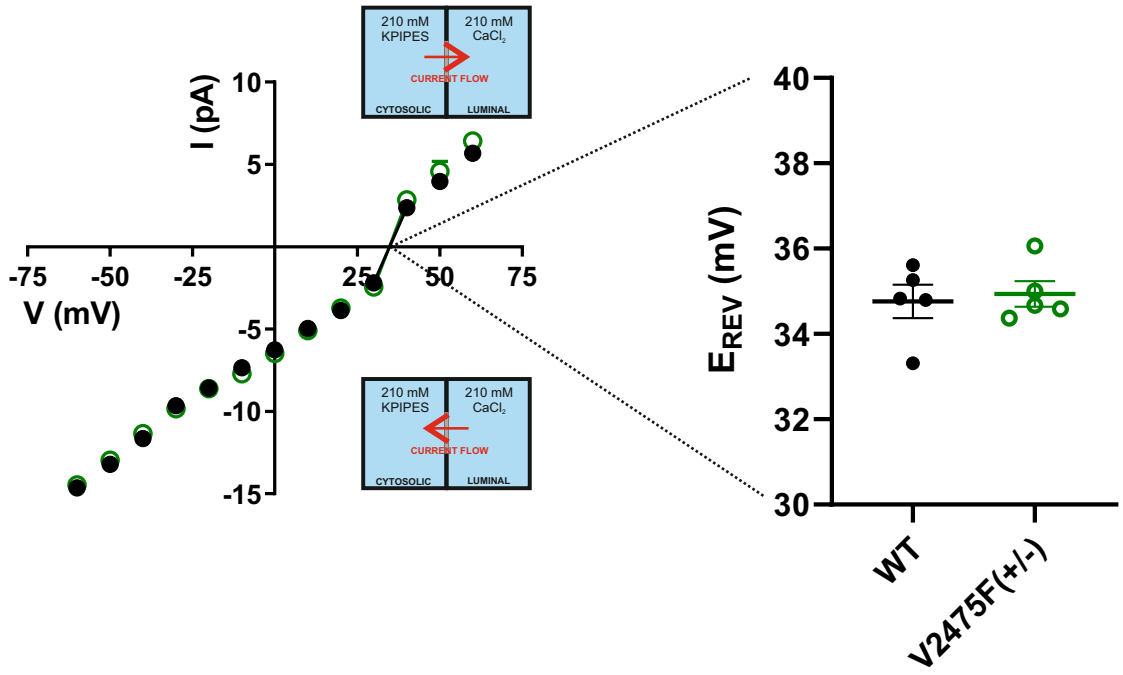


Figure 3.6: Comparison of single-channel relative Ca^{2+}/K^{+} permeability of RyR2 channels from WT and V2475F(+/-) mice Left: The single-channel current-voltage relationships with the same solutions as Fig. 3.5 are shown. Mean ± SEM, n = 5, for WT (black filled circles) and V2475F(+/-) (green open circles) channels are shown. Where not shown, error bars are within the symbol. Right: The individual E_{REV} values of WT (black) and V2475F(+/-) (green) channels (Mean ± SEM; p = 0.73) are plotted.

An increased prevalence of sub-conductance states has been suggested to be associated with the pathophysiology of CPVT1 (Wehrens et al., 2003; Meli et al., 2011). Sub-conductance state analysis was therefore performed on channels in which a sub-conductance state could be defined. As the openings of the RyR2 channels were typically very brief and close to the minimum duration resolvable, in order to be sure than an event was a 'sub-conductance state' rather than an event truncated by filtering it was important to only monitor events that were longer than the minimum resolvable event duration. Since the filtering rate used here was 800 Hz, events shorter than 2 ms were not included in the analysis. With this precondition, only one WT channel and two V2475F(+/-) channels were identified as gating in sub-conductance states in the total population of channels that were recorded in the same conditions. This accounts for sub-conductance states being observed in only 1.7% of WT and 2.8% of V2475F(+/-) channels in these same

conditions (χ^2, p = 0.68). Therefore, there was no evidence that sub-conductance states were more frequently observed in V2475F(+/-) channels compared to WT. The mean values of the single-channel sub-conductance levels appeared similar for WT and V2475F(+/-) channels at 2.50 pA for the one WT RyR2 channel, and 2.15 pA and 2.07 pA for the two V2475F(+/-) RyR2 channels.

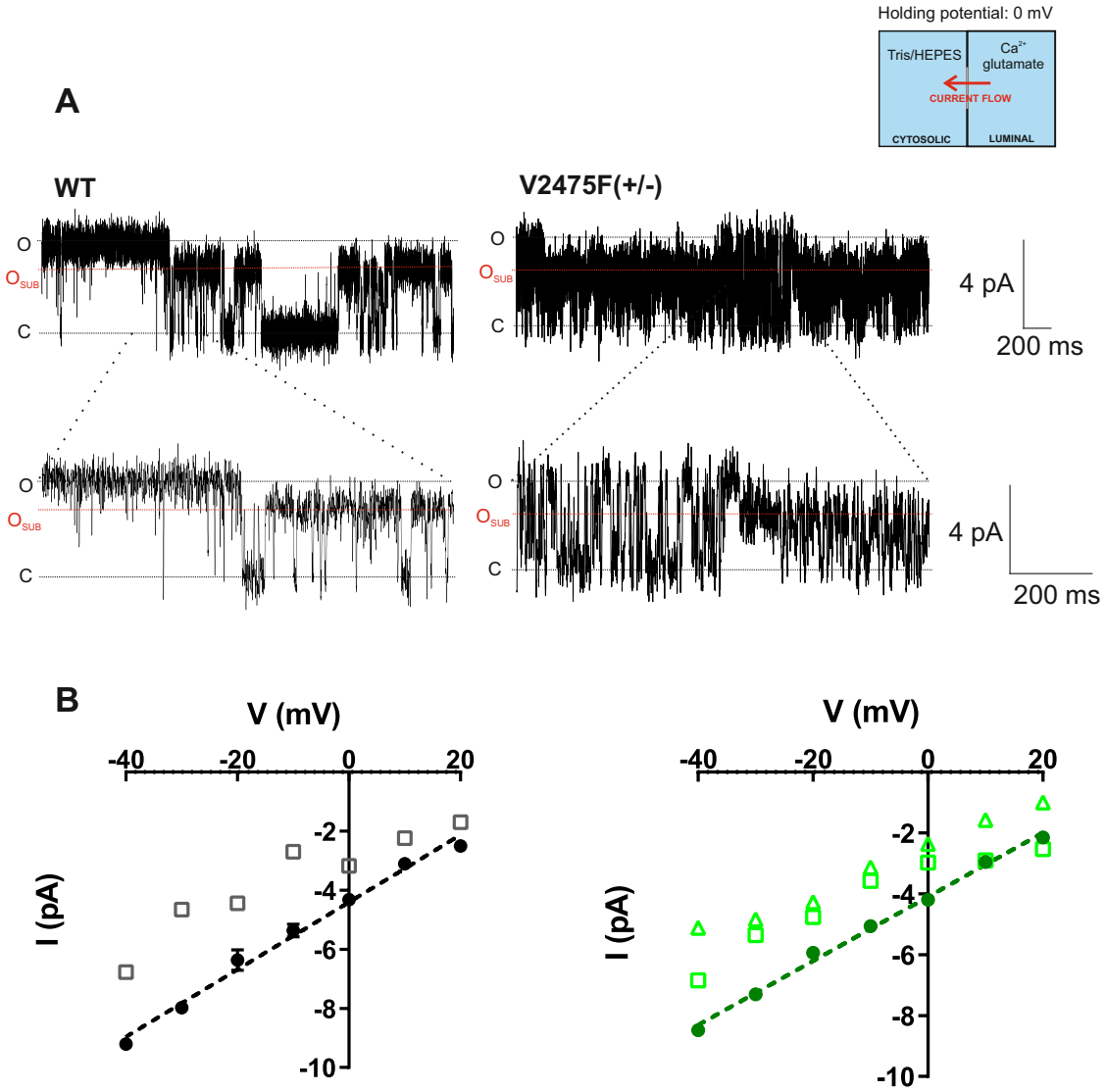


Figure 3.7: Comparison of the sub-conductance states of RyR2 channels from WT and V2475F(+/-) mice (A) Representative single-channel recordings in Tris/HEPES (cytosolic) and Ca^{2+} glutamate solutions (luminal) illustrating single-channel sub-conductance states for a WT (left) and V2475F(+/-) (right) RyR2 channel. The luminal Ca^{2+} was approximately 50 mM and the cytosolic free [Ca^{2+}] was 1 μM, with Ca^{2+} as the permeant ion. The holding potential was 0 mV. O and C represent the fully open and closed levels, respectively. O_{SUB} in red indicates the sub-conductance open levels. Traces were filtered at 800 Hz. The top traces show a 3 s recording, and the bottom traces show an expanded recording illustrating the transitions between a full opening and a sub-conductance opening. **(B)** Single-channel current-voltage relationships with the same solutions as (A) are shown for WT (black, left) and V2475F(+/-) (green, right) RyR2 channels. The filled symbols indicate the current-voltage relationships of full single-channel openings in Ca^{2+} which are taken from Fig. 3.2A. The open symbols indicate the current-voltage relationships of the individual channels gating in a sub-conductance state. A different symbol shape indicates a different channel.

3.3 Comparison of the RyR2 channel response to cytosolic Ca^{2+} from WT and V2475F(+/-) hearts

The response of WT and V2475F(+/-) derived RyR2 channels to increased cytosolic [Ca^{2+}] with Ca^{2+} as the permeant ion is displayed in Fig. 3.8. The representative channels shown in Fig. 3.8A illustrate that most WT and V2475F(+/-) derived RyR2 channels were completely closed (Po = 0) at 100 nM free [Ca^{2+}] (top traces). When [Ca^{2+}] was increased to 1 μM Ca^{2+}, Po increased in both groups of channels, although this was more marked in the V2475F(+/-) channels. At 1 μM Ca^{2+}, in both groups of channels, gating was characterised by very short open and closed events (middle traces). The bottom traces show how 1 mM Ca^{2+} was much more effective at inactivating V2475F(+/-) channels than WT channels. The V2475F(+/-) channels were almost fully inactivated by 1 mM Ca^{2+}, whereas the WT channels were still gating with a high Po. No other ligands were present to ensure the different response was solely because of cytosolic Ca^{2+}.

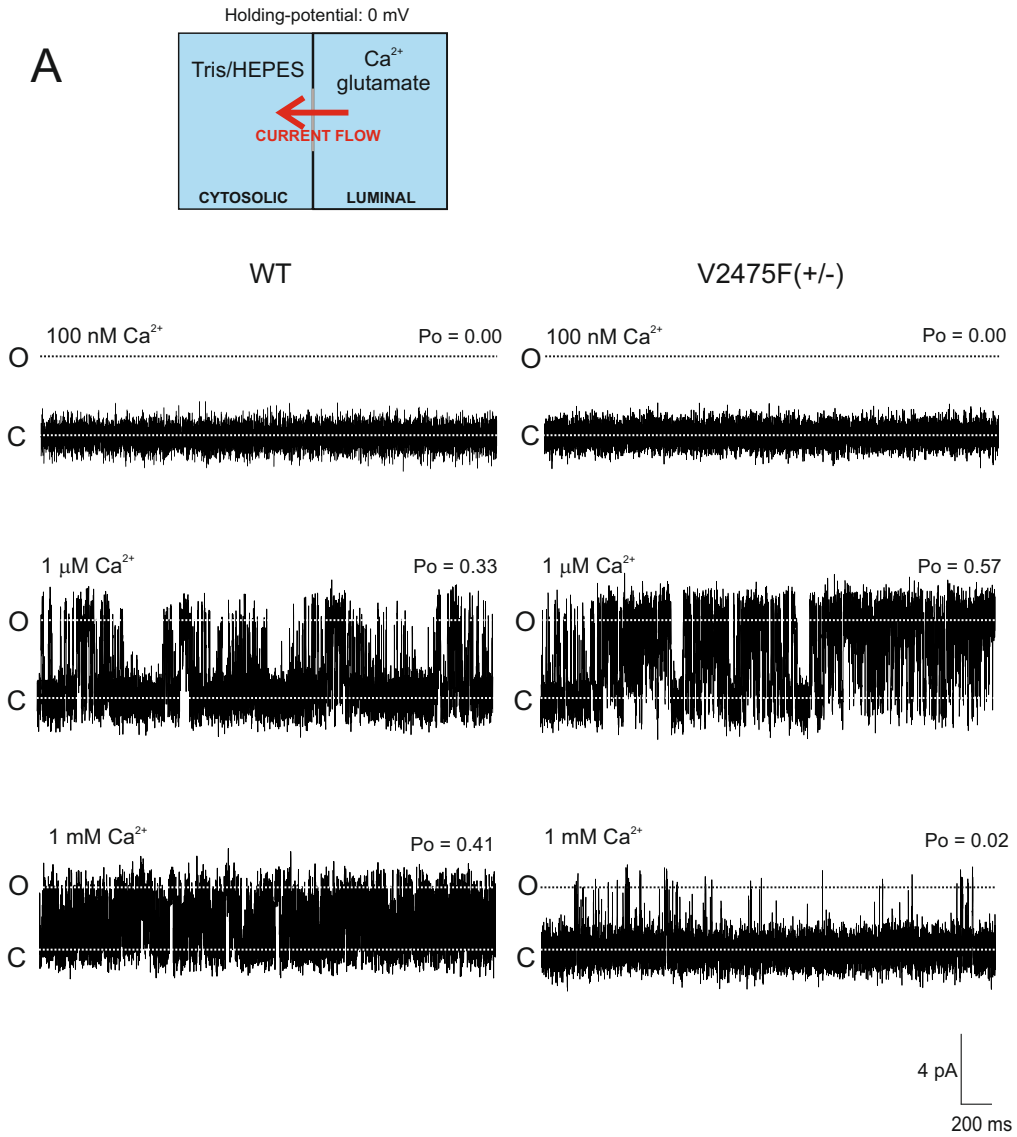


Figure 3.8: Effects of the V2475F mutation on the response of RyR2 channels to cytosolic Ca^{2+} (A) Representative single-channel traces in Tris/HEPES and Ca^{2+}-glutamate solutions, illustrating the effects of varying cytosolic Ca^{2+} on gating and conductance for WT (left panel) and V2475F(+/-) (right panel) RyR2 channels. The holding potential was 0 mV. Cytosolic free [Ca^{2+}] was 1 μM and luminal Ca^{2+} was approximately 50 mM, therefore, Ca^{2+} was the permeant ion flowing in the luminal to cytosolic direction. A simplified model of the experimental conditions is shown above the traces. Traces were filtered at 800 Hz. Po displayed above the traces was the average Po measured over 3 min of recording. O and C represent the fully open and closed levels, respectively.

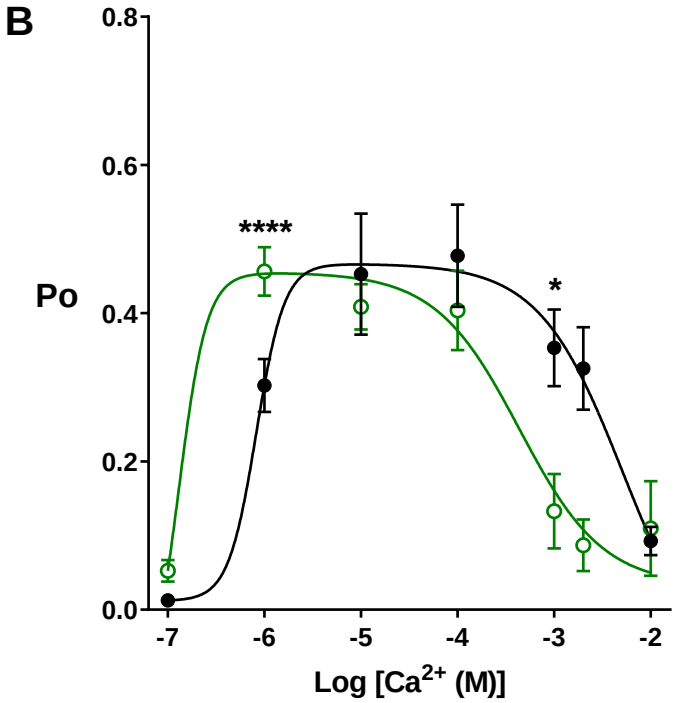


Figure 3.8: (Cont.) Effects of the V2475F mutation on the response of RyR2 channels to cytosolic Ca^{2+} (B) Relationship between [Ca^{2+}] and Po values for RyR2 channels derived from WT (black) or V2475F(+/-) (green) mouse hearts. Two-way ANOVA: Ca^{2+}-by-genotype interaction, $p < 0.0001$; main effect of Ca^{2+}, $p < 0.0001$; no main effect of genotype $p = 0.07$. Post-hoc multiple comparisons with Sidak's correction comparing WT and V2475F(+/-) at each [Ca^{2+}]: significant differences between WT and V2475F(+/-) are indicated by **** for $p < 0.0001$ at 1 μM Ca^{2+}, and by * for $p = 0.04$ at 1 mM Ca^{2+}. For clarity, only significant differences across genotype are shown. Each point represents n = 8 – 110 for WT and n = 5 – 95 for V2475F(+/-) channels. Lines display non-linear bell-shaped fitted curves. EC_{50} values were 0.83 μM for WT and 0.17 μM for V2475F(+/-), and IC_{50} values were 5.18 mM for WT and 0.43 mM for V2475F(+/-).

Fig. 3.8B shows the mean data comparing the response of the WT and V2475F(+/-) derived channels. Both groups presented a biphasic response to the full range of activating and inactivating cytosolic [Ca^{2+}]. Although most of the channels did not open at 100 nM Ca^{2+}, it is important to note that 14% of WT and 20% of the V2475F(+/-) channels did open at 100 nM Ca^{2+} and the gating properties of this critical subset of channels are illustrated later in this chapter. Fig. 3.8B clearly illustrates that the mutation causes a leftward shift in the bell-shaped [Ca^{2+}]-response relationship and at 1 μM cytosolic Ca^{2+} the Po of the V2475F(+/-) RyR2 channels was significantly higher than that of WT channels.

Based on the line fitted through the points, the EC_{50} values were 0.83 μM for WT and 0.17 μM for V2475F(+/-) derived channels.

The plateau of the [Ca^{2+}]-response relationship indicated that the maximum response of WT channels occurred at approximately 100 μM Ca^{2+}, similar to sheep cardiac RyR2 (Ashley and Williams, 1990; Sitsapesan and Williams, 1994a), whereas the V2475F(+/-) channels appeared to already be maximally activated at 1 μM. In the millimolar Ca^{2+} range, the V2475F(+/-) channels were more readily inactivated; IC_{50} values were 5.18 mM for WT and 0.43 mM for V2475F(+/-) channels and at 1 mM cytosolic Ca^{2+} the Po of the V2475F(+/-) RyR2 channels was significantly lower than that of WT channels. With further increase of cytosolic Ca^{2+} to 10 mM, both the WT and V2475F(+/-) channels were inactivated by Ca^{2+}.

Unless otherwise stated, all the subsequent experiments in this chapter were performed using the same recording conditions as used in Fig. 3.8 which is displayed in the schematic of the bilayer recording chambers shown above the traces.

To understand the mechanisms underlying the different response to Ca^{2+} resulting from the V2475F mutation, mean open and closed times were evaluated. Fig. 3.9A demonstrates the trend for Ca^{2+}-induced decreases in mean open time. This relationship was more pronounced for V2475F(+/-) channels than for WT channels with a 3.7-fold reduction versus a 2.1-fold reduction, respectively, when Ca^{2+} was increased from 100 nM to 1 μM. At 10 μM Ca^{2+} the mean open times of WT channels were variable, possibly because of some longer opening states as the maximally activated [Ca^{2+}] for WT was approached. In contrast, the open times of the V2475F(+/-) channels were always brief at [Ca^{2+}] above 1 μM. The longest open times were observed at 100 nM Ca^{2+} in those channels that did open, and the V2475F(+/-) channels were characterised by significantly longer openings than WT channels at this [Ca^{2+}]. The gating characteristics at 100 nM Ca^{2+} are explored in more detail later in Section 3.4.

Although mean open times changed with increasing [Ca^{2+}] for both WT and V2475F(+/-) channels, the primary mechanism producing Ca^{2+}-activation was an

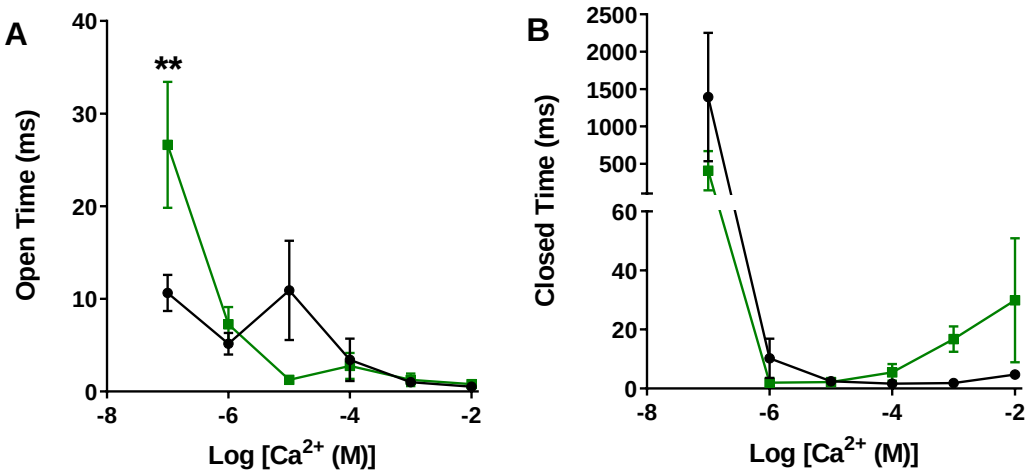


Figure 3.9: The effects of cytosolic Ca^{2+} on RyR2 channel mean open and closed times from WT or V2475F(+/-) mouse hearts with Ca^{2+} as the permeant ion (A) Mean open times (n $\geq$ 5) for RyR2 derived from WT (black) and V2475F(+/-) (green) mice with increasing cytosolic Ca^{2+}. At pCa = 7, only channels that opened at this low [Ca^{2+}] were included. Where not shown, error bars are within the symbol. Two-way ANOVA: Ca^{2+}-by-genotype interaction, p =0.03; main effect of Ca^{2+}, p < 0.0001; no main effect of genotype p = 0.57. Post-hoc multiple comparisons with Sidak's correction comparing WT and V2475F(+/-) for each [Ca^{2+}]: significant differences between WT and V2475F(+/-) are indicated by ** for p = 0.002 at 100 nM Ca^{2+}. For clarity, only significant differences across genotype are shown. (B) Mean closed times (n $\geq$ 5) for RyR2 derived from WT (black) and V2475F(+/-) (green) mice with increasing cytosolic Ca^{2+}. At pCa = 7, only the closed times for channels that opened were included. Where not shown, error bars are within the symbol. Two-way ANOVA: no Ca^{2+}-by-genotype interaction, p = 0.65; no main effect of Ca^{2+}, p = 0.06; no main effect of genotype p = 0.55.

increase in the frequency of channel opening as shown by the marked decrease in mean closed times (Fig. 3.9B) following the increase in cytosolic [Ca^{2+}] from 100 nM to 1 μM. In V2475F(+/-) channels, this was more pronounced with a 208-fold decrease in comparison to the 136-fold decrease for WT channels.

In both WT and V2475F(+/-) channels, Ca^{2+}-induced inactivation appeared to be caused by the combination of a decrease in mean open times and a more marked decrease in the frequency of openings. The V2475F(+/-) channels had a more prominent increase in mean closed times at millimolar [Ca^{2+}] suggesting that this mechanism is important for the more readily inactivated V2475F(+/-)

channels. For example, at 1 mM Ca^{2+}, the mean closed times were 8.8-fold greater for V2475F(+/-) channels compared to WT.

Lifetime analysis was performed across the range of $[Ca^{2+}]$ to elucidate alterations to gating components caused by the V2475F mutation. Only experiments where a single channel was present in the bilayer could be used for this analysis. The representative open and closed lifetime distributions of a typical RyR2 channel derived from WT (black) or V2475F(+/-) (green) mouse hearts are illustrated in Fig. 3.10 and 3.11 for 1 μM and 1 mM Ca^{2+}, respectively. Representative lifetime analysis was displayed to compare the $[Ca^{2+}]$ in which the significant difference in Po caused by the mutation was observed (Fig. 3.8), at 1 μM and 1 mM cytosolic $[Ca^{2+}]$.

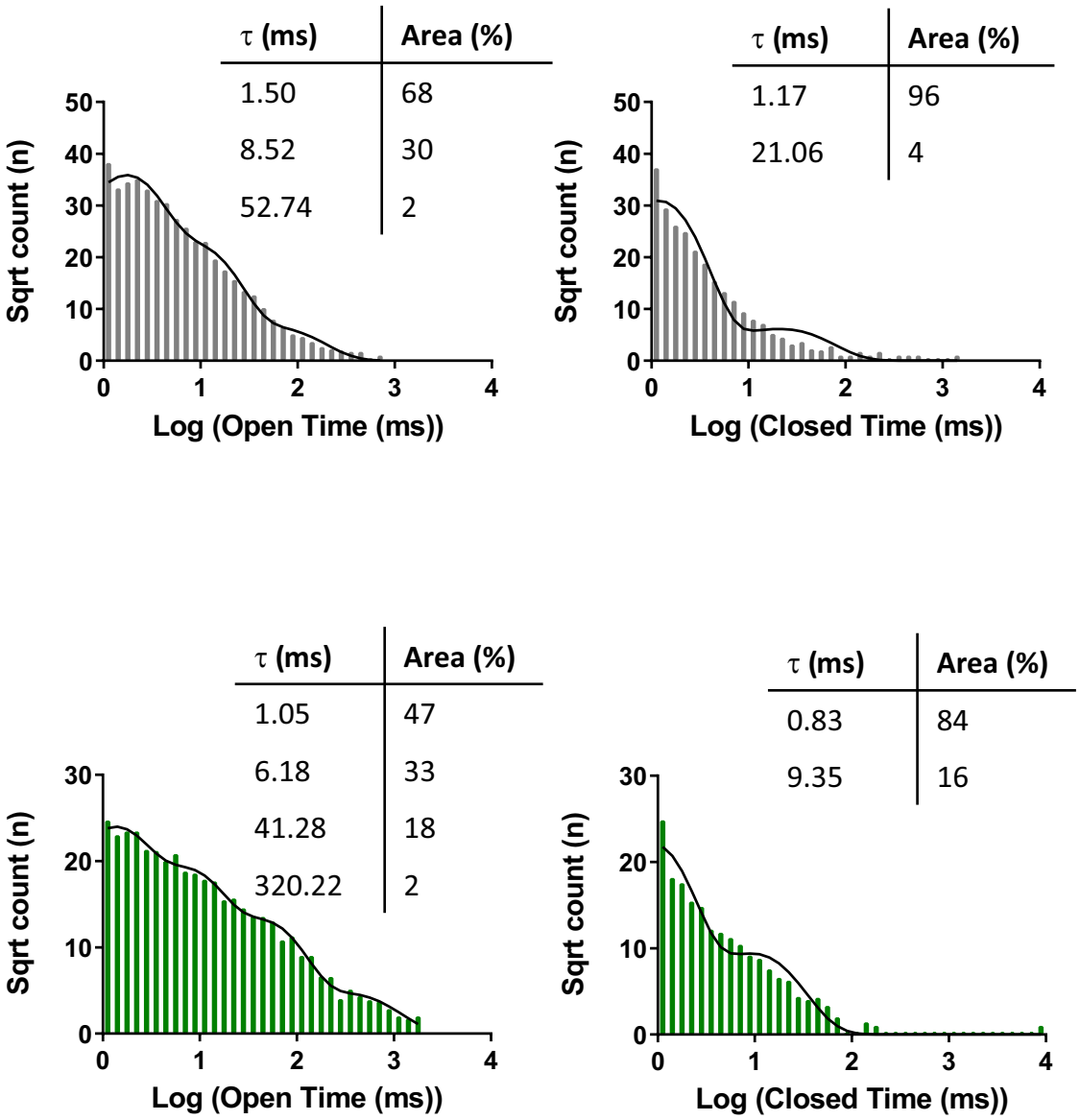


Figure 3.10: Representative open and closed lifetime distributions of single RyR2 channels in response to 1 μM cytosolic Ca^{2+} Lifetime distributions and pdfs for a typical single RyR2 derived from WT (grey) or V2475F(+/-) (green) mouse hearts are shown. The best fits to the data were obtained by the method of maximum likelihood and the resulting time constants (τ, ms) and percentage areas (%) are displayed next to each graph.

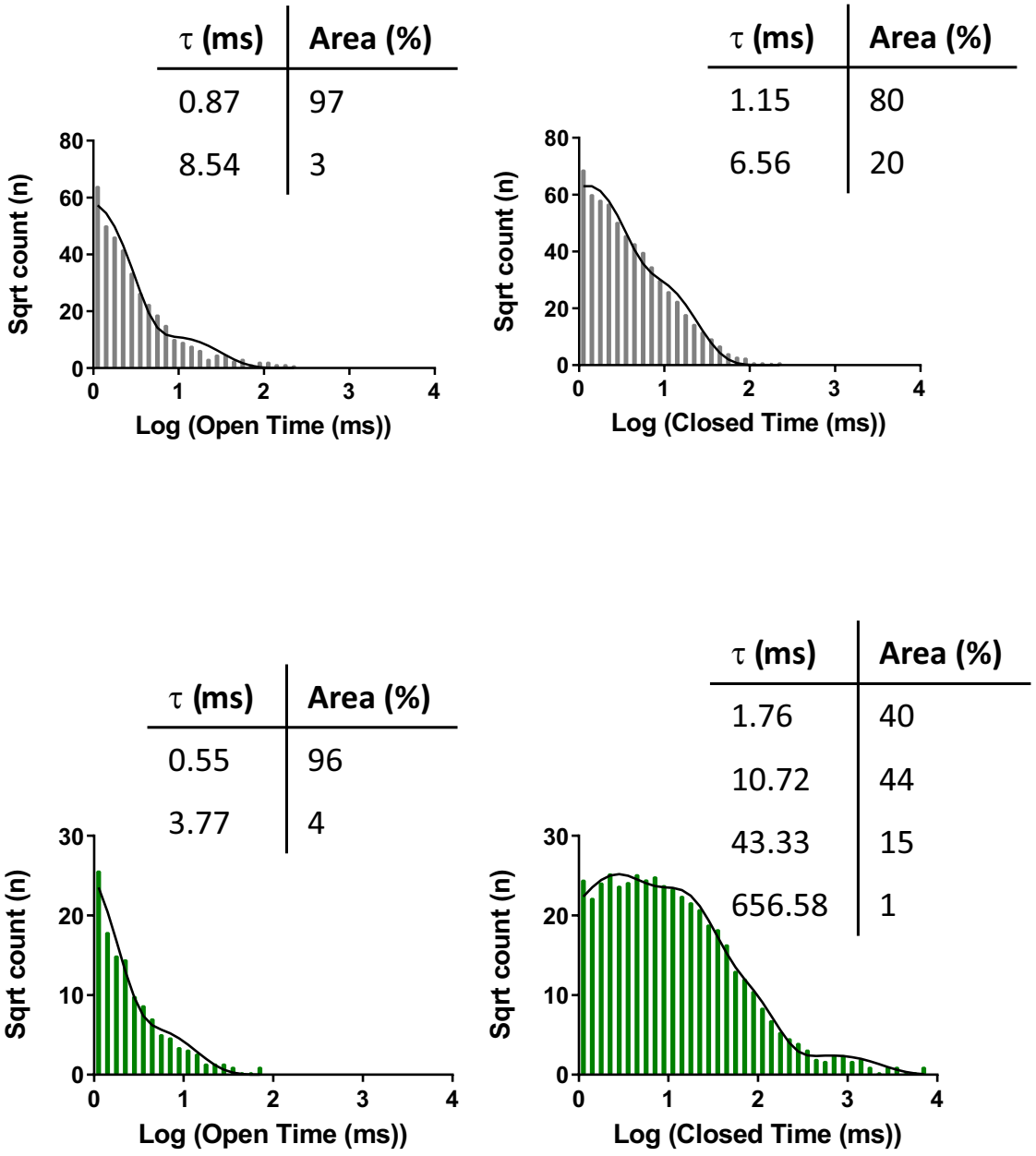


Figure 3.11: Representative open and closed lifetime distributions of single RyR2 channels in response to 1 mM cytosolic Ca^{2+} Lifetime distributions and pdfs for typical single RyR2 channels derived from WT (grey) or V2475F(+/-) (green) mouse hearts are shown. The best fits to the data were obtained by the method of maximum likelihood and the resulting time constants (τ, ms) and percentage areas (%) for the representative single RyR2 channel are displayed next to each graph.

As shown in Fig. 3.10, at 1 μM Ca^{2+}, the open lifetime distribution for the V2475F(+/-) channel could be fit to an extra fourth tau (τ) exponential which does not exist in the WT distribution, indicating an extra exponential of long

openings. 38% of the V2475F(+/-) single channels analysed were fit to a fourth open exponential compared to 0% of WT channels. The closed lifetime distribution displays a similar distribution for WT and V2475F(+/-) channels, but with shorter τ values at every exponential for V2475F(+/-) channels. This was in line with the shorter mean closed time observed at 1 μM Ca^{2+} in Fig. 3.9.

As shown in Fig. 3.11, at 1 mM Ca^{2+}, the closed lifetime distributions for V2475F(+/-) channels were frequently fit to an extra long fourth exponential. In comparison, the closed lifetime distributions of WT channels were usually best fit by only two exponentials at this [Ca^{2+}] although a third longer exponential representing only a few longer closings was sometimes present. Thus, 60% of the V2475F(+/-) channels at 1 mM exhibited four closed time constants, whereas 0% of WT channels were fit to this many exponentials. The open lifetime distributions appeared similar for WT and V2475F(+/-) channels at 1 mM Ca^{2+}, indicating that the important mechanism causing the difference in Ca^{2+} inactivation in V2475F(+/-) channels was the slowed rate of channel opening.

Lifetime analysis as in the representative examples of Fig. 3.10 and 3.11 was conducted on all single channels across the range of [Ca^{2+}]. The mean values of the calculated pdf parameters are summarised in Fig. 3.12A/B and 3.12C/D to allow comparison of the important lifetime features of the WT and V2475F(+/-) channels. In the activating range of cytosolic Ca^{2+}, the trends for decreasing open lifetime τ values with increasing cytosolic [Ca^{2+}] were demonstrated for both WT and V2475F(+/-) channels. However, with the exception of the shortest time constant, all τ values were longer for V2475F(+/-) channel open lifetimes compared to WT (Fig. 3.12). Further, WT channel distributions did not display the third and fourth longest time constants which occurred in some V2475F(+/-) channels (Fig. 3.12).

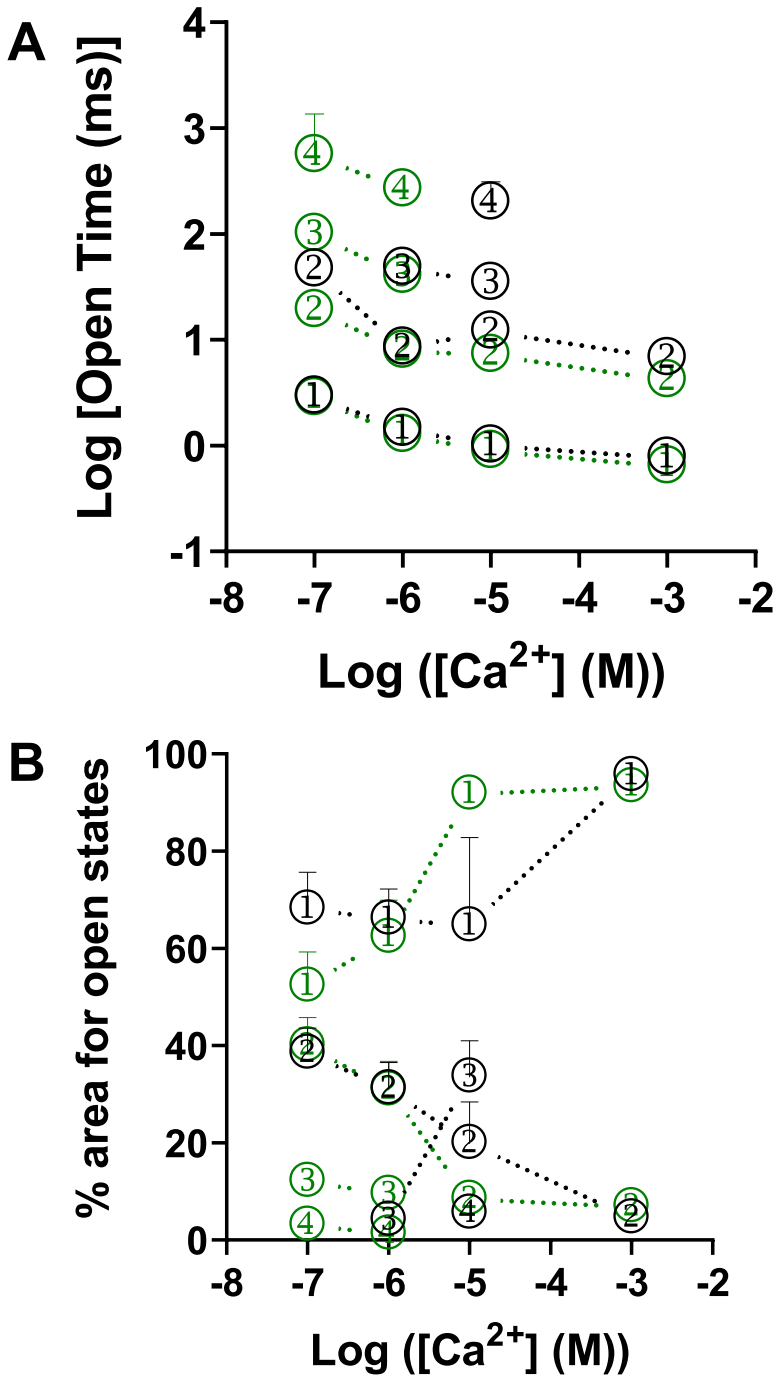


Figure 3.12: Comparison of the mean open lifetime parameters with increasing cytosolic [Ca^{2+}] for single RyR2 channels derived from WT (black) or V2475F(+/-) (green) mouse hearts The numbers within the symbols refer to the 1st (shortest), 2nd, 3rd, and 4th time constants (τ). Mean ± SEM, n ≥ 4 (except for long open 3rd or 4th exponentials which did not occur in all channels where n ≥ 2). **(A)** The relationship between cytosolic [Ca^{2+}] and the open time constants (τ) of the pdfs to the open lifetime distributions **(B)** and their respective % areas.

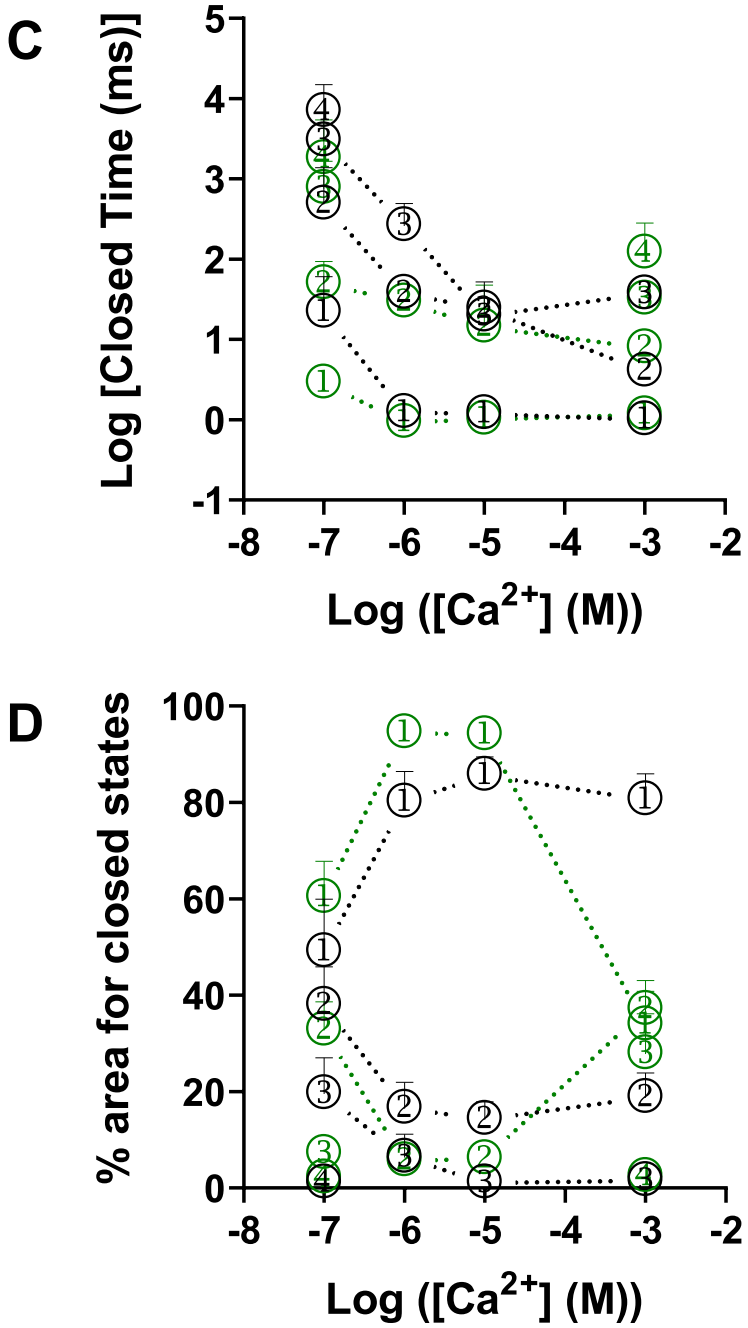


Figure 3.12: (Cont.) Comparison of the mean closed lifetime parameters with increasing cytosolic [Ca^{2+}] for single RyR2 channels derived from WT (black) or V2475F(+/-) (green) mouse hearts The numbers within the symbols refer to the 1st (shortest), 2nd, 3rd, and 4th time constants (τ). Mean ± SEM, n ≥ 4 **(C)** The relationship between cytosolic [Ca^{2+}] and the closed time constants (τ) of the pdfs to the closed lifetime distributions **(D)** and their respective % areas.

At 100 nM, both WT and V2475F(+/-) channels exhibited long closed time constants; this feature was investigated in more detail later in section 3.4. As Ca^{2+} was raised from 100 nM to 1 μM, the closed τ values became shorter for both WT and mutant channels, however, a higher proportion of closings occurred to the shortest exponential (τ1) in the V2475F(+/-) distributions (Fig. 3.12D). For example, at 1 μM cytosolic Ca^{2+}, on average, 80% of WT closings compared to 94% of mutant channel closings occurred to the shortest closed exponential. This greater increase in frequency of opening of the V2475F(+/-) channels explains the lower EC_{50} value and the higher Po activity at 1 μM Ca^{2+} compared to WT (Fig. 3.8)

Lifetime analysis also elucidated mechanisms causing the hyper-sensitivity of V2475F(+/-) channels to Ca^{2+} induced inactivation. At high [Ca^{2+}], the V2475F(+/-) channel open lifetime distributions lose the third and fourth long open exponentials that can be observed at lower [Ca^{2+}] (Fig. 3.12). WT and V2475F(+/-) channels exhibited similar duration and distribution of open lifetime parameters at 1 mM Ca^{2+}, with very brief open durations shorter (< 1 ms) than is fully resolvable at this filtering rate (Fig. 3.12). The key difference at 1 mM cytosolic Ca^{2+} between the two genotypes was the proportion of closings that were brief; 34% of closings occur to the shortest time constant for V2475F(+/-) channels in comparison to 81% in WT (Fig. 3.12D). This results in the frequency of openings being greatly reduced in the V2475F(+/-) channels, thereby reducing the V2475F(+/-) channel activity.

3.4 Effects of the V2475F mutation on channel response to 100 nM [Ca^{2+}]

100 nM is a critical [Ca^{2+}] to investigate since the cytosolic [Ca^{2+}] during diastole in a cardiomyocyte is approximately this concentration (Eisner et al., 2020). As shown earlier in the top traces of Fig. 3.8, at 100 nM Ca^{2+}, most WT (86%; n = 115) and V2475F(+/-) mutant (80%; n = 95) channels did not open at all (Fig. 3.13A), and only opened after increasing Ca^{2+} to 1 μM. Some channels did open at 100 nM Ca^{2+}, but there was no significant difference in the proportion of

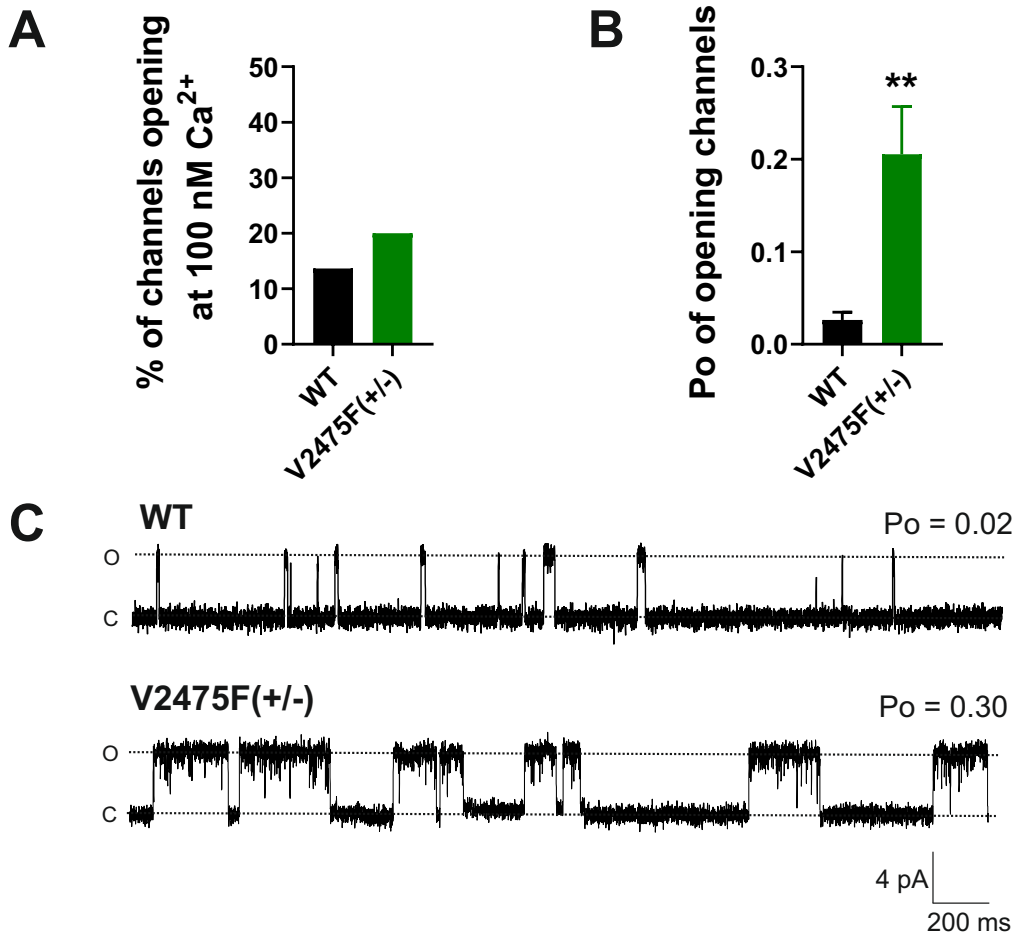


Figure 3.13: The effect of the V2475F mutation on the response of RyR2 channels to 100 nM cytosolic Ca^{2+} (A) The proportion of channels that opened at 100 nM Ca^{2+} is shown as a percentage (%) with n = 110 and n = 95 for WT and V2475F(+/-) channels, respectively (χ^2: no significant difference, p = 0.22). **(B)** The mean Po values ± SEM of single channels that opened at 100 nM Ca^{2+} are displayed. Only channels that did open at 100 nM Ca^{2+} were included for WT (n = 15) and V2475F(+/-) (n = 19) Unpaired t-test: significant differences between WT and V2475F(+/-) are indicated by ** for p = 0.005. **(C)** Representative single-channel recordings from RyR2 derived from WT and V2475F(+/-) hearts that did open in response to 100 nM cytosolic Ca^{2+}. Po displayed was for the full 3 min recording. C and O indicate the closed and open states, respectively.

V2475F(+/-) channels that opened compared to that of WT channels. However, when V2475F(+/-) channels did open, they did so with significantly higher Po than WT channels (Fig. 3.13B). Representative single channel recordings (Fig. 3.13C) demonstrate the typically longer openings of the V2475F(+/-) channels at 100 nM Ca^{2+}. As already shown in Fig. 3.9, mean open times were significantly longer for V2475F(+/-) channels than for WT channels at 100 nM Ca^{2+}.

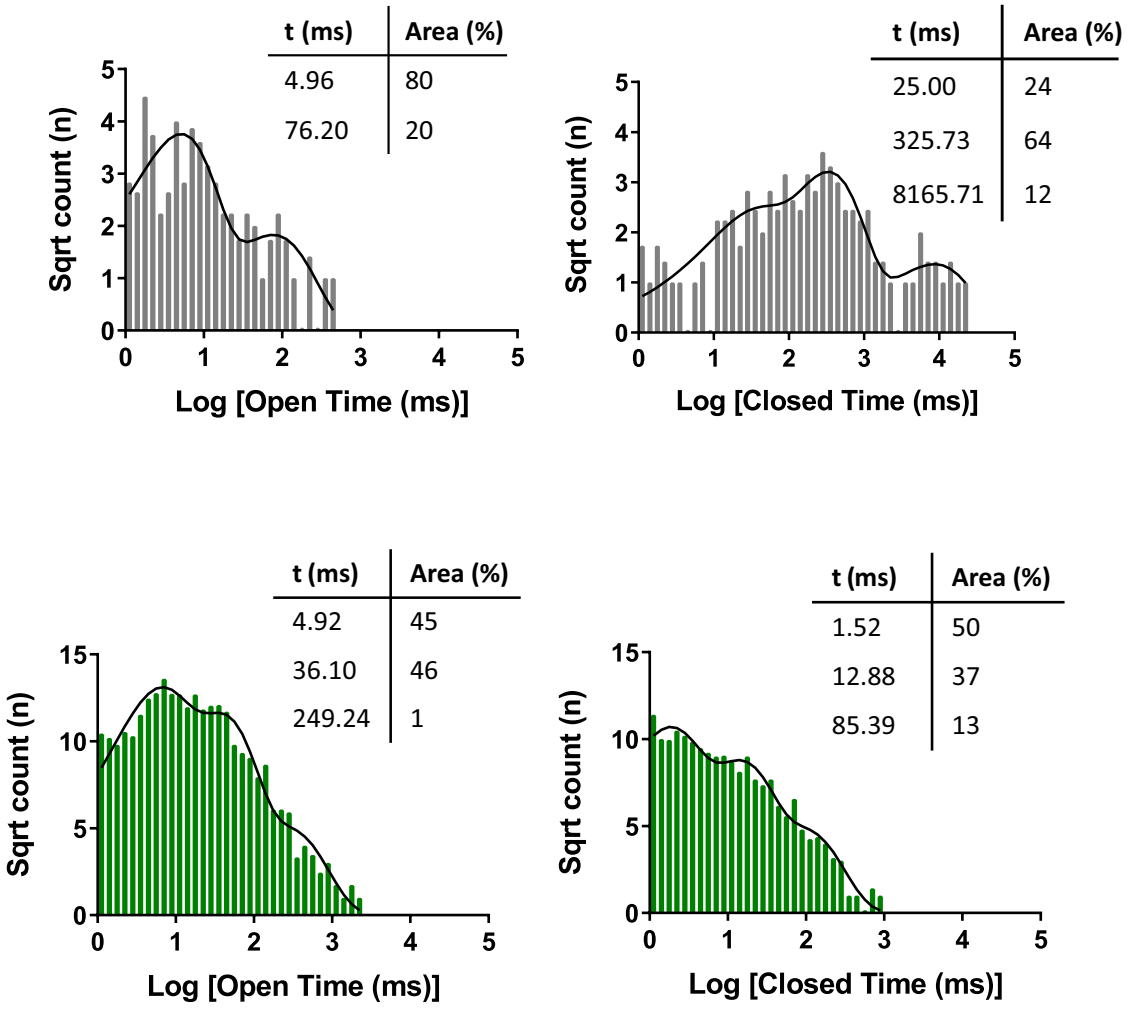


Figure 3.14: Effects of the V2475F mutation on open and closed lifetime distributions at 100 nM cytosolic [Ca^{2+}] Open (left) and closed (right) lifetime distributions and pdfs are displayed for representative single RyR2 channels derived from WT (black) or V2475F(+/-) (green) mice in the presence of 100 nM cytosolic Ca^{2+}. The best fits to the data were obtained by the method of maximum likelihood and the resulting time constants (τ) and percentage areas (%) for the representative single RyR2 channels are displayed next to each histogram.

Lifetime analysis provided further insight into the altered gating behaviour of mutant channels that opened at 100 nM Ca^{2+}. Only experiments where a single channel was present in the bilayer which opened at 100 nM were used for this analysis. The open and closed lifetime distributions for a typical WT and V2475F(+/-) channel that opened at 100 nM cytosolic Ca^{2+} are shown in Fig. 3.14 with the mean lifetime parameters of all single channels recorded at this

concentration detailed earlier in Fig. 3.12A/B and 3.12C/D. The open lifetime distributions of WT channels at 100 nM Ca^{2+} were best fit by one or two short time constants. In contrast, three or four exponentials were required to best fit the open lifetime distributions of V2475F(+/-) channels, and there was a greater proportion of long open events. This is also clearly shown in the trace in Fig. 3.13C.

The closed lifetime distributions of both WT and V2475F(+/-) channels were both usually described by at least three time constants. WT channels tended to have some very long closed states, whereas for V2475F(+/-) channels this was less common. A large proportion of the V2475F(+/-) channel closings occurred to the shortest time constant, close to the minimum resolvable event duration (< 1 ms). As exemplified in the trace in Fig. 3.13C, these very brief closings occurred within bursts of openings. Burst analysis was therefore performed to further understand these gating characteristics at 100 nM Ca^{2+}.

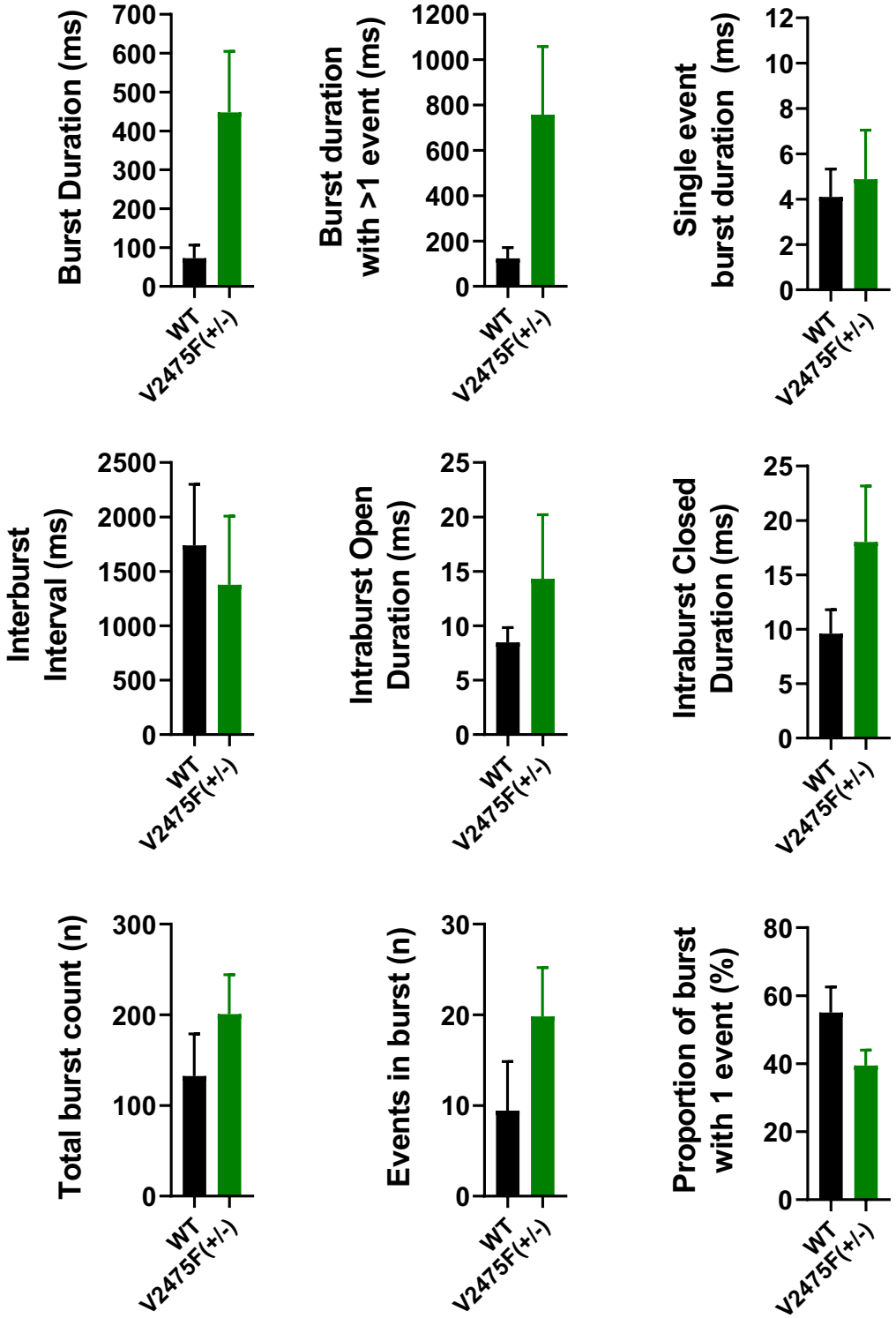


Figure 3.15: Burst analysis parameters at 100 nM cytosolic Ca^{2+} comparing WT (black) and V2475F(+/-) (green) single channels Burst analysis was performed on single channels at 100 nM cytosolic Ca^{2+} in those channels that did open. Burst parameters are compared in bar charts as mean ± SEM with n = 6 for WT and n = 10 for V2475F(+/-) channels. The y-axes are not equivalent scales nor units.

Table 3.1: Burst analysis parameters at 100 nM cytosolic Ca^{2+} comparing WT and V2475F(+/-) single-channels The same data for burst analysis as in Fig. 3.15 is displayed in a table to compare differences between WT and V2475F(+/-) channels. The burst parameter and appropriate units are listed in the first column, and the data is displayed as mean ± SEM. Significant differences between WT and V2475F(+/-) channels were computed from an unpaired t-test, and the p value is given in the final column.

PARAMETER	**WT**	**V2475F(+/−)**	**p-value**
	MEAN ± SEM	**MEAN** ± SEM	
Burst duration (ms)	72.7 ± 33.8	447.7 ± 157.2	0.09
Burst duration with >1 event (ms)	123.3 ± 48.4	757.5 ± 300.6	0.13
Burst duration of 1 event (ms)	4.1 ± 1.2	4.9 ± 2.2	0.80
Interburst interval (ms)	1739.6 ± 559.9	1377.9 ± 629.7	0.70
Intraburst open duration (ms)	8.5 ± 1.4	14.3 ± 5.9	0.46
Intraburst closed duration (ms)	9.6 ± 2.2	18.0 ± 5.1	0.24
Total burst count (n)	132.5 ± 46.5	200.7 ± 43.5	0.33
Events in burst (n)	9.4 ± 5.4	19.8 ± 5.4	0.22
Proportion of bursts with 1 event (%)	55.0 ± 7.5	39.4 ± 4.6	0.08

The burst analysis showed that, comparing WT and V2475F(+/-) derived RyR2 channels, there was no difference in the interburst interval and the intraburst closed time was not shorter. This suggested that Ca^{2+} binding to the closed state of the channel to cause channel opening was not affected by the V2475F mutation. This was also confirmed by the fact that the proportion of channels that do open was not significantly different between WT and V2475F(+/-) derived channels (Fig. 3.13A). As shown previously, the Po in response to Ca^{2+} was altered by the V2475F mutation (Fig. 3.8). Notably, at 100 nM Ca^{2+}, the V2475F(+/-) channels that did open exhibited significantly higher Po than that of WT channels (Fig. 3.13B). V2475F(+/-) RyR2 channels displayed a 6.15-fold elongation of burst duration, and bursts with > 1 opening were also 6.14-times longer compared to WT channels.

Further, although not significant, there were trends towards a greater proportion of bursts with more than 1 event and for an increased number of events within each burst for V2475F(+/-) channels in comparison to WT channels. Taken together, the evidence from burst analysis suggests that, at this [Ca^{2+}], the V2475F mutation increases the affinity for Ca^{2+} to the open state, thereby prolonging open event duration.

3.5 Populations of V2475F(+/-) channels

Since the V2475F(+/-) mouse model is heterozygous for the mutation, a mixed population of RyR2 channels with varying numbers of mutated monomers in each tetrameric RyR2 channel was expected. Assuming equal synthesis of each monomer type and random assembly of a binomial distribution, the populations of different channels were expected to exist in the proportions shown in the schematic in Fig. 3.16. The presence of population groups within the data obtained was therefore examined.

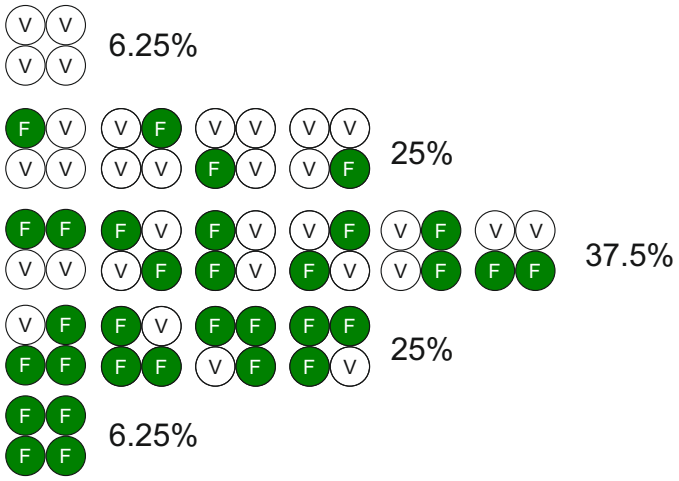


Figure 3.16: Populations of RyR2 channels derived from V2475F(+/-) hearts Schematic showing the proportions (%) of each population expected of RyR2s isolated from V2475F heterozygous mouse tissue. A different number of mutated monomers are expected in each tetrameric channel. A white circle with V indicates a WT monomer with a valine at amino acid position 2475, and a green circle with F indicates a V2475F mutated monomer with a phenylalanine at position 2475.

As large data sets for Po values at 1 μM cytosolic Ca^{2+} were collected, it was possible to examine the population distribution. Po-frequency histograms for WT and V2475F(+/-) channels were plotted and pdf fitting was attempted (Fig. 3.17). The WT channel data was best fit by a single exponential indicating one single population characterised by a Po of 0.10. The Po-frequency distribution for V2475F(+/-) mutated channels could not be fitted with a pdf. However, apparent Po populations were observed in the frequency histogram for V2475F(+/-) channels. A kernel density estimate (KDE) was therefore used to identify these different

populations of V2475F(+/-) channels according to their activity (Fig. 3.17B, bottom). The KDE suggested the presence of four populations indicated by the green triangles on four peaks, including several populations of Po values higher than observed for WT channels. The four peaks corresponded to Po values of 0.07, 0.33, 0.61 and 0.89. The traces corresponding to each population provide examples of the type of gating exhibited by the V2475F(+/-) channels at these variable activity levels (Fig. 3.17C).

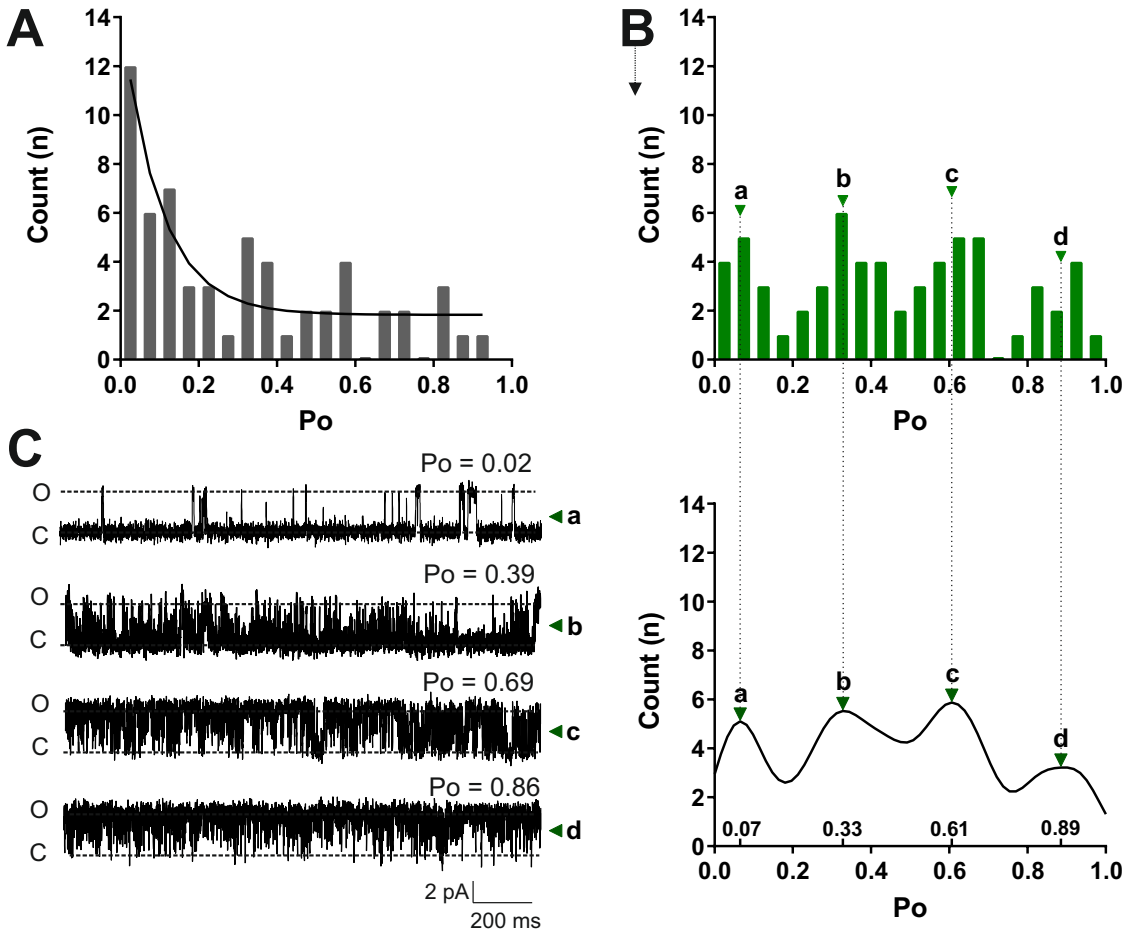


Figure 3.17: The V2475F mutation changes the population frequency of high Po RyR2 channels isolated from heterozygous mouse cardiac muscle The Po values of individual channels were plotted as frequency distributions for WT (**(A)**, n = 59) and V2475F(+/-) (**(B)** top, n = 62) channels in the presence of 1 μM cytosolic Ca^{2+}. The WT distribution was best fit by a pdf determined by maximum likelihood fitting to one exponential, showing a Po constant of 0.10 with an area of 100%. The V2475F(+/-) channel distribution could not be fitted using this method (**(B)**, top). A kernel density estimate (KDE) (**(B)** bottom) was subsequently computed which estimated 4 peaks, and therefore the presence of at least four different populations of activity. The gating behaviour of typical V2475F(+/-) channels drawn from these populations are shown in the four traces in **(C)** labelled a-d and indicated by the green triangle for the corresponding exponential from the KDE. O and C are the open and closed levels, respectively. Po displayed above the traces was the average Po measured over 3 min of recording.

Fig. 3.2B illustrated that there was a wide range of single-channel Ca^{2+} conductance values for the V2475F(+/-) channels (from 90.5 to 118.7 pS). Since populations of Po were observed in the V2475F(+/-) channels in response to 1 μM cytosolic Ca^{2+} (Fig. 3.17) it was therefore investigated whether differences in single-channel Ca^{2+} conductance were related to the Po recorded from the same channel (Fig. 3.18). The best-fit linearisation of the relationship between single-channel Ca^{2+} conductance and Po was not statistically distinguishable from a slope of zero ($p = 0.38$). This suggested that the single-channel Ca^{2+} conductance may not be correlated with channel activity.

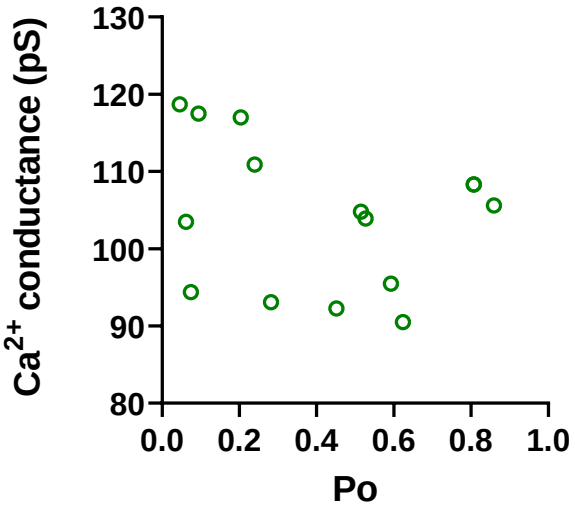


Figure 3.18: The relationship between single-channel Ca^{2+} conductance and Po for V2475F(+/-) channels Single-channel Ca^{2+} conductance values, taken from Fig. 3.2 (n = 15) were plotted against the Po for each channel. Po was measured in the same solutions as the Ca^{2+} conductance measurements with 1 μM cytosolic [Ca^{2+}] but held at a constant holding potential of 0 mV for the 3 min recordings.

Since the V2475F(+/-) RyR2 tetramers assemble with variable numbers of mutated and WT monomers (Fig. 3.16), it was possible that some combinations may produce non-functional channels that would not be recorded in bilayer experiments. Joined data points in Fig. 3.19A indicate WT and V2475F(+/-) RyR2 bands in side-by-side lanes that were loaded with the same protein concentration and stained simultaneously on the same membrane in a Western blot procedure. Following quantifcation of these bands, there did not appear to be a consistently lower RyR2

band intensity in the V2475F(+/-) preparations compared to WT. Further, the protein concentration measured by the Bradford technique between SR preparations was not significantly different (Fig. 3.19B).

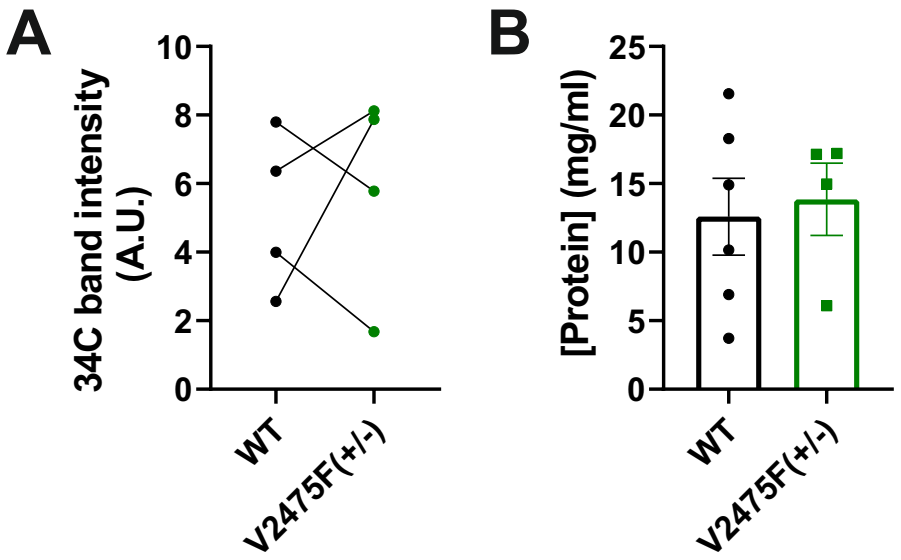


Figure 3.19: The quantification of protein concentration from WT and V2475F(+/-) SR vesicle isolations (A) The intensity of RyR2 bands stained using the 34C antibody from Western blot membranes with equal protein concentration of SR vesicle preparations from each genotype loaded in each well on the same gel. The connected points indicate the intensity of the band stained simultaneously on the same membrane. Unpaired t-test: no significant difference, p = 0.76 **(B)** The crude protein concentration of SR vesicle preparations measured by the Bradford protein quantification technique. Unpaired t-test: no significant difference, p = 0.73

To investigate whether Po is influenced by the number of RyR2 channels in the bilayer, experiments were separated into two groups: those where only a single channel was gating in the bilayer and those where multiple channels were gating in the bilayer. As described in Fig. 3.8, Po is greater for V2475F(+/-) channels than WT in response to 1 μM Ca^{2+}, and Po is lower for V2475F(+/-) channels than WT in response to 1 mM Ca^{2+}. However, for both WT and V2475F(+/-) channel groups, at either 1 μM Ca^{2+} or 1 mM Ca^{2+}, the number of channels present in the bilayer did not appear to influence Po.

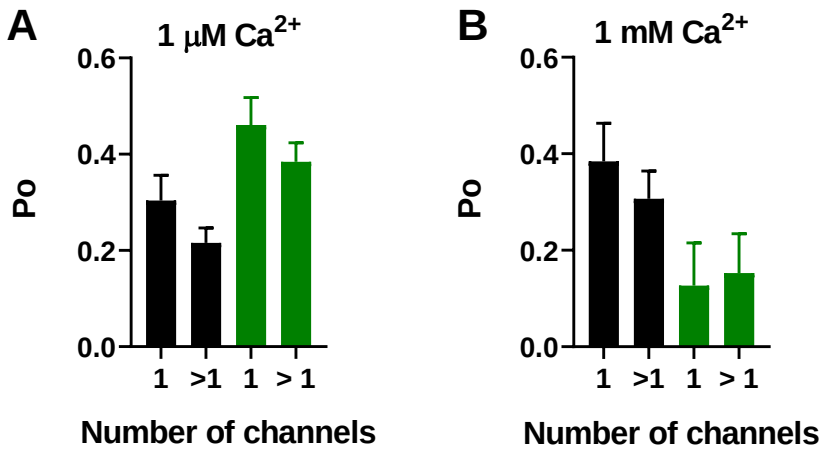


Figure 3.20: Investigating differences in Po with single channels or multiple channels gating in the bilayer (A) Mean Po values ± SEM for WT (black) and V2475F(+/-) (green) RyR2 channels were grouped depending on whether a single channel was gating alone in the bilayer (1) or multiple channels were gating in the bilayer (> 1) in response to 1 μM cytosolic Ca^{2+}. 2-way ANOVA: no channel number-by-genotype interaction, p = 0.91, no main effect of channel number, p = 0.10, main effect of genotype, p = 0.002 **(B)** Mean Po values ± SEM for WT (black) and V2475F(+/-) (green) RyR2 channels are grouped depending on whether a single channel was gating alone in the bilayer (1) or multiple channels were gating in the bilayer (> 1) in response to 1 mM cytosolic Ca^{2+}. 2-way ANOVA: no channel number-by-genotype interaction, p = 0.59, no main effect of channel number, p = 0.79, main effect of genotype, p = 0.046.

3.6 Alterations to other key regulators of RyR2

In line with previous work, ATP was very effective at activating RyR2 in the presence of activating levels of Ca^{2+} (Kermode et al., 1998; Lindsay et al., 2018). In response to ATP addition, the gradient of the line that indicates increase in Po from control was similar for WT and V2475F(+/-) RyR2 channels, and there was no interaction between ATP and genotype. Although the V2475F(+/-) channels were activated to a level above that of the WT, the Po was increased to a similar degree considering the already higher Po at 1 μM Ca^{2+} alone.

Adenosine does not chelate Ca^{2+} or Mg^{2+} and cannot phosphorylate RyR2 via endogenous kinases, so it is a useful tool to measure adenine nucleotide effects without these confounding factors. In subsequent experiments shown below, adenosine was therefore used to activate channels before the addition of Mg^{2+}.

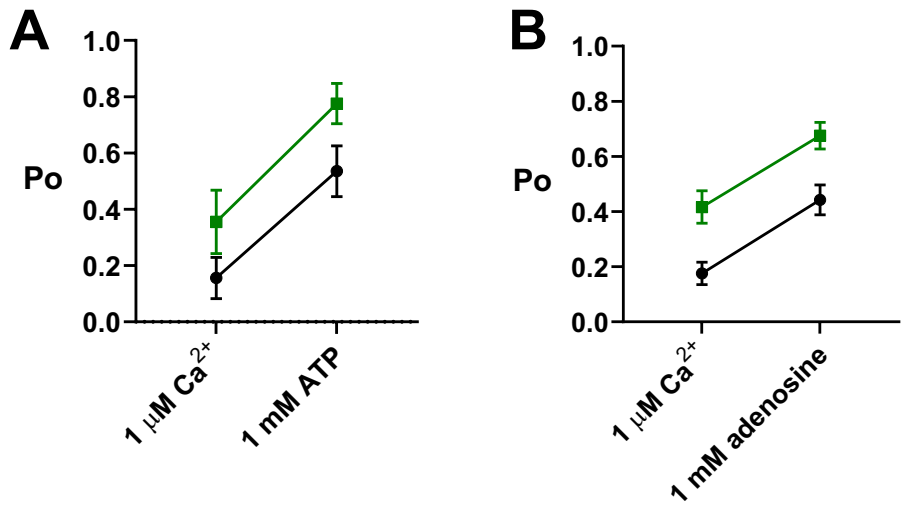


Figure 3.21: Comparison of adenosine-based ligand activation of RyR2 from WT or V2475F(+/-) mouse hearts (A) shows the activation of WT (black) and V2475F(+/-) (green) channels by ATP. Two-way ANOVA: no ATP-by-genotype interaction, p = 0.82; main effect of ATP, p = 0.0002; main effect of genotype, p = 0.02. Mean ± SEM, n = 7 for WT and n = 5 for V2475F. **(B)** shows the activation of WT (black) and V2475F(+/-) (green) channels by adenosine. Two-way ANOVA: no adenosine-by-genotype interaction, p = 0.94; main effect of adenosine, p < 0.0001; main effect of genotype, p < 0.0001. Mean ± SEM; n = 21 for WT and n = 33 for WT. In both cases, control channels were activated solely by 1 μM cytosolic Ca^{2+} and the free [Ca^{2+}] was maintained at 1 μM after ATP or adenosine addition as described in Methods.

Adenosine and ATP are thought to bind at the same sites on RyR2 but adenosine acts as a partial agonist and, unlike ATP, because its action is purely sensitisation to cytosolic Ca^{2+}, it does not increase Po above the level seen with Ca^{2+} as the sole activator (Kermode et al., 1998; Chan et al., 2000; Lindsay et al., 2018). Similarly to the effects with ATP, adenosine activates both WT and V2475F(+/-) channels by a comparable extent, as there was no interaction of adenosine by genotype and the gradient of the Po increase from control was similar. As expected from our previous work, adenosine was less effective than ATP at activating RyR2 (Lindsay et al., 2018). Adenosine increased Po by 81% and 87% of that of ATP activation observed in the WT and V2475F(+/-) channels, respectively.

WT channels were not activated above the maximal Po response observed in Ca^{2+} alone. However, both adenosine and ATP activated V2475F(+/-) RyR2 channels above the observed maximal level of activation with Ca^{2+} alone as seen in the plateaued responses shown in Fig. 3.8, in which the maximal activation for

WT and V2475F(+/-) channels is similar at a Po of approximately 0.45.

The effects of the V2475F mutation on RyR2 channels in response to Mg^{2+} is shown in Fig. 3.22. The addition of 500 μM cytosolic free Mg^{2+} to WT channels, activated by 1 μM free Ca^{2+} and 1 mM adenosine, consistently decreased Po by > 80%. An example of this consistent and potent inhibition is shown in Fig. 3.22A, in which a high WT channel was chosen to compare the V2475F(+/-) to a comparable control. Over the 3 s of recording trace shown, there are only two very brief channel openings after addition of 500 μM Mg^{2+} for the WT channel. In contrast, Mg^{2+} exerted a much weaker inhibitory action on the gating of V2475F(+/-) channels. As can be seen in the trace in Fig. 3.22A, Po is still 0.87 with a high frequency of openings upon the addition of 500 μM Mg^{2+}.

The relationship between Po and free cytosolic [Mg^{2+}] yielded an IC_{50} of 86 μM for WT channels (Fig. 3.22B). The inhibitory effect of Mg^{2+} on V2475F(+/-) channels was highly variable and, at the concentrations used, did not bring Po down to low levels. As Mg^{2+} is a permeant ion, it was difficult to accurately assess Po at cytosolic concentrations above 2 mM as the current amplitude becomes small due to competition within the pore for Ca^{2+} flowing through from the luminal side. As a result, it was not possible to compute an accurate IC_{50} value.

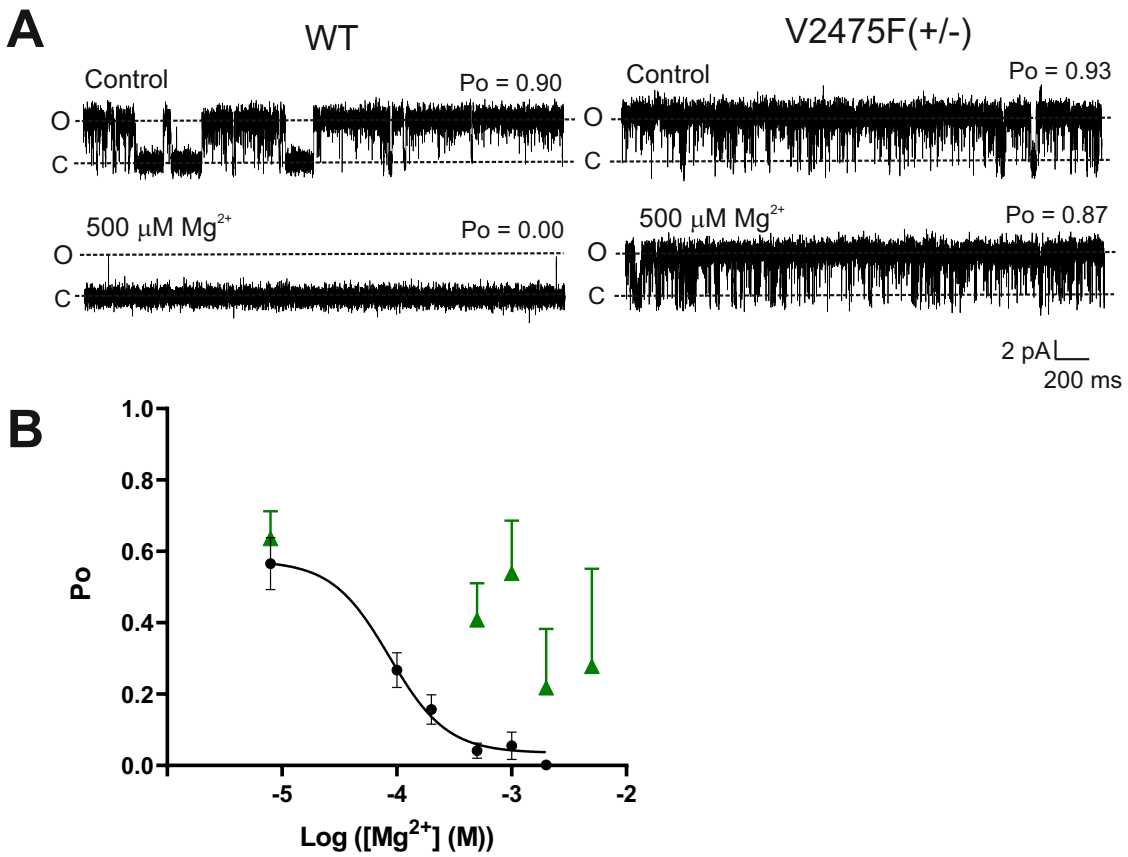


Figure 3.22: Comparison of the effect of cytosolic Mg^{2+} on the gating of WT and V2475F(+/-) channels (A) Representative single-channel recordings from WT (left) and V2475F(+/-) (right) channels before and after adding 500 μM free cytosolic [Mg^{2+}] in the presence of 1 mM adenosine and 1 μM free cytosolic [Ca^{2+}] (control). To directly compare the ability of Mg^{2+} to inhibit WT and V2475F(+/-) channels, recordings from channels with a similar Po under control conditions were chosen. O and C indicate the open and closed states, respectively. **(B)** The relationship between Po and free [Mg^{2+}] for WT (black) and V2475F(+/-) (green) channels is displayed in the presence of 1 μM free Ca^{2+} and 1 mM adenosine. Mean ± SEM, n $\geq$ 5. The log([Mg^{2+}])-response non-linear variable slope was computed only for WT channels since a good fit could not be obtained for V2475F(+/-) channels.

To understand the mechanisms underlying the alterations to Mg^{2+} sensitivity resulting from the V2475F mutation, mean open and closed times were evaluated. For WT channels, the addition of 500 μM Mg^{2+} reduced mean open time and exerted a substantial reduction in frequency of opening as indicated by the 264-fold increase in mean closed time (Fig. 3.23).

To compare, although the addition of 500 μM Mg^{2+} to V2475F(+/-) channels decreased mean open time, the mean open times of the V2475F(+/-) channels was

highly variable, and decreased to a value 20.7-fold greater than WT. The most substantial defect for V2475F(+/-) channels was observed in the modest decrease in the frequency of openings as indicated by a relatively small 2.3-fold increase in mean closed time with the addition of 500 μM Mg^{2+} compared to WT (Fig. 3.23). This is also clearly observed in the representative trace in Fig. 3.22A.

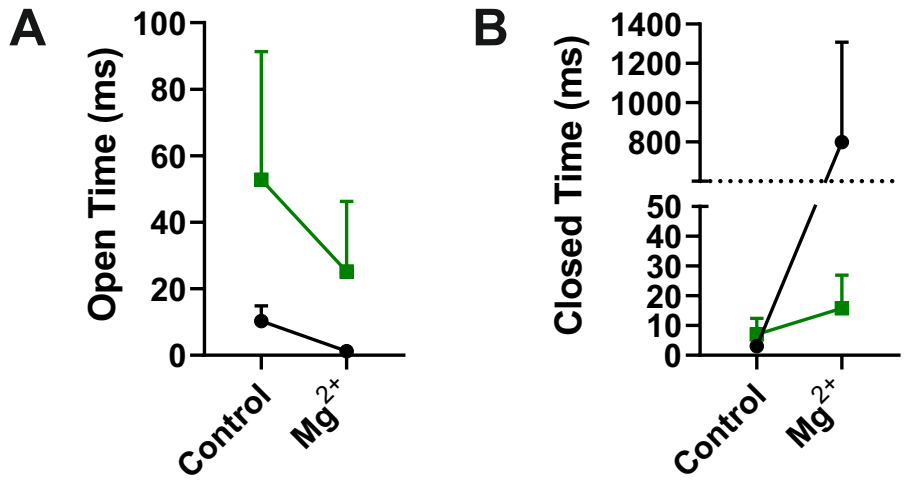


Figure 3.23: The effects of cytosolic 500 μM Mg^{2+} on RyR2 channel mean open and closed times from WT or V2475F(+/-) mouse hearts Mean ± SEM open **(A)** and closed **(B)** times (n = 3 for WT and n = 5 for V2475F(+/-) channels) for RyR2 derived from WT (black) and V2475F(+/-) (green) mouse hearts in the presence of 1 μM Ca^{2+} and 1 mM adenosine, before and after addition of 500 μM Mg^{2+}. Statistical analysis was not conducted due to low n numbers.

As shown in Fig. 3.22, V2475F(+/-) channels had a reduced sensitivity to inhibition by Mg^{2+}. The percentage inhibition in Po from 1 μM Ca^{2+} and 1 mM adenosine (control) following the addition of 500 μM Mg^{2+} was calculated. For all V2475F(+/-) channels, the mean percentage inhibition was significantly lower than the mean inhibition in Po for WT channels. With the addition of 500 μM cytosolic Mg^{2+}, WT channels displayed a range of inhibition from 82.8 to 99.9% decrease from control. Since populations of V2475F(+/-) channels have been observed to respond differently to cytosolic Ca^{2+} (Fig. 3.17), and V2475F(+/-) channels displayed a highly variable Po in response to Mg^{2+} as can be observed by the large error bars in Fig. 3.22, the response to cytosolic Mg^{2+} for each individual channel was investigated further. On closer inspection of the individual channel recordings, there

appeared to be at least three types of channel in respect to their response to Mg^{2+}: 1. "inhibited": those channels that were inhibited by >80% (4 of 13 channels) and thus appeared similar to WT channels in their response; 2. "intermediate": those channels that were inhibited by < 80% (6 of 13 channels) and 3. "activated": those channels that were activated by 500 μM Mg^{2+} (3 of 13 channels). Representative examples of V2475F(+/-) single-channel recordings of RyR2 channels in these groups gating in response to 500 μM Mg^{2+} are shown in Fig. 3.24A.

The mean Po of the channels separated into these different groups is displayed in Fig. 3.24B, with the n number for each group indicated on the bar. Most V2475F(+/-) channels (46%) displayed an intermediate response to inhibition by 500 μM Mg^{2+}. Some V2475F(+/-) channels (31%) behaved like WT channels. Remarkably, some V2475F(+/-) channels (23%) even presented an increase in Po in response to 500 μM Mg^{2+}, displaying a completely opposite activation effect compared to WT channels.

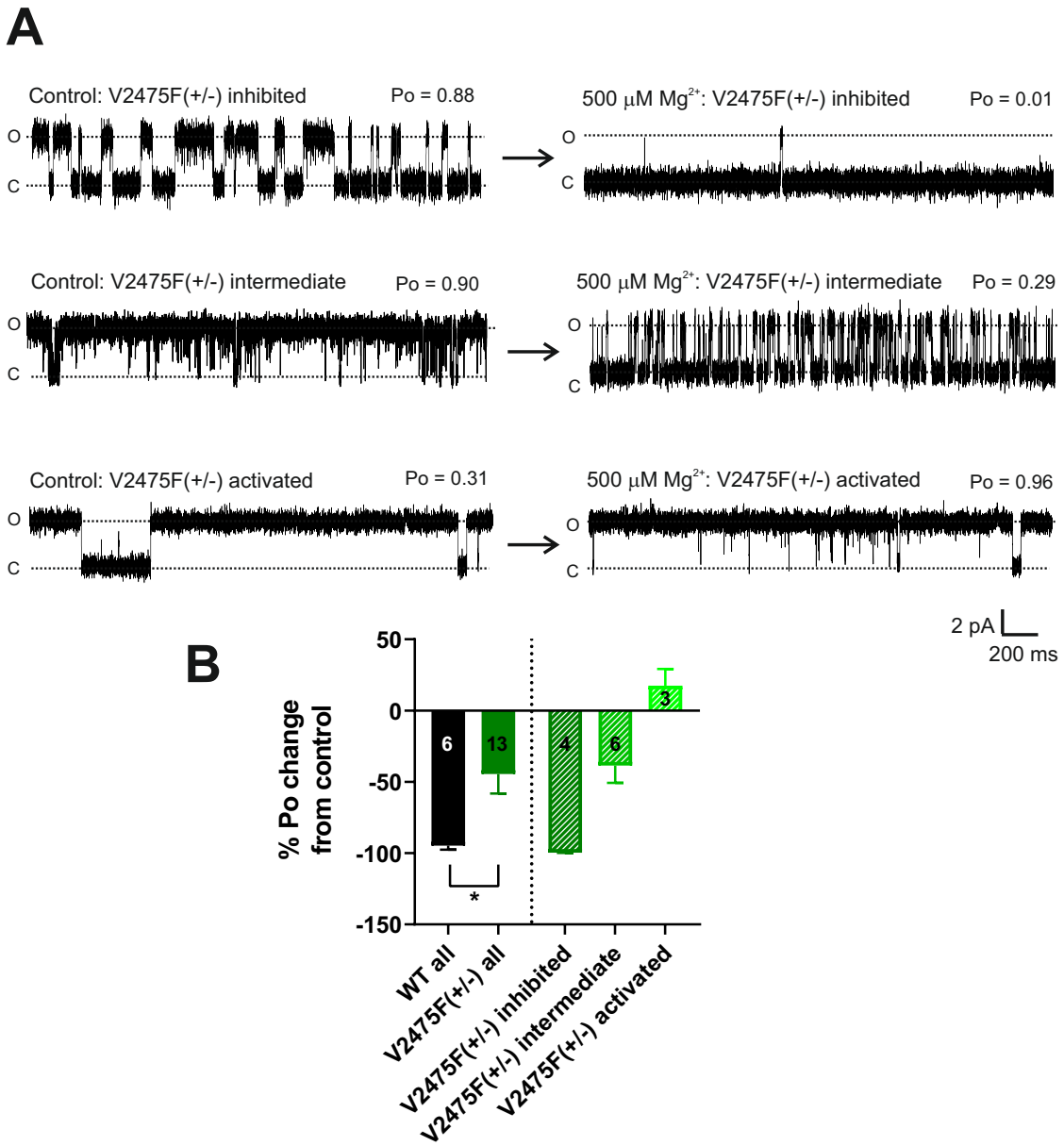


Figure 3.24: Populations of V2475F(+/-) channels that respond differently to Mg^{2+} inhibition (A) Representative single-channel traces displaying examples of the gating behaviour of V2475F(+/-) channels showing WT-like inhibition (top trace, >80% inhibition), intermediate inhibition (middle trace, < 80% inhibition) and activation (bottom trace, increase in Po from control) in response to 500 μM Mg^{2+}. O and C indicate the open and closed levels, respectively. **(B)** Left of the dashed line: comparison of the percentage inhibition of Po induced by 500 μM Mg^{2+} in all WT (black) and all V2475F(+/-) (green) channels (unpaired t-test: significant difference between all WT and all V2475F(+/-) channels indicated by * for p = 0.03). Right of the dashed line: percentage change in Po of V2475F(+/-) channels after the channels are separated into 3 groups: those channels inhibited to within the range of inhibition expected for WT channels (>80% inhibition, n = 4), those channels inhibited to a reduced or intermediate extent (<80% inhibition, n = 6) and those channels that were activated (increase in Po, n = 3) by Mg^{2+}. The number of replicates for each group are indicated on the bars.

Representative lifetime distributions gave further insight to the mechanisms governing the V2475F(+/-) activation in response to 1 μM Ca^{2+} and 1 mM adenosine (control) and the V2475F(+/-) channel insensitivity to inhibitory Mg^{2+}. For this analysis, a single channel from the "V2475F intermediate" group as shown in Fig. 3.24 was selected, which was the most common response of a V2475F(+/-) channel to Mg^{2+}.

At control, 99% of closed events were fit to the shortest exponential in the closed lifetime distribution for the V2475F(+/-) channel. In comparison, there were still some longer closed exponentials in the WT, with only 66% of events gating in the shortest exponential (Fig. 3.25). For the open lifetime distribution, the WT channel can be fit to three exponentials, whereas the V2475F(+/-) channel can be fit to four exponentials indicating an extra exponential with very long openings.

The alterations to the lifetime distributions in response to the addition of 500 μM Mg^{2+} are strikingly different when comparing WT and V2475F(+/-) channels. As expected, with the addition of Mg^{2+}, the WT channel displayed an increase in the proportion and duration of long closed exponentials. Further, the open events for WT decreased in duration and frequency so that they were too brief to fit a pdf (Fig. 3.25). In contrast, the representative V2475F(+/-) channel displayed a similar lifetime distribution for closed times with or without the presence of 500 μM Mg^{2+}, with only slight increase in the duration of each exponential. 99% of events were still represented by the shortest exponential following the addition of 500 μM Mg^{2+}, suggesting almost no change in gating in response to Mg^{2+}. The Mg^{2+} open lifetime distribution was also very similar to control for the V2475F(+/-) channel, with only a modest reduction in the open time duration for every exponential, and surprisingly, four exponentials were still present for the V2475F(+/-) channel. This suggested some of the V2475F(+/-) channels had almost no sensitivity to inhibition by cytosolic Mg^{2+}.

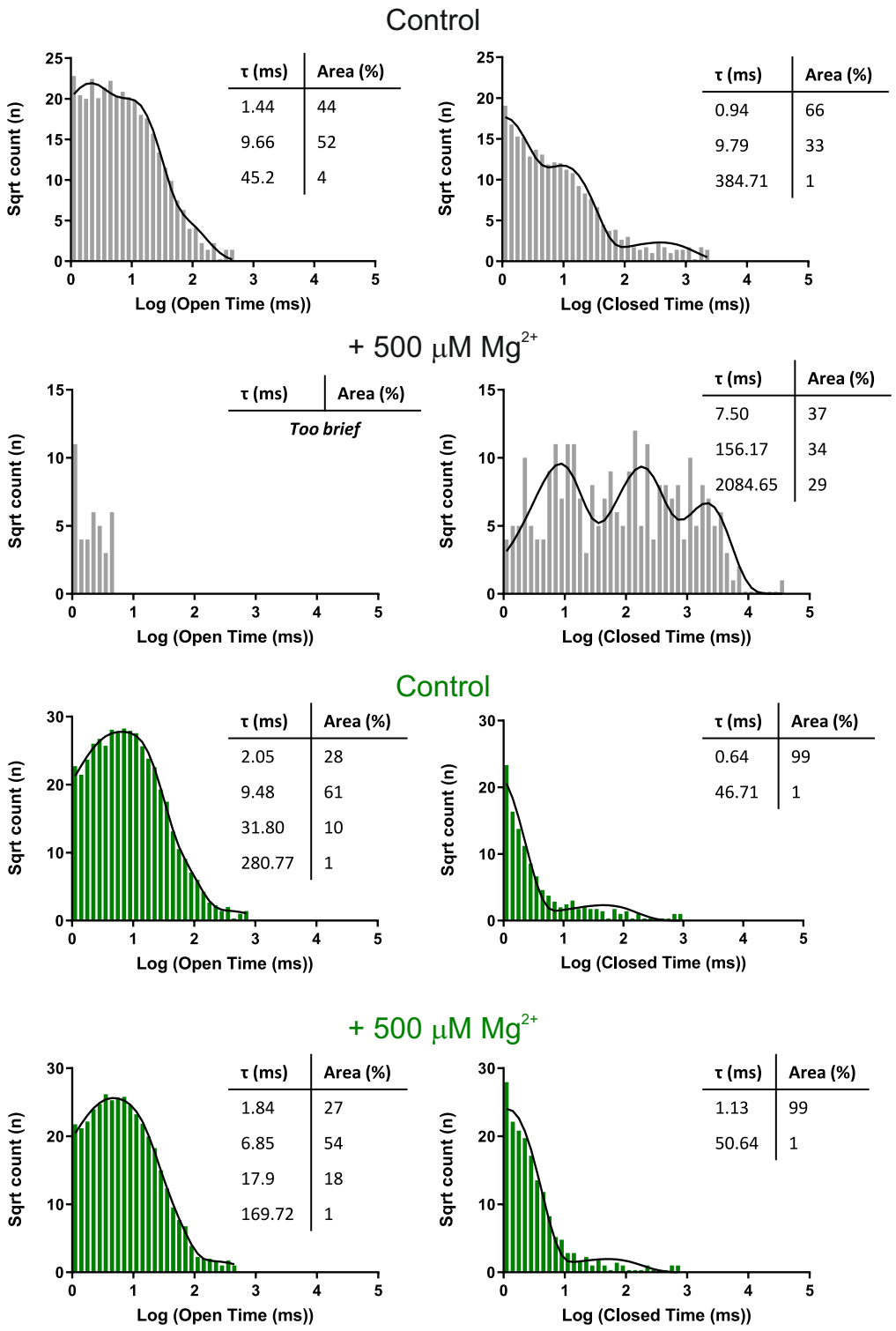


Figure 3.25: Effects of the V2475F mutation on open and closed lifetime distributions with the addition of 500 μM Mg^{2+} Open (left) and closed (right) lifetime distributions and pdfs for representative single RyR2 channels derived from WT (grey) or V2475F(+/-) (green) hearts in the presence of 1 μM Ca^{2+} and 1 mM adenosine, or with the addition of 500 μM Mg^{2+}. The best fits to the data were obtained by the method of maximum likelihood and the resulting time constants (τ, ms) and percentage areas (%) for the representative single RyR2 channel are displayed next to each pdf.

Luminal Ca^{2+} regulation of V2475F(+/-) channels was investigated using symmetrical K^+ as the permeant ion with increasing permeation by Ca^{2+} as the luminal [Ca^{2+}] was raised. Recordings were made at the holding potential of -30 mV so that current flowed in the physiological luminal to cytosolic direction. Experiments were performed in the presence of 1 μM free cytosolic Ca^{2+} and 1 mM ATP since luminal Ca^{2+} alone does not activate normal channels and a cytosolic activator plus Ca^{2+} is required for a maximum response (Sitsapesan and Williams, 1994b). Fig. 3.26A shows the gating characteristics of WT (left) and V2475F(+/-) (right) single RyR2 channels. In the absence of luminal Ca^{2+} (<1 nM due to chelation via EGTA), Po is extremely low for WT and V2475F(+/-) (top trace), indicating the potentiating action of luminal Ca^{2+} for channel opening. When luminal Ca^{2+} is increased to 10 μM (middle trace) and 1 mM Ca^{2+} (bottom traces), Po increases for both groups, with a slightly higher Po for V2475F(+/-) channels.

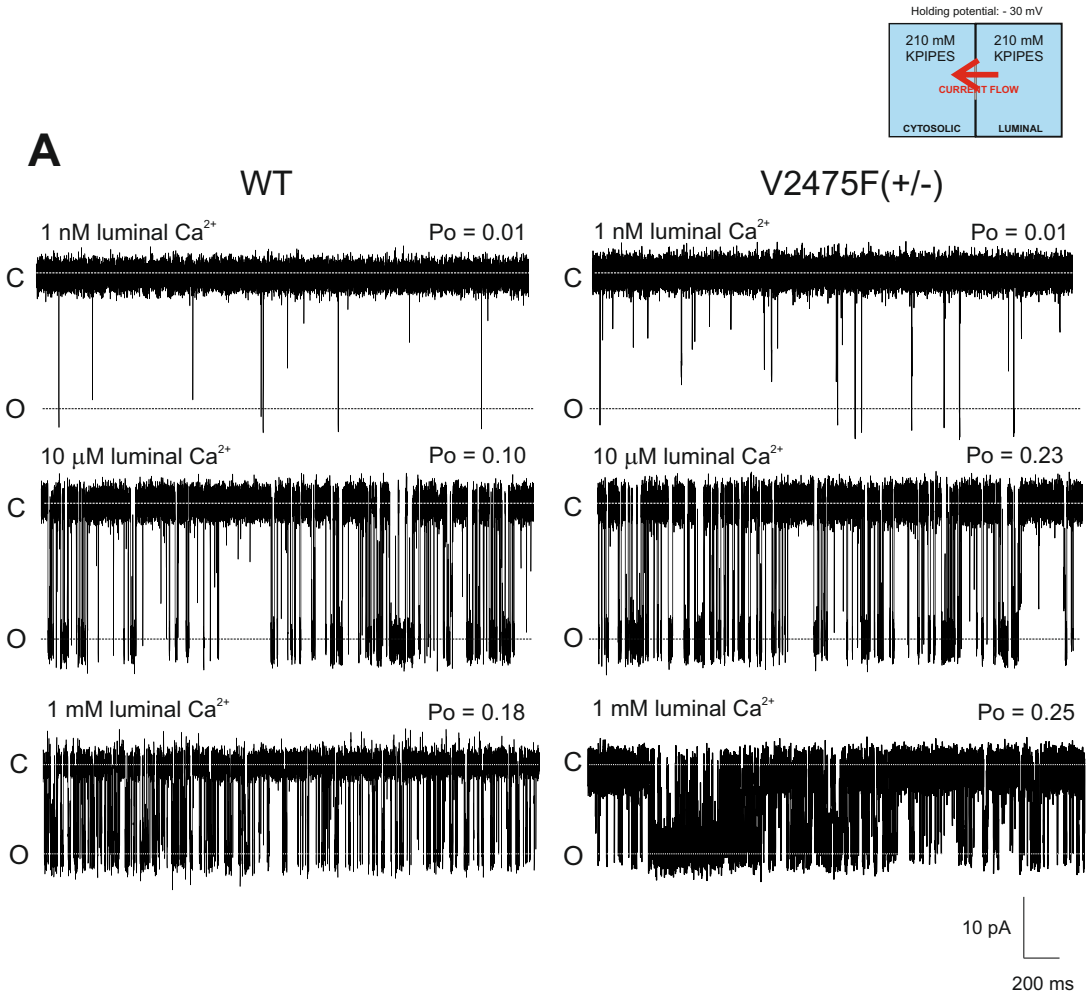


Figure 3.26: Luminal Ca^{2+} regulation of WT and V2475F(+/-) channel gating **(A)** Representative recordings of WT and V2475F(+/-) channels in symmetrical 210 mM KPIPES solutions in the presence of cytosolic activators 1 μM Ca^{2+} and 1 mM ATP at the indicated luminal [Ca^{2+}]. A simplified model of the experimental conditions is shown above the traces. The holding potential was -30 mV and current flow was in the luminal to cytosolic direction with K^+ as the permeant ion. Traces were filtered at 2 kHz. O and C indicate the open and closed states, respectively.

Fig. 3.26B displays the relationship between Po and luminal [Ca^{2+}] for WT and V2475F(+/-) channels. There was a trend for higher Po values for V2475F(+/-) channels compared to WT up to 1 mM Ca^{2+}. However, between 1 nM to 1 mM Ca^{2+} there was no significant difference between WT and V2475F(+/-) channel Po values at each [Ca^{2+}] that Po was measured.

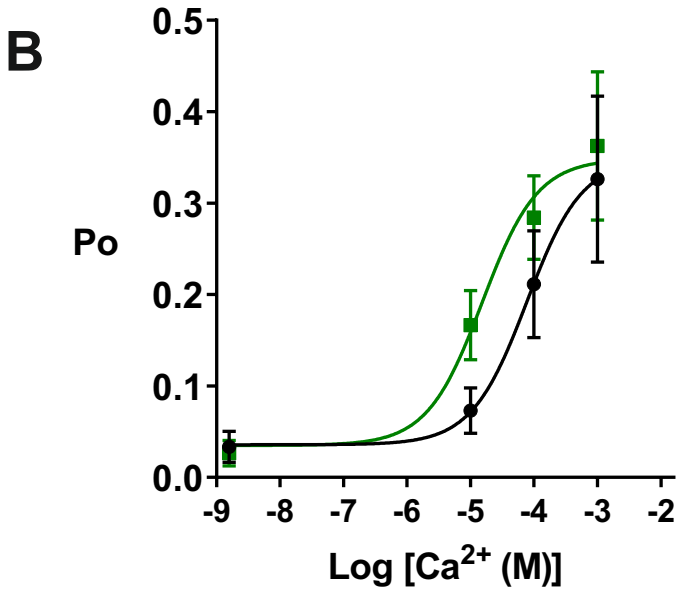


Figure 3.26: (Cont.) Luminal Ca^{2+} regulation of WT and V2475F(+/-) channel gating (B) The relationship between mean Po ± SEM (n ≥ 5) and luminal [Ca^{2+}] for WT (black) and V2475F(+/-) (green) channels activated by cytosolic 1 μM Ca^{2+} and 1 mM ATP in the same conditions as (A). Two-way ANOVA: no luminal Ca^{2+}-by-genotype interaction, p = 0.87; main effect of luminal Ca^{2+}, p < 0.0001; no main effect of genotype, p = 0.26. The data was fit to a log([Ca^{2+}])-response non-linear variable slope.

4

Phosphorylation and the V2475F mutation

Contents

4.1 Introduction 112
4.2 Phosphorylation at the single-channel level 112
4.3 Quantifying phosphorylation levels 116
4.4 β-adrenergic stimulation at the cardiomyocyte level . 117

4.1 Introduction

CPVT1 is a disease triggered by physical or emotional stress, in which catecholamine release is thought to contribute to the generation of arrhythmogenic episodes (Priori et al., 2001). The classical adrenergic pathway that is upregulated in this mechanism is conducted through activation of PKA, and leads to phosphorylation of various targets in a cardiomyocyte, including RyR2, to stimulate increased Ca^{2+} cycling and ultimately increased cardiac output of the heart, as described in the introduction (Bers, 2001).

This chapter therefore investigated whether the functional responses of V2475F mutated RyR2 channels to phosphorylation by PKA are different to those responses observed in normal WT RyR2 channels. Experiments were performed in which single RyR2 channels incorporated into bilayers were subject to phosphorylation and dephosphorylation directly in the bilayer by using activated PKA or PP1. In the SR vesicles used for the bilayer experiments, the level of phosphorylation of V2475F and WT RyR2 at S2808 under basal, phosphorylated, and de-phosphorylated conditions were quantified by western blot using antibodies specific for the phosphorylation or dephosphorylation state of S2808 (Rodriguez et al., 2003).

4.2 Phosphorylation at the single-channel level

As is shown earlier in this thesis (Chapter 3, Fig. 3.21), the Po in response to 1 μM Ca^{2+} and 1 mM adenosine is greater for RyR2 channels derived from V2475F(+/-) compared to WT hearts. After recording control Po, PP1 and $MnCl_2$ was applied to the cytosolic side of the RyR2 for 10 mins at RT. Following PP1 treatment, the required kinases and $MnCl_2$ was perfused out of the cytosolic chamber, and 1 μM Ca^{2+} and 1 mM adenosine was added back to the channel to observe the same conditions as before treatment. In both genotypes, there was a trend for a decrease in Po from basal levels, but the Po was not reduced to the same level in RyR2 from WT and V2475F(+/-) following abolishment of basal phosphorylation levels.

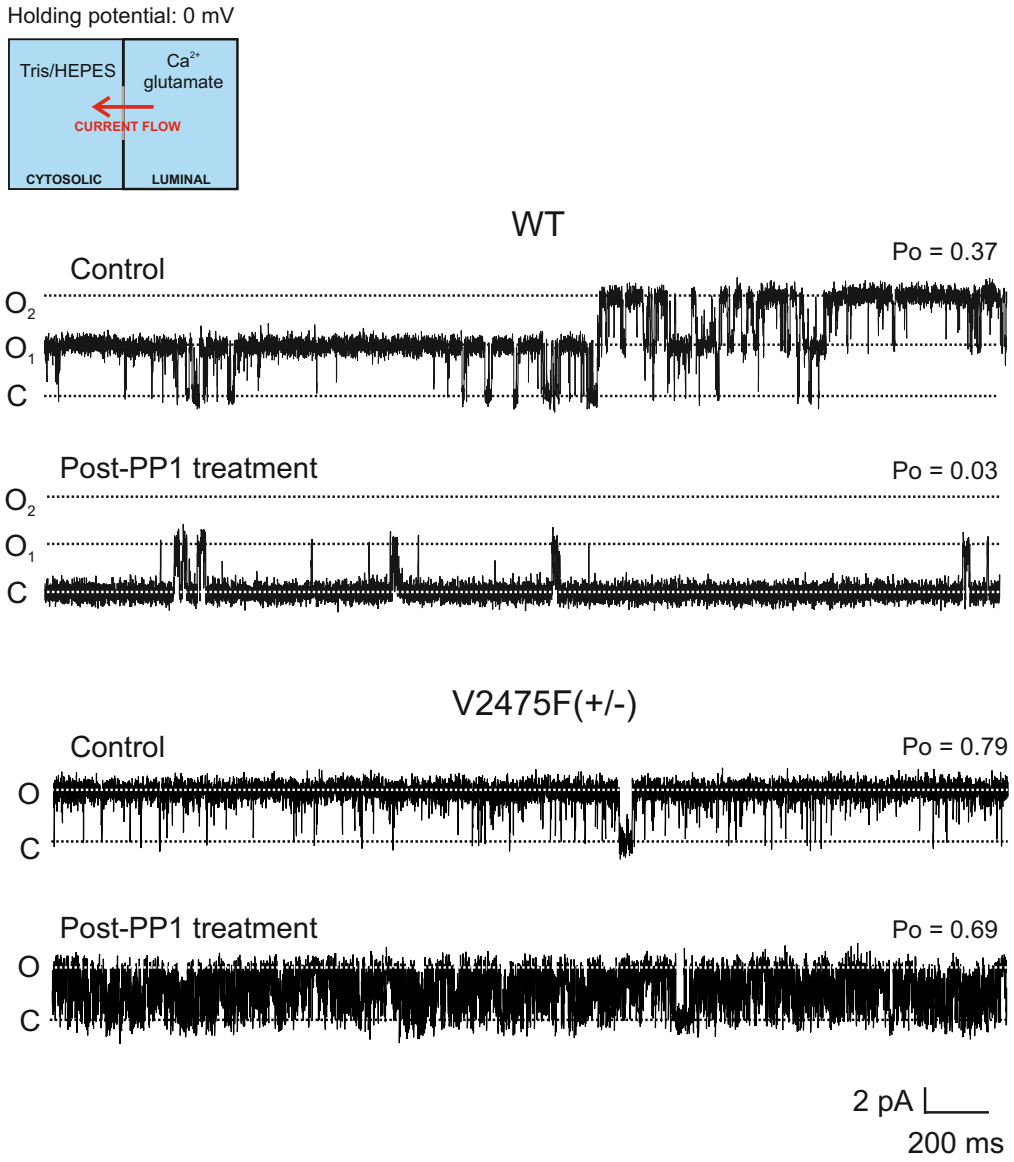


Figure 4.1: The contribution of phosphorylation to WT and V2475F(+/-) RyR2 gating Representative recordings from a single channel derived from WT (top) or V2475F(+/-) (bottom) hearts. The solutions used were Tris/HEPES in the cytosolic chamber buffered to 1 μM Ca^{2+}, and Ca^{2+} glutamate in the luminal chamber with approximately 50 mM luminal Ca^{2+} as displayed in the schematic. Ca^{2+} was the permeant ion. The top traces are two WT channels gating together in the bilayer, and the bottom traces are a single V2475F (+/-) channel gating alone. Po displayed is for the full 3 min recording. C and O indicate the closed and open states, respectively. O1 and O2 refer to the open level with one or two channels. Control displays the gating of an RyR2 channel in response to 1 μM cytosolic Ca^{2+} and 1 mM adenosine prior to treatment. Post-PP1 treatment indicates the gating of the same channel in response to 1 μM Ca^{2+} and 1 mM adenosine following 10 min treatment with PP1 and $MnCl_2$ which was subsequently washed out.

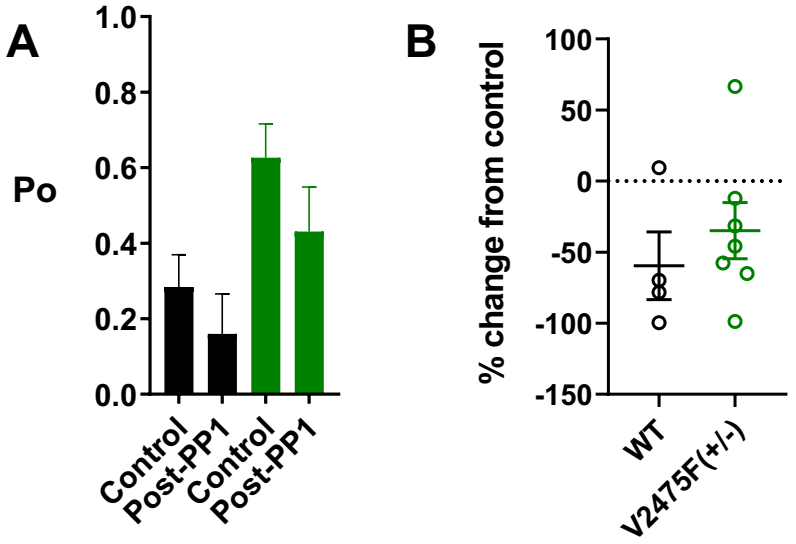


Figure 4.2: The contribution of phosphorylation to WT and V2475F(+/-) channel Po (A) Mean RyR2 Po ± SEM at basal phosphorylation levels (control, 1 μM Ca^{2+} + 1 mM adenosine) and following 10 min PP1 treatment (Post-PP1, 1 μM Ca^{2+} + 1 mM adenosine added back), for WT (black) and V2475F(+/-) (green) derived channels. n = 4 for WT, n = 7 for V2475F(+/-). The conditions are the same as Fig. 4.1. Two-way ANOVA: no treatment-by-genotype interaction, p = 0.68; no main effect of treatment, p = 0.08; main effect of genotype, p = 0.04. **(B)** Percentage change from control of Po for each channel following PP1 treatment. Bars indicate mean ± SEM.

As described previously in Chapter 3 (Fig. 3.8), RyR2-V2475F(+/-) channels have increased sensitivity to 1 μM cytosolic Ca^{2+}. Post-PKA treatment, the cytosolic chamber was washed out, and 1 μM Ca^{2+} was added back to the channel to apply the same conditions as before treatment. In both genotypes, there was a trend for reduction in Po following PKA treatment.

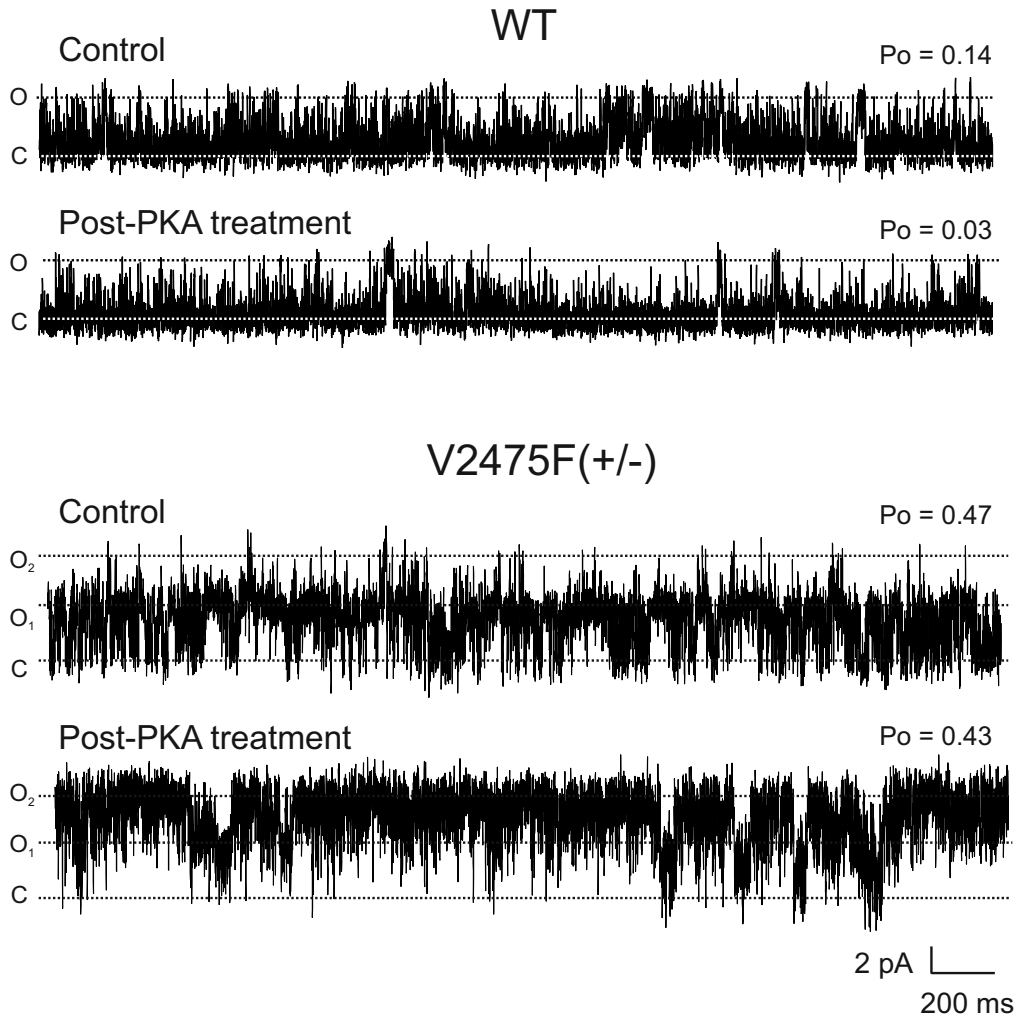


Figure 4.3: The response of RyR2 gating with increased phosphorylation Representative recordings from channels derived from WT and V2475F(+/-) hearts. The top traces are a WT single channel, and the bottom traces are two V2475F (+/-) channels gating together in the bilayer. Po displayed is for the full 3 min recording. C and O indicate the closed and open states respectively. O1 and O2 indicate the open level of two channels gating in the same bilayer. The solutions used were Tris/HEPES in the cytosolic chamber buffered to 1 μM Ca^{2+}, and Ca^{2+} glutamate in the luminal chamber with approximately 50 mM luminal Ca^{2+}. Ca^{2+} was the permeant ion. Control indicates the gating of RyR2 channels in 1 μM cytosolic Ca^{2+} before treatment, post-PKA treatment indicates the gating of the same channel following washout back to 1 μM Ca^{2+}, after 10 min incubation with the PKA treatment.

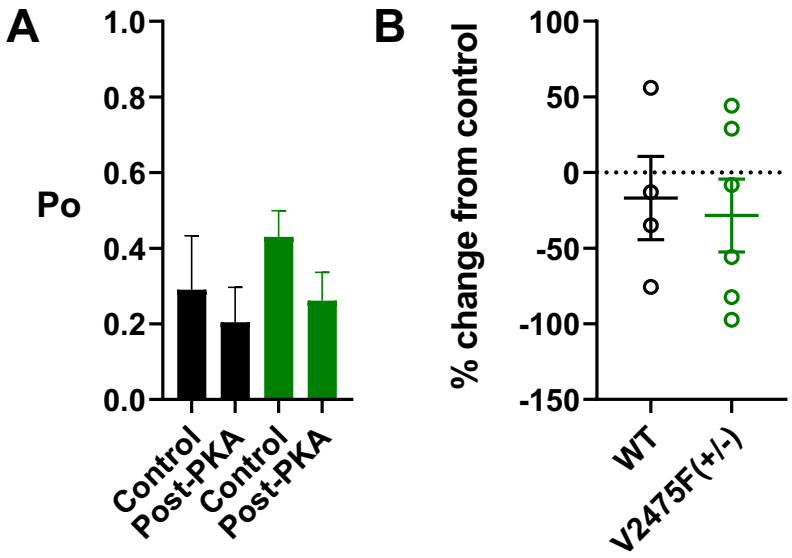


Figure 4.4: The response of RyR2 Po with increased phosphorylation (A) Native RyR2 activity level at basal phosphorylation levels (control, 1 μM Ca^{2+}) and following 10 min PKA treatment (Post-PKA, 1 μM Ca^{2+} added back) for WT (black) and V2475F(+/-) (green) derived channels. Mean ± SEM, n = 4 for WT and n = 6 for V2475F(+/-). Two-way ANOVA: no treatment-by-genotype interaction, p = 0.59; no main effect of treatment, p = 0.12; no main effect of genotype, p = 0.39. **(B)** Percentage change from control of Po for each channel following PKA treatment. Bars indicate mean ± SEM.

4.3 Quantifying phosphorylation levels

To ascertain the phosphorylation status at site S2808, native RyR2 channels derived from WT and V2475F(+/-) mouse hearts were run on western blots and stained with phospho-specific RyR2 antibodies. The treatments used on SR vesicle preparations in these studies (Fig. 4.5) were designed to recapitulate those in the cytosolic chamber of the bilayer in the previous experiments. Experiments were conducted at RT for the same duration with comparable concentrations of PKA, PP1 and required ligands (see Methodology, Chapter 2). Basal phosphorylation levels, and the resulting phosphorylation level in response to phosphorylating or de-phosphorylating treatments were similar for RyR2 in WT and V2475F(+/-) SR vesicle preparations. Phosphorylation by PKA increased phosphorylation levels by 14 % to a similar level for WT and V2475F(+/-). Further, PP1 reduced phosphorylation but this effect was similar for WT and V2475F(+/-) derived SR.

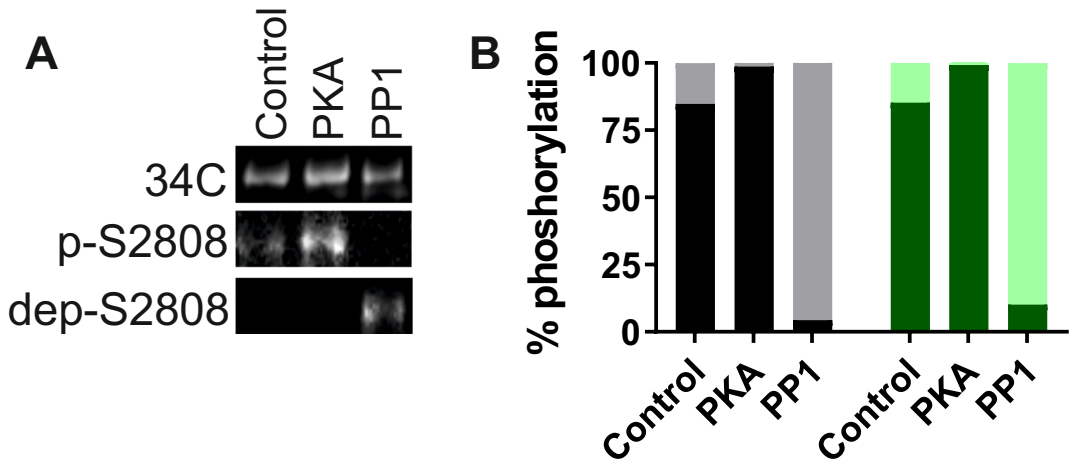


Figure 4.5: Phosphorylation level of native RyR2 from SR vesicle preparations following phosphorylation or dephosphorylation treatment (A) Representative western blot using the antibody for RyR2 (34C), the phospho-S2808 antibody for the phosphorylated site at S2808 (p-S2808) and the dephospho-S2808 antibody for the unphosphorylated site at S2808 (dep-S2808). **(B)** Relative fluorescence quantified by normalising to RyR2 protein level (34C antibody) and percentage of phosphorylation relative to phospho-S2808 (black, dark green) and dephospho-S2808 (grey, light green) staining of RyR2 derived from WT (black, grey) and V2475F(+/-) (green) mouse hearts. Mean, n = 3 independent western blots.

4.4 β-adrenergic stimulation at the cardiomyocyte level

To investigate the effects of stimulating the β-adrenergic stimulation pathway at the whole cell level, a β-adrenergic stress protocol was designed to compare Ca^{2+} release in intact cardiomyocytes isolated from WT or V2475F(+/-) mouse hearts in response to isoprenaline (ISO). Cardiomyocytes were perfused with 50 nM ISO in Kreb's solution with 1 mM free Ca^{2+}, (Table 2.7) and paced at 0.5 Hz. Ca^{2+} release activity outside of the pacing stimulation was considered spontaneous activity; this was quantified using the fluorescent Ca^{2+} dye, Fluo4-AM (further described in the Methodology (Chapter 2)). An example of the fluorescence indicating Ca^{2+} release recorded from cardiomyocytes and how spontaneous activity was determined is illustrated in Fig. 4.6.

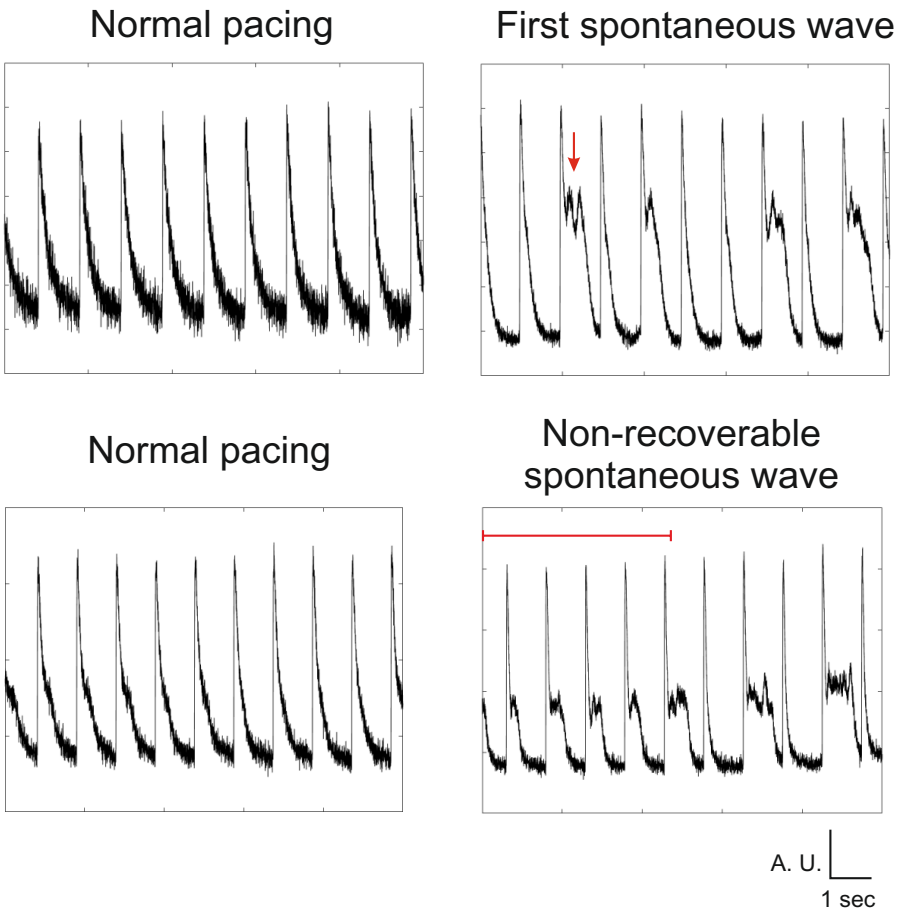


Figure 4.6: Ca^{2+} release measured from intact cardiomyocytes isolated from mouse hearts Ca^{2+} release was quantified by fluorescence of Fluo-4 AM as arbitrary units (A. U.), over time (s). Figures above display fluorescence (A. U.) over a 10 s recording. Top figures were selected as an example of a cardiomyocyte releasing Ca^{2+} only under pacing stimulus (normal pacing), then with the first spontaneous Ca^{2+} release event (first spontaneous wave) indicated on the figure by the red arrow. Bottom figures were selected as an example of a cardiomyocyte releasing Ca^{2+} only under pacing stimulus (normal pacing), then spontaneous Ca^{2+} release events that do not recover (non-recoverable spontaneous wave) indicated by the red bar which highlights 5 s of several spontaneous Ca^{2+} release events.

There was slight tendency for shorter latency to first spontaneous wave for V2475F(+/-) cardiomyocytes compared to WT (63.03 ± 12.8 s and 77.7 ± 15.2 s for V2475F(+/-) and WT respectively, mean ± SEM; unpaired t-test, p = 0.46), and a significantly shorter latency to non-recoverable spontaneous waves for V2475F(+/-) compared to WT ISO-treated cardiomyocytes (94.2 ± 15.3 s and 144.0 ± 18.5 s for V2475F(+/-) and WT respectively, mean ± SEM; unpaired t-test, p = 0.04). This data was then plotted as survival curves for cardiomyocytes isolated from

each genotype. The log-rank survival test (Bland and Altman, 2004) indicated a significantly shorter latency for non-recoverable survival for the V2475F(+/-) cardiomyocytes compared to WT (p = 0.04) (Fig. 4.7). There was no significant difference in the survival curve for first spontaneous wave.

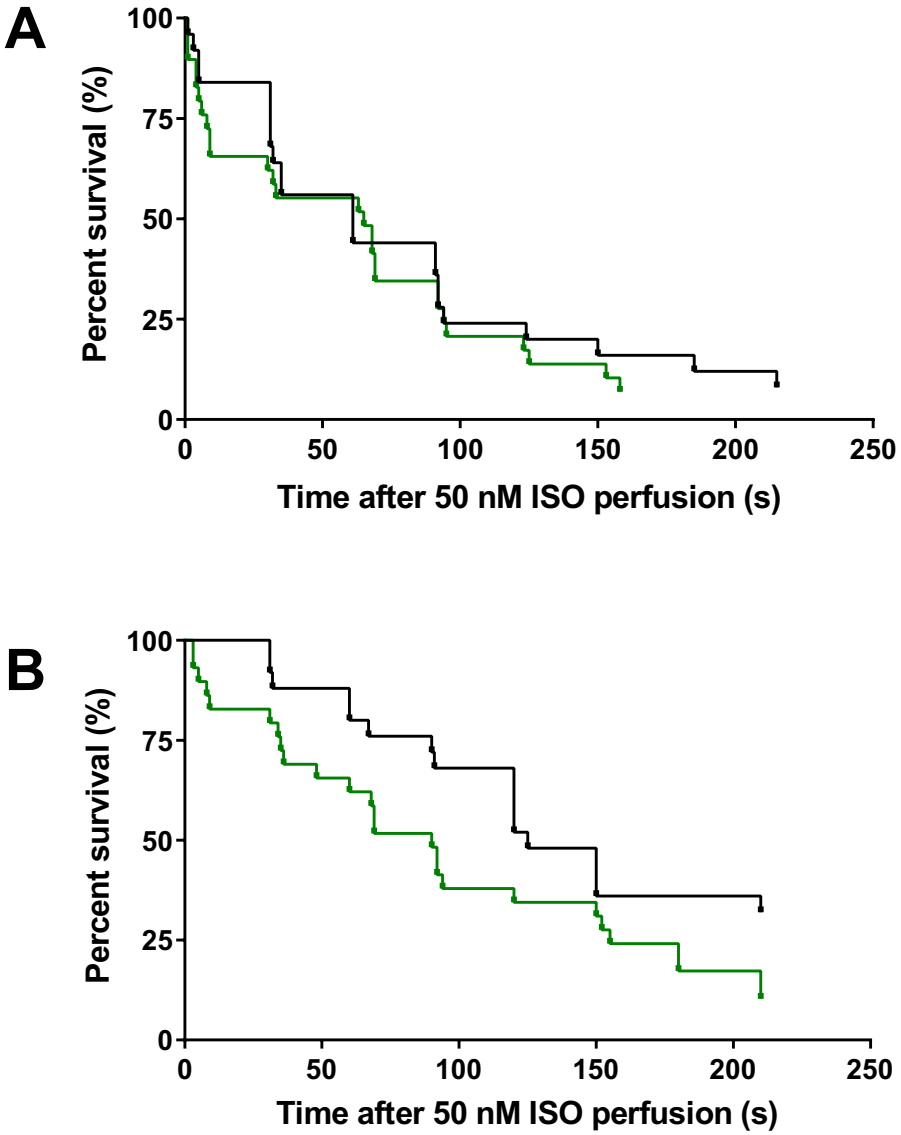


Figure 4.7: Survival of intact cardiomyocytes isolated from WT (black) or V2475F(+/-) hearts following β-adrenergic stress protocol treatment (A) Percent survival of cardiomyocytes quantified by first spontaneous wave at time point (s) after perfusion with 50 nM ISO. Log-rank survival test; p = 0.63. **(B)** Percent survival of cardiomyocytes quantified by non-recoverable spontaneous waves at time point (s) after perfusion with 50 nM ISO. Log-rank survival test; p = 0.04. n = 27 and n = 32 cells for WT and V2475F(+/-) respectively, n = 3 animals in each genotype.

5

RyR2 and statins

Contents

5.1 Introduction 121
5.2 Comparison of native and purified RyR2 channels . . 123
5.3 The effect of atorvastatin on purified RyR2 125
5.4 Atorvastatin modulation on a CPVT1- mutated RyR2 136

5.1 Introduction

RyR2 channels that open more than usual during diastole are thought to cause DADs that trigger arrhythmias (described in further detail section 1.3.3) (Mohamed et al., 2007). It was found in Chapter 3 that RyR2 channels derived from V2475F(+/-) cardiac tissue were 'hyperactive' at nanomolar and low micromolar cytosolic [Ca^{2+}]. In particular, the V2475F(+/-) channels that opened did so with a higher Po than WT channels at 100 nM Ca^{2+} (Fig. 3.13).

As described in section 1.4, there is clinical and experimental evidence of a reduction in arrhythmic events in the heart by statin therapy (De Sutter et al., 2000; Siu et al., 2003; Fauchier et al., 2008; Liu et al., 2009). Furthermore, previous publications from our laboratory have characterised the interactions of statins with RyR2 (Venturi et al., 2018). Critically, there is complex regulation of RyR2, in which statins inhibit RyR2 activity at low concentrations and activate RyR2 at high concentrations (Venturi et al., 2018; Wilson et al., 2018). As the inhibitory 'low concentrations' of statins appear similar to those concentrations of statins that accumulate in the hearts of patients treated with statins (Jirásko et al., 2014; Higgins et al., 2014), it was hypothesised that this inhibitory effect of statins at low doses could modulate the high Po V2475F(+/-) channels at low micromolar cytosolic [Ca^{2+}] and thereby reverse the hyperactivity at this [Ca^{2+}]. Atorvastatin was chosen for these experiments since it is the most prescribed statin for lowering cholesterol (Connor, 2019) and it would be advantageous to repurpose such a highly prescribed drug in the clinic due to its established safety in hypercholesterolemic patients (Armitage, 2007).

Initially, the effect of statins on purified sheep RyR2 was studied. The native RyR2 recordings presented so far in this thesis were obtained from a mixed membrane preparation following a one-step ultra-centrifugation to obtain mixed SR membranes of cardiac tissue from the RyR2-V2475F mutated mouse model (Loaiza et al., 2013). For purification of RyR2, because of the very small amount of tissue in a mouse ventricle, sheep hearts were used instead so that a high yield of protein

could be obtained with few hearts. Mouse and sheep RyR2 are known to be highly similar (Table 1.1). Briefly, the SR membranes were separated into a heavy and light fraction on a discontinuous sucrose gradient as previously published (Sitsapesan et al., 1991). The heavy SR fraction was solubilised with a detergent and phospholipid (CHAPS/PC) mixture then ultra-centrifugated on a continuous sucrose gradient (Sitsapesan and Williams, 1994a; Sigalas et al., 2009b). Certain fractions from this gradient contain high levels of RyR2 but without SR Cl^- and K^+ channels and many other SR proteins and therefore produces a 'functionally' purified RyR2 fraction to be reconstituted into artificial planar bilayers (Pessah et al., 1985; Sitsapesan and Williams, 1994a). This is described in more detail in the Methodology in section 2.2.3 and 2.2.4.

Although experiments with K^+ as the permeant ion were possible after incorporating native RyR2 from mixed membrane vesicles into bilayers, this was nontrivial. Mixed membrane preparations contain a variety of ion channel species and therefore KPIPES was used in those experiments to eliminate currents through SR Cl^- channels. However, recordings from RyR2 channels incorporated in this way also required that a low number of SR K^+ channels co-incorporated into the bilayer to allow for accurate visualisation of RyR2 currents, and it was found that these experiments could only be conducted in the first few days after isolating the SR vesicles. The method described above for functionally purifying RyR2 such that other SR ion channel species, like SR K^+ channels and/or Cl^- channels, were not present, made it possible to record current fluctuations through RyR2 in KCl solutions (Lindsay et al., 1991). This meant that K^+ could be robustly used as the permeant ion, allowing improved resolution of RyR2 gating characteristics and therefore was useful to determine how statins affected RyR2 channel gating.

The purification procedure described here not only removes other ion channels that are present in the SR but also removes some associated proteins that are normally bound to RyR2. This is an advantage because possible confounding interactions of drugs with RyR2-associated proteins which are present in native RyR2 are reduced, thereby increasing the likelihood that any observed change in

RyR2 function is caused by direct binding of the drug to RyR2. For example, CASQ2 and triadin were found to be present in mixed membrane but not in purified SR preparations (Beard et al., 2002). Isolation protocols from our laboratory have found that separation of a mixed membrane into heavy and light SR fraction using a high salt solution does remove FKBP associated proteins from sheep RyR2 (Galfré et al., 2012), however, some studies of FKBP have shown it is tightly bound and still associated with murine RyR2 following purification (Timerman et al., 1994, 1996). This observed difference may be due to the species used for the isolation. Taken together, the purified sheep RyR2 were therefore used to investigate if statins can bind directly with RyR2 and to determine how statins modify purified RyR2 channel gating. Subsequent experiments then examined the effects of atorvastatin on the V2475F-mutated native RyR2 channels isolated from mouse cardiac tissue.

5.2 Comparison of native and purified RyR2 channels

Initially, the gating and single-channel conductance properties of the purified sheep RyR2 channels in symmetrical 210 mM KCl solutions were compared with those of the native mouse RyR2 channels in 210 mM KPIPES solution as shown in Fig. 5.1. The current-voltage relationships suggest that the K^+ conductance of sheep and mouse RyR2 isoforms was similar (698.4 ± 18.6 pS for native mouse RyR2 and 724.3 ± 6.8 pS for purified sheep RyR2).

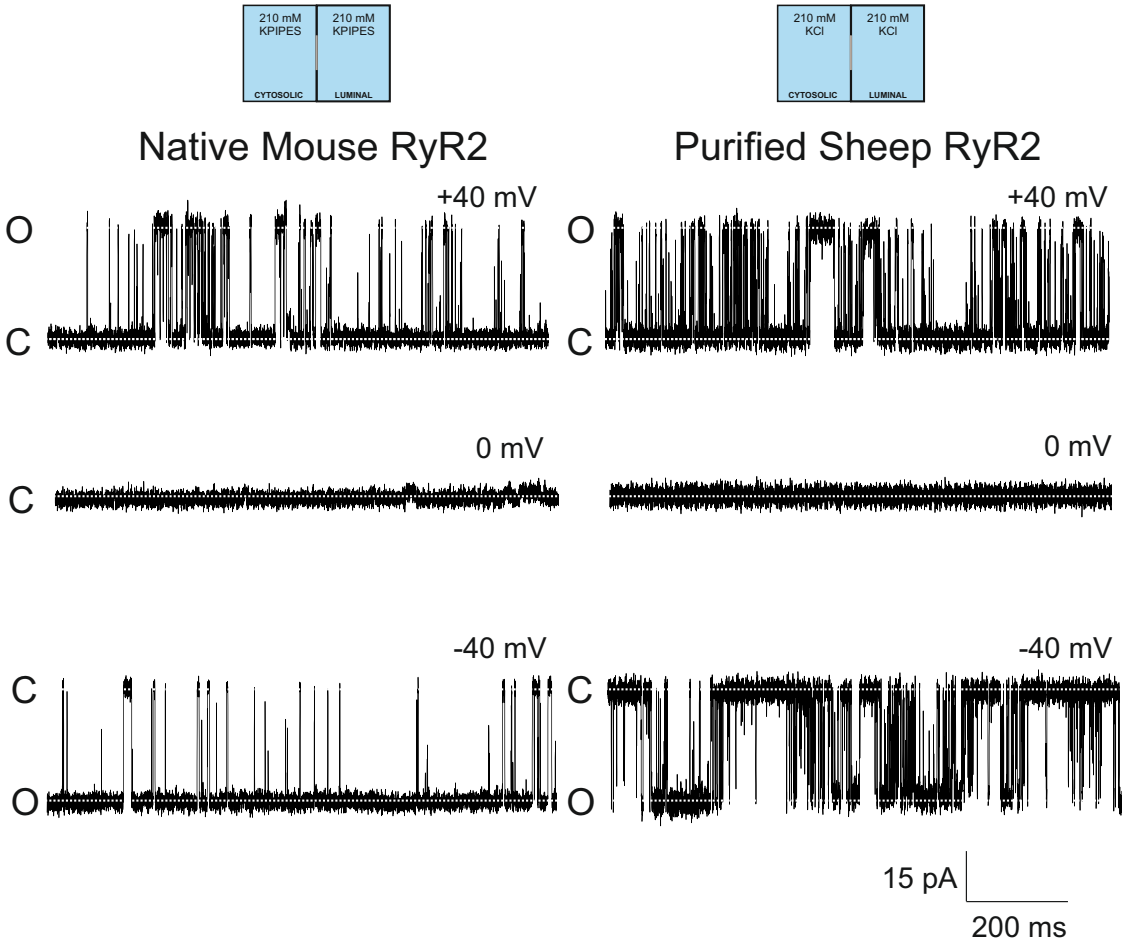


Figure 5.1: Comparison of single-channel K^+ current fluctuations of native RyR2 channels from WT mouse cardiac tissue and purified RyR2 channels from sheep cardiac tissue Representative single-channel recordings illustrating the effects of varying holding potentials as indicated, on gating and current amplitude in symmetrical 210 mM KPIPES for native mouse RyR2 channels (left) and symmetrical 210 mM KCl for purified sheep RyR2 channels (right). A simplified model of the experimental conditions is shown above the traces. Traces were filtered at 2 kHz in both conditions for this figure. O and C represent the fully open and closed levels, respectively.

Fig. 5.2B shows the mean Po of RyR2 channels in K^+ solutions derived from native mouse hearts or purified sheep preparations. The recording conditions were slightly different for each RyR2 preparation type: native mouse RyR2 Po was measured in symmetrical 210 mM KPIPES held at – 30 mV in order to minimise current from other ion channel species; the purified sheep RyR2 Po was measured in symmetrical 210 mM KCl held at - 40 mV. These two solutions had a different contaminant free [Ca^{2+}], with 2 μM free Ca^{2+} in the KPIPES solutions and 10 μM free Ca^{2+} in the KCl solution.

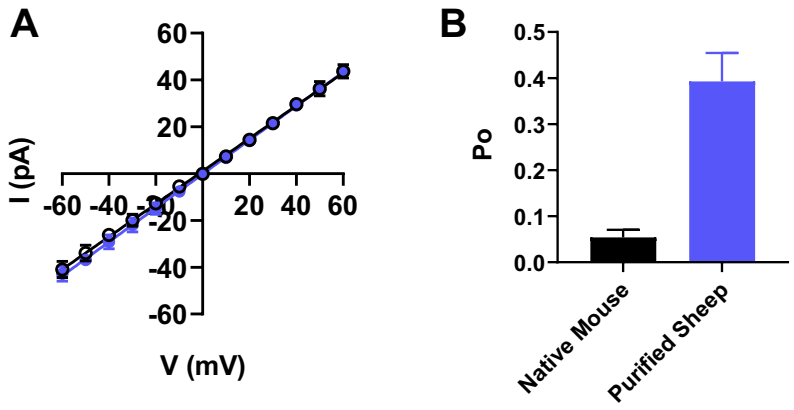


Figure 5.2: Comparison of current-voltage relationships in K^+ and Po in K^+ solutions of RyR2 channels derived from native mouse cardiac or purified from sheep cardiac tissue (A) Single-channel current-voltage relationships with the same solutions as in Fig. 5.1. Mean values ± SEM for native mouse (black, n = 7) and purified sheep (blue, n = 4) derived channels. Where not shown, error bars are within the symbol. **(B)** Mean Po ± SEM of channels derived from native mouse hearts (black, n = 8) in 210 mM symmetrical KPIPES (2 μM contaminant free Ca^{2+}) held at -30 mV or purified from sheep hearts (blue, n = 19) in 210 mM symmetrical KCl (10 μM contaminant free Ca^{2+}) held at -40 mV.

5.3 The effect of atorvastatin on purified RyR2

To investigate the effect of atorvastatin on purified RyR2 channel gating, a range of atorvastatin concentrations was added to the cytosolic side of purified RyR2 derived from sheep cardiac tissue in the presence of 10 μM Ca^{2+}. The representative traces in Fig. 5.3 show the alterations to RyR2 channel gating after the addition of atorvastatin. The RyR2 channel was inhibited by 20 nM

atorvastatin as observed by the reduction in Po relative to control conditions (Fig. 5.3). This inhibition was reversed with increasing levels of atorvastatin and activation was observed with 50 μM atorvastatin.

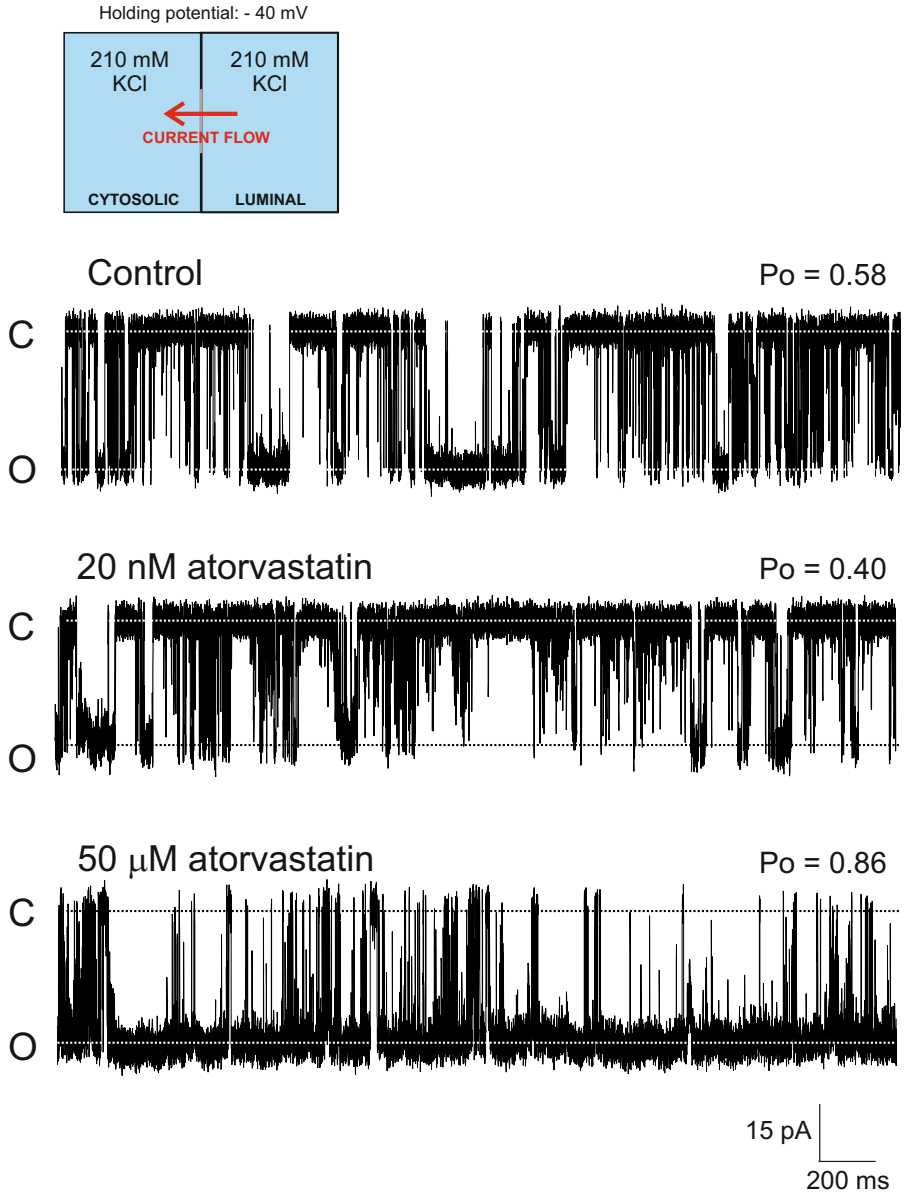


Figure 5.3: Effects of atorvastatin on purified RyR2 channel gating Representative single-channel traces in symmetrical 210 mM KCl and 10 μM free Ca^{2+}. The holding potential was - 40 mV, therefore K^+ was the permeant ion flowing in the luminal to cytosolic direction. A simplified model of the experimental conditions is shown above the traces. Traces were filtered at 4 kHz. Po displayed above the traces was the average Po measured over 3 min of recording. O and C represent the fully open and closed levels, respectively.

Fig. 5.4 displays the mean voltage-current relationships with and without the addition of 50 μM atorvastatin to the cytosolic chamber. There was no alteration to the voltage-current relationship for purified RyR2 channels in the presence of 50 μM atorvastatin. The single-channel conductance was 727 pS for both conditions.

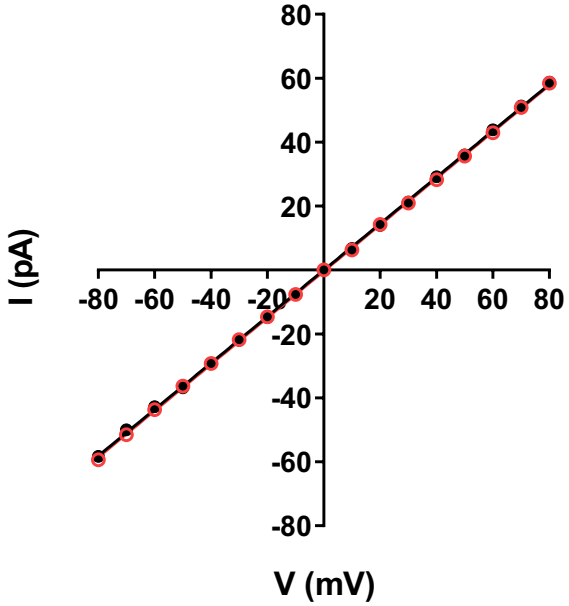


Figure 5.4: The effect of atorvastatin on purified RyR2 current-voltage relationships Single-channel current-voltage relationships of RyR2 purified from sheep cardiac tissue in symmetrical 210 mM KCl with 10 μM free Ca^{2+} before (black, filled circles) and after addition of 50 μM atorvastatin to the cytosolic chamber (red, empty circles). Points are mean values ± SEM, n = 4. Where not shown, error bars are within the symbol. Linear single-channel conductance values were obtained by plotting a straight line of best fit between holding potentials of -60 to +60 mV. With K^+ as the permeant ion, single-channel conductance was 727 ± 5 pS and 727 ± 1 pS for control and 50 μM atorvastatin, respectively. Linear regression for the two conditions were not significantly different, p = 0.73.

Fig. 5.5 shows the mean data of purified RyR2 channels in response to cytosolic atorvastatin, in the same conditions as shown in the representative traces in Fig. 5.3. The inhibition by atorvastatin reduced Po 2.3-fold from control. This inhibition was reversed with increasing levels of atorvastatin and significant activation was observed with 50 μM atorvastatin, with a 1.5-fold increase in Po from control.

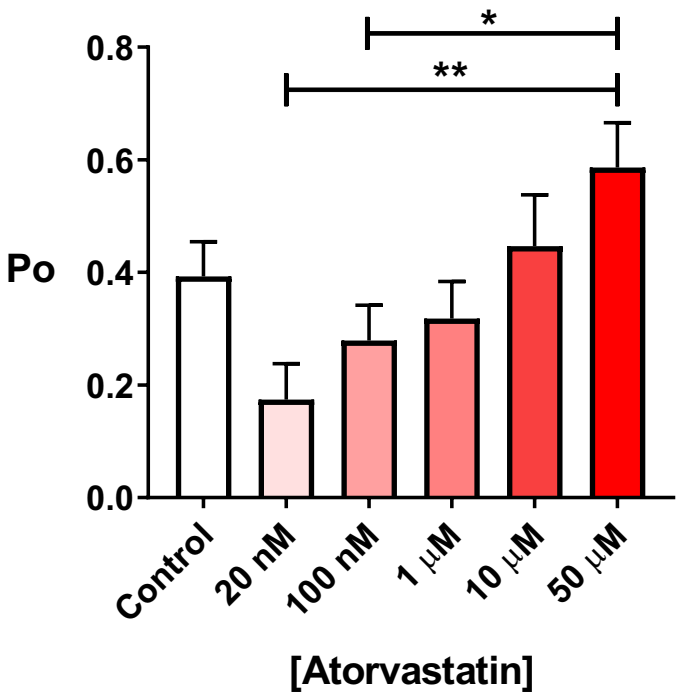


Figure 5.5: Effects of atorvastatin on purified RyR2 channel gating Mean Po values ± SEM for control (10 μM Ca^{2+}) and with the indicated concentration of atorvastatin, in the same conditions as (Fig. 5.3). Each point represents n $\geq$ 7. One-way ANOVA: p $<$ 0.0001. Post-hoc multiple comparisons with Sidak's correction: significant differences between 20 nM and 50 μM atorvastatin are indicated by ** for p = 0.004, significant differences between 100 nM and 50 μM atorvastatin are indicated by * for p = 0.04.

To understand the mechanisms underlying the RyR2 Po response to atorvastatin, mean open and closed times were evaluated. Open and closed dwell times were obtained from RyR2 channels gating in the bilayer as single channels. As shown in Fig. 5.6, following the addition of 20 nM atorvastatin, mean closed time appeared similar to control, but the average mean open time for the two experiments where there were singles was 2.3-fold lower than control. Above 100 nM atorvastatin, the trends were for slight decreases in mean closed times and more obvious increases in mean open times including a 5.4-fold increase in mean open time from control to 50 μM atorvastatin. The variability in mean open time at 50 μM was caused by some channels exhibiting super-long mean open durations of $>$ 20 ms.

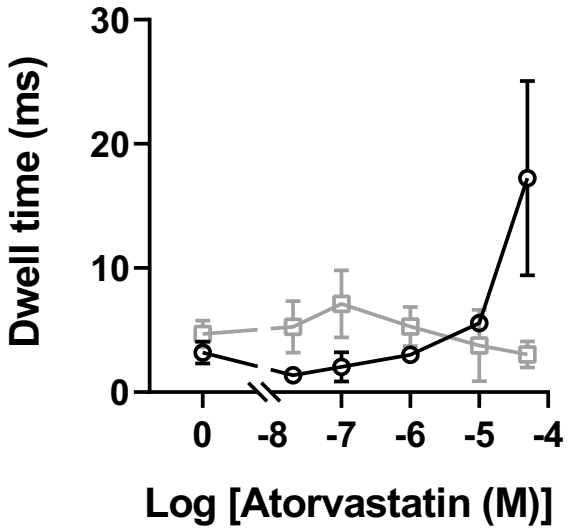


Figure 5.6: Relationships between dwell times and increasing [atorvastatin] Mean open (black) and closed (grey) time ± SEM of purified RyR2 in the same conditions as Fig. 5.2, with increasing [atorvastatin] added to the cytosolic side. The x-axis is segmented to display "0" which indicates control with no atorvastatin and 10 μM cytosolic Ca^{2+}. Since only single channels could be used for analysis, some of the n numbers are low: at 0 n = 9; at 20 nM n = 2, at 100 nM n = 3; at 1 μM n = 2; at 10 μM n = 2; at 50 μM n = 7.

Lifetime analysis was then performed comparing control, 20 nM and 50 μM atorvastatin to elucidate alterations to gating exponentials by atorvastatin. Representative lifetime histograms and pdfs are displayed in Fig. 5.7 with the mean lifetime parameters shown in Fig. 5.8. The lifetime analysis indicated that there was a slight decrease in duration of τ values at all open exponentials with the addition of 20 nM atorvastatin. However, the greatest effect was observed in the mean proportion of events that resided in the shortest exponential of the open lifetime distribution from all single channels analysed, increasing from 54% to 76% with the addition of 20 nM atorvastatin (Fig. 5.8). This can also be observed in the representative channel in Fig. 5.7, in which the open lifetime distribution could also be fitted to a fewer number of exponentials with 20 nM atorvastatin compared to control. Only minor alterations to the closed lifetime distribution parameters were observed with the addition of 20 nM atorvastatin (Fig. 5.8), indicating that the primary mechanism of inhibition by low concentrations of atorvastatin was shortening of the duration of openings.

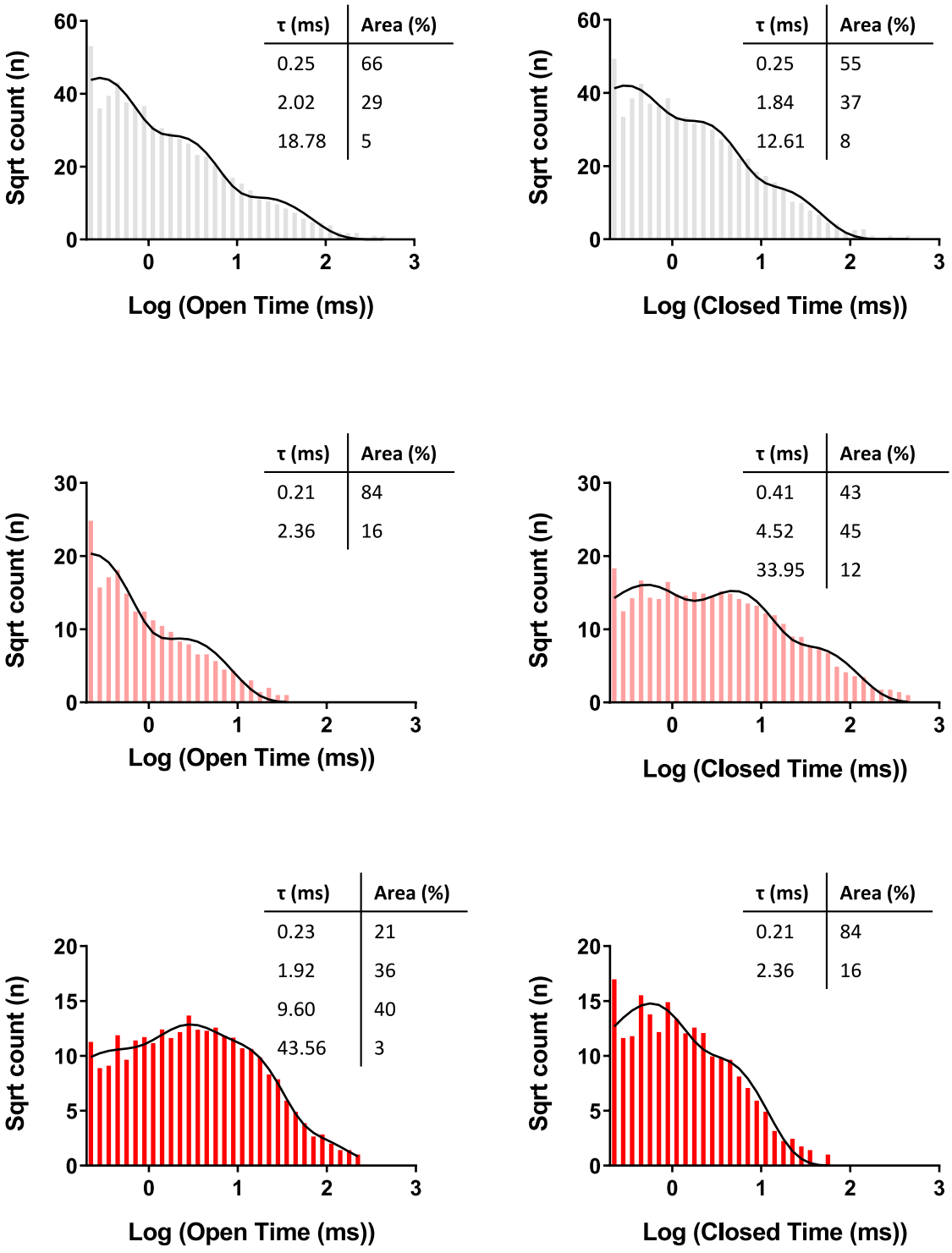


Figure 5.7: Representative open and closed lifetime distributions of single purified RyR2 channels in response to 20 nM and 50 μM atorvastatin Open (left) and closed (right) lifetime distributions and pdfs for representative single purified RyR2 channels held at -40 mV in the presence of 10 μM cytosolic free Ca^{2+} (grey), 20 nM atorvastatin (pink) or 50 μM atorvastatin (red). The best fits to the data were obtained by the method of maximum likelihood and the resulting time constants (τ, ms) and percentage areas (%) for each lifetime distribution are shown with each histogram.

Lifetime analysis also helped describe the mechanism for activation by micromolar atorvastatin on RyR2. With the addition of 50 μM atorvastatin, the open lifetime distributions of just over half (57%) of all single channels were best fit to four open exponentials. In control conditions, most of the single channels (86%) were best fit to three exponentials, with no individual channel lifetimes best fit to a fourth long open exponential. This indicated a new exponential of long open gating induced by 50 μM atorvastatin. A representative example of one of these channels is shown in Fig. 5.7 in which the open lifetime distribution is shifted to the right with the proportion of openings gating in the shortest exponential reduced. Overall, a greater proportion of closings resided in the shortest exponential for the closed lifetime distributions, with an increase from 53% for control to 80% following the addition of 50 μM atorvastatin (Fig. 5.8). This indicated the mechanism for activation by 50 μM atorvastatin was via an increase in frequency of openings, as well as an increase in duration of openings.

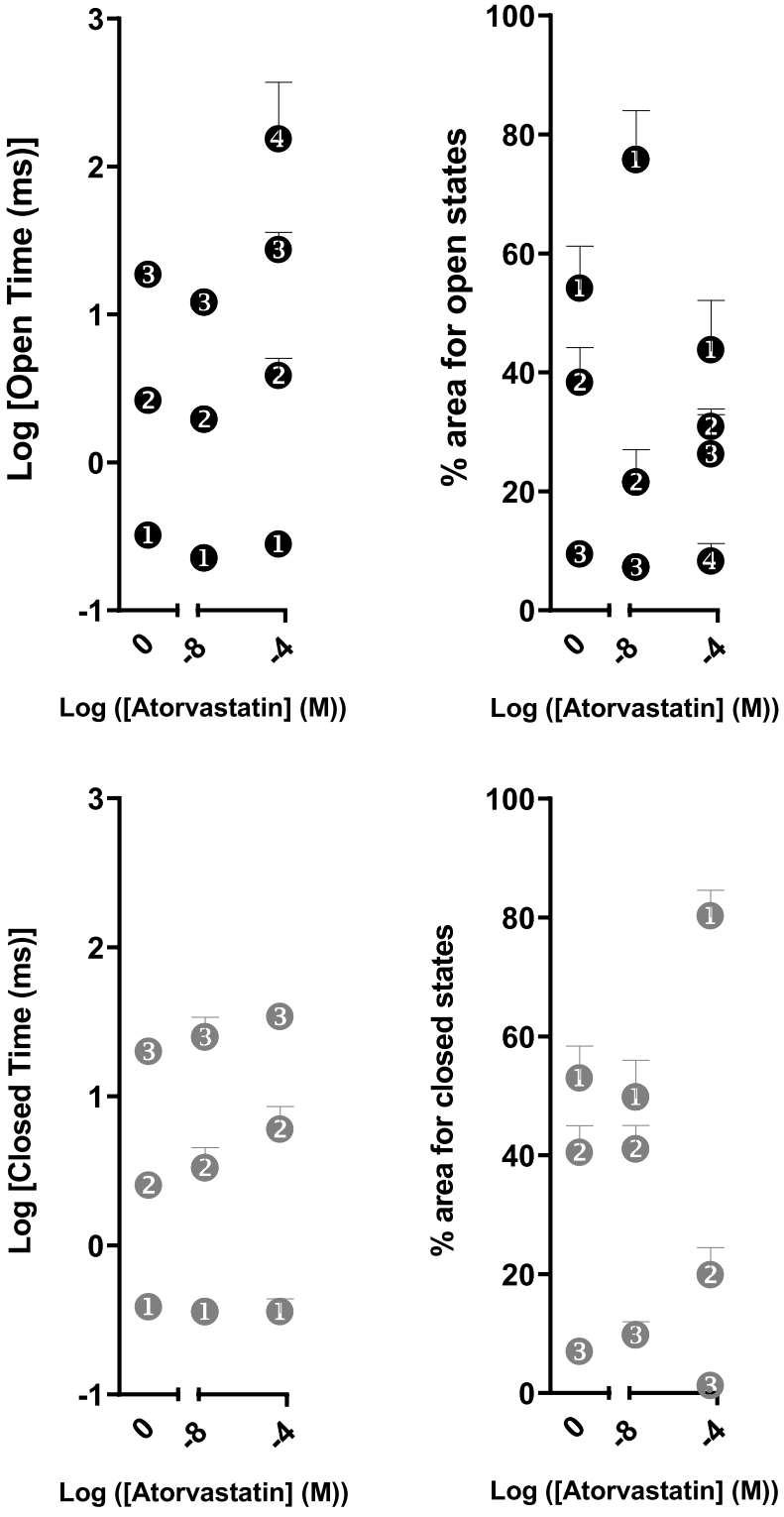


Figure 5.8: Effects of atorvastatin on mean open and closed lifetime parameters for single purified RyR2 channels Mean lifetime parameters ± SEM for pdfs on single lifetime parameters from purified RyR2 channels for open (top, black) and closed (bottom, grey) lifetime parameters. Log dwell times (left) and their respective percentage area (right) of pdfs are plotted against each [atorvastatin] in 10 μM Ca^{2+}. The numbers within the symbols refer to the 1st (shortest), 2nd, 3rd and 4th time constants.

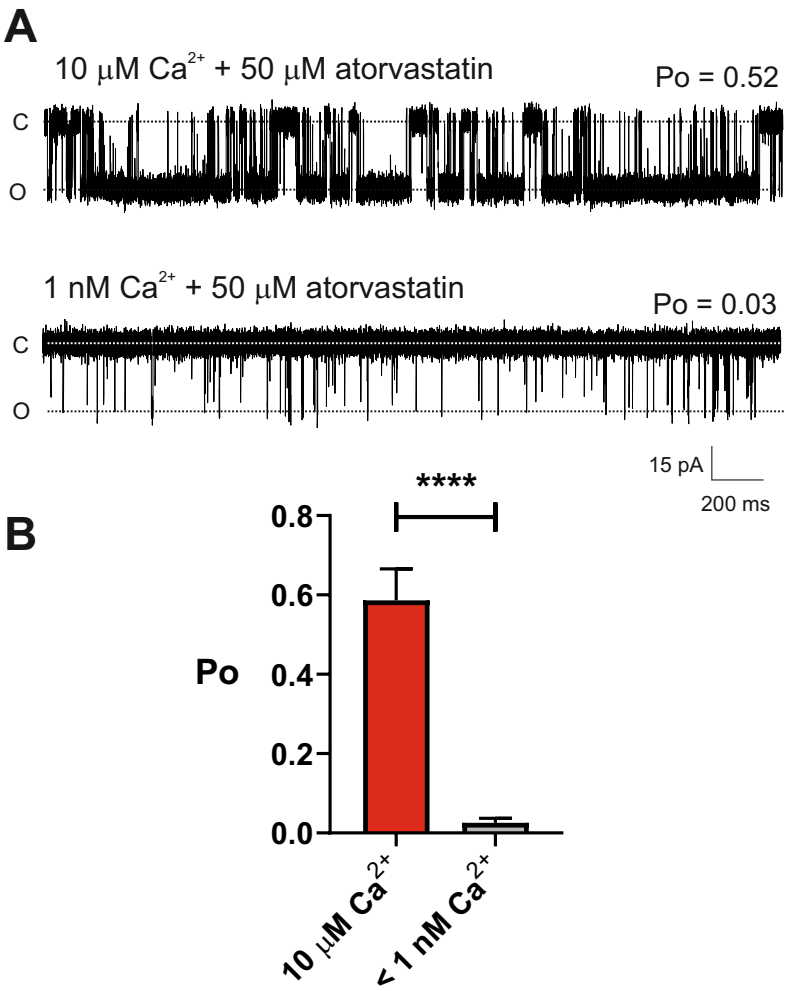


Figure 5.9: Evidence of Ca^{2+}-independent openings with 50 μM atorvastatin **(A)** A typical purified RyR2 single-channel recording in symmetrical KCl with 10 μM free Ca^{2+} held at – 40 mV. The top trace displays the gating of RyR2 with 50 μM atorvastatin and 10 μM free Ca^{2+} in the cytosolic chamber, and the bottom trace displays the same channel after addition of 1 mM cytosolic EGTA, therefore chelation of $[Ca^{2+}]$ to < 1 nM, still in the presence of 50 μM atorvastatin. C and O represent the closed and open states, respectively. **(B)** Mean Po values ± SEM for 50 μM atorvastatin with the indicated cytosolic $[Ca^{2+}]$, in the same conditions as (A). Data for 10 μM Ca^{2+} with 50 μM atorvastatin is the same data as in Fig. 5.5. Each bar represents n $\geq$ 7. Unpaired t-test: significant difference indicated by **** for $p < 0.0001$.

At the sub-activating free cytosolic $[Ca^{2+}]$ of < 1 nM, in the absence of other cytosolic activators, it would be expected that Po would be zero (Walweel et al., 2014). The representative trace in Fig. 5.9A showed that after Ca^{2+} was lowered to < 1 nM in the presence of 50 μM atorvastatin, channel openings were not completely abolished. Further, the mean Po values given in Fig. 5.9B showed that Po was not reduced to zero. These remaining openings were therefore induced by 50 μM

atorvastatin itself. Hence, at high micromolar concentrations, atorvastatin can induce openings in a Ca^{2+}-independent manner, as has previously been reported for simvastatin (Venturi et al., 2018). Lifetime analysis was thereby conducted to explore this mechanism further.

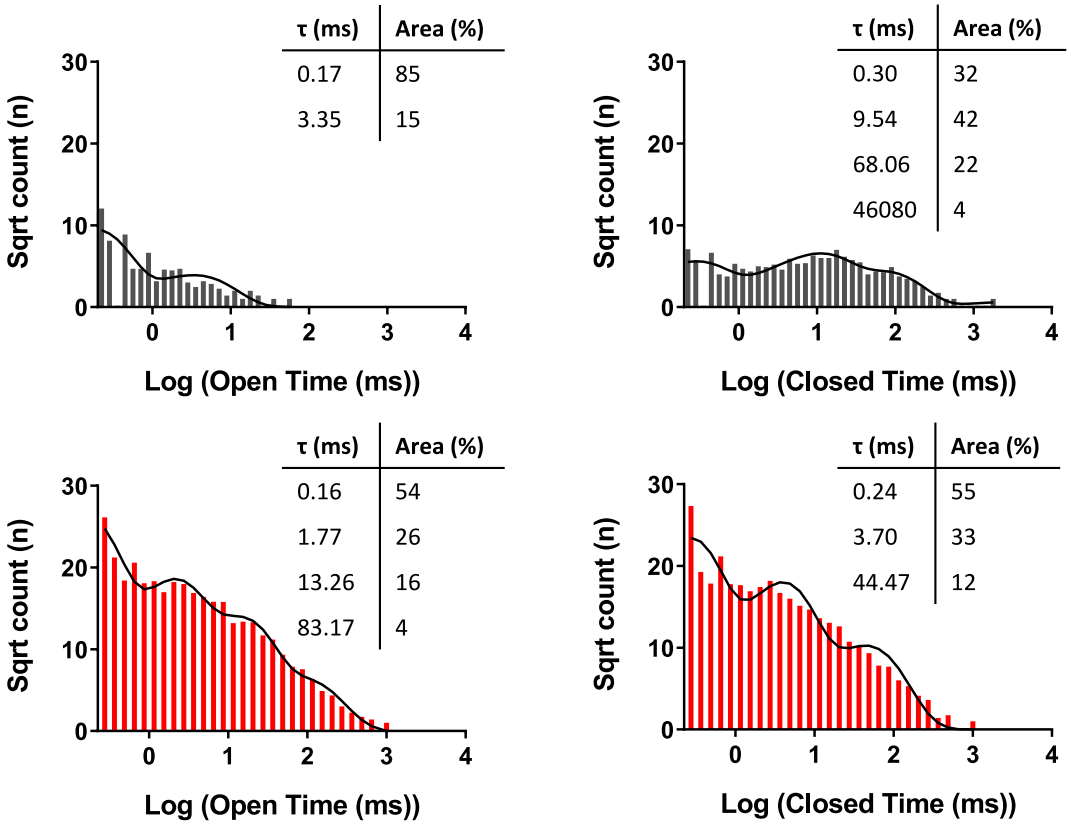


Figure 5.10: Evidence of Ca^{2+}-independent openings with 50 μM atorvastatin Open (left) and closed (right) lifetime distributions and pdfs for representative single purified RyR2 channels in the same conditions as Fig. 5.9 in the presence of 50 μM atorvastatin and $<$ 1 nM Ca^{2+} (black) or 50 μM atorvastatin with 10 μM cytosolic free Ca^{2+} (red). The best fits to the data were obtained by the method of maximum likelihood and the resulting time constants (τ, ms) and percentage areas (%) for each lifetime distribution are shown with each histogram.

Examples of lifetime analyses in Fig. 5.10 demonstrated that the increase of free cytosolic [Ca^{2+}] from $<$ 1 nM Ca^{2+} to 10 μM in the presence of 50 μM atorvastatin increased the number of exponentials that the open lifetime distribution is best fit to with the addition of the long opening exponentials associated with activation by 50 μM atorvastatin in activating [Ca^{2+}] (10 μM). Additionally, the closed lifetime distribution was best fit to a fewer number of exponentials with sub-activating

cytosolic Ca^{2+}; closed lifetime distributions at 1 nM Ca^{2+} were best fit to four exponentials whereas closed lifetime distributions at 10 μM Ca^{2+} were best fit to two exponentials. This indicated that in the presence of 50 μM atorvastatin, raising cytosolic [Ca^{2+}] increased the frequency of openings that is associated with an increase in [Ca^{2+}] (Sitsapesan and Williams, 1994a), as well as increasing the duration of openings. Nevertheless, atorvastatin does induce Ca^{2+}-independent openings as shown in Fig 5.10; the open lifetime distribution with 1 nM Ca^{2+} and 50 μM atorvastatin can still be fit to two exponentials indicating some longer opening events even in sub-activating [Ca^{2+}].

5.4 Atorvastatin modulation on a CPVT1-mutated RyR2

Fig. 5.11 compares the effects of low nanomolar and high micromolar concentrations of atorvastatin on native RyR2 channels derived from WT or V2475F(+/-) mouse hearts. In the RyR2 channels derived from WT mouse cardiac tissue, there was a similar pattern of gating in response to atorvastatin as observed in the purified sheep RyR2 channels (Fig. 5.3); a biphasic response of apparent inhibition at low concentrations and activation at higher concentrations. The average response of these native mouse RyR2 channels differed from that of that purified sheep RyR2 since the lowest Po value was obtained with 1 nM atorvastatin rather than 20 nM atorvastatin (although lower atorvastatin concentrations were not tested on the purified sheep RyR2s). As described in chapter 3, WT channels presented a lower Po at 1 μM cytosolic free Ca^{2+} (control) compared to V2475F(+/-). However, in contrast to WT channels, there was no evidence for an inhibitory action of atorvastatin at 1 nM in the RyR2 channels derived from V2475F(+/-) mouse hearts. RyR2 channels derived from V2475F(+/-) hearts were activated to a higher mean Po level than WT in response to 50 μM atorvastatin, however, since the control Po was higher at 1 μM Ca^{2+} the fold-increase in Po was similar (1.55-fold and 1.58-fold increase for WT and V2475F(+/-) channels, respectively).

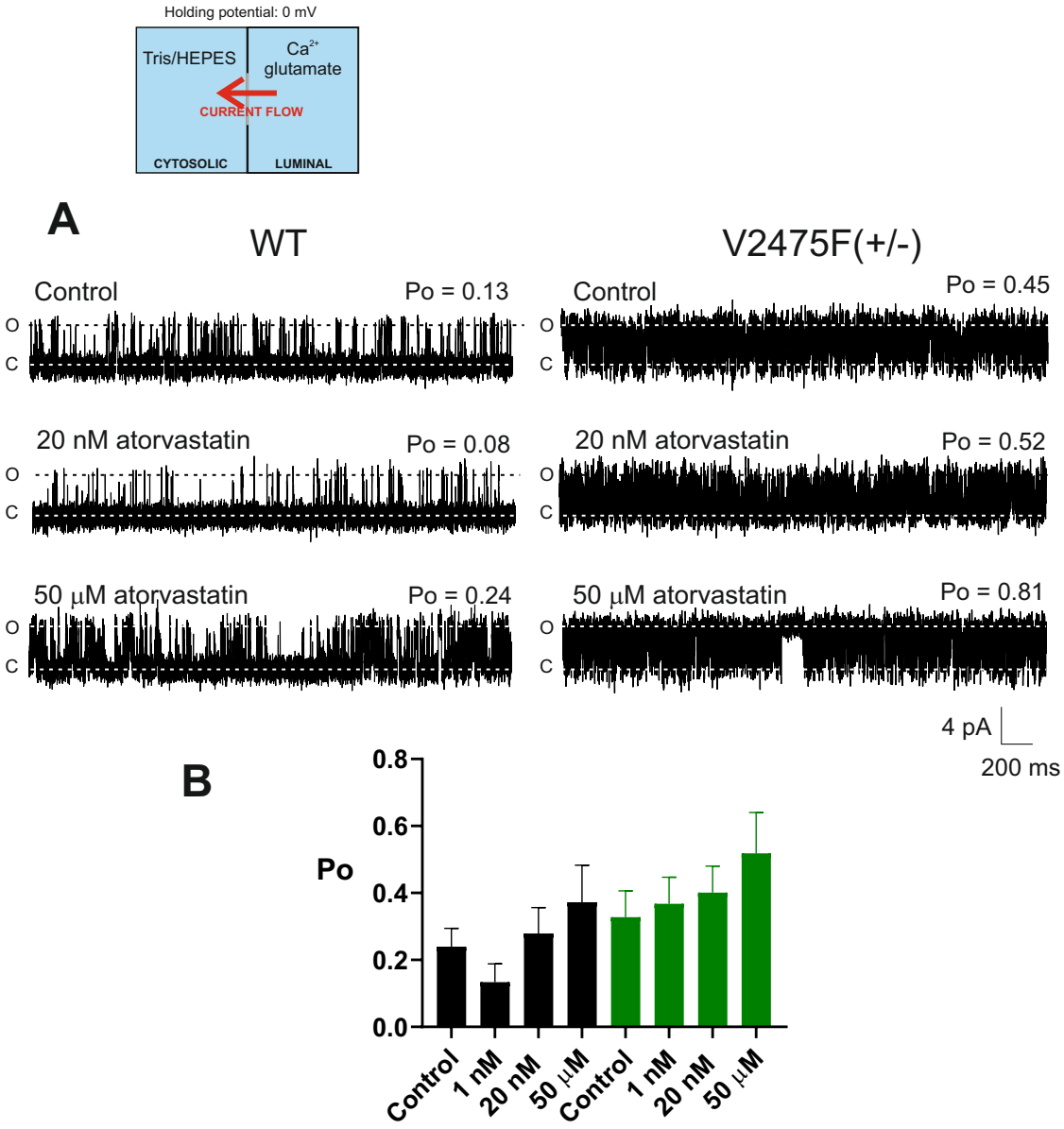


Figure 5.11: Effects of atorvastatin on mouse native RyR2 channel gating **(A)** A typical native RyR2 channel isolated from V2475F(+/-) mouse cardiac tissue in Tris/HEPES and Ca^{2+}-glutamate solutions, held at 0 mV, with Ca^{2+} as the permeant ion. A simplified model of the experimental conditions is shown above the traces. Control indicates 1 μM cytosolic Ca^{2+}, and the [atorvastatin] added to the cytosolic side is indicated above. Po displayed above the traces was the average Po measured over 3 min of recording. Traces were filtered at 800 Hz. O and C represent the fully open and closed levels, respectively **(B)** Mean Po values ± SEM at control (1 μM cytosolic Ca^{2+}) and with increasing [atorvastatin] added to the cytosolic side. Native RyR2 channels isolated from WT (black) or V2475F(+/-) (green) mouse cardiac tissue. (Two-way ANOVA: Ca^{2+}-by-genotype interaction, $p = 0.98$; no main effect of statin, $p = 0.14$, main effect of genotype, $p = 0.02$. Mean ± SEM; $n \geq 5$).

As described in Chapter 3, channels derived from heterozygous V2475F(+/-) mouse hearts can be divided into populations of channels, grouped by their different Po in response to both cytosolic Ca^{2+} or Mg^{2+}. Consequently, the behaviour of individual channels in response to atorvastatin was examined. In response to 1 nM atorvastatin (Fig. 5.12), 67% of WT channels were inhibited in comparison to 29% of V2475F(+/-) channels. In response to 50 μM atorvastatin, a similar proportion of channels were activated; 78% of WT channels were activated by 50 μM atorvastatin in comparison to 63% of V2475F(+/-) channels (Fig. 5.12).

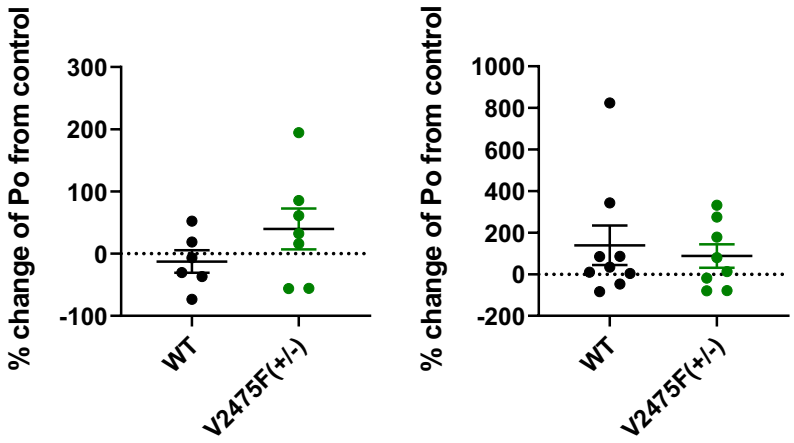


Figure 5.12: Percentage change in Po of mouse native RyR2 in response to 1 nM (A) or 50 μM (B) atorvastatin Percentage change of Po from control (1 μM cytosolic Ca^{2+}) in response to 1 nM or 50 μM cytosolic atorvastatin, calculated from data in Fig. 5.11 from native RyR2 channels isolated from WT (black) or V2475F(+/-) (green) mouse cardiac tissue. Each point represents an individual channel.

To investigate this mechanism further, lifetime analysis was conducted on two V2475F(+/-) channels, one that was inhibited and one that was not inhibited by 1 nM atorvastatin to investigate the difference in two individual channel's response derived from the same V2475F(+/-) cardiac tissue.

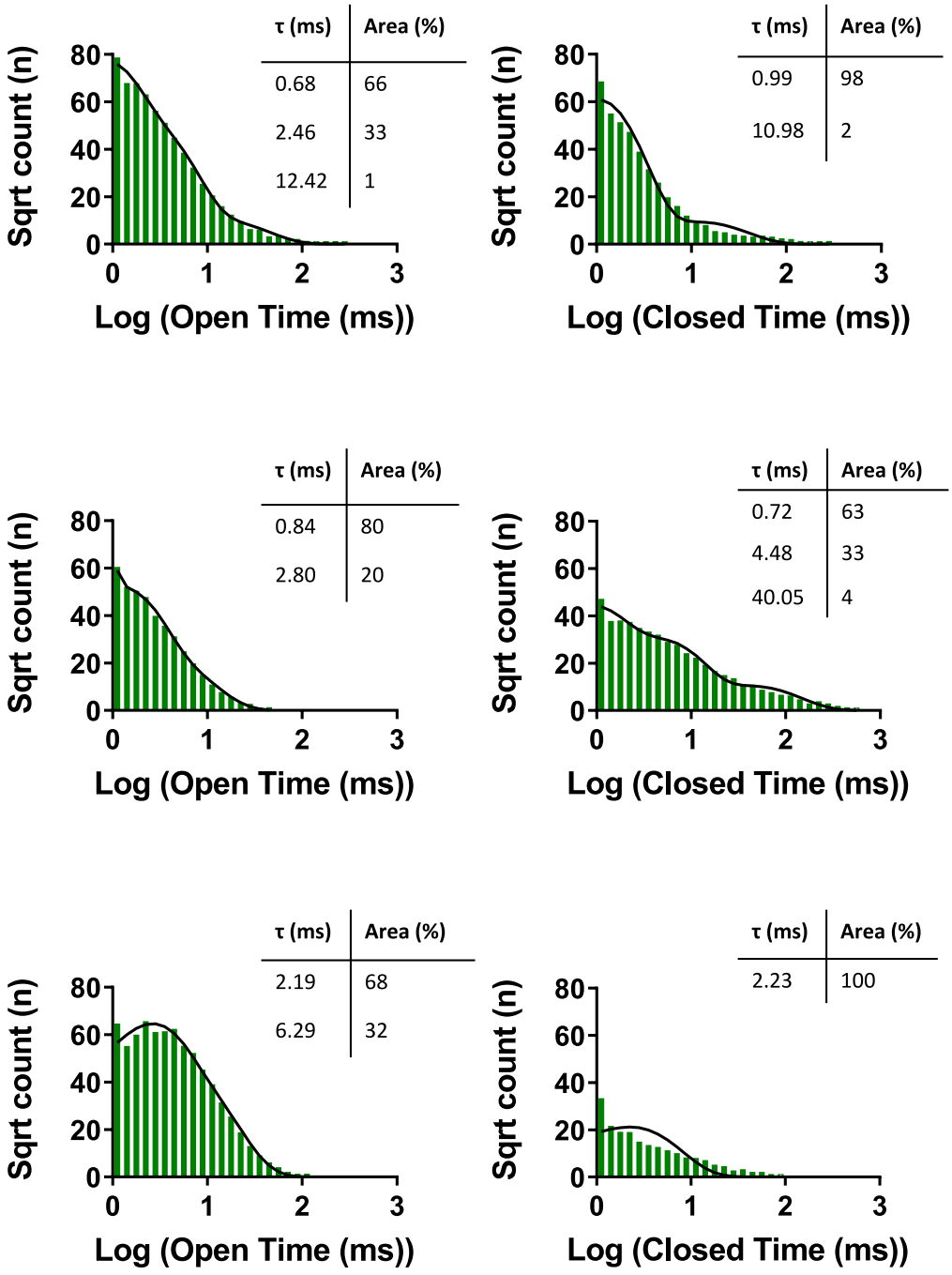


Figure 5.13: Open and closed lifetime distributions of a single RyR2 channel derived from V2475F(+/-) tissue that behaves similarly to a WT channel in response to 1 nM and 50 μM atorvastatin Lifetime distributions and pdfs for a single RyR2 channel derived from V2475F(+/-) mouse hearts are shown. The best fits to the data were obtained by the method of maximum likelihood and the resulting time constants (τ, ms) and percentage areas (%) for the representative single RyR2 channel are displayed next to each graph. The top figures correspond to control (1 μM Ca^{2+}), the middle figures correspond to 1 nM atorvastatin and the bottom figures correspond to 50 μM atorvastatin added to the cytosolic face of the channel.

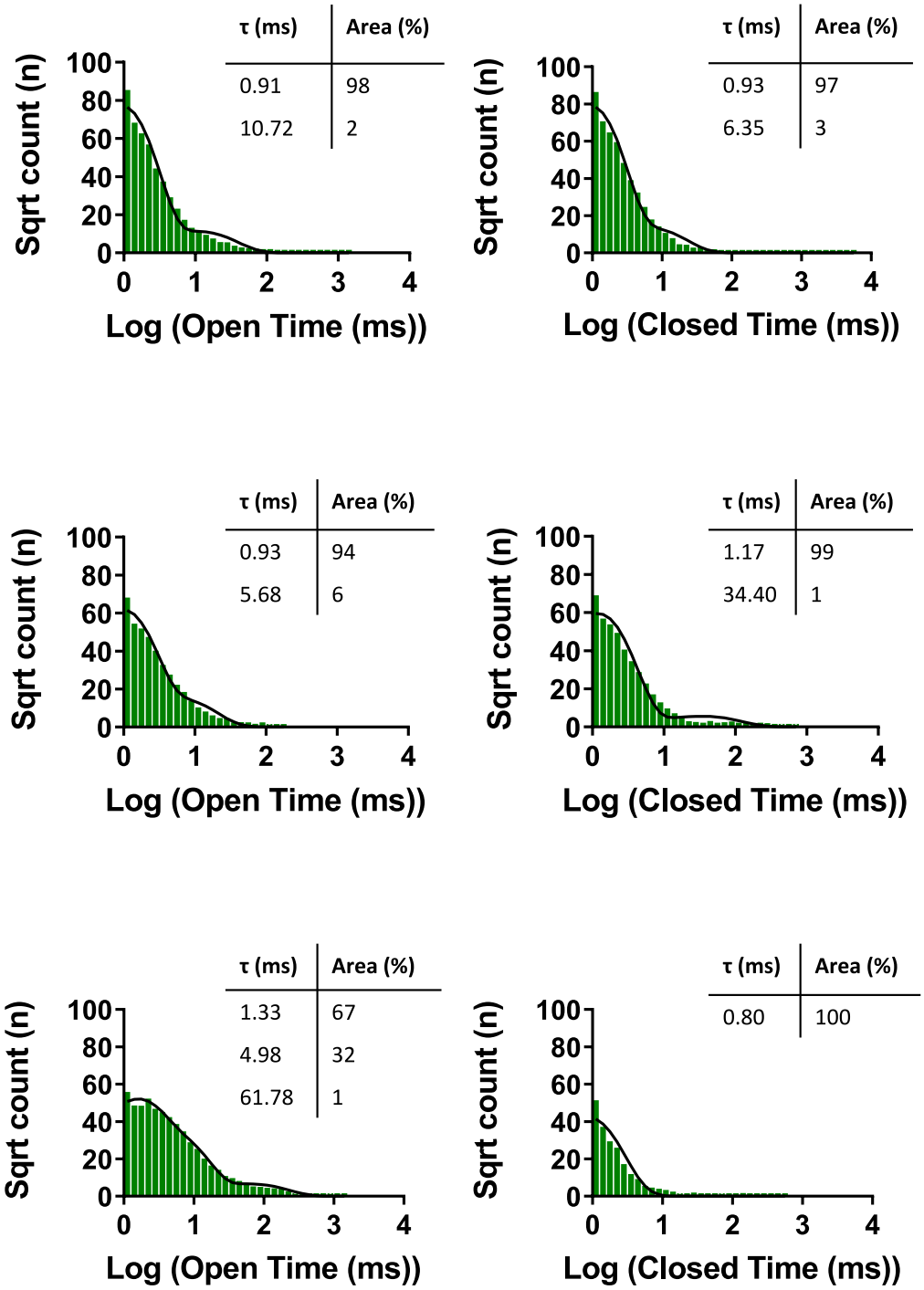


Figure 5.14: Open and closed lifetime distributions of a single RyR2 channel derived from V2475F(+/-) tissue that behaves differently to a WT channel in response to 1 nM and 50 μM atorvastatin Lifetime distributions and pdfs for a single RyR2 channel derived from V2475F(+/-) mouse hearts are shown. The best fits to the data were obtained by the method of maximum likelihood and the resulting time constants (τ, ms) and percentage areas (%) for the representative single RyR2 channel are displayed next to each graph. The top figures correspond to control (1 μM Ca^{2+}), the middle figures correspond to 1 nM atorvastatin and the bottom figures correspond to 50 μM atorvastatin.

Fig. 5.13 displays lifetime analysis for a channel derived from V2475F(+/-) cardiac tissue that was inhibited at 1 nM atorvastatin and therefore behaved similar to a WT channel. Fig. 5.14 displays the lifetime analysis for a V2475F(+/-) channel that was not inhibited by 1 nM atorvastatin, and therefore differed from WT. Although these observations are only based on one representative channel in each case, the trends observed that may indicate a mechanism for this inter-channel variation are as follows.

With the addition of 1 nM atorvastatin to the cytosolic face of the channel, the number of exponentials that the open lifetime distribution was best fit to decreased alongside an increase in the proportions of openings that resided in the smallest exponential (Fig. 5.13). The closed lifetime distribution was altered with a decrease in the proportion of closings in the shortest exponential (Fig. 5.13). Following the increase of atorvastatin to 50 μM, the greatest effect on the lifetime distributions was observed to the closed distribution, reducing the number of exponentials that the distribution was best fit to from three to one. The closed and open lifetime distribution at control and 50 μM atorvastatin were similar comparing the two single channels both derived from WT channels (Fig 5.14). The open lifetime distributions with 1 nM atorvastatin were similar. However, the closed lifetime distribution at 1 nM atorvastatin differed between the two V2475F(+/-) channels. In this example, the alteration was observed in the closed lifetime distribution, in which there was a greater proportion of closings in the shortest exponential, and the distribution was best fit to only two exponentials. On account of this, the proposed difference between the two channels may be the absence of a decrease in the frequency of openings with the addition of 1 nM atorvastatin in the channel displayed in 5.14, whereas frequency of openings were decreased in the channel displayed in Fig. 5.13.

6

Discussion

Contents

6.1 The pathophysiological effects of the V2475F mutation at single-channel RyR2 144
6.1.1 Alterations to modulation by cytosolic Ca^{2+} 144
6.1.2 Alterations to modulation by cytosolic Ca^{2+} at 100 nM 147
6.1.3 Alterations to modulation by cytosolic Mg^{2+} 148
6.1.4 Differences in other key activators 150
6.1.5 Alterations to single-channel conductance 151
6.2 The contribution of phosphorylation to CPVT1 pathophysiology 153
6.2.1 Phosphorylation levels at S2808 were not altered 153
6.2.2 The relationship between S2808 phosphorylation levels and RyR2 single-channel function 154
6.2.3 β-adrenergic stimulation at the cardiomyocyte level . . 156
6.3 The interaction between RyR2 and atorvastatin 159
6.3.1 Comparison of purified and native RyR2 159
6.3.2 Atorvastatin modulates purified RyR2 gating 160
6.3.3 Statins as a therapeutic intervention for arrhythmic heart disease 162
6.4 Populations of single-channel behaviour 164
6.5 Structure-function relationship 170
6.6 Summary 172
6.6.1 Physiological implications 172
6.6.2 Other potential mechanisms 175
6.6.3 Generalised models of CPVT1 175
6.6.4 Concluding remarks 176

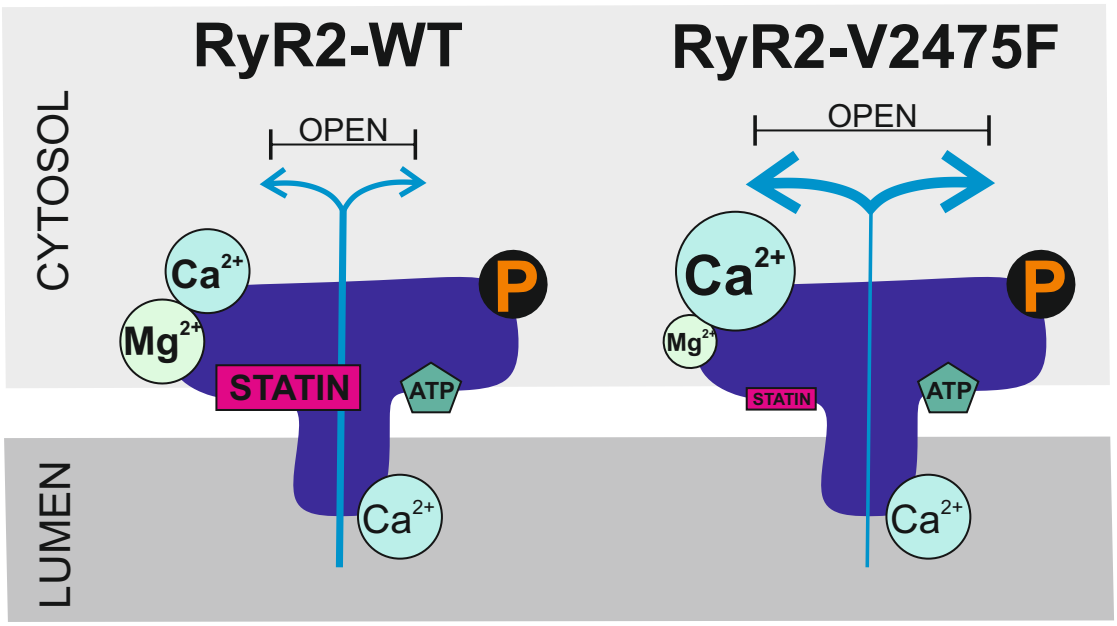


Figure 6.1: Schematic depicting the alterations at RyR2 caused by the V2475F mutation These alterations were observed at the single-channel level and by western blots in this thesis. The change in size of the icon for each regulatory ligand or drug indicates an increase, decrease or no change in sensitivity caused by the V2475F mutation compared to WT. The black circle with the orange P indicates phosphorylation levels at S2808.

This thesis reveals aberrant ligand regulation of RyR2 caused by the V2475F mutation, in addition to alteration of Ca^{2+} ion flux through the pore. By individually examining dysregulation in response to key aspects of the complex regulation of RyR2, the critical dysfunction in response to cytosolic Ca^{2+} and Mg^{2+} has been identified. The degree of these deviant behaviours could be associated with the number of mutated monomers in the heterozygous V2475F(+/-) RyR2 channels. Alterations in response to adenosine-based ligands, luminal Ca^{2+}, and K^{+} conductance properties were also characterised, but were not identified to be significant factors contributing to the CPVT1 phenotype in this mutation. Furthermore, basal phosphorylation levels at S2808 did not appear altered, but Po was greater for V2475F(+/-) mutated RyR2 at all levels of S2808 phosphorylation compared to WT. In line with the disruption observed at the single-channel level, β-adrenergic-stimulated cardiomyocytes isolated from V2475F(+/-) hearts

exhibited a shorter latency to spontaneous Ca^{2+} release compared to WT cardiomyocytes. Alongside an aberrant response to endogenous ligands, RyR2 channels with the V2475F mutation also responded differently to atorvastatin compared to WT. These finding are summarised in Fig. 6.1.

6.1 The pathophysiological effects of the V2475F mutation at single-channel RyR2

6.1.1 Alterations to modulation by cytosolic Ca^{2+}

The modifications to the RyR2 response to cytosolic Ca^{2+} observed here are likely to have crucial implications for the pathogenesis of CPVT1. At 1 μM Ca^{2+}, the V2475F(+/-) channels have significantly higher activity than WT channels (Fig. 3.8). The increase in activation from 100 nM to 1 μM Ca^{2+} is very steep for mouse RyR2, and particularly steep for the V2475F(+/-) channels with an EC_{50} of 0.17 μM (Fig. 3.8). Since the activation portion of the curve was so steep, this EC_{50} calculation will not be precise. However, the collection of further data points on this steep part of the curve was not attempted because of the error in measuring the free [Ca^{2+}] in this range. Nevertheless, it is evident that at low micromolar [Ca^{2+}] the V2475F(+/-) derived channels were more sensitive to the activating effects of cytosolic Ca^{2+} compared to WT channels. At 1 μM Ca^{2+}, the [Ca^{2+}]-response relationship had already reached its maximal activation. This does not occur until between 10 to 100 μM for WT channels (Fig. 3.8). The increase in Po from 100 nM to 1 μM was driven by the increase in frequency of channel opening, but for V2475F(+/-) channels this effect was much greater, contributing to the higher Po observed (Fig. 3.9). Additionally, the best fit to the open lifetime distributions of a proportion of the V2475F(+/-) channels, required an additional long fourth exponential which was not observed in any WT channels, indicating that the mutation causes RyR2 to open to an additional long open state. (Fig. 3.10). This also contributed to the higher Po of the V2475F(+/-) channels at 1 μM Ca^{2+} 3.8. At 1 μM cytosolic Ca^{2+}, RyR2 channels derived from V2475F(+/-)

preparations could be separated into four groups dependent on their Po values (Fig. 3.17). Since CPVT1 is caused by a heterozygous mutation at RyR2, this may be linked to the different number of monomers per RyR2 (Fig. 3.16). The contribution of the heterozygosity of the V2475F(+/-) channels in response to 1 μM cytosolic Ca^{2+} is discussed further in Section 6.4.

It is important to note that although the V2475F(+/-) channels appear to be more sensitive to cytosolic Ca^{2+}, on average, the peak Po that V2475F(+/-) channels achieve is no higher than that of WT channels. Both WT and V2475F(+/-) mouse RyR2 channels reach a maximal activation Po of approximately 0.45 in Ca^{2+} alone (Fig. 3.8). Under similar experimental conditions, it has been shown previously that cytosolic Ca^{2+} alone cannot fully activate native RyR2 channels derived from mice (Salvage et al., 2019) and from other species like sheep (Sitsapesan and Williams, 1994a; Laver et al., 1995) and dog (Chu et al., 1993), indicating that cytosolic Ca^{2+} is a partial agonist for RyR2 channels. The results in this thesis show that this is also true for the V2475F(+/-) mouse RyR2 channels. However, this characteristic of Ca^{2+} activation does not always remain when RyR2 is purified before reconstitution into bilayers. Some groups have shown that purified mouse RyR2 displays maximal activation with a Po > 0.9 in response to cytosolic Ca^{2+} alone (Li and Chen, 2001), alongside other groups showing maximal activation with other species of purified RyR2 in cytosolic Ca^{2+} alone (Mukherjee et al., 2012). It is possible that the methods for purifying and reconstituting RyR2 may disrupt its normal behaviour. For example, in the study by Li and Chen (2001), the RyR2 channels were recombinantly expressed in a human embryonic kidney 293 (HEK) cell before purification. Firstly, the synthesis of RyR2 in a HEK cell means that some cardiac RyR2-associated proteins will not be present endogenously, or may be present but at different levels, which may affect the resultant Po of the RyR2 channel. For example, HEK cells do not express CASQ which is reported to modify RyR Po differently depending on the luminal free [Ca^{2+}] (Beard et al., 2002; Györke et al., 2004). Secondly, HEK-cell derived RyR2 may not be subjected to the same post-translational modifications that would alter RyR2 gating in their

native environment within cardiomyocytes, such as oxidation or phosphorylation (Niggli et al., 2013; Denniss et al., 2018). In these experiments, we used NaF as a phosphatase inhibitor when isolating RyR2 from cardiac tissue in order to maintain basal phosphorylation levels (Chapter 2). The process of purification may also affect RyR2 function. However, the method of purification used previously in the Sitsapesan laboratory had found similar gating behaviour between native and purified sheep RyR2 (Sitsapesan and Williams, 1994a). Nonetheless, different groups use varying concentrations of CHAPS and phospholipid mixtures, with some reports of purification causing damage to RyR2, affecting not only its ability to gate in response to ligands (Laver and Lamb, 1998) but also affecting the conducting properties of the channel (Lai et al., 1988b). Purified RyR2 may again have extra loss of associated proteins due to the solubilisation procedure (Timerman et al., 1994; Györke et al., 2004). Taken together, we propose that the partial agonism of cytosolic Ca^{2+} exhibited by the mouse native RyR2 in this thesis, and by other authors, is more likely to reflect how a cardiac RyR2 *in situ*, devoid of intervention by recombinant expression procedures or purification protocols, would respond to cytosolic Ca^{2+}. The single-channel bilayer experiments are still a reductionist approach that can not exactly mimic physiological conditions, but by investigating the individual effects of various ligands on native RyR2 function, we hope to reveal basic mechanisms of RyR2 channel gating and conduction that are altered in patients with this CPVT1-mutation.

As the cytosolic [Ca^{2+}] was increased above 1 μM Ca^{2+}, V2475F(+/-) channels exhibited a shortening of open times and a decrease in the frequency of openings (Fig. 3.9). Furthermore, the single-channel recordings in 1 μM cytosolic Ca^{2+} (Fig. 3.8) displayed a distinctive 'flickering' type of rapid channel gating; the frequency of channel opening was high but the channels only briefly resided in the open state. At 1 mM cytosolic Ca^{2+}, the closed lifetime distributions for V2475F(+/-) channels had a high proportion of closings occurring in the shortest exponential which was not observed in the distributions for WT channels (Fig. 3.11). This contributed to the significantly lower Po in V2475F(+/-) channels at 1 mM Ca^{2+} and the 12-fold

lower IC_{50} value. Overall, these observations evidenced that, alongside the rapid activation in response to 1 μM cytosolic Ca^{2+}, the V2475F-mutated RyR2 channels also displayed an increased sensitivity to inactivation in response to cytosolic [Ca^{2+}] above 1 μM [Ca^{2+}]. It is possible that Ca^{2+} had a greater affinity at the cytosolic inactivation site/s for V2475F(+/-) channels than for WT channels.

At 10 μM Ca^{2+}, as the Po single-channel activity is similar between the WT and mutant RyR2 channels, it was therefore informative to compare the lifetime analysis at this cytosolic [Ca^{2+}] as shown in Fig. 3.12. The open lifetimes appear to differ the most between WT and V2475F(+/-) channels. The open lifetimes for WT channels can be fit to a greater number of exponentials compared to that of the V2475F(+/-) channels. Further, a higher proportion of events exist in the shortest exponential for V2475F(+/-) channels, with 92 % of events in the shortest exponential for V2475F(+/-) channels compared to 65 % of events in the shortest exponential for WT channels (Fig. 3.12). The closed lifetime distributions appeared similar when comparing WT and V2475F(+/-) at 10 μM cytosolic Ca^{2+}. Although the mean Po activity at 10 μM Ca^{2+} is similar between WT and V2475F(+/-) channels, this indicates that the sensitivity to Ca^{2+} inactivation is already taking effect, as observed by the briefer closing events, further evidencing that the V2475F(+/-) channels are more sensitive to the cytosolic effects of Ca^{2+}.

6.1.2 Alterations to modulation by cytosolic Ca^{2+} at 100 nM

Of particular interest was the alteration to the mechanism of Ca^{2+} regulation of V2475F(+/-) channels in the presence of 100 nM cytosolic Ca^{2+} as this is the approximate concentration of Ca^{2+} during diastole in a ventricular cardiomyocyte (Eisner et al., 2020). Most WT and V2475F(+/-) channels remained closed at 100 nM Ca^{2+}, but those V2475F(+/-) channels that opened did so with a higher Po and a prolonged duration of openings (Fig. 3.13 and 3.14. Burst analysis was used to elucidate the Ca^{2+} binding kinetics that caused this abnormality (Fig. 3.15 and Table. 3.1). The normal mechanism for Ca^{2+}-induced activation of

RyR2 is increased binding of Ca^{2+} to the closed state of the channel (Sitsapesan and Williams, 1994a). However, because the interburst intervals for V2475F(+/-) channels and WT channels were similar at 100 nM Ca^{2+}, this suggests that Ca^{2+} did not bind more frequently to the closed state of the V2475F(+/-) channels than to the closed state of the WT channels and therefore this mechanism was not the cause for higher Po of the V2475F(+/-) channels. Instead, at 100 nM Ca^{2+}, burst analysis indicated an increased burst duration and a greater proportion of bursts with more than one event in V2475F(+/-) channels compared to the WT channels (Fig. 3.15). Furthermore, a prolonged duration of openings was observed in the V2475F(+/-) channels compared to WT (Fig. 3.9). Additionally, the open lifetime distributions at 100 nM Ca^{2+} were best fit to three or four exponentials compared to WT channels which were best fit to one or two exponentials (Fig. 3.14 and 3.12). Taken together, these results suggest that at 100 nM cytosolic Ca^{2+}, Ca^{2+} may have bound more readily to the open state of the channel, in other words, the Ca^{2+} dissociated more slowly which resulted in the sustained bursts and prolonged openings observed. Perhaps a similar mechanism also contributes to the heightened sensitivity to Ca^{2+}-inactivation; slower Ca^{2+} dissociation from the inhibitory cation binding site could cause enhanced inhibition (Fig. 3.8). However, it was not possible to conduct burst analysis at 1 mM cytosolic Ca^{2+} due to an insufficient number of recordings with only single channels gating in the bilayer in these conditions.

6.1.3 Alterations to modulation by cytosolic Mg^{2+}

Cytosolic Mg^{2+} is a key ligand in the regulation of RyR2 as it inhibits RyR2 activity. Since the V2475F mutation caused abnormalities in the response to cytosolic Ca^{2+}, and since Mg^{2+} competes with Ca^{2+} for the activation and inhibitory sites on RyR2 (Pessah et al., 1985; Meissner et al., 1986; Smith et al., 1986) it is not unexpected that alterations to normal Mg^{2+} function were also observed. As discussed previously, the binding of Ca^{2+} to RyR2 appears altered but without an apparent change in efficacy in terms of Po, since the maximal activation of V2475F(+/-) channels is similar to that of WT channels (Fig. 3.8). However, the

efficacy for Mg^{2+} does appear to be altered. The mean inhibitory effect of Mg^{2+} was reduced in V2475F(+/-) channels, and surprisingly, Mg^{2+} behaved as an agonist in 23% of experiments. Most channels (46%) were partially inhibited, but not to the same extent as WT, whereas 31% of V2475F(+/-) channels were inhibited to the same extent as WT channels. In response to 1 μM cytosolic Ca^{2+}, the data in Fig. 3.17 indicated that there may be different populations of V2475F(+/-) channels based on their Po values. Heterozygous RyR2 mutations cause CPVT1 (Priori et al., 2001), and since our mouse model was heterozygous for the V2475F mutation (Loaiza et al., 2013), it is tempting to speculate that the different channel behaviours could be modelled to the expected distribution of the number of mutated monomers per RyR2 (Fig. 3.16). If so, it seems logical to suggest that a tetrameric RyR2 with zero or only one mutated monomer would have a similar channel response to Mg^{2+} as WT, two mutated monomers might induce an intermediate response, while three to four mutated monomers might be required to cause such extreme channel disruption that Mg^{2+} behaves as an agonist. This is displayed as a schematic in Fig. 6.3 and the contribution of the heterozygosity of the V2475F(+/-) channels is discussed in more detail in Section 6.4.

This is the first time in single-channel experiments that Mg^{2+} has been shown to have an agonistic effect. It has been suggested from radioligand binding assays that Mg^{2+} can reduce the inactivating effects of Ca^{2+} (Chugun et al., 2007), but at 1 μM [Ca^{2+}] as in the experiments in Fig. 3.22 this is unlikely to be the mechanism involved since Ca^{2+} normally inactivates RyR2 only at high micromolar or millimolar concentrations (Laver et al., 1995). It is possible that the observed reduction in the Ca^{2+} off rate at the activation site may shift binding in favour of Ca^{2+} over Mg^{2+} in the intermediately effected channels, and therefore Mg^{2+} is less able to compete with Ca^{2+} due to site occupancy at the cation activation site. However, the observation that some channels can in fact be activated by Mg^{2+} suggests that the mutation enables a bound Mg^{2+} to cause a different effect on RyR2 in which RyR2 responds to Mg^{2+} more similarly to the way it responds to Ca^{2+}, albeit with a much lower efficacy. As discussed previously, the increased sensitivity of V2475F(+/-) channels

to millimolar Ca^{2+} at the inactivation site could have indicated that the sensitivity of V2475F(+/-) channels to Mg^{2+} inhibition would also change. This may be in part what happens since, although not calculated, the IC_{50} appears to have shifted to the right. However, since Mg^{2+} can also activate some channels, it appears that a change to the interactions between Mg^{2+} and the Ca^{2+}-activation site is also implicated in the abnormal Mg^{2+} modulation of RyR2 in V2475F(+/-) channels.

In recombinant CPVT1 channels, the P2328S, Q4201R and V4653F mutations were also shown to reduce the inhibitory action of Mg^{2+} in single channel experiments (Lehnart et al., 2004), and the R2474S and K4750Q mutations decreased the ability of Mg^{2+} to inhibit ryanodine binding (Uehara et al., 2017). All these mutant RyR2s also display increased sensitivity to cytosolic Ca^{2+}. Since the similarity in increased sensitivity to Ca^{2+} and reduction of Mg^{2+} inhibition was also observed in multiple HD1 domain mutations (P2328S by Salvage et al. (2019) and R2474S by Uehara et al. (2017), this suggests a mutation in HD1 has a direct impact on mechanisms of Ca^{2+} and Mg^{2+} modulation.

6.1.4 Differences in other key activators

Compared to WT channels, the V2475F(+/-) derived RyR2 channels displayed a non-significant trend for increased sensitivity to luminal Ca^{2+} within physiological ranges (Fig. 3.26). It had previously been reported that the homozygous V2475F(+/+) channels exhibited heightened sensitivity to the activating effects of luminal Ca^{2+} (Loaiza et al., 2013) however, an important difference in the experiment displayed in Fig. 3.26 was the presence of cytosolic ATP since the potentiating effects of luminal Ca^{2+} are greater when cytosolic activators in additon to cytosolic Ca^{2+} are present (Sitsapesan and Williams, 1994b). The experiments in this thesis also used native V2475F(+/-) channels rather than homozygous recombinant channels (Loaiza et al., 2013), therefore factors such as differences in the number of mutated monomers or disruptions to the interactions with associated proteins such as CASQ2 may impact

the resultant finding. Our results are similar to those found in native HD1-mutated RyR2s with the P2328S mutation (Salvage et al., 2019).

V2475F(+/-) channels had a greater Po in response to 1 μM cytosolic Ca^{2+} alone compared to WT channels (Fig. 3.8). However, both the WT and V2475F(+/-) RyR2 channels showed an increase in Po as expected from the addition of 1 mM adenosine or ATP in the presence of cytosolic Ca^{2+} (McGarry and Williams, 1994; Kermode et al., 1998). Although, adenosine-based ligands appeared to increase the Po of V2475F(+/-) channels to a higher level than that of the WT channels, this Po increase was to a similar relative extent from their activation level with 1 μM Ca^{2+} alone (Fig. 3.21). The response of the RyR2 channels to adenosine as well as to ATP was investigated. Although adenosine was less effective than ATP at activating RyR2 as expected, adenosine will not induce phosphorylation and does not chelate Ca^{2+}, so we can be certain that the effect was dependent solely on the activation at the nucleotide-binding site. Lifetime analysis for V2475F(+/-) channels in the presence of cytosolic 1 μM Ca^{2+} and 1 mM adenosine showed that their open lifetime distribution was best fit to a fourth exponential that was absent in the open lifetime distributions for WT channels in the same conditions (Fig. 3.25, top panels). The mechanism for adenosine-based ligands to increase RyR2 Po is via increasing open durations, as well as the frequency of openings (Kermode et al., 1998). The additional exponential that the V2475F(+/-) channel open lifetime distributions were best fit to therefore suggested that the V2475F(+/-) channels had an exaggerated increase in duration of channel openings in response to the synergistic effect of cytosolic 1 μM Ca^{2+} and adenosine compared to WT channels.

6.1.5 Alterations to single-channel conductance

Alongside the modifications of RyR2 sensitivity to cytosolic ligands, the V2475F mutation also caused significant alterations to the single-channel conductance. As shown in Fig 3.1 and 2, channels derived from V2475F(+/-) hearts displayed a mean 8.6% reduction in Ca^{2+} conductance compared to WT channels. This alteration to

Ca^{2+} conductance was initially unexpected since the mutation site is far from the pore. Since conductance through the pore of RyR2 for a permeant ion is dependent on the affinity of that ion with binding sites within the conduction pathway (Lindsay et al., 1991; Tinker and Williams, 1992) it may be that the mutation caused a fractional alteration in the affinity for Ca^{2+} in the pore. RyR2 cytosolic Ca^{2+} activation sites are shielded from the flux through its own pore (Liu et al., 2010), so this reduction in Ca^{2+} conductance is unlikely to affect the activity of the same channel. In fact, there was no observed correlation between single-channel conductance and Po (Fig. 3.18). To our knowledge, this is the first time conductance properties of an RyR2 have been shown to be altered with a CPVT1 mutation. Since the luminal [Ca^{2+}] in these experiments was approximately 50 mM the Ca^{2+} current was around 4.2 pA, which is much greater than the proposed 0.5 pA flux through RyR2 in physiological conditions inside a cardiomyocyte (Mejía-Alvarez et al., 1999; Kettlun et al., 2003; Gillespie and Fill, 2008). Therefore, it is uncertain how this observed difference will affect the cytosolic [Ca^{2+}] at neighbouring RyR2 channels following SR Ca^{2+} release in physiological conditions. Future experiments could measure the alterations to conductance of Mg^{2+} and the relative permeability of Ca^{2+} to Mg^{2+}, as it is conceivable that this could also be altered. There appeared to be no alteration to K^+ conductance. Further, the relative permeability of Ca^{2+} to K^+ was not observed to be different between WT and V2475F(+/-) channels and was similar to values measured in previous studies (Tinker and Williams, 1992).

An increased incidence of sub-conductance states has been reported to occur with CPVT1-mutated RyR2 channels that are depleted of some associated proteins like FKBP12.6 (Wehrens et al., 2003; Meli et al., 2011). Incidences of sub-conductance states were therefore quantified to compare WT and V2475F(+/-) channels (Fig. 3.7), but the incidence of sub-conductance gating states was infrequent and there was no apparent difference between WT and V2475F(+/-) channels. On the basis on these results, it did not appear that sub-conductance states impacted the pathophysiology of the V2475F-mutated RyR2 channels.

6.2 The contribution of phosphorylation to CPVT1 pathophysiology

6.2.1 Phosphorylation levels at S2808 were not altered

The western blots shown in Fig. 4.5 indicated that there was no difference in the levels of phosphorylation of WT or V2475F(+/-) derived RyR2 channels at S2808. At basal levels, in which all experiments in Chapter 3 and 5 were conducted, the phosphorylation level at S2808 was approximately 85% for both WT and V2475F(+/-) channels (Fig. 4.5). This was similar to the basal phosphorylation level observed in sheep RyR2 of 75% (Carter et al., 2006) and in agreement with measurements by Valdivia's group for WT mouse native RyR2 (Alvarado et al., 2017). In line with our findings, other studies have shown that the CPVT1 mutations do not alter basal phosphorylation of S2808 (Sedej et al., 2010; Meli et al., 2011; Shan et al., 2012). The conditions used in the treatment of the SR vesicles for western blot experiments paralleled those in the bilayer experiments. The same temperature, same duration of kinase or phosphatase incubation, and comparative concentrations of ligands were used in order to create conditions as similar as possible to the bilayer experiments to estimate the levels of RyR2-S2808 phosphorylation in the single-channel experiments. This suggested that the Po values observed in the bilayer experiments may correspond to near maximal phosphorylation of S2808 (99%) following the phosphorylation treatment with PKA, and to near zero (4% for WT and 10% for V2475F(+/-)) phosphorylation following the de-phosphorylation treatment with PP1 (Fig. 4.5). Although the S2808 phosphorylation levels appeared similar in the WT and CPVT1-mutated RyR2, the functional response to phosphorylation may still be different. However, the only way to determine this is by comparing single-channel activity of the same channel incorporated into a bilayer before and after incubation by kinases or phosphatases.

6.2.2 The relationship between S2808 phosphorylation levels and RyR2 single-channel function

A key finding in Chapter 4 was that with the reduction of phosphorylation at S2808 of RyR2 by PP1, the Po of V2475F(+/-) channels did not decrease to the same level of the WT RyR2 channels (Fig. 4.2). This suggests that the intrinsic alterations to RyR2 channel gating caused by the V2475F mutation may be independent of the phosphorylation level at S2808. Other studies have also demonstrated increased CPVT1-RyR2 channel activity without additional phosphorylation (Uchinoumi et al., 2010; Sedej et al., 2010). The V2475F(+/-) derived channels, like WT channels, still displayed functional sensitivity to dephosphorylation by PP1 at S2808, since the relative decrease in Po was similar to that of WT channels (Fig. 4.2).

The RyR2 channels derived from mouse cardiac tissue in these experiments do not increase in Po when incubated with PKA (Fig. 4.4). In response to incubation with PKA, western blots suggest that the mouse RyR2 channels become hyperphosphorylated (Fig. 4.5 but the Po in the bilayer experiments was decreased (Fig. 4.4). This suggests that they do not become uncoupled from Ca^{2+} regulation with hyperphosphorylation, as is the case for sheep RyR2 (Carter et al., 2011). Previous studies in WT mouse have also shown a decrease in Po in response to treatment by PKA (Benkusky et al., 2007). It is possible that this disparity observed was due to species differences. For example, different species may have differences in the expression of endogenous kinases or other proteins associated with RyR2 that may affect the functional response to PKA phosphorylation (Carter et al., 2011; O'Brien et al., 2015).

In the study by Wehrens et al. (2003) investigating the changes in RyR2 function caused by the CPVT1 mutation, R2474S, it was reported that the Po of the R2474S channels was no different to that of the WT channels in the presence of 150 nM free cytosolic Ca^{2+}. However, upon phosphorylation by PKA, the R2474S channels subsequently displayed a significantly greater Po than the WT channels. Despite R2474S neighbouring the V2475F studied here, these results were different to

the results described in this thesis in Chapter 3 and 4. It is possible that the different mutations could cause different gating changes, despite being neighbouring residues. However, there are also differences in the experimental procedures that may explain these different functional changes. The RyR2 channels used by Wehrens et al. (2003) were recombinant RyR2 expressed in non-cardiac cells, and therefore the large number of proteins normally associated with native RyR2 extracted from cardiac tissue, as in the experiments in this thesis, are likely to be different. Further, the basal phosphorylation or the phosphorylation observed following PKA treatment at S2808 was not quantified in these experiments by Wehrens et al. (2003), so it is possible that the measured Po in these conditions do not relate to the phosphorylation levels we observe. In the experiments in Chapter 4, the Po following PKA incubation was measured after the PKA and required co-factors for phosphorylation were perfused out. This does not appear to be the case in experiments by Wehrens et al. (2003), so co-factors added to the bilayer may have an effect on Po independent of phosphorylation levels at S2808.

A key aspect of the data in this thesis is that experiments were performed on native RyR2 channels rather than using purified or recombinant channels. It is possible that the basal phosphorylation level of the native RyR2 channels will be more similar to that of channels in cardiomyocytes. It is also known that purification of RyR2 can affect gating behaviour (Li and Chen, 2001), therefore it seems possible that the use of native channels will provide a better understanding of the changes to RyR2 function in relation to phosphorylation that result in patients with CPVT1.

Carter et al. (2006) demonstrated that the relationship between phosphorylation of the native sheep cardiac RyR2 at S2808 and Po appeared to be biphasic in nature since basal levels of phosphorylation (75% phosphorylation of the maximum) at this site were associated with lower Po than that observed at near zero levels of phosphorylation (following PP1 treatment) or maximum levels of phosphorylation following incubation with PKA. In Chapter 4, the results indicate that basal levels of phosphorylation of native mouse RyR2 at S2808 (75% of maximum) were similar to those of sheep RyR2 as were the levels of phosphorylation that occurred after

incubation with PP1 or PKA. However, the Po associated with those levels of phosphorylation at S2808 in mouse RyR2 appeared to be very different to those of sheep RyR2. It appeared that the mouse RyR2 were phosphorylated to a level that gave the maximal functional response at basal, since both increasing and decreasing the phosphorylation level causes a reduction in Po from basal control levels. A schematic of this effect is illustrated in Fig. 6.2. Although there is high homology between different species for RyR2, with 91.7% identity sequence alignment between mouse and sheep (Table. 1.1), this different response to phosphorylation may still be due to species differences. Although both preparations used in this example were native and thereby isolated from cardiac tissue, the mouse preparation is composed of mixed membranes, whereas the sheep native preparation undergoes another enrichment step to separate heavy SR vesicles from light SR (Section 2.2.3). It is possible that this modification could remove an important protein associated with phosphorylation. For example, RyR2 has been found to be associated with PKA, PKA regulatory subunits, PP1, protein phosphatase 2A (PP2A) and muscle A kinase anchoring protein (mAKAP) in canine ventricular tissue (Marx et al., 2000). It is possible that one of these associated proteins was removed in the enrichment step, or that a species difference exists between the mouse and sheep in the expression of these associated proteins. Futhermore, in normal physiology, different species may require different regulation of RyR2 as it is known that cardiac Ca^{2+} homeostasis varies between species. For example, smaller mammals generally require much faster Ca^{2+} cycling and so may require modification to the regulation of RyR2 function of a larger mammal like the sheep (Milani-Nejad and Janssen, 2013). All these factors could play a role in the different functional outcomes observed.

6.2.3 β-adrenergic stimulation at the cardiomyocyte level

Fig. 6.2 shows that although RyR2 channels isolated from V2475F(+/-) cardiac tissue exhibit higher Po than WT channels, overall, a similar pattern of Po changes were observed after PP1 or PKA incubation and with the level of phosphorylation at S2808. This is a simplified picture of the effects of phosphorylation and does

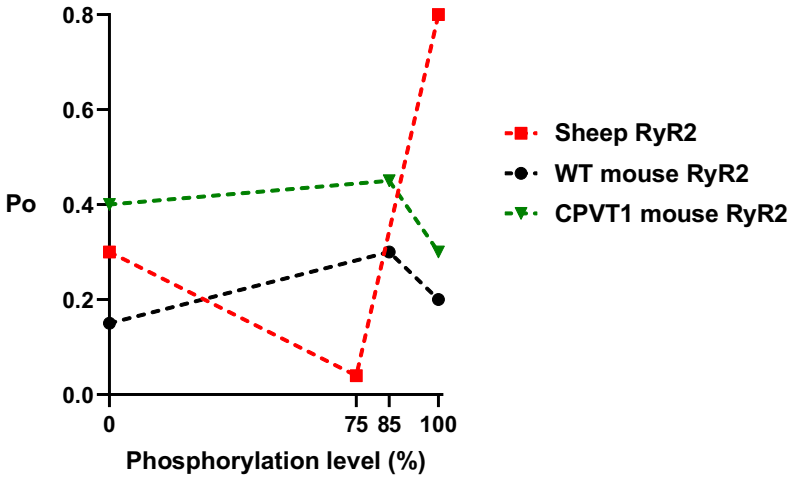


Figure 6.2: Schematic describing the complex non-linear relationship between RyR2 phosphorylation and Po Increasing Po is indicated by the y-axis, and level of phosphorylation at S2808 is indicated on the x-axis. The Po change for RyR2 channels derived from WT (black) or V2475F(+/-) (green) mouse hearts displays a similar relationship, but the Po level is generally higher for channels derived from V2475F(+/-) hearts at low micromolar [Ca^{2+}], as measured in Chapter 4 of this thesis. The RyR2 derived from sheep displays an opposite relationship to the mouse with an uncoupling from cytosolic Ca^{2+} sensitivity at maximal phosphorylation levels, as described by (Carter et al., 2006, 2011; O'Brien et al., 2015); this was not observed in these experiments in the mouse RyR2. This schematic is only an approximate comparison of Po values; the respective conditions at each phosphorylation level in the mouse RyR2 experiments were the same, however the cytosolic [Ca^{2+}] was different between the sheep and mouse RyR2 experiments, as is their cytosolic Ca^{2+} sensitivity (Walweel et al., 2014).

not account for changes in phosphorylation at other sites. To understand how the changes in RyR2 function may be linked with changes in SR Ca^{2+} release in cardiomyocytes, the effect of isoprenaline on the spontaneous Ca^{2+} release from the SR in WT and mutant cardiomyocytes was investigated. Perfusion of isolated mouse hearts with isoprenaline has been shown to increase the phosphorylation level of RyR2-S2808 (Benkusky et al., 2007). The perfusion of cardiomyocytes with isoprenaline containing solution (Fig. 4.7) would therefore be predicted to increase the S2808 phosphorylation levels at RyR2.

Since arrhythmogenesis and sudden cardiac death in CPVT1 is triggered in situations of high circulating catecholamine levels (Priori et al., 2001), there has been much interest in the idea that hyperphosphorylation of RyR2 is linked to increased tendency for arrhythmias (Wehrens et al., 2003; Van Oort et al., 2010), however, this

remains a controversial topic (Dobrev and Wehrens, 2014). The results of Fig. 4.7 show that, after isoprenaline exposure, the latency to non-recoverable spontaneous Ca^{2+} release in the V2475F(+/-) isolated cardiomyocytes was significantly shorter than that of WT cardiomyocytes, implicating β-adrenoceptor and downstream PKA activation as important for the increased likelihood of developing arrhythmias in the V2475F mutation. Although the single-channel experiments revealed that Po in both WT and V2475F(+/-) channels decreases following PKA incubation (Fig. 4.4), the V2475F(+/-) channels still exhibited a higher Po than WT channels over the range of S2808 phosphorylation levels (Fig. 6.2). It is possible that a decrease in Po of mouse RyR2 upon PKA-phosphorylation is a physiological mechanism to decrease the risk for diastolic Ca^{2+} release during β-adrenergic stimulation since SR Ca^{2+} levels increase (Bers, 2002). Perhaps the higher Po at maximal phosphorylation at S2808 for V2475F(+/-) channels compared to WT is an important contributing factor to the increased incidence of spontaneous Ca^{2+} release in the cardiomyocyte experiment, elevating the RyR2 activity to a level of increased likelihood for diastolic Ca^{2+} release. However, isoprenaline has many downstream targets for phosphorylation, including various sites of phosphorylation at RyR2, like S2030 and S2814, and also phosphorylates other proteins important in Ca^{2+} cycling, for example SERCA and phospholamban, (Bers, 2002; Huke and Bers, 2008) as detailed in the Introduction (Chapter 1). Further investigation is therefore required to isolate the complex role of RyR2 phosphorylation in arrhythmia generation in CPVT1.

The experiments in this thesis focused on just the one phosphorylation site of RyR2-S2808. A complete understanding of the functional role of RyR2 phosphorylation in CPVT1 is more complex. As described in the Introduction, there are many phosphorylation sites on RyR2 and phospho-specific antibodies have been developed for S2814 (a CaMKII specific site) and S2030 (a PKA specific site), hence these phosphorylation sites have been the most extensively characterised (Rodriguez et al., 2003; Wehrens et al., 2004; Xiao et al., 2006; Huke and Bers, 2008; Potenza et al., 2019). For example, since S2808 already has high basal phosphorylation, and since Xiao et al. (2006) demonstrated that S2030 has

low basal phosphorylation but is increased by β-adrenoceptor activation, this is possibly an important site for CPVT1, and may display more striking differences in phosphorylation levels between CPVT1-mutated and WT RyR2s. However, the commercially available S2030 antibody has a poor signal and so this site was not investigated here.

Mass spectrometry studies were planned to be conducted alongside the single-channel experiments, in order to investigate phosphorylation levels more accurately and across every serine site of the RyR2 protein. Preliminary optimisation experiments evidenced that mass spectrometry of the RyR2 peptides had good coverage at S2030, S2814 as well as S2808 (data not shown), and therefore would have allowed a more in-depth comparison of the global changes to RyR2 phosphorylation with various physiological kinases to mimic β-adrenoceptor stimulation in both WT and V2475F(+/-) derived RyR2 channels. Due to time limitations these experiments were not possible but should be the subject of a future investigation.

6.3 The interaction between RyR2 and atorvastatin

6.3.1 Comparison of purified and native RyR2

Both functionally purified sheep RyR2 and mouse native RyR2 preparations were used to study the mechanisms of atorvastatin modulation of RyR2 gating in Chapter 5. The mouse and sheep sequence identity alignment of RyR2 is similar at 91.7% (Table. 1.1), but there are some reported species differences in sensitivity to cytosolic divalent cations (Walweel et al., 2014). This method of RyR2 functional purification has previously found similar gating mechanisms between native and purified preparations (Sitsapesan and Williams, 1994a). However, as shown in Fig. 5.2, the Po was higher than previously measured from purified sheep RyR2 (Sitsapesan and Williams, 1994a). In studies by other groups on purified mouse

RyR2, the Po was also higher than we observed with native mouse RyR2 in Chapter 3 (Li and Chen, 2001). The purified mouse RyR2 in the study by Li and Chen (2001) displayed a greater maximal activation with cytosolic Ca^{2+}, in comparison to that more typically observed in native preparations (Fig. 3.8) (Sitsapesan and Williams, 1994a; Laver et al., 1995). As discussed previously, it is possible that some associated proteins that inhibit RyR2 gating that are normally present in purification methods had been removed, for example CASQ2 which in most conditions inhibits RyR2 activity (Beard et al., 2002; Györke et al., 2004), however this was not specifically quantified. There are advantages to using purified preparations for experiments with a ligand such as atorvastatin. Fewer RyR2-associated proteins to which atorvastatin could bind were therefore present and the bilayers did not contain other ion channel species such as the SR K^+ and Cl^- channels which make the interpretation of RyR2 channel recordings more challenging and means that K^+-containing recording conditions are difficult. Using purified RyR2, it was also therefore possible to use solutions with K^+ as the permeant ion, which allowed for improved resolution of brief events for lifetime analysis. For these reasons, the Po values between the native and purified preparations in Chapter 5 were not directly comparable, but the similar pharmacology observed has still given insights into the action of atorvastatin directly on RyR2.

6.3.2 Atorvastatin modulates purified RyR2 gating

Chapter 5 further elucidates the complex modulation of atorvastatin with RyR2. Atorvastatin modulated sheep purified RyR2 in a biphasic manner; at high concentrations (50 μM) functionally purified RyR2 were activated, whereas at low concentrations (20 nM) atorvastatin inhibited RyR2 (Fig. 5.3 and 5.2). There was no alteration to conductance suggesting no interaction with the pore region of RyR2 (Fig. 5.4). The biphasic gating response that we observed is similar to that observed with simvastatin and atorvastatin with native RyR2 channels (Venturi et al., 2018; Wilson et al., 2018). The biphasic response suggests that statins could be interacting with two different sites: a high affinity site associated with inhibition,

and a lower affinity site associated with RyR2 activation. By using purified RyR2 and still observing these two effects suggests that statins could be binding directly to RyR2 rather than to an associated protein or ion channel to modulate activity.

Only single channels incorporated into the bilayer could be used for mean dwell time calculations, so at some concentrations there are a small number of replications (Fig. 5.6). However, the data still provides some information regarding the potential mechanism for atorvastatin-induced alterations to RyR2 single-channel activity. The inhibitory action of 20 nM atorvastatin was inferred to be caused by a reduction in the duration of openings, with no effect on the frequency of openings (Fig. 5.6). Further, lifetime analysis showed a greater proportion of openings that resided in the shortest exponential following the addition of 20 nM atorvastatin compared to control (Fig. 5.7). These results suggest that the primary mechanism of inhibition by nanomolar atorvastatin was shortening of the duration of openings, in which nanomolar atorvastatin exerted its effect while the channel was in the open state. The activation by atorvastatin overrides the inhibitory effect in the micromolar range, with mean open duration increasing and mean closed times decreasing in an [atorvastatin]-dependent manner above 100 nM atorvastatin (Fig. 5.6). Furthermore, lifetime analysis displayed an additional exponential in most of the channels with the addition of 50 μM atorvastatin that was not detected in control conditions (Fig. 5.7). Thus, activation by 50 μM atorvastatin occurred by increasing the frequency of openings as well as increasing the duration of openings, suggesting that 50 μM atorvastatin binds to both the open and closed state of the channel.

Cytosolic Ca^{2+} activates RyR2 via increasing the frequency of openings (Sitsapesan and Williams, 1994a). High concentrations of atorvastatin appeared to cause sensitisation to the effects of Ca^{2+} since atorvastatin increased the frequency of openings in a concentration-dependent manner. However, 50 μM atorvastatin also induced an increase in mean open time, inferring that a Ca^{2+}-independent mechanism could also be involved. This was confirmed by the addition of 1 mM EGTA to chelate cytosolic Ca^{2+} to approximately 1 nM free [Ca^{2+}] in the presence of 50 μM atorvastatin, in which Ca^{2+}-independent openings were still observed

(Fig. 5.9). At this cytosolic [Ca^{2+}], you would not expect to observe any channel openings. Lifetime analysis of these Ca^{2+}-independent openings at 50 μM atorvastatin displayed open lifetime distributions that were best fit to two exponentials; this indicated that some of the openings were relatively long compared to very brief openings fit by the first exponential (Fig. 5.10). This is typical of Ca^{2+}-independent openings (Kermode et al., 1998).

6.3.3 Statins as a therapeutic intervention for arrhythmic heart disease

It is important to consider the relevant clinical dose of atorvastatin. A standard oral dose of 20 mg of atorvastatin can give up to 10 ng/ml peak plasma concentration (Pasanen et al., 2007), and the IC_{50} of statins against its primary target to reduce cholesterol, HMG-CoA reductase, is in the nanomolar range (Dansette et al., 2000), which is similar to the concentration range which was found to inhibit RyR2 single-channel activity in Chapter 5. The clearance of atorvastatin from plasma occurs via organic anion transporting polypeptide (OATP) transporters into hepatocytes (Matsushima et al., 2005). These transporters are also highly expressed in cardiac tissue, in particular the OATP2B1 transporter which has a high affinity for atorvastatin (Grube et al., 2006). Therefore, atorvastatin has been found to penetrate tissues and accumulate in cardiac tissue above the level of that in plasma in several studies (Jiráško et al., 2014; Higgins et al., 2014). Taken together, a low nanomolar concentration of atorvastatin in the intracellular cardiac environment appears to be a clinically relevant concentration to investigate.

The effect of atorvastatin on WT native mouse RyR2 channels has strong similarities to the effect observed on RyR2 purified sheep channels (Fig. 5.5). A low concentration (1 nM) of atorvastatin inhibited RyR2 and a high concentration (50 μM) activated WT RyR2 channels from control (Fig. 5.11). What is particularly interesting, is that the V2475F(+/-) RyR2 channels were not inhibited by atorvastatin at 1 or 20 nM. In retrospect perhaps this is not surprising; as shown in Chapter 3, Mg^{2+} no longer exerts the same level of inhibitory action on

V2475F(+/-) channels compared to WT channels, and V2475F(+/-) channels are hyperactive in response to 1 μM Ca^{2+} compared to WT channels, suggesting that the V2475F mutation causes disruption to the normal RyR2 response to ligands that modulate activity. Thus, if atorvastatin was effective in reducing diastolic Ca^{2+} leak from the SR in normal patients, it would seem likely that this would not be the case in RyR2-mutated CPVT1 patients. In consequence, this experiment highlights the critical importance of understanding the effect of any drugs that may be administered to patients with RyR2 mutations, since drugs may have a different effect to that expected in normal RyR2 in healthy patients. In fact, a number of studies have highlighted potential risk factors in administering statins to patients with malignant hyperthermia, concluding that a pre-existing impairment in Ca^{2+} handling caused by an RyR1 mutation can predispose patients to the known myotoxic side effects of statins (Guis et al., 2006; Metterlein et al., 2010).

The binding site for atorvastatin on RyR2 is unknown. Since the response of RyR2 to ligands that regulate the channel are altered in the V2475F-mutated RyR2 channels, for example cytosolic Ca^{2+} and Mg^{2+}, it is comprehensible that the response to drugs may also be altered. On the grounds of this, if there are two sites of action of statins on RyR2, one activation site and one inhibition site, perhaps the affinity for the activation site is increased relative to that of the inhibitory site due to the global structural change caused by the V2475F mutation. This would link to the observation that the maximal Po at 50 μM atorvastatin for V2475F(+/-) channels was greater than that for WT channels (Fig. 5.11).

The potential of atorvastatin as a treatment to reduce the risk of arrhythmias in CPVT1 via inhibition of mutated RyR2s requires further basic science understanding. Atorvastatin is a synthetic molecule, compared to other statins like simvastatin which are based upon a more complex natural product core (Schachter, 2005; Venturi et al., 2018). It is therefore easier to manipulate the chemical structure of atorvastatin compared to simvastatin. If the binding site of atorvastatin could be identified, then perhaps a more potent and inhibitory-specific compound could be synthesised to modulate RyR2 channels in CPVT1 that are hyperactive at nanomolar and

low micromolar concentrations of cytosolic Ca^{2+}. Future experiments within the Sitsapesan group have been proposed to investigate the binding site of atorvastatin with RyR2 via cryogenic electron microscopy (Ma et al., 2020), which may give us further insight into the interaction between RyR2 and statins.

6.4 Populations of single-channel behaviour

Disparity in inter-channel behaviour was observed in most experiments where the V2475F(+/-) channels were studied. This was expected as the mouse model and human genotype is heterozygous for the mutation (Priori et al., 2001; Loaiza et al., 2013). The expected populations of channels are illustrated in Fig. 3.16. It is more common for recombinantly expressed and detergent purified CPVT1-RyR2 channels to be researched (Liu et al., 2017; Uehara et al., 2017; Wang et al., 2017). However, this does not reflect the expression of heterozygous channels that exists in patients with CPVT1. Previous studies highlighted the variable nature of gating when RyR2 channels from the hearts of V2475F(+/-)-mutated mice were incorporated into bilayers (Loaiza et al., 2013) and other groups have found that heterologous co-expression of WT and CPVT1-E3987A mutated DNA gave rise to channels with Po values intermediate to that of WT or homozygous E3987A mutated channels containing four mutated monomers (Li and Chen, 2001). However, to our knowledge, this is the first comprehensive study of native CPVT1-mutated RyR2 channels that have explored different populations of the RyR2 channels in such detail and with such large numbers of replications.

Fig. 3.17 indicates that RyR2 channels from V2475F(+/-) preparations can be grouped into four populations of channel activity, suggesting that the number of mutated monomers in an RyR2 tetramer makes a significant difference to the gating behaviour of the channel, with a low Po population equivalent to WT activity, and three further groups of channels with greater activity than WT. The data indicates that whether RyR2 tetramers contain one, two, three or four mutated monomers makes a significant difference to the gating behaviour of the

channel. This gives further evidence for the critical importance to study native RyR2 channels to try to recapitulate the most similar RyR2 channel behaviour that would exist in a patient with CPVT1.

The single-channel response to cytosolic Mg^{2+} could also be grouped into different channel populations. The most surprising result was that Mg^{2+} behaved as an agonist in 23% of experiments. Most channels were partially inhibited, but not to the same extent as WT, whereas 31% of V2475F(+/-) channels were inhibited similarly to WT channels. As discussed previously, these different channel behaviours were compared against the expected distribution of number of mutated monomers, again suggesting that a scaled level of dysfunction could be dependent on the number of mutated monomers. If so, it seems most likely that three to four mutated monomers might cause such channel disruption that Mg^{2+} behaves as an agonist (Fig. 6.3).

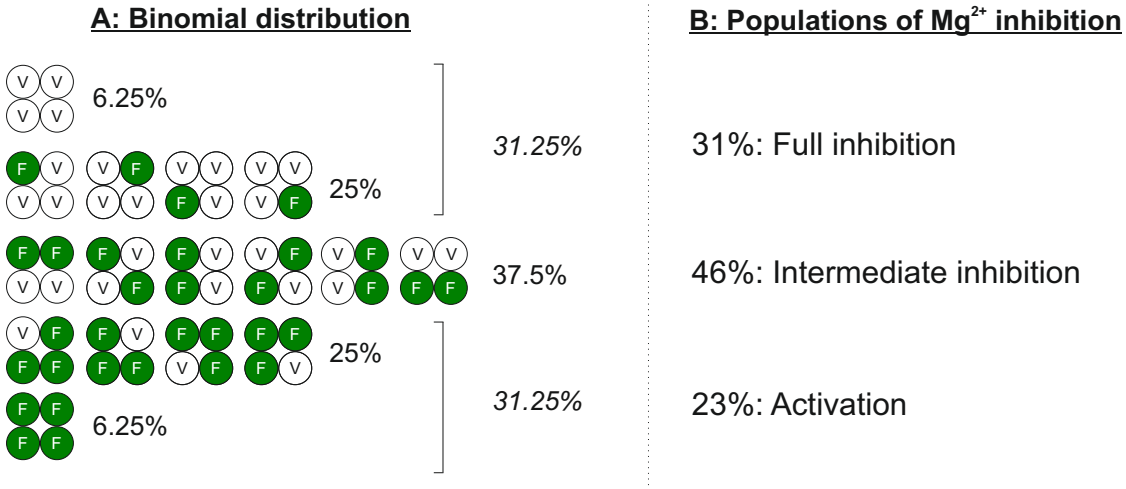


Figure 6.3: Schematic relating (A) the distribution of V2475F(+/-) channel populations and (B) the proportion of V2475F(+/-) channels with different behaviours to Mg^{2+} The proportion of channels was calculated by a binomial distribution, the percentage of channels in each Mg^{2+} behaviour type calculated from data shown in Fig. 3.24

Lifetime analysis of V2475F(+/-) channels also indicated a proportion of channels with behaviours that deviated from WT. For example, at 1 μM cytosolic Ca^{2+}, 38% of the V2475F(+/-) channels in which lifetime analysis was conducted showed an open lifetime distribution that was best fit to four exponentials whereas only three exponential were required to fit the open lifetime distribution of WT channels (Fig.

3.10). This would contribute to the significantly higher Po of the V2475F(+/-) channels compared to WT channels. This proportion of channels (38%) correlates with the population size of having three or four mutated monomers (31.25%), and in fact, all these channel exhibited a Po that was > 0.8, linking to the high Po populations observed by the KDE in Fig. 3.17. This gives further evidence that an alteration to the overall channel behaviour could be dependent on the number of mutated monomers (Fig. 6.4). Further, at 1 mM cytosolic Ca^{2+}, lifetime analysis on the closed lifetime distributions found that 60% of the V2475F(+/-) channels were best fit to a fourth long exponential that was absent in any closed lifetime distribution produced from a WT channel. Perhaps two or more mutated monomers in the channel can cause this extra-long closing exponential that contributes to the rapid Ca^{2+}-dependent inactivation of V2475F(+/-) channels (Fig. 3.11).

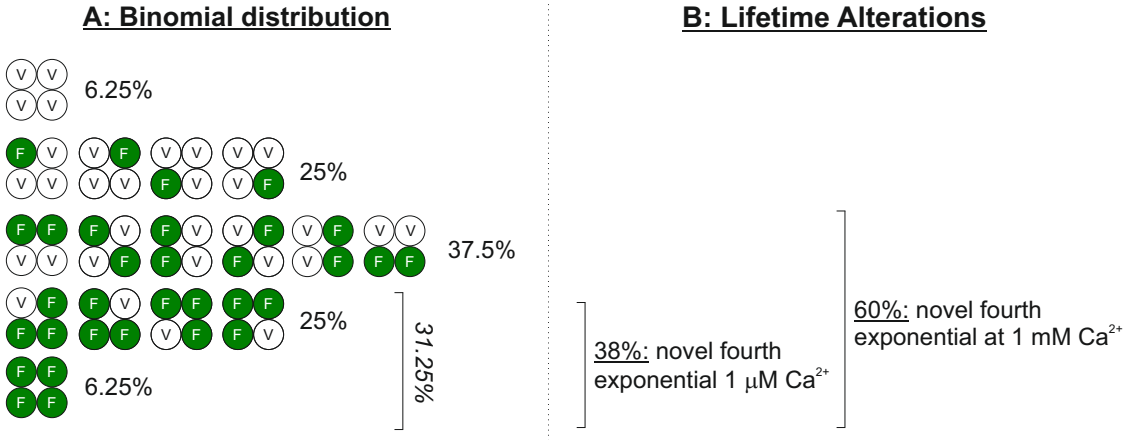


Figure 6.4: Schematic relating (A) the distribution of V2475F(+/-) channel populations, and (B) novel τ exponentials evidenced in lifetime analysis of open events at 1 μM and closed events at 1 mM cytosolic Ca^{2+} Proportion of channels calculated by a binomial distribution, percentage of V2475F(+/-) channels that could be fit to an extra τ exponential.

Disparate channel behaviour was also observed in the Ca^{2+} conductance of V2475F(+/-) channels (Fig. 3.2), however this did not correlate with channel activity (Fig. 3.18), and so may not be dependent on the number of mutated monomers. However, perhaps the symmetricity of the mutated monomers was important for permeation properties. In other words, having two mutated monomers side-by-side versus two mutated monomers diagonally opposite may impact channel conductance

differently whilst having equal effects on channel activity due to maintaining the same number of mutated binding sites.

As shown in Fig. 6.5, a 38% smaller proportion of channels derived from V2475F(+/-) cardiac tissue were inhibited in response to 1 nM atorvastatin compared to WT. Similarly to the disparity in response of V2475F(+/-) channels that were shown in Chapter 3, this percentage roughly equates to that percentage of channels that have three or four mutated monomers within the RyR2 tetramer. Perhaps a subset of the mutated RyR2 channels are insensitive to inhibition by low concentrations of atorvastatin and therefore contribute to a mean Po value that is not lower than the control value (Fig. 5.11). This was explored further by investigating lifetime analysis of two V2475F(+/-) derived channels that responded differently to inhibition by 1 nM atorvastatin as seen in WT channels (Fig. 5.13 and 5.14). Although underpowered due to a limited number of single channel experiments, one could speculate that, comparing these two representative channels suggested that the insensitivity to inhibition was due to the lack of reduction in frequency of openings. Perhaps modulation of sensitivity to Ca^{2+} by atorvastatin was not possible in some channels, for example, those channels with three or four mutated monomers. To investigate this possibility, a greater number of experiments are required.

In order to determine whether the RyR2 channels with four mutated monomers do exhibit the most aberrant channel behaviour discussed here, a future experiment could use the recombinant V2475F(+/+) RyR2 channels. If we then observe consistent activation in response to cytosolic Mg^{2+}, a channel with a Po of approximately 0.89 in response to 1 μM Ca^{2+} with their open lifetime distribution best fit to four exponentials, and a consistent insensitivity to inhibition by nanomolar atorvastatin, then this would help prove these predictions that channel behaviour was related to specific numbers of mutated monomers. However, since recombinantly produced RyR2 may have different associated proteins and will be subject to purification procedures, these channels will still be different to the native V2475F(+/-) RyR2 channels and results should be examined with caution.

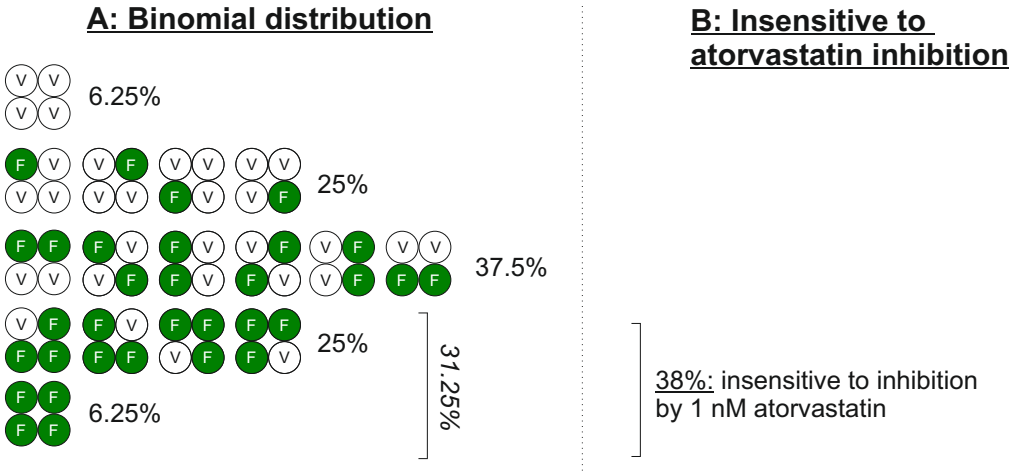


Figure 6.5: Schematic relating (A) the distribution of V2475F(+/-) channel populations, and (B) the proportion of channels from V2475F(+/-) preparations that are insensitive to 1 nM inhibition by atorvastatin different to WT. Proportion of channels calculated by a binomial distribution, percentage of channels that are not inhibited based on percentage change of Po from control following the addition of 1 nM atorvastatin.

RyR2 channels in cardiac junctional SR are situated in clusters of various sizes, (Franzini-Armstrong et al., 1999) the distribution and size of which can vary by altering the ionic conditions, degree of phosphorylation and association of regulatory ligands and proteins, and are found to be altered in some cardiac diseases (Asghari et al., 2014, 2020). Heterogeneity amongst RyR2 channels in clusters within cardiomyocytes may have implications on cluster dynamics. Greater sensitivity of the V2475F-mutated RyR2s to cytosolic [Ca^{2+}] between 100 nM and 1 μM Ca^{2+}, as shown in Chapter 3, are predicted to steepen the relationship between Ca^{2+} spark frequency and cluster size (Galice et al., 2018), and the heterogeneity is likely to impact on the consistency of local SR Ca^{2+}-release events. Simulations show that small clusters potentiate Ca^{2+} waves due to their enhanced SR Ca^{2+} load which then triggers propagation from larger neighbouring clusters (Xie et al., 2019). Small clusters of 8-10 RyRs are capable of producing a Ca^{2+} release event (Galice et al., 2018). With a large number of RyR2 channels in a cluster, they are most likely to have different numbers of mutated monomers in each channel distributed binomially as in Fig. 3.16, meaning large clusters will be relatively similar to other large clusters. On this account, there is a greater chance for heterogeneity

in small clusters, since the random incidence of a cluster with a high proportion of V2475F(+/-) RyR2s with multiple mutated monomers only and fewer WT-like channels is more likely as there are fewer overall channels. Therefore, there may be specific small clusters that exhibit a high propensity for inappropriate Ca^{2+} release and therefore generation of DADs. This mechanism could be common across various heterozygous CPVT1 mutations at RyR2 and requires further investigation.

Taken together with the evidence in Chapter 3 and Chapter 5, it appears that certain subsets of the channels derived from V2475F(+/-) mutated cardiac tissue contribute most strongly to the detrimental CPVT1 phenotype. In a study by Bongianino et al. (2017), the authors used an allele-specific silencing by RNA interference to downregulate synthesis of the mutant allele in a heterozygous R4496C-RyR2 mutated mouse line (Bongianino et al., 2017). They calculated that this gene silencing shifted the proportion of the expression of either three or four mutated monomers per RyR2 from 31.25% to 11.1%, enough of a shift to show a robust anti-arrhythmic effect compared to control (Bongianino et al., 2017). This study agrees with the findings in this thesis that a population subset of the V2475F(+/-) channels with high numbers of mutated monomers are having the greatest contribution to the aberrant phenotype of the CPVT1 disease in which these channels exhibit long openings at 100 nM cytosolic Ca^{2+}, increased sensitivity to 1 μM cytosolic Ca^{2+}, an agonist response to Mg^{2+} and the insensitivity of the V2475F(+/-) derived RyR2s to inhibition by nanomolar statin concentrations. Low concentrations of simvastatin in cardiomyocytes has been shown to inhibit Ca^{2+} sparks (Venturi et al., 2018). Since V2475F(+/-) channels exist as a heterozygous mixture of channels, could inhibiting just WT RyR2, or RyR2 channels with two or less mutated V2475F mutated monomers (Fig. 6.5), result in an intermediate regulation of Ca^{2+} release? Or would this produce further disparity in the activity of WT versus mutant RyR2 channels between clusters in a cardiomyocyte? Further experiments are required to investigate the ability of statins to alter spontaneous Ca^{2+} release in permeabilised cardiomyocytes derived from CPVT1 mouse models

to establish this further, and were originally planned to be conducted in this thesis but were not possible due to time constraints.

6.5 Structure-function relationship

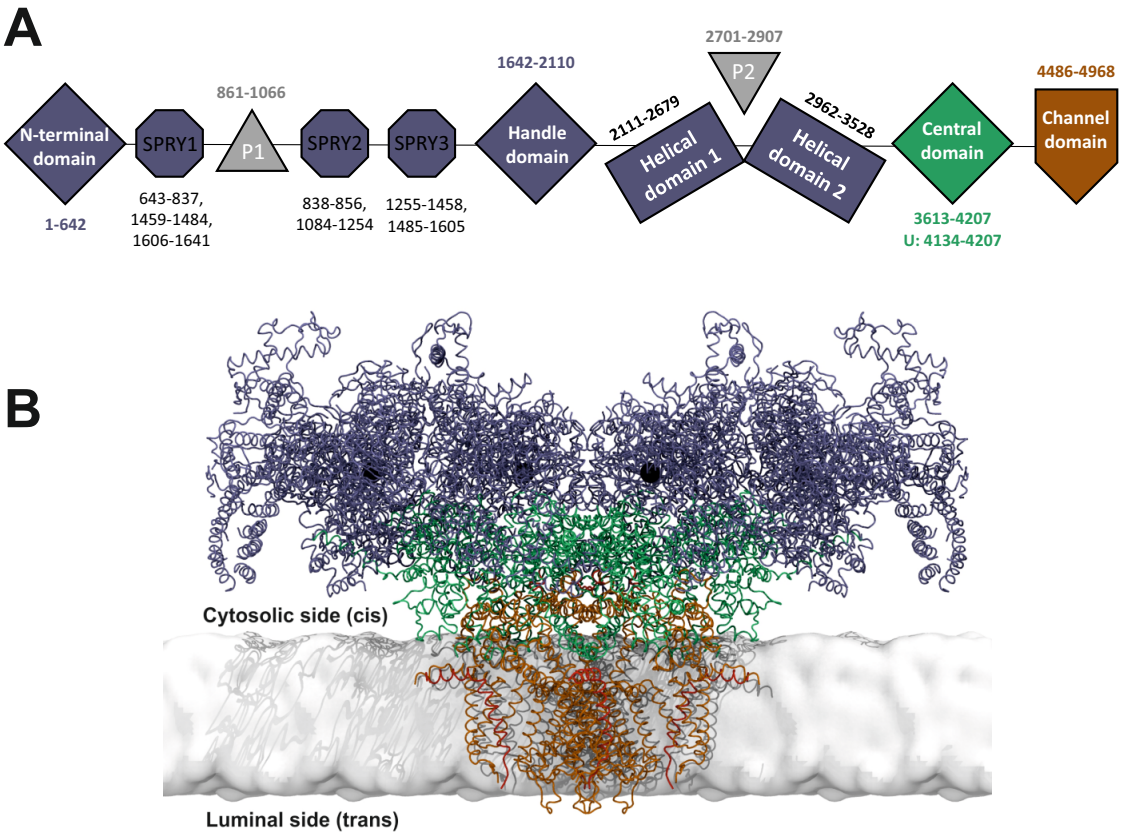


Figure 6.6: Structural domains of RyR2 (A) Domain organisation of an RyR2 protomer. The amino acid sequences are numbered alongside each domain. P1 and P2 in grey indicate phosphorylation sites. Figure adapted from (Peng et al., 2016) **(B)** A single RyR2 channel incorporated into a lipid bilayer. Colours of domain are coordinated with those of the domain organisation in (A). The black bead indicates the site(s) of the V2475F mutation. Structural images were created in VMD.

Although the HD1 domain is, in terms of the vast structure of RyR2, a long way from the pore or gate region (Fig. 6.6), it has been suggested that structural changes to this domain can still influence channel gating. This is because both the HD1 domain and the central domain have been suggested to synchronise with the expansion of the channel domain and the N-terminal domain during channel openings, when comparing the proposed open and closed structure using cryogenic

electron microscopy (Peng et al., 2016). It is therefore tempting to speculate that the alterations to the HD1 structure could have a far-reaching structural changes thereby implicating the wide range of disruption observed in this thesis to normal RyR2 function caused by the V2475F mutation. It is interesting that the HD1 mutations, (P2328S, R2474S and V2475F) have similar alterations in their regulation by Ca^{2+} and Mg^{2+} as central and channel domain mutations (Q4201R, V4653F and K4750Q) described in section 6.1, suggesting that these neighbouring domains may be interlinked in their structure to function relationships (Lehnart et al., 2004; Loaiza et al., 2013; Uehara et al., 2017; Salvage et al., 2019). The field is currently limited by the computational power required to model the complex interactions across all domains in such a large ion channel such as RyR2. Although through molecular dynamics it has been possible to model a single domain of the RyR2 molecule (Zheng and Liu, 2017; Miranda et al., 2018), it is not currently possible to simulate the effects that a single point mutation causes to the entire structure of the huge RyR2 molecule.

The structural change caused by the V2475F mutation likely causes the alterations to cytosolic Ca^{2+} or Mg^{2+} interactions observed; perhaps the transition between the open and closed state is energetically changed due the structural alteration in HD1 caused by the mutation. For example, at 100 nM cytosolic Ca^{2+}, as discussed previously, the V2475F(+/-) RyR2 channels appear to have a greater tendency to remain in their open state once opened. It could thereby be postulated that the structural change at HD1 of RyR2 confers a more "stable" open state at this nanomolar [Ca^{2+}]. The lifetime analysis for the open state of V2475F(+/-) channels in 1 μM cytosolic Ca^{2+} identified an extra exponential that did not exist in the open lifetime distribution of WT channels. This may suggest that the channel can open to an additional long open state that was induced by the effect of the mutation at the HD1 region.

As described in Fig. 3.17, it was found that V2475F(+/-) channels clustered in four distinct populations of channels with Po values increasingly deviating from that of WT channels. Previous studies of E3987A CPVT-mutated channels have

also found intermediate RyR2 activity levels when using a mixed expression of WT and E3987A mutated RyR2 DNA (Li and Chen, 2001). It could be postulated that the greater number of monomers in RyR2 with the mutation, as suggested with the V2475F(+/-) mutated channels, causes an increasingly aberrant overall ion channel structure, thus resulting in the scaled degree of functional alteration from the WT control, as observed in the response to both cytosolic Ca^{2+} and Mg^{2+}. Since all RyR2 mutated CPVT1 patients are heterozygous for the mutation, this could be a universal pathophysiological mechanism that encompasses all mutations of the disease.

It is possible that a structural change such as that in the HD1 domain caused by the V2475F mutation could also affect inter-RyR2 interactions, particularly since the highly flexible HD1 is distal to HD2 which interacts directly with neighbouring RyR2 in adjoining configurations as described in section 1.2.7 (Cabra et al., 2016). However, alteration in channel activity dependent on the number of channels in the bilayer was not observed experimentally (Fig. 3.20). Additional experiments are therefore required to understand the implication of CPVT1 mutations on inter-RyR2 interactions.

6.6 Summary

6.6.1 Physiological implications

The dysfunction to cytosolic regulation by Ca^{2+} caused by the V2475F mutation at RyR2 described so far is expected to have serious physiological implications. The increased sensitivity for channel activation between 100 nM and 1 μM would increase the likelihood for RyR2 channel openings (Fig. 3.8 and 3.13). This would likely be further exacerbated by the changes in Mg^{2+} regulation (Fig. 3.22). These observed changes in Mg^{2+} sensitivity may remove the inhibitory regulator of Ca^{2+} activation to further augment the probability of RyR2 opening. Furthermore, upon PKA-mediated phosphorylation as would be the case when CPVT1 cardiac events occur, the Po of V2475F(+/-) channels was higher than for WT RyR2 (Fig. 4.4)

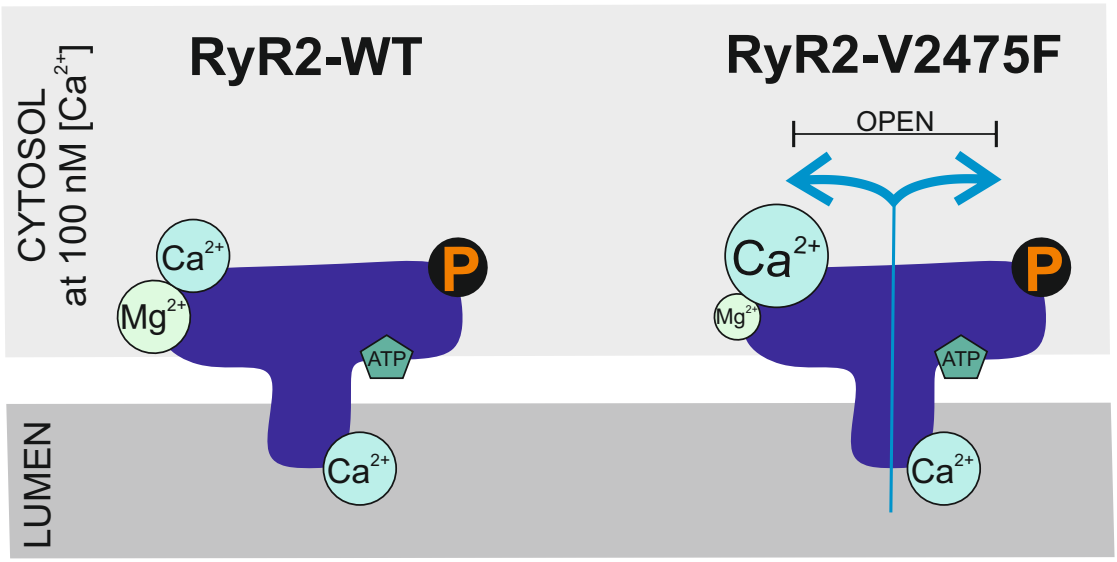


Figure 6.7: Schematic depicting the predicted RyR2 behaviour of RyR2 channel derived from WT or V2475F(+/-) cardiac tissue in diastolic conditions in a cardiomyocyte The expected alterations observed in this thesis at the single-channel level would be expected to increase the risk of RyR2-V2475F(+/-) channel opening during diastole in which the cytosolic [Ca^{2+}] is around 100 nM.

thereby further increasing the likelihood for RyR2 channel opening. Taken together, these aberrant RyR2 behaviours are likely to contribute towards to the increased likelihood of Ca^{2+}-triggered events during diastole in which the cytosolic [Ca^{2+}] is around 100 nM, as depicted in Fig. 6.7.

Our results indicate some of the V2475F mutated RyR2 channels would be more likely to open and release Ca^{2+} from the SR during diastole, meanwhile possibly triggering the opening of local neighbouring RyR2 channels (Bers, 2002). As discussed in section 6.4, this mechanism will be at particularly high risk of occurring in those most aberrant channels with three to four mutated monomers. This will cause activation of NCX to extrude the excess intracellular Ca^{2+}, which causes a transient inward Na^{+} current that will trigger a DAD (Bers, 2001). As shown in Fig. 6.8, this mechanism triggers DADs that are characteristic of CPVT1 pathophysiology with this mutation (Loaiza et al., 2013), leading to arrhythmogenesis in patients with this disease. The characteristics of the V2475F mutation described in this thesis provide insight into the possible underlying mechanisms that take place at the level of the RyR2 molecule and that could alter Ca^{2+} dynamics within

cardiomyocytes to the extent that sudden cardiac death can occur in a patient with this mutation (Tester et al., 2005). For CVPT1, this is a crucial advancement for understanding the mechanisms driving arrhythmogenesis and which would have been otherwise missed due to the lack of a fully comprehensive study of a range of key ligands involved in the regulation of RyR2.

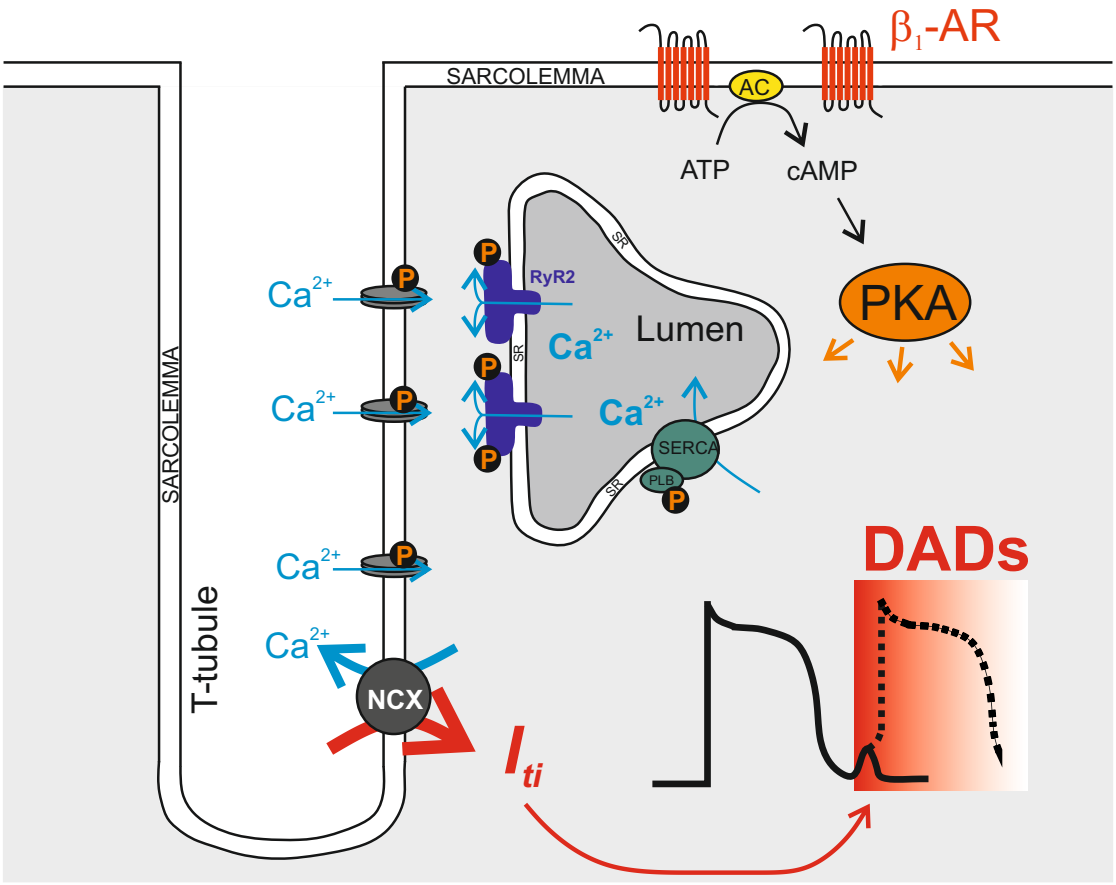


Figure 6.8: Adapted figure from the introduction displaying the pathophysiological mechanisms that lead to the induction of delayed-after-depolarisations (DADs) in CPVT1 caused by the mutation at V2475F The RyR2 channels with the V2475F mutation would be expected to release Ca^{2+} inappropriately during diastole, as shown in Fig. 6.7. This would cause NCX to extrude excess Ca^{2+}, thereby creating a transient inward current (I_{ti}). This would lead to a depolarisation of the cardiomyocyte causing DADs, and if large enough could induce an action potential.

6.6.2 Other potential mechanisms

It is uncertain what effect the increased sensitisation of V2475F(+/-) channels to millimolar inactivating levels of cytosolic Ca^{2+} will have in a cardiomyocyte (Fig. 3.8). Single-channel experiments that investigate a range of cytosolic [Ca^{2+}]s in the presence of quasi-physiological solutions with Mg^{2+} and ATP should be the subject of future investigation. Additionally, the high V2475F(+/-) channel activity with elongated open events in response to adenosine-based ligands (Fig. 3.25) may further contribute to the hyperactive RyR2 behaviour observed at 100 nM cytosolic Ca^{2+} in the mutant since adenosine-based ligands are constitutively present *in situ* inside cardiomyocytes (Lindsay et al., 2018). This may further elicit opening events at sub-activating Ca^{2+} concentrations and should be investigated further.

6.6.3 Generalised models of CPVT1

Results from this thesis suggest that the mechanisms that cause CPVT1 due to RyR2 mutations should not be over-generalised. In particular, the burst analysis suggested that the dysfunction at RyR2 caused by the V2475F mutation observed at 100 nM Ca^{2+} was due to a reduction in the Ca^{2+} off rate once bound to the open state of RyR2 (Fig. 3.15). A generalised mechanism in an attempt to explain all CPVT1 mutations has previously been postulated, stating that CPVT1-mutated RyR2 exhibit "unzipping" of domains within the channel as the mutation destabilises the closed state of the channel, thereby allowing Ca^{2+} leak through the SR (Yamamoto et al., 2008; Uchinoumi et al., 2010). However, the mechanisms observed from the burst analysis in this thesis suggest an inversed mechanism; the V2475F mutation stabilises the open channel state instead. Another proposed generalised mechanism for CPVT1 describes that the threshold for Ca^{2+} release from the SR is lowered due to increased sensitivity of RyR2 to luminal Ca^{2+}, thereby allowing inappropriate Ca^{2+} release from the SR during diastole (Jiang et al., 2004, 2005). It is well characterised that RyR2 channels are regulated by luminal [Ca^{2+}] (Sitsapesan and Williams, 1994b). However, some CPVT1 mutations display a decreased sensitivity

to luminal Ca^{2+} (Jiang et al., 2007). Further, in the experiments in this thesis, there was no observed significant increase in luminal Ca^{2+} sensitivity (Fig. 3.26), as is the case for other HD1 mutations investigated by other groups (Salvage et al., 2019). This observation suggests that not all CPVT1 can be classified under the general theory of alterations to SR thresholds for Ca^{2+} release.

It is tempting to over-generalise mechanisms that cause CPVT1 in an attempt to suggest targets of treatment that could help all patients. However, the observations described here suggest that mechanisms for CPVT1 should not be over-generalised as this may suggest incorrect mechanisms for some mutations. Mutations at different locations of the large RyR2 protein appear to impact the normal functioning of RyR2 in different ways. On this account, perhaps CPVT1 patients with RyR2 mutations in different residue locations should be treated differently, dependent on how the mutation directly impacts the RyR2 channel function at the molecular level. On the other hand, results from the characterisation of V2475F in Chapter 3 do align more closely to other published HD1 mutations in their cytosolic Ca^{2+} and Mg^{2+} sensitivity, as well as the luminal Ca^{2+} sensing behaviours (Uehara et al., 2017; Salvage et al., 2019). Perhaps pathophysiological mechanisms could be generalised for each domain of RyR2 that the mutation resides in. Since RyR2 is such a vast ion channel, this could provide a conceivable way to group CPVT1 patient types and their treatment requirements. Further comprehensive exploration at the single-channel level of other mutations is required to examine whether this could be possible.

6.6.4 Concluding remarks

To conclude, the V2475F(+/-) mutation does not simply cause one alteration in the channel's normal function, but a wide and heterogenous alteration in RyR2 channel response to cytosolic ligands and ion permeation (Fig. 6.1). The major defects arise from alterations to the interactions of both cytosolic Ca^{2+} and Mg^{2+}, with a variance in the extent of alteration from WT dependent on the number of mutated

monomers within the RyR2 tetramer. The research in this thesis has revealed the importance of studying the dysfunctional behaviour of native derived RyR2 channels at the molecular level with the aim to recapitulate the behaviour of an aberrant channel in a patient with CPVT1. Overall, this work has elucidated some key mechanisms in this CPVT1 mutant. Ultimately, the greater our understanding of the pathophysiological mechanisms involved in this devastating disease, the greater our chances of finding effective treatments to treat CPVT1 patients.

References

Ackers-Johnson, Matthew et al. (2016). "A Simplified, Langendorff-Free Method for Concomitant Isolation of Viable Cardiac Myocytes and Nonmyocytes from the Adult Mouse Heart". In: *Circulation Research* 119.8, pp. 909–920.

Ahern, Gerard P., Pauline R. Junankar, and Angela F. Dulhunty (1997). "Subconductance states in single-channel activity of skeletal muscle ryanodine receptors after removal of FKBP12". In: *Biophysical Journal*.

Alvarado, Francisco J, Xi Chen, and Héctor H Valdivia (2017). "Ablation of the cardiac ryanodine receptor phospho-site Ser2808 does not alter the adrenergic response or the progression to heart failure in mice. Elimination of the genetic background as critical variable". In: *Journal of Molecular and Cellular Cardiology* 103, pp. 40–47.

Alvarez, Osvaldo (1986). "How to set up a Bilayer System". In: *Ion Channel Reconstitution*. Ed. by Christopher Miller. Boston, MA: Springer US, pp. 115–130.

Amar, David et al. (2005). "Statin use is associated with a reduction in atrial fibrillation after noncardiac thoracic surgery independent of C-reactive protein". In: *Chest* 128.5, pp. 3421–3427.

Armitage, Jane (2007). "The safety of statins in clinical practice". In: *Lancet* 370.9601, pp. 1781–1790.

Asghari, Parisa et al. (2014). "Nonuniform and variable arrangements of ryanodine receptors within mammalian ventricular couplons". In: *Circulation Research* 115.2, pp. 252–262.

Asghari, Parisa et al. (2020). "Cardiac ryanodine receptor distribution is dynamic and changed by auxiliary proteins and post-translational modification". In: *eLife* 9.

Ashley, R H and A J Williams (1990). "Divalent cation activation and inhibition of single calcium release channels from sheep cardiac sarcoplasmic reticulum". In: *Journal of General Physiology* 95.5, pp. 981–1005.

Bai, Xiao Chen et al. (2016). "The Central domain of RyR1 is the transducer for long-range allosteric gating of channel opening". In: *Cell Research* 26.9, pp. 995–1006.

Balshaw, David M. et al. (2001). "Calmodulin Binding and Inhibition of Cardiac Muscle Calcium Release Channel (Ryanodine Receptor)". In: *Journal of Biological Chemistry* 276.23, pp. 20144–20153.

Bannister, Mark L. et al. (2015). "The mechanism of flecainide action in CPVT does not involve a direct effect on RyR2". In: *Circulation Research* 116.8, pp. 1324–1335.

Bassani, J. W., R. A. Bassani, and D. M. Bers (1994). "Relaxation in rabbit and rat cardiac cells: species-dependent differences in cellular mechanisms." In: *The Journal of Physiology*.

Bassani, R. A., J. W. Bassani, and D. M. Bers (1992). "Mitochondrial and sarcolemmal Ca2+ transport reduce [Ca2+]i during caffeine contractures in rabbit cardiac myocytes." In: *The Journal of Physiology*.

Bean, Bruce P. (1985). "Two kinds of calcium channels in canine atrial cells: Differences in kinetics, selectivity, and pharmacology". In: *Journal of General Physiology*.

Beard, Nicole A. et al. (2002). "Calsequestrin is an inhibitor of skeletal muscle ryanodine receptor calcium release channels". In: *Biophysical Journal* 82.1, pp. 310–320.

Benkusky, Nancy A. et al. (2007). "Intact β-adrenergic response and unmodified progression toward heart failure in mice with genetic ablation of a major protein kinase A phosphorylation site in the cardiac ryanodine receptor". In: *Circulation Research* 101.8, pp. 819–829.

Bers, D. M. and J. H.B. Bridge (1989). "Relaxation of rabbit ventricular muscle by Na-Ca exchange and sarcoplasmic reticulum calcium pump. Ryanodine and voltage sensitivity". In: *Circulation Research*.

Bers, Donald (2001). *Excitation-contraction coupling and cardiac contractile force*. 2nd. Springer Science & Business Media.

Bers, Donald M. (2002). "Cardiac excitation-contraction coupling". In: *Nature* 415.6868, pp. 198–205.

Berti, Claudio et al. (2017). "Sarcoplasmic reticulum Ca2+, Mg2+, K+, and Cl concentrations adjust quickly as heart rate changes". In: *Journal of Molecular and Cellular Cardiology* 103, pp. 31–39.

Bland, J. Martin and Douglas G. Altman (2004). "Statistics notes: The logrank test". In: *British Medical Journal*.

Bongianino, Rossana et al. (2017). "Allele-specific silencing of mutant mRNA rescues ultrastructural and arrhythmic phenotype in mice carriers of the R4496C mutation in the ryanodine receptor gene (RYR2)". In: *Circulation Research* 121.5, pp. 525–536.

Bradford, Marion M (1976). *A Rapid and Sensitive Method for the Quantitation of Microgram Quantities of Protein Utilizing the Principle of Protein-Dye Binding*, pp. 248–254.

Cabra, Vanessa, Takashi Murayama, and Montserrat Samsó (2016). "Ultrastructural Analysis of Self-Associated RyR2s". In: *Biophysical Journal* 110.12, pp. 2651–2662.

Camors, Emmanuel and Héctor H. Valdivia (2014). "CaMKII regulation of cardiac ryanodine receptors and inositol triphosphate receptors". In: *Frontiers in Pharmacology* 5 MAY.

Campbell, K P et al. (1987). "Identification and characterization of the high affinity [3H]ryanodine receptor of the junctional sarcoplasmic reticulum Ca2+ release channel." In: *Journal of Biological Chemistry* 262.14, pp. 6460–6463.

Capel, Rebecca A et al. (2015). "Two-pore channels (TPC2s) and nicotinic acid adenine dinucleotide phosphate (NAADP) at lysosomal-sarcoplasmic reticular junctions contribute to acute and chronic β-adrenoceptor signaling in the heart". In: *Journal of Biological Chemistry* 290.50, pp. 30087–30098.

Carl, Stephanie Lewis et al. (1995). "Immunolocalization of sarcolemmal dihydropyridine receptor and sarcoplasmic reticular triadin and ryanodine receptor in rabbit ventricle and atrium". In: *Journal of Cell Biology*.

Carter, Simon, John Colyer, and Rebecca Sitsapesan (2006). "Maximum phosphorylation of the cardiac ryanodine receptor at serine-2809 by protein kinase A produces unique modifications to channel gating and conductance not observed at lower levels of phosphorylation". In: *Circulation Research* 98.12, pp. 1506–1513.

Carter, Simon et al. (2011). "Ca2+-dependent phosphorylation of RyR2 can uncouple channel gating from direct cytosolic Ca2+ regulation". In: *Journal of Membrane Biology* 240.1, pp. 21–33.

Chan, Wei Mun, William Welch, and Rebecca Sitsapesan (2000). "Structural factors that determine the ability of adenosine and related compounds to activate the cardiac ryanodine receptor". In: *British Journal of Pharmacology* 130.7, pp. 1618–1626.

Charatan, Fred (2001). "Bayer decides to withdraw cholesterol lowering drug". In: *BMJ (Clinical research ed.)* 323.7309, p. 359.

Chen, Haiyan et al. (2013). "Mechanism of calsequestrin regulation of single cardiac ryanodine receptor in normal and pathological conditions". In: *Journal of General Physiology* 142.2, pp. 127–136.

Chen, Wenqian et al. (2014). "The ryanodine receptor store-sensing gate controls Ca 2+ waves and Ca2+-triggered arrhythmias". In: *Nature Medicine* 20.2, pp. 184–192.

Cheng, H., W. J. Lederer, and M. B. Cannell (1993). "Calcium sparks: Elementary events underlying excitation-contraction coupling in heart muscle". In: *Science* 262.5134, pp. 740–744.

Cheng, H. et al. (1996). "Calcium sparks and [Ca2+]i waves in cardiac myocytes". In: *American Journal of Physiology - Cell Physiology*.

Cheng, Heping and W. J. Lederer (2008). "Calcium sparks". In: *Physiological Reviews* 88.4, pp. 1491–1545.

Ching, Li Lien, Alan J. Williams, and Rebecca Sitsapesan (2000). "Evidence for Ca2+ activation and inactivation sites on the luminal side of the cardiac ryanodine receptor complex". In: *Circulation Research* 87.3, pp. 201–206.

Choi, Grace et al. (2004). "Spectrum and frequency of cardiac channel defects in swimming-triggered arrhythmia syndromes". In: *Circulation* 110.15, pp. 2119–2124.

Chu, A. et al. (1993). "Cytoplasmic Ca2+ does not inhibit the cardiac muscle sarcoplasmic reticulum ryanodine receptor Ca2+ channel, although Ca2+-induced Ca2+ inactivation of Ca2+ release is observed in native vesicles". In: *The Journal of Membrane Biology* 135.1, pp. 49–59.

Chugun, Akihito et al. (2007). "Mg2+ activates the ryanodine receptor type 2 (RyR2) at intermediate Ca2+ concentrations". In: *American Journal of Physiology - Cell Physiology* 292.1.

Clapham, David E. (2007). "Calcium Signaling". In: *Cell*.

Cohen, Fredric S (1986). "Fusion of Liposomes to Planar Bilayers". In: *Ion Channel Reconstitution*. Ed. by Christopher Miller. Boston, MA: Springer US, pp. 131–139.

Collins, Rory et al. (2016). "Interpretation of the evidence for the efficacy and safety of statin therapy". In: *The Lancet* 388.10059, pp. 2532–2561.

Colquhoun, David and F. J. Sigworth (1995). "Fitting and Statistical Analysis of Single-Channel Records". In: pp. 483–587.

Connor, Stewart (2019). "Leading chemical drugs dispensed in England 2019 from Statista". In:

Coronado, Roberto, Robert L. Rosenberg, and Christopher Miller (1980). "Ionic selectivity, saturation, and block in a K+-selective channel from sarcoplasmic reticulum". In: *Journal of General Physiology* 76.4, pp. 425–446.

Dansette, P M, M Jaoen, and C Pons (2000). "HMG-CoA reductase activity in human liver microsomes: Comparative inhibition by statins". In: *Experimental and Toxicologic Pathology* 52.2, pp. 145–148.

De Sutter, Johan et al. (2000). "Lipid lowering drugs and recurrences of life-threatening ventricular arrhythmias in high-risk patients". In: *Journal of the American College of Cardiology* 36.3, pp. 766–772.

Denniss, Amanda, Angela F. Dulhunty, and Nicole A. Beard (2018). *Ryanodine receptor Ca 2+ release channel post-translational modification: Central player in cardiac and skeletal muscle disease*.

Des Georges, Amédée et al. (2016). "Structural Basis for Gating and Activation of RyR1". In: *Cell* 167.1, 145–157.e17.

Di Barletta, Marina Raffaele et al. (2006). "Clinical phenotype and functional characterization of CASQ2 mutations associated with catecholaminergic polymorphic ventricular tachycardia". In: *Circulation* 114.10, pp. 1012–1019.

Diszházi, Gyula et al. (2019). "Dantrolene requires MG2+ and ATP to inhibit the ryanodine receptor". In: *Molecular Pharmacology* 96.3, pp. 401–407.

Dobrev, Dobromir and Xander H.T. Wehrens (2014). "Role of RyR2 phosphorylation in heart failure and arrhythmias: Controversies around ryanodine receptor phosphorylation in cardiac disease". In: *Circulation Research*.

Eckhardt, Jan et al. (2019). "Extraocular muscle function is impaired in ryr3-/- mice". In: *Journal of General Physiology* 151.7, pp. 929–943.

Eisner, David A. et al. (2020). "The Control of Diastolic Calcium in the Heart: Basic Mechanisms and Functional Implications". In: *Circulation Research*, pp. 395–412.

Elison, C. and D. J. Jenden (1967). "The effects of ryanodine on model systems derived from muscle-II. Myofibrils and natural actomyosin". In: *Biochemical Pharmacology* 16.7, pp. 1347–1354.

Fabiato, A (1985). "Time and calcium dependence of activation and inactivation of calcium-induced release of calcium from the sarcoplasmic reticulum of a skinned canine cardiac Purkinje cell". In: *J Gen Physiol* 85.2, pp. 247–289.

— (1983). "Calcium-induced release of calcium from the cardiac sarcoplasmic reticulum". In: *American Journal of Physiology - Cell Physiology* 14.1.

Fabiato, Alexandre and Françoise Fabiato (1979). "Use of chlorotetracycline fluorescence to demonstrate Ca 2+-induced release of Ca2+ from the sarcoplasmic reticulum of skinned cardiac cells [14]". In:

Fatt, P and B L Ginsborg (1958). "The ionic requirements for the production of action potentials in crustacean muscle fibres". In: *The Journal of Physiology* 142.3, pp. 516–543.

Fauchier, Laurent et al. (2008). "Antiarrhythmic Effect of Statin Therapy and Atrial Fibrillation". In: *Journal of the American College of Cardiology* 51.8, pp. 828–835.

Faul, Franz et al. (2007). "G*Power 3: A flexible statistical power analysis program for the social, behavioral, and biomedical sciences". In: *Behavior Research Methods*. Vol. 39. 2. Psychonomic Society Inc., pp. 175–191.

Fawcett, D. W. and N. S. McNutt (1969). "The ultrastructure of the cat myocardium. I. Ventricular papillary muscle." In: *The Journal of cell biology*.

Fenwick, Nicole, Gilly Griffin, and Clément Gauthier (2009). "The welfare of animals used in science: how the "Three Rs" ethic guides improvements." In: *The Canadian veterinary journal = La revue veterinaire canadienne*.

Fernández-Velasco, María et al. (2009). "Increased Ca2+ sensitivity of the ryanodine receptor mutant RyR2R4496C underlies catecholaminergic polymorphic ventricular tachycardia". In: *Circulation Research*.

Festing, Michael F.W. and Douglas G. Altman (2002). "Guidelines for the design and statistical analysis of experiments using laboratory animals". In: *ILAR Journal* 43.4, pp. 244–257.

Fill, Michael and Julio A. Copello (2002). "Ryanodine receptor calcium release channels". In: *Physiological Reviews* 82.4, pp. 893–922.

Fink, R. H.A. and C. Veigel (1996). "Calcium uptake and release modulated by counter-ion conductances in the sarcoplasmic reticulum of skeletal muscle". In: *Acta Physiologica Scandinavica*.

Fisher, R A (1992). *Statistical Methods for Research Workers*. Springer, New York, NY, pp. 66–70.

Franzini-Armstrong, Clara and Feliciano Protasi (1997). "Ryanodine receptors of striated muscles: A complex channel capable of multiple interactions". In: *Physiological Reviews*.

Franzini-Armstrong, Clara, Feliciano Protasi, and Venkat Ramesh (1999). "Shape, size, and distribution of Ca2+ release units and couplons in skeletal and cardiac muscles". In: *Biophysical Journal* 77.3, pp. 1528–1539.

Galfré, Elena et al. (2012). "Fkbp12 activates the cardiac ryanodine receptor ca 2+-release channel and is antagonised by fkbp12.6". In: *PLoS ONE* 7.2.

Galice, Samuel et al. (2018). "Size matters: Ryanodine receptor cluster size affects arrhythmogenic sarcoplasmic reticulum calcium release". In: *Journal of the American Heart Association* 7.13.

George, Christopher H., Gemma V. Higgs, and F. Anthony Lai (2003). "Ryanodine Receptor Mutations Associated With Stress-Induced Ventricular Tachycardia Mediate Increased Calcium Release in Stimulated Cardiomyocytes". In: *Circulation Research* 93.6, pp. 531–540.

Gillespie, Dirk (2008). "Energetics of divalent selectivity in a calcium channel: The ryanodine receptor case study". In: *Biophysical Journal* 94.4, pp. 1169–1184.

Gillespie, Dirk and Michael Fill (2008). "Intracellular calcium release channels mediate their own countercurrent: The ryanodine receptor case study". In: *Biophysical Journal* 95.8, pp. 3706–3714.

Gillespie, Dirk, Le Xu, and Gerhard Meissner (2014). "Selecting ions by size in a calcium channel: The ryanodine receptor case study". In: *Biophysical Journal* 107.10, pp. 2263–2273.

Ginsburg, Kenneth S. and Donald M. Bers (2004). "Modulation of excitation-contraction coupling by isoproterenol in cardiomyocytes with controlled SR Ca2+ load and Ca2+ current trigger". In: *Journal of Physiology* 556.2, pp. 463–480.

Grube, M et al. (2006). "Organic anion transporting polypeptide 2B1 is a high-affinity transporter for atorvastatin and is expressed in the human heart". In: *Clin Pharmacol Ther* 80.6, pp. 607–620.

Guis, S et al. (2006). "In vivo and in vitro characterization of skeletal muscle metabolism in patients with statin-induced adverse effects". In: *Arthritis Care and Research* 55.4, pp. 551–557.

Guo, Tao et al. (2011). "FRET detection of calmodulin binding to the cardiac RyR2 calcium release channel". In: *Biophysical Journal* 101.9, pp. 2170–2177.

Györke, Inna et al. (2004). "The Role of Calsequestrin, Triadin, and Junctin Conferring Cardiac Ryanodine Receptor Responsiveness to Luminal Calcium". In: *Biophysical Journal* 86.4, pp. 2121–2128.

Györke, Sandor (2009). "Molecular basis of catecholaminergic polymorphic ventricular tachycardia". In: *Heart Rhythm*.

Haji-Ghassemi, Omid, Zhiguang Yuchi, and F. Van Petegem (2019). "The Cardiac Ryanodine Receptor Phosphorylation Hotspot Embraces PKA in a Phosphorylation-Dependent Manner". In: *Molecular Cell* 75.1, 39–52.e4.

Hazle, Matthew A. et al. (2013). "Arrhythmogenic channelopathy syndromes presenting as refractory epilepsy". In: *Pediatric Neurology* 49.2, pp. 134–137.

Higgins, J. William et al. (2014). "Utility of oatp1a/1b-knockout and OATP1B1/3-humanized mice in the study of OATP-mediated pharmacokinetics and tissue distribution: Case studies with pravastatin, atorvastatin, simvastatin, and carboxydichlorofluorescein". In: *Drug Metabolism and Disposition*.

Hill, Peter D. (1985). "Kernel Estimation of a Distribution Function". In: *Communications in Statistics - Theory and Methods* 14.3, pp. 605–620.

Hodgkin, A. L. and A. F. Huxley (1952). "A quantitative description of membrane current and its application to conduction and excitation in nerve". In: *The Journal of Physiology* 117.4, pp. 500–544.

Huang, Xiaojun et al. (2013). "Two potential calmodulin-binding sequences in the ryanodine receptor contribute to a mobile, intra-subunit calmodulin-binding domain". In: *Journal of Cell Science* 126.19, pp. 4527–4535.

Huke, Sabine and Donald M. Bers (2008). "Ryanodine receptor phosphorylation at Serine 2030, 2808 and 2814 in rat cardiomyocytes". In: *Biochemical and Biophysical Research Communications* 376.1, pp. 80–85.

Hwang, Hyun Seok et al. (2011). "Inhibition of cardiac Ca2+ release channels (RyR2) determines efficacy of class i antiarrhythmic drugs in catecholaminergic polymorphic ventricular tachycardia". In: *Circulation: Arrhythmia and Electrophysiology* 4.2, pp. 128–135.

Jiang, Dawei et al. (2004). "RyR2 mutations linked to ventricular tachycardia and sudden death reduce the threshold for store-overload-induced Ca2+ release (SOICR)". In: *Proceedings of the National Academy of Sciences of the United States of America* 101.35, pp. 13062–13067.

Jiang, Dawei et al. (2005). "Enhanced Store Overload–Induced Ca ²⁺ Release and Channel Sensitivity to Luminal Ca ²⁺ Activation Are Common Defects of RyR2 Mutations Linked to Ventricular Tachycardia and Sudden Death". In: *Circulation Research* 97.11, pp. 1173–1181.

Jiang, Dawei et al. (2007). "Loss of luminal Ca2+ activation in the cardiac ryanodine receptor is associated with ventricular fibrillation and sudden death". eng. In: *Proc Natl Acad Sci U S A* 104.46, pp. 18309–18314.

Jirásko, Robert et al. (2014). "Distribution study of atorvastatin and its metabolites in rat tissues using combined information from UHPLC/MS and MALDI-Orbitrap-MS imaging". In: *Analytical and Bioanalytical Chemistry*.

Jones, Larry R et al. (1979). *Separation of Vesicles of Cardiac Sarcolemma from Vesicles of Cardiac Sarcoplasmic Reticulum COMPARATIVE BIOCHEMICAL ANALYSIS OF COMPONENT ACTIVITIES**. 2, pp. 530–539.

Jung, C B et al. (2012). "Dantrolene rescues arrhythmogenic RYR2 defect in a patient-specific stem cell model of catecholaminergic polymorphic ventricular tachycardia". In: *EMBO Mol Med* 4.3, pp. 180–191.

Kashimura, Takeshi et al. (2010). "In the RyR2R4496C mouse model of CPVT, β-adrenergic stimulation induces ca waves by increasing SR Ca content and not by decreasing the threshold for Ca Waves". In: *Circulation Research*.

Kawai, Makoto, Munir Hussain, and Clive H. Orchard (1999). "Excitation-contraction coupling in rat ventricular myocytes after formamide-induced detubulation". In: *American Journal of Physiology - Heart and Circulatory Physiology*.

Kentish, Jonathan C. et al. (2001). "Phosphorylation of troponin I by protein kinase A accelerates relaxation and crossbridge cycle kinetics in mouse ventricular muscle". In: *Circulation Research*.

Kermode, Helen, Alan J. Williams, and Rebecca Sitsapesan (1998). "The interactions of ATP, ADP, and inorganic phosphate with the sheep cardiac ryanodine receptor". In: *Biophysical Journal* 74.3, pp. 1296–1304.

Kettlun, Claudia et al. (2003). "Unitary Ca2+ current through mammalian cardiac and amphibian skeletal muscle ryanodine receptor channels under near-physiological ionic conditions". In: *Journal of General Physiology* 122.4, pp. 407–417.

Khori, Vahid et al. (2015). "Acute effects of simvastatin to terminate fast reentrant tachycardia through increasing wavelength of atrioventricular nodal reentrant tachycardia circuit". In: *Fundamental and Clinical Pharmacology* 29.1, pp. 41–53.

Krzywinski, Martin and Naomi Altman (2014). *Two-factor designs*.

Kunst, Gudrun et al. (2000). "Myosin binding protein C, a phosphorylation-dependent force regulator in muscle that controls the attachment of myosin heads by its interaction with myosin S2". In: *Circulation Research*.

Lai, Anthony F. et al. (1988a). "Purification and reconstitution of the calcium release channel from skeletal muscle". In: *Nature* 331.6154, pp. 315–319.

Lai, F. Anthony et al. (1988b). "Evidence for a Ca2+ channel within the ryanodine receptor complex from cardiac sarcoplasmic reticulum". In: *Biochemical and Biophysical Research Communications*.

Laver, D R, T M Baynes, and A F Dulhunty (1997). "Magnesium inhibition of ryanodine-receptor calcium channels: Evidence for two independent mechanisms". In: *Journal of Membrane Biology* 156.3, pp. 213–229.

Laver, D R and G D Lamb (1998). "Inactivation of Ca2+ release channels (ryanodine receptors RyR1 and RyR2) with rapid steps in [Ca2+] and voltage". In: *Biophysical Journal* 74.5, pp. 2352–2364.

Laver, D. R. et al. (1995). "Cytoplasmic Ca2+ inhibits the ryanodine receptor from cardiac muscle". In: *The Journal of Membrane Biology* 147.1, pp. 7–22.

Lehnart, Stephan E. et al. (2008). "Leaky Ca2+ release channel/ryanodine receptor 2 causes seizures and sudden cardiac death in mice". In: *Journal of Clinical Investigation* 118.6, pp. 2230–2245.

Lehnart, Stephan E et al. (2004). "Sudden death in familial polymorphic ventricular tachycardia associated with calcium release channel (ryanodine receptor) leak." In: *Circulation* 109.25, pp. 3208–3214.

Li, Li et al. (2000). "Phosphorylation of phospholamban and troponin I in β-adrenergic-induced acceleration of cardiac relaxation". In: *American Journal of Physiology - Heart and Circulatory Physiology*.

Li, Pin and S. R.Wayne Chen (2001). "Molecular basis of Ca2+ activation of the mouse cardiac Ca2+ release channel (ryanodine receptor)". In: *Journal of General Physiology* 118.1, pp. 33–44.

Lindsay, A. R., S. D. Manning, and A. J. Williams (1991). "Monovalent cation conductance in the ryanodine receptor-channel of sheep cardiac muscle sarcoplasmic reticulum." In: *The Journal of Physiology*.

Lindsay, Chris et al. (2018). "Promiscuous attraction of ligands within the ATP binding site of RyR2 promotes diverse gating behaviour". In: *Scientific Reports* 8.1, pp. 1–13.

Liu, Nian et al. (2006). "Arrhythmogenesis in catecholaminergic polymorphic ventricular tachycardia: Insights from a RyR2 R4496C knock-in mouse model". In: *Circulation Research*.

Liu, Yen Bin et al. (2009). "Effects of simvastatin on cardiac neural and electrophysiologic remodeling in rabbits with hypercholesterolemia". In: *Heart Rhythm* 6.1, pp. 69–75.

Liu, Yingjie et al. (2017). "CPVT-associated cardiac ryanodine receptor mutation G357S with reduced penetrance impairs Ca2+ release termination and diminishes protein expression". In: *PLoS ONE* 12.9, e0184177.

Liu, Yiwei et al. (2010). "Flux regulation of cardiac ryanodine receptor channels". In: *Journal of General Physiology* 135.1, pp. 15–27.

Loaiza, Randall et al. (2013). "Heterogeneity of ryanodine receptor dysfunction in a mouse model of catecholaminergic polymorphic ventricular tachycardia". In: *Circulation Research* 112.2, pp. 298–308.

Ma, Ruifang et al. (2020). "Structural basis for diamide modulation of ryanodine receptor". In: *Nature Chemical Biology*, pp. 1–9.

Madamanchi, Aasakiran (2007). "β-adrenergic receptor signaling in cardiac function and heart failure". In: *McGill Journal of Medicine*.

Magleby, K L and B S Pallotta (1983). "Burst kinetics of single calcium-activated potassium channels in cultured rat muscle." In: *The Journal of Physiology* 344.1, pp. 605–623.

Marban, E., S. W. Robinson, and W. G. Wier (1986). "Mechanisms of arrhythmogenic delayed and early afterdepolarizations in ferret ventricular muscle". In: *Journal of Clinical Investigation*.

Marx, Steven O. et al. (2000). "PKA phosphorylation dissociates FKBP12.6 from the calcium release channel (ryanodine receptor): Defective regulation in failing hearts". In: *Cell* 101.4, pp. 365–376.

Matsushima, Soichiro et al. (2005). "Identification of the hepatic efflux transporters of organic anions using double-transfected Madin-Darby canine kidney II cells expressing human organic anion-transporting polypeptide 1B1 (OATP1B1)/multidrug resistance-associated protein 2, OATP1B1/multid". In: *Journal of Pharmacology and Experimental Therapeutics* 314.3, pp. 1059–1067.

McGarry, S. J. and A. J. Williams (1994). "Adenosine discriminates between the caffeine and adenine nucleotide sites on the sheep cardiac sarcoplasmic reticulum calcium-release channel". In: *The Journal of Membrane Biology*.

Meissner, G. (1984). "Adenine nucleotide stimulation of Ca2+-induced Ca2+ release in sarcoplasmic reticulum". In: *Journal of Biological Chemistry*.

Meissner, Gerhard (2017). "The structural basis of ryanodine receptor ion channel function". In: *Journal of General Physiology* 149.12, pp. 1065–1089.

Meissner, Gerhard, Edward Darling, and Julia Eveleth (1986). "Kinetics of Rapid Ca2+ Release by Sarcoplasmic Reticulum. Effects of Ca2+, Mg2+, and Adenine Nucleotides". In: *Biochemistry* 25.1, pp. 236–244.

Mejía-Alvarez, Rafael et al. (1999). "Unitary Ca 2 Current through Cardiac Ryanodine Receptor Channels under Quasi-Physiological Ionic Conditions". In: *J. Gen. Physiol* 113, pp. 177–186.

Meli, Albano C. et al. (2011). "A novel ryanodine receptor mutation linked to sudden death increases sensitivity to cytosolic calcium". In: 109.3, pp. 281–290.

Metterlein, T et al. (2010). "Statins Alter Intracellular Calcium Homeostasis in Malignant Hyperthermia Susceptible Individuals". In: *Cardiovascular Therapeutics* 28.6, pp. 356–360.

Milani-Nejad, Nima and Paul M L Janssen (2013). "Small and Large Animal Models in Cardiac Contraction Research: Advantages and Disadvantages". In:

Miller, Christopher (1978). *Voltage-Gated Cation Conductance Channel from Fragmented Sarcoplasmic Reticulum" Steady-State Electrical Properties*. Tech. rep., pp. 1–23.

Miller, Christopher and Robert L. Rosenberg (1979). "A Voltage-Gated Cation Conductance Channel from Fragmented Sarcoplasmic Reticulum. Effects of Transition Metal Ions". In: *Biochemistry* 18.7, pp. 1138–1145.

Miranda, Williams E. et al. (2018). "Molecular Mechanism of Conductance Enhancement in Narrow Cation-Selective Membrane Channels". In: *Journal of Physical Chemistry Letters* 9.12, pp. 3497–3502.

Miyake, C Y et al. (2013). "Efficacy of implantable cardioverter defibrillators in young patients with catecholaminergic polymorphic ventricular tachycardia: success depends on substrate". In: *Circ Arrhythm Electrophysiol* 6.3, pp. 579–587.

Mohamed, Uwais, Carlo Napolitano, and Silvia G. Priori (2007). "Molecular and electrophysiological bases of catecholaminergic polymorphic ventricular tachycardia". In: *Journal of Cardiovascular Electrophysiology*.

Mukherjee, Saptarshi, N. Lowri Thomas, and Alan J. Williams (2012). "A mechanistic description of gating of the human cardiac ryanodine receptor in a regulated minimal environment". In: *Journal of General Physiology* 140.2, pp. 139–158.

Murayama, Takashi and Yasuo Ogawa (1996). "Properties of Ryr3 ryanodine receptor isoform in mammalian brain". In: *Journal of Biological Chemistry*.

Murayama, Takashi et al. (2018). "Efficient high-throughput screening by endoplasmic reticulum Ca 2+ measurement to identify inhibitors of ryanodine receptor Ca 2+ -release channels". In: *Molecular Pharmacology* 94.1, pp. 722–730.

Napolitano, Carlo, Silvia G Priori, and Raffaella Bloise (2016). "Catecholaminergic Polymorphic Ventricular Tachycardia". In: *GeneReviews®*. University of Washington, Seattle.

Niggli, Ernst et al. (2013). "Posttranslational modifications of cardiac ryanodine receptors: Ca2+ signaling and EC-coupling". In: *Biochimica et Biophysica Acta - Molecular Cell Research* 1833.4, pp. 866–875.

Nyquist, H. (1928). "Certain Topics in Telegraph Transmission Theory". In: *Transactions of the American Institute of Electrical Engineers* 47.2, pp. 617–644.

O'Brien, Fiona, Elisa Venturi, and Rebecca Sitsapesan (2015). "The ryanodine receptor provides high throughput Ca2+-release but is precisely regulated by networks of associated proteins: A focus on proteins relevant to phosphorylation". In: *Biochemical Society Transactions* 43.3, pp. 426–433.

Ogawa, Yasuo and Masaru Tanokura (1984). "Calcium binding to calmodulin: Effects of ionic strength, MG, ph and temperature1". In: *Journal of Biochemistry* 95.1, pp. 19–28.

Ohata, Hisayuki et al. (1999). "Confocal imaging analysis of intracellular ions in mixed cellular systems or in situ using two types of confocal microscopic systems". In: *Methods in Enzymology* 307, pp. 425–441.

Oo, Ye Win et al. (2015). "Essential Role of Calmodulin in RyR Inhibition by Dantrolene." In: *Molecular pharmacology* 88.1, pp. 57–63.

Otsu, K et al. (1990). "Molecular cloning of cDNA encoding the Ca2+ release channel (ryanodine receptor) of rabbit cardiac muscle sarcoplasmic reticulum". In: *J Biol Chem* 265.23, pp. 13472–13483.

Page, E. and M. Surdyk-Droske (1979). "Distribution, surface density, and membrane area of diadic junctional contacts between plasma membrane and terminal cisterns in mammalian ventricle". In: *Circulation Research*.

Pan, B. S. and R. J. Solaro (1987). "Calcium-binding properties of troponin C in detergent-skinned heart muscle fibers." In: *Journal of Biological Chemistry*.

Pasanen, M K et al. (2007). "Different effects of SLCO1B1 polymorphism on the pharmacokinetics of atorvastatin and rosuvastatin". In: *Clin Pharmacol Ther* 82.6, pp. 726–733.

Pearson, Karl (1900). "X. On the criterion that a given system of deviations from the probable in the case of a correlated system of variables is such that it can be reasonably supposed to have arisen from random sampling". In: *The London, Edinburgh, and Dublin Philosophical Magazine and Journal of Science* 50.302, pp. 157–175.

Peng, Wei et al. (2016). "Structural basis for the gating mechanism of the type 2 ryanodine receptor RyR2". In: *Science* 354.6310.

Perez, Claudio F., José R. López, and Paul D. Allen (2005). "Expression levels of RyR1 and RyR3 control resting free Ca2+ in skeletal muscle". In: *American Journal of Physiology - Cell Physiology*.

Pessah, Isaac N., Andrew L. Waterhouse, and John E. Casida (1985). "The calcium-Ryanodine receptor complex of skeletal and cardiac muscle". In: *Biochemical and Biophysical Research Communications* 128.1, pp. 449–456.

Pitt, Samantha J. et al. (2010). "Charade of the SR K+-channel: Two ion-channels, TRIC-A and TRIC-B, masquerade as a single K -channel". In: *Biophysical Journal*.

Postma, A V et al. (2005). "Catecholaminergic polymorphic ventricular tachycardia: RYR2 mutations, bradycardia, and follow up of the patients". In: *J Med Genet* 42.11, pp. 863–870.

Potenza, Duilio M. et al. (2019). "Phosphorylation of the ryanodine receptor 2 at serine 2030 is required for a complete β-adrenergic response". In: *Journal of General Physiology* 151.2, pp. 131–145.

Potter, James D. et al. (1983). "Ca2+ Binding to Calmodulin". In: *Methods in Enzymology* 102.C, pp. 135–143.

Priori, S. G. and P. B. Corr (1990). "Mechanisms underlying early and delayed afterdepolarizations induced by catecholamines". In: *American Journal of Physiology - Heart and Circulatory Physiology*.

Priori, Silvia G. and S. R.Wayne Chen (2011). "Inherited dysfunction of sarcoplasmic reticulum Ca2+ handling and arrhythmogenesis". In: *Circulation Research* 108.7, pp. 871–883.

Priori, Silvia G. et al. (2001). "Mutations in the cardiac ryanodine receptor gene (hRyR2) underlie catecholaminergic polymorphic ventricular tachycardia". In: *Circulation*.

Priori, Silvia G et al. (2002). "Clinical and molecular characterization of patients with catecholaminergic polymorphic ventricular tachycardia". In: *Circulation* 106.1, pp. 69–74.

Protasi, Feliciano (2002). "Structural interaction between RYRs and DHPRs in calcium release units of cardiac and skeletal muscle cells." In: *Frontiers in bioscience : a journal and virtual library* 7.

Rebbeck, Robyn T. et al. (2017). "High-throughput screens to discover small-molecule modulators of ryanodine receptor calcium release channels". In: *SLAS Discovery* 22.2, pp. 176–186.

Respress, Jonathan L et al. (2012). "Role of RyR2 phosphorylation at S2814 during heart failure progression". In: *Circulation Research* 110.11, pp. 1474–1483.

Ringer, Sydney (1883). "A further Contribution regarding the influence of the different Constituents of the Blood on the Contraction of the Heart". In: *The Journal of Physiology*.

Rodriguez, Patricia, Moninder S. Bhogal, and John Colyer (2003). "Stoichiometric phosphorylation of cardiac ryanodine receptor on serine 2809 by calmodulin-dependent kinase II and protein kinase A". In: *Journal of Biological Chemistry* 278.40, pp. 38593–38600.

Rousseau, E., M. Roberson, and G. Meissner (1988). "Properties of single chloride selective channel from sarcoplasmic reticulum". In: *European Biophysics Journal* 16.3, pp. 143–151.

Rousseau, E., J. S. Smith, and G. Meissner (1987). "Ryanodine modifies conductance and gating behavior of single Ca2+ release channel". In: *American Journal of Physiology - Cell Physiology* 253.3.

Rudy, Yoram (2008). "Molecular basis of cardiac action potential repolarization". In: *Annals of the New York Academy of Sciences*.

Saftenku, Elena, Alan J. Williams, and Rebecca Sitsapesan (2001). "Markovian models of low and high activity levels of cardiac ryanodine receptors". In: *Biophysical Journal* 80.6, pp. 2727–2741.

Salvage, Samantha C. et al. (2019). "Ion channel gating in cardiac ryanodine receptors from the arrhythmic RyR2-P2328S mouse". In: *Journal of Cell Science* 132.10, jcs229039.

Samsó, Montserrat (2017). "A guide to the 3D structure of the ryanodine receptor type 1 by cryoEM". In: 26.1, pp. 52–68.

Samsó, Montserrat, Xiaohua Shen, and Paul D. Allen (2006). "Structural characterization of the RyR1-FKBP12 interaction". In: *Journal of Molecular Biology*.

Sanchez, Colline et al. (2018). "Tracking the sarcoplasmic reticulum membrane voltage in muscle with a FRET biosensor". In: *Journal of General Physiology*.

Schachter, Michael (2005). "Chemical, pharmacokinetic and pharmacodynamic properties of statins: An update". In: *Fundamental and Clinical Pharmacology*.

Schirris, Tom J J et al. (2015). "Clinical and Translational Report Statin-Induced Myopathy Is Associated with Mitochondrial Complex III Inhibition Cell Metabolism Clinical and Translational Report Statin-Induced Myopathy Is Associated with Mitochondrial Complex III Inhibition". In: *Cell Metabolism* 22, pp. 399–407.

Scoote, Mark and Alan J. Williams (2002). "The cardiac ryanodine receptor (calcium release channel): Emerging role in heart failure and arrhythmia pathogenesis". In: *Cardiovascular Research* 56.3, pp. 359–372.

Sedej, Simon et al. (2010). "Na+-dependent SR Ca2+ overload induces arrhythmogenic events in mouse cardiomyocytes with a human CPVT mutation". In: *Cardiovascular Research*.

Sekulic-Jablanovic, Marijana et al. (2015). "Characterization of excitation-contraction coupling components in human extraocular muscles". In: *Biochemical Journal* 466.1, pp. 29–36.

Severini, Alberto and Richard Morgan (1991). "An assay for proteinases and their inhibitors based on DNA/ethidium bromide fluorescence". In: *Analytical Biochemistry* 193.1, pp. 83–89.

Sham, J. S.K., L. Cleemann, and M. Morad (1995). "Functional coupling of Ca2+ channels and ryanodine receptors in cardiac myocytes". In: *Proceedings of the National Academy of Sciences of the United States of America* 92.1, pp. 121–125.

Shan, Jian et al. (2010). "Role of chronic ryanodine receptor phosphorylation in heart failure and β-adrenergic receptor blockade in mice". In: *Journal of Clinical Investigation* 120.12, pp. 4375–4387.

Shan, Jian et al. (2012). "Calcium leak through ryanodine receptors leads to atrial fibrillation in 3 mouse models of catecholaminergic polymorphic ventricular tachycardia". In: *Circulation Research* 111.6, pp. 708–717.

Shen, Jian Xin (2006). "Isoprenaline enhances local Ca2+ release in cardiac myocytes". In: *Acta Pharmacologica Sinica*.

Shepherd, James et al. (1995). "Prevention of coronary heart disease with pravastatin in men with hypercholesterolemia". In: *New England Journal of Medicine*.

Šidák, Zbyněk (1967). "Rectangular Confidence Regions for the Means of Multivariate Normal Distributions". In: *Journal of the American Statistical Association* 62.318, pp. 626–633.

Sigalas, C. et al. (2009a). "Ca 2+-calmodulin can activate and inactivate cardiac ryanodine receptors". In: *British Journal of Pharmacology* 156.5, pp. 794–806.

Sigalas, Charalambos et al. (2009b). "Ca2+-calmodulin increases RyR2 open probability yet reduces ryanoid association with RyR2". In: *Biophysical Journal* 97.7, pp. 1907–1916.

Sigworth, F. J. and S. M. Sine (1987). "Data transformations for improved display and fitting of single-channel dwell time histograms". In: *Biophysical Journal* 52.6, pp. 1047–1054.

Sirtori, Cesare R. (2014). "The pharmacology of statins". In: *Pharmacological Research* 88, pp. 3–11.

Sitsapesan, R. and A. J. Williams (1994a). "Gating of the native and purified cardiac SR Ca(2+)-release channel with monovalent cations as permeant species". In: *Biophysical Journal* 67.4, pp. 1484–1494.

— (1994b). "Regulation of the gating of the sheep cardiac sarcoplasmic reticulum ca2+-release channel by luminal Ca2+". In: *The Journal of Membrane Biology* 137.3, pp. 215–226.

Sitsapesan, R et al. (1991). "Sheep cardiac sarcoplasmic reticulum calcium-release channels: modification of conductance and gating by temperature." In: *The Journal of Physiology* 434.1, pp. 469–488.

Siu, Chung Wah, Chu Pak Lau, and Hung Fat Tse (2003). "Prevention of atrial fibrillation recurrence by statin therapy in patients with lone atrial fibrillation after successful cardioversion". In: *American Journal of Cardiology* 92.11, pp. 1343–1345.

Smith, G. L. and S. C. O'Neill (2001). "A comparison of the effects of ATP and tetracaine on spontaneous Ca2+ release from rat permeabilised cardiac myocytes". In: *Journal of Physiology* 534.1, pp. 37–47.

Smith, Jeffrey S., Roberto Coronado, and Gerhard Meissner (1986). "Single channel measurements of the calcium release channel from skeletal muscle sarcoplasmic reticulum: Activation by Ca2+ and ATP and Modulation by Mg2+". In: *Journal of General Physiology* 88.5, pp. 573–588.

Smith, Jeffrey S. et al. (1988). "Purified ryanodine receptor from rabbit skeletal muscle is the calcium-release channel of sarcoplasmic reticulum". In: *Journal of General Physiology*.

Stern, M. D. (1992). "Theory of excitation-contraction coupling in cardiac muscle". In: *Biophysical Journal* 63.2, pp. 497–517.

Sulakhe, Prakash V. and Xuan T. Vo (1995). "Regulation of phospholamban and troponin-I phosphorylation in the intact rat cardiomyocytes by adrenergic and cholinergic stimuli: roles of cyclic nucleotides, calcium, protein kinases and phosphatases and depolarization". In: *Molecular and Cellular Biochemistry*.

Sun, X. H. et al. (1995). "Molecular architecture of membranes involved in excitation-contraction coupling of cardiac muscle". In: *Journal of Cell Biology* 129.3, pp. 659–671.

Szent-Györgyi, A. G. (1975). "Calcium regulation of muscle contraction". In: *Biophysical Journal*.

Takeshima, Hiroshi et al. (1989). "Primary structure and expression from complementary DNA of skeletal muscle ryanodine receptor". In: *Nature*.

Tester, David J. et al. (2005). "Pathogenesis of unexplained drowning: New insights from a molecular autopsy". In: *Mayo Clinic Proceedings* 80.5, pp. 596–600.

Tewari, Rita et al. (2010). "Armadillo-repeat protein functions: Questions for little creatures". In: *Trends in Cell Biology* 20.8, pp. 470–481.

The UniProt Consortium (2017). "UniProt: the universal protein knowledgebase". eng. In: *Nucleic acids research* 45.D1, pp. D158–D169.

Timerman, Anthony P. et al. (1994). "The ryanodine receptor from canine heart sarcoplasmic reticulum is associated with a novel FK-506 binding protein". In: *Biochemical and Biophysical Research Communications* 198.2, pp. 701–706.

Timerman, Anthony P. et al. (1996). "Selective binding of FKBP12.6 by the cardiac ryanodine receptor". In: *Journal of Biological Chemistry*.

Tinker, Andrew, Allan R.G. Lindsay, and Alan J. Williams (1993). "Cation conduction in the calcium release channel of the cardiac sarcoplasmic reticulum under physiological and pathophysiological conditions". In: *Cardiovascular Research*.

Tinker, Andrew and Alan J. Williams (1992). "Divalent cation conduction in the ryanodine receptor channel of sheep cardiac muscle sarcoplasmic reticulum". In: *Journal of General Physiology* 100.3, pp. 479–493.

Torres, Natalia S. et al. (2014). "A modified local control model for Ca2+ transients in cardiomyocytes: Junctional flux is accompanied by release from adjacent non-junctional RyRs". In: *Journal of Molecular and Cellular Cardiology* 68, pp. 1–11.

Towbin, H., T. Staehelin, and J. Gordon (1979). "Electrophoretic transfer of proteins from polyacrylamide gels to nitrocellulose sheets: Procedure and some applications". In: *Proceedings of the National Academy of Sciences of the United States of America*.

Tripathy, A. et al. (1995). "Calmodulin activation and inhibition of skeletal muscle Ca2+ release channel (ryanodine receptor)". In: *Biophysical Journal*.

Uchinoumi, Hitoshi et al. (2010). "Catecholaminergic polymorphic ventricular tachycardia is caused by mutation-linked defective conformational regulation of the ryanodine receptor". In: *Circulation Research* 106.8, pp. 1413–1424.

Uehara, Akira et al. (2017). "Extensive Ca2+ leak through K4750Q cardiac ryanodine receptors caused by cytosolic and luminal Ca2+ hypersensitivity". In: *Journal of General Physiology*.

Valdivia, H H et al. (1995). "Rapid adaptation of cardiac ryanodine receptors: modulation by Mg2+ and phosphorylation." In: *Science (New York, N.Y.)* 267.5206, pp. 1997–2000.

Van Oort, Ralph J. et al. (2010). "Ryanodine receptor phosphorylation by calcium/calmodulin-dependent protein kinase II promotes life-threatening ventricular arrhythmias in mice with heart failure". In: *Circulation* 122.25, pp. 2669–2679.

Venetucci, Luigi et al. (2012). "Inherited calcium channelopathies in the pathophysiology of arrhythmias". In: *Nature Reviews Cardiology* 9.10, pp. 561–575.

Venturi, Elisa et al. (2013). "TRIC-B channels display labile gating: Evidence from the TRIC-A knockout mouse model". In: *Pflugers Archiv European Journal of Physiology*.

Venturi, Elisa et al. (2018). "Simvastatin activates single skeletal RyR1 channels but exerts more complex regulation of the cardiac RyR2 isoform". In: *British Journal of Pharmacology* 175.6, pp. 938–952.

Wagenknecht, Terence et al. (1996). "Cryoelectron microscopy resolves FK506-binding protein sites on the skeletal muscle ryanodine receptor". In: *Biophysical Journal*.

Walweel, K. et al. (2017). "Ryanodine receptor modification and regulation by intracellular Ca2+ and Mg2+ in healthy and failing human hearts". In: *Journal of Molecular and Cellular Cardiology* 104, pp. 53–62.

Walweel, Kafa et al. (2014). "Differences in the regulation of RyR2 from human, sheep, and rat by Ca2+ and Mg2+ in the cytoplasm and in the lumen of the sarcoplasmic reticulum". In: *Journal of General Physiology*.

Wang, Yanwen et al. (2016). "Optogenetic Control of Heart Rhythm by Selective Stimulation of Cardiomyocytes Derived from Pnmt + Cells in Murine Heart". In: *Nature Publishing Group*.

Wang, Yue Yi et al. (2017). "RyR2R420Q catecholaminergic polymorphic ventricular tachycardia mutation induces bradycardia by disturbing the coupled clock pacemaker -suplement". In: *JCI insight* 2.8.

Watanabe, Hiroshi et al. (2009). "Flecainide prevents catecholaminergic polymorphic ventricular tachycardia in mice and humans". In: *Nature Medicine* 15.4, pp. 380–383.

Wehrens, Xander H T et al. (2003). "FKBP12.6 deficiency and defective calcium release channel (ryanodine receptor) function linked to exercise-induced sudden cardiac death". In: *Cell* 113.7, pp. 829–840.

Wehrens, Xander H.T. et al. (2004). "Ca2+/calmodulin-dependent protein kinase II phosphorylation regulates the cardiac ryanodine receptor." In: *Circulation research* 94.6.

Wei, Risheng et al. (2016). "Structural insights into Ca2+-activated long-range allosteric channel gating of RyR1". In: *Cell Research* 26.9, pp. 977–994.

Welch, B L (1951). "On the Comparison of Several Mean Values: An Alternative Approach". In: *Biometrika* 38.3/4, p. 330.

White, Stephen H. (1986). "The Physical Nature of Planar Bilayer Membranes". In: *Ion Channel Reconstitution*. Springer US, pp. 3–35.

Wilson, Abigail D. et al. (2018). "Statins Bind to Cardiac Ryanodine Receptor (RyR2) Channels to Alter Opening Frequency". In: *Biophysical Journal* 114.3, 621a–622a.

Xiao, Bailong et al. (2004). "Protein Kinase A Phosphorylation at Serine-2808 of the Cardiac Ca 2+-Release Channel (Ryanodine Receptor) Does Not Dissociate 12.6-kDa FK506-Binding Protein (FKBP12.6)". In: *Circulation Research* 94.4, pp. 487–495.

Xiao, Bailong et al. (2006). "Ser-2030, but not Ser-2808, is the major phosphorylation site in cardiac ryanodine receptors responding to protein kinase A activation upon

β-adrenergic stimulation in normal and failing hearts". In: *Biochemical Journal* 396.1, pp. 7–16.

Xiao, Jianmin et al. (2007). "Removal of FKBP12.6 does not alter the conductance and activation of the cardiac ryanodine receptor or the susceptibility to stress-induced ventricular arrhythmias". In: *Journal of Biological Chemistry*.

Xie, Yuanfang et al. (2019). "Size Matters: Ryanodine Receptor Cluster Size Heterogeneity Potentiates Calcium Waves". In: *Biophysical Journal* 116.3, pp. 530–539.

Yamamoto, Takeshi et al. (2008). "Identification of target domains of the cardiac ryanodine receptor to correct channel disorder in failing hearts". In: *Circulation* 117.6, pp. 762–772.

Yazawa, Masayuki et al. (2007). "TRIC channels are essential for Ca2+ handling in intracellular stores". In: *Nature* 448.7149, pp. 78–82.

Ye, Chen Izu et al. (2000). "G(i)-dependent localization of β2-adrenergic receptor signaling to L-type Ca2+ channels". In: *Biophysical Journal*.

Zhao, Xiao Lan et al. (1994). "The α1-subunit of skeletal muscle L-type Ca channels is the key target for regulation by A-kinase and protein phosphatase-1C". In: *Biochemical and Biophysical Research Communications*.

Zhao, Y T et al. (2015). "Arrhythmogenesis in a catecholaminergic polymorphic ventricular tachycardia mutation that depresses ryanodine receptor function". eng. In: *Proc Natl Acad Sci U S A* 112.13, E1669–77.

Zheng, Wenjun and Zheng Liu (2017). "Investigating the inter-subunit/subdomain interactions and motions relevant to disease mutations in the N-terminal domain of ryanodine receptors by molecular dynamics simulation". In: *Proteins: Structure, Function and Bioinformatics* 85.9, pp. 1633–1644.

Zsolnay, Vilmos, Michael Fill, and Dirk Gillespie (2018). "Sarcoplasmic Reticulum Ca2+ Release Uses a Cascading Network of Intra-SR and Channel Countercurrents". In: *Biophysical Journal*.